REPUBLIC OF TURKEY

YILDIZ TECHNICAL UNIVERSITY

GRADUATE SCHOOL OF NATURAL AND APPLIED SCIENCES

MULTISCALE DRUG REPURPOSING STUDY FOR THE TREATMENT OF THE ALZHEIMER DISEASE: A COMBINED *IN SILICO* AND *IN VITRO* STUDY

Hind ALJANABI

DOCTOR OF PHILOSOPHY THESIS

Department of Chemistry

Chemistry Program

Supervisor

Prof. Dr. Barbaros NALBANTOĞLU

Co-Advisor

Prof. Dr. Serdar DURDAĞI

January, 2022

REPUBLIC OF TURKEY

YILDIZ TECHNICAL UNIVERSITY

GRADUATE SCHOOL OF NATURAL AND APPLIED SCIENCES

MULTISCALE DRUG REPURPOSING STUDY FOR THE TREATMENT OF THE ALZHEIMER DISEASE: A COMBINED *IN SILICO* AND *IN VITRO* STUDY

A thesis submitted by Hind ALJANABI in partial fulfillment of the requirements for the degree of **DOCTOR OF PHILOSOPHY** is approved by the committee on 20.01.2022 in Department of Chemistry, Chemistry (English) Program.

Prof. Dr. Barbaros NALBANTOĞLU	Prof. Dr. Serdar DURDAĞI
Yıldız Technical University	Bahçeşehir University
Supervisor	Co-Advisor

Approved By the Examining Committee

Prof. Dr. Barbaros NALBANTOĞLU, Advisor _____

Yıldız Technical University

Assoc. Prof. Dr. Volkan SÖZER, Member _____

Yıldız Technical University

Prof. Dr. Turgay ÇAKMAK, Member _____

Istanbul Medeniyet University

Assist. Prof. Dr. Çiğdem BILEN, Member _____

Yıldız Technical University

Assoc. Prof. Dr. Mustafa YAMAN, Member _____

Istanbul Sabahattin Zaim University

I hereby declare that I have obtained the required legal permissions during data collection and exploitation procedures, that I have made the in-text citations and cited the references properly, that I haven't falsified and/or fabricated research data and results of the study and that I have abided by the principles of the scientific research and ethics during my Thesis Study under the title of "Multiscale Drug Repurposing Study for the Treatment of the Alzheimer Disease: A Combined *in silico* and *in vitro* Study", supervised by my supervisor, Prof. Dr. Barbaros NALBANTOĞLU. In the case of a discovery of false statement, I am to acknowledge any legal consequence.

Hind ALJANABI

Signature

Dedicated to

The soul of my dear parents,

My husband Ali

My daughters Maryam and Sarah

My sister Suadad

And to all my family and friends

ACKNOWLEDGEMENTS

I would like to express my sincere gratitude and my special thanks to my supervisor Prof. Dr. Barbaros NALBANTOĞLU for his pure-hearted support, help and guidance during the last 6 years of my Ph.D journey. I would like to express my gratitude and thanks to my co-supervisor Prof. Dr. Serdar DURDAĞI for allowing me to work on this project, for his guidance and his kind advices through my Ph.D research.

I would like to express my thank to Prof. Dr. Murat Senturk from department of basic sciences of pharmacy, Pharmacy Faculty, Ağri Ibrahim Çecen University for helping and supporting my Ph.D study and research, I'm really grateful to him.

I also would like to thank Bahçeşehir University for giving me this opportunity to work in computational biology and molecular simulations laboratory and for supporting this project with the necessary equipment.

I thank the graduate school of and all the teaching staff for their efforts, their commitment and their help during the first part of my Ph.D.

I would like to thank all my colleagues and members of (Durdağı Lab.) for collaboration and support especially; Ismail Erol, Fareed Assad, Dr. Busecan Aksoydan, Dr. Kadar Şahin, Lalehan Oktay, and Saima had imaginable experience to share with me. Ismail was the most helpful person I have ever met. Thank you for your help, companionship, providing a pleasurable and friendly work atmosphere.

Big thanks to my best friends during this Ph.D journey in YTU, Dr. Wissem Mhiri, Dr. Mohammad Haddad and Dr. Tuğba Dayioğlu for their support, their help, and for all moment we shared, you are unforgettable.

Ultimately, to the best people in my life, I express my extreme gratitude for my husband (Ali), my sister (Suadad) and my daughters (Maryam and Sarah) for their unconditional supportive, have always been proud and for their help and their love. Concisely, all these people reminded me that I would never walk alone

in different parts of my life. Without their supports, I would not be able to come to this point. Everyone who has made this achievement possible, I'm grateful to you all.

Hind ALJANABI

TABLE OF CONTENTS

LIST OF SYMBOLS

α	Alpha
Å	Angstrom
β	Beta
ΔG	Binding Free Energy
γ	Gamma
IC_{50}	Half Maximal Inhibitory Concentration
K	Kelvin
Kcal	Kilocalories
μM	Micro molar
mg	Milligrams
ml	Milliliters
M	Molar
mol	Mole
ns	Nano Second
%	Percentage
π	Pi
τ	Tau

LIST OF ABBREVIATIONS

2D	Two – Dimensional
3D	Three-Dimensional
α-Sec	Alpha Secretase
β-Sec	Beta Secretase
γ-Sec	Gamma Secretase
τ	Tau
Aβ	Beta Amyloid
ACh	Acetylcholine
AChE	Acetylcholinesterase Enzyme
AD	Alzheimer's Disease
ADME	Available Absorption, Distribution, Metabolism, and Excretion
ADP	Adenosine Diphosphate
AICD	APP Intracellular Domain
ALA	Alanine
APOE	Apolipoprotein
APP	Amyloid Precursor Protein
APPsα	Amyloid Precursor Protein Secretase Alpha
APPsβ	Amyloid Precursor Protein Secretase Beta
AS	Anionic Substrate
ASP	Aspartate
ASN	Asparagine
ATP	Adenosine Triphosphate
BBB	Blood-Brain Barrier
BuChE	Butyrylcholinesterase Enzyme

CADD	Computer-Aided Drug Designed
CDK5	Cyclin-Dependent Kinase 5
ChE	Cholinesterase
ChEIs	Cholinesterase Inhibitors
CNS	Central Nervous System
CT	Computed Tomography
CTFβ	β-Secretase-Derived C-Terminal Fragment
Cu	Copper
ER	Endoplasmic Reticulum
ES	Esteratic Subsite
ETC	Electron Transport Chain
FAD	Familial Alzheimer's Disease
FDA	Food and Drug Administration
Fe	Iron
FEP	Free Energy Perturbation
GBSA	Generalized Born Surface Area
GLN	Glutamine
GLU	Glutamate
GLY	Glycine
GSK3β	Glycogen Synthase Kinase 3
hERG	Human Ether a-go-go-Related Gene
HIS	Histidine
HTS	High-Throughput Screening
LBDD	Ligand-Based Drug Design
IFD	Induced Fit Docking
LIE	Ligand Efficiency

MCC	Matthews Correlation Coefficient
MCI	Mild Cognitive Impairment
MD	Molecular Dynamics
MM	Molecular Mechanics
MM/GBSA	Molecular Mechanics Generalized Born Surface Area
MMP	Matched Molecular Pairs
MRI	Magnetic Resonance Imaging
MTL	Medial Temporal lobe
NAD	Nicotinamide Adenine Dinucleotide
NADH	Nicotinamide Adenine Dinucleotide Hydrogen
NCGC	NIH Chemical Genomics Center
NFTs	Neurofibrillary Tangles
NMDA	N-Methyl-D-Aspartate
NPC	NIH Pharmaceutical Collection
NPT	Isothermal – Isobaric Ensemble
PDB	Protein Data Bank
PET	Positron Emission Tomography
PHE	Phenylalanine
PNS	Peripheral Nervous System
PRO	Proline
PSEN	Presenilins
QOL	Quality of Life
QPLD	Quantum Mechanics-Polarized Ligand Docking
QSAR	Quantitative Structure - Activity Relationship
RMSD	Root Mean Square Deviation
RMSF	Root Mean Square Fluctuation

RNS	Reactive Nitrogen Species
ROS	Reactive Oxygen Species
SAPPα	Secreted APP Alpha
sAPPβ	Secreted APP Beta
SAD	Sporadic Alzheimer's Disease
SER	Serine
SGA	Second-Generation Antipsychotic
SI	Selectivity Index
SP	Standard Precision
SPC	Single Point Charge
SBDD	Structure-Based Drug Design
TAV	Therapeutic Activity Values
TRP	Tryptophan
TYR	Tyrosine
Zn	Zinc

LIST OF FIGURES

LIST OF TABLES

ABSTRACT

Drug Repurposing Effort for the Novel Acetylcholinesterase and Butyrylcholinesterase Targets: A Combined *in silico* and *in vitro* Study

Hind ALJANABI

Department of Chemistry

Doctor of Philosophy Thesis

Advisor: Prof. Dr. Barbaros NALBANTOĞLU

Co-advisor: Prof. Dr. Serdar DURDAGI

Alzheimer's disease (AD) is a central nervous system chronic condition that causes a decrease in cognitive control and language capacity. AD is associated with cholinergic deficiency, and various cholinesterase inhibitors, including naturally derived inhibitors, synthetic analogs, and hybrids have been developed to treat AD. The drugs available for AD are currently mainly cholinesterase inhibitors. However, the efficacy of these drugs was limited, as they can cause adverse side effects and are unable to stop the progression disease entirely.

Initially, in the current study, 7922 small compounds were retrieved from NIH Chemical Genomics Center (NCGC) pharmaceutical collection (NPC) library to be screened through QSAR model developed from targets against AD. The molecules with higher AD therapeutic activity values (>0.75) were then used in the 26 different toxicity-QSAR models. Binary QSAR models resulted in 10 hits that have high AD therapeutic activity and no toxicity. The selected hits were then screened against acetylcholinesterase (AChE), and butyrylcholinesterase (BuChE) targets using standard precision docking (SP), induce fit docking (IFD) and quantum

mechanics-polarized ligand docking (QPLD). Top IFD docking poses for five compounds were used in, initially, short (50 ns), and then long (100 ns) molecular dynamics (MD) simulations. Molecular Mechanics/Generalized Born Surface Area (MM/GBSA) binding free energy calculations were performed for the five top compounds. A similar protocol was also applied for three of the known AChE and BuChE inhibitors. Finally, based on MM/GBSA scores and their corresponding docking scores, three compounds were ordered, and their in vitro tests were performed. All compounds showed nM-level inhibition for both AChE and BuChE targets. The outcomes of this study may open a new perspective for the development of novel drugs with reduced toxicity and preserved pharmacological activity against AD.

Keywords: Alzheimer disease, acetylcholinesterase, butyrylcholinesterase, molecular docking, MD simulations.

ÖZET

Yeni Asetilkolinesteraz ve Butirilkolinesteraz Hedefleri için İlaç Yeniden Konumlandırma Çabası: Bir Birleşik *in siliko* ve *in vitro* Çalışma

Hind ALJANABI

Kimya Bölümü

Doktora Tezi

Danışman: Prof. Dr. Barbaros NALBANTOĞLU

Eş-Danışman: Prof. Dr. Serdar DURDAGI

Alzheimer hastalığı (AH) bilişsel kontrol ve konuşma kapasitesinde düşüşe sebep olan kronik bir merkezi sinir sistemi rahatsızlığıdır. AH kolinerjik yetersizlik ile ilişkilendirildiğinden, doğal bileşik türevleri, sentetik analoglar, hibrit molekülleri de içeren bir çok kolinesteraz inhibitörleri geliştirilmiştir. Ancak, bu moleküllerin etkinliği kısıtlıdır, çünkü bu moleküllerin hastalığın ilerlemesi tamamen durduramadığı gibi, olumsuz yan etkilere de olmaktadır.

NIH Kimyasal Genomik Merkez (NKGM) dan elde edilen 7922 moleküle sahip farmasötik molekül koleksiyonu (NPC) kütüphanesi AH'a karşı kantitatif yapı-aktivite ilişkisi (KYAİ) modelleriyle sanal olarak taranmıştır. Bu moleküllerden AH terapötik aktivitesi 0,75' ten büyük olan moleküller, bir sonraki aşamada 26 farklı toksisite-KYAİ modelleriyle analiz edilmişler ve toksisite gösterip göstermedikleri tahmin edilmiştir. İkili KYAİ modelleri, AH terapötik aktivite değerleri yüksek ve toksisite göstermeyen 10 hit molekülü tahmin etmiştir. Bu 10 molekül, asetilkolin esteraz (AKE) ve butirilkolin esteraz (BKE) enzimlerine standard hassasiyetli (SH)

kenetleme, indüklenmiş uyum (IU) kenetleme ve kuantum polarized ligand (KPL) kenetleme yöntemleriyle bağlanmalarının enerjileri ölçülmüştür.

En yüksek IU kenetleme pozları öncelikle 50 nanosaniyelik (ns) kısa, ardından 100 ns lik uzun moleküler dinamik (MD) simulasyonlarına tabi tutulmuşlardır. Moleküler mekanik genelleştirilmiş Born yüzey alanı (MM/GBYA) bağlanma enerji hesaplamaları seçilen 5 molekül için yapılmıştır. Son olarak, moleküler kenetleme ve MMGBYA enerji skorlarına göre 3 molekül sipariş edilmiş, ve bu moleküllerin AKE ve BKE enzimlerine bağlanmaları in vitro testlerle belirlenmiştir. Her iki hedef için de, seçilen moleküller nanomolar (nM) afinite göstermişlerdir. Bu tez çalışmasının sonuçları, AH' na karşı azaltılmış toksisite ve bunun yanında korunmuş farmakolojik aktiviteye sahip yeni ilaçların geliştirilmesi için yeni bir perspektif açabileceği düşünülmektedir.

Anahtar Kelimeler: Alzheimer hastalığı, asetilkolinestaz, butirilkolinesteraz, moleküler yerleştirme, MD simülasyonları.

1
INTRODUCTION

1.1 Literature Review

Alzheimer's disease (AD) is a type of irreversible brain disease that creates memory, consideration, and behavior problems. AD affects around 50 million people worldwide and gets worse with severe behavioral and psychological symptoms over the long term [1, 2]. Symptoms firstly appear in most people with AD in their mid-60s [3]. Scientists keep sorting out the complicated brain alterations involved with AD onset and progress. It seems that brain alterations may start a decade or more before memory and other cognitive problems emerge. Through this pre-clinical stage of AD people seem devoid of symptoms, even while toxic changes occur in the brain. Neurological changes associated with AD include sediments of abnormal, stable, and insoluble protein throughout the brain. These sediments will congeal into what are known as amyloid plaques, and tau tangles and healthy neurons will cease to function, lose connections, and die in the presence of other neurons [3, 4]. It is also believed that numerous additional complicated brain alterations will play a part in the development of Alzheimer's disease. So far, scientists could not predict what the actual causes (i.e., exact etiology) behind AD are; however, the disease exhibits some associations with a combination of factors related to genetics, environment, and lifestyle. In the USA, Alzheimer's disease (AD) is presently classified as the sixth greatest cause of death, but new estimates indicate that it may really be the third biggest cause of mortality for older people, after heart disease and cancer [5]. AD is generally characterized via a deficiency in the amount of neurotransmitter acetylcholine (ACh) in the brain. Therefore, inhibitors of cholinesterase (ChE) are the 1st-line pharmacological agents used to treat AD [3]. Damage to the cholinergic neurotransmission that produces ACh has been shown to be related to memory disorders in patients with AD. Some of the cognitive habits were correlated with ACh existing in the brain cortex and plasticity [6, 7]. The enzyme class of ChE

consists primarily of 2 target proteins, namely, acetylcholinesterase (AChE, E.C. 3.1.1.7) and butyrylcholinesterase (BuChE, E.C. 3.1.1.8). The sequence identity between the AChE and BuChE is very high (nearly 84%); thus, the responses they give each other match[8]. They are found mainly in the central nervous system and in vertebrate cholinergic synapses [9].

AChE plays a key role in regulating several physiological reactions via hydrolyzing the ACh into cholinergic synapses. BuChE is expressed in neuroglia, on the other hand, and is located in the stomach, liver, heart, kidney, lungs, and serum. It plays a significant role in compound-containing ester metabolism. AChE may also be hydrolyzed, and its level does not decrease, or it can even rise in AD. AChE is usually prevalent in the brain, but BuChE activity increases when AChE activity stays unchanged or decreases in AD patients. The cessation of cholinergic signaling via hydrolyzing AChE is responsible for both enzymes. Therefore, a medication that inhibits both AChE and BuChE can be preferable to selective inhibitors of AChE or BuChE.

So far, the US Food and Drug Administration (FDA) has approved five medications for treating AD. Four of them (tacrine, donepezil, rivastigmine, and galantamine) are AChE antagonists, and memantine is the N-Methyl-D-Aspartate (NMDA) receptor antagonist [10]. Such licensed AChE inhibitors block metabolite products from forming in ACh. Insufficient levels of the neurotransmitter ACh at the synaptic cleft contribute to AD. Nevertheless, current ChE inhibitors have some drawbacks due to the side effects, including bradycardia, syncope, nausea, diarrhea, anorexia, migraine, insomnia, and muscle cramps [11, 12]. The current therapies only prolong the development of AD-related symptoms. Hence, the need for effective treatment is crucial. The current therapies only prolong the development of AD-related symptoms. Hence, the need for effective treatment is crucial. Recent development in computational biology approaches and molecular modeling techniques lead new opportunities for the detection, diagnosis, and design/development of more effective treatments against both common and rare diseases. Many data types, including molecular, medical, and epidemiological data, are becoming publicly available at comparable rates. It is possible to use

these databases including small molecule libraries against specific target proteins to find new uses for existing therapies [13]. Naturally derived and synthesized compounds as AChE and BuChE inhibitors are a promising area of interest. many hybrids are also being developed. Some hybrids utilize completely new materials, while others depend on existing AChEI materials and are attempting to improve upon their performance. Several researches have been conducted on the actions of AChE and BuChE inhibitors that are employed in the treatment of Alzheimer's disease [14], [15], [16], [17], [18-20] and other neurodegenerative diseases.

1.2 Objective of the thesis

The target of this research is to reveal the potential use of new small known molecules against AD which were previously used for different purposes. For this aim, a small molecule library which has approved drugs and compounds tested in clinical phase studies is virtually screened initially in ligand-based AD model, then; the binding sites of AChE and BuChE were identified as essential targets in the therapy of AD. Not only we focused on identifying the therapeutic compounds targeting AChE and BuChE, but the search also established pharmacokinetic and toxicity profiles of selected hit ligands. Selected hits based on the multiscale ligand and structure-driven methods contribute to discovering new hits that are closely related to AChE and BuChE targets. The identifying hit compounds were then tested via in vitro experiments.

1.3 Hypothesis

Treatment with AChE and BuChE inhibitors is commonly one aspect of the package of care required for AD patients. Therefore, investigating the effects of molecules via inhibiting or activating on esterase activities of AChE and BuChE is essential for drug design used to treat AD diseases. At the same time, the drugs may inhibit or activate other enzymes that belong to the same group lead to disease as an unknown side effect of used drugs. Therefore, the findings of this study may be led to consider these drugs as new inhibitors for AChE and BuChE via *in vitro* esterase activity. However, other in vivo investigations are also required to understand these enzymes' inhibition activity.

2

ALZHEIMER'S DISEASE

2.1 Overview of Alzheimer's Disease

Alzheimer's disease (AD) is a kind of irreversible brain illness that causes memory, decision-making, and behavioral difficulties in affected individuals. AD affects millions of individuals across the globe and worsens with time, causing severe behavioral and psychiatric symptoms [4]. In the globe, about 50 million individuals are affected via Alzheimer's disease, with more than 10 million new cases being identified each year. With an aging population, it is projected that the number of Alzheimer's sufferers would exceed 130 million via 2050, resulting in significant implications for healthcare [21]. The majority of Alzheimer's patients have their 1st symptoms in their mid-60s [4].

Scientists are still trying to figure out the complicated brain changes that occur Through the development and course of Alzheimer's disease. It seems probable that brain alterations begin a decade or more before memory loss and other cognitive problems manifest themselves. When people are at this preclinical stage of Alzheimer's disease, they do not seem to be experiencing any symptoms, despite the fact that harmful changes are occurring in the brain [3]. In recent years, estimates have shown that the Alzheimer's disease (AD) condition may be the third largest cause of mortality in older adults, after heart disease and cancer [5]. The goal of this research is to discover more about Alzheimer's disease, including its history, symptoms, diagnosis, and chances for a cure, in order to better understand it.

2.2 History of Alzheimer's Disease

Alzheimer's disease was first discovered in 1906, but it wasn't until around 70 years ago that it was recognized as a common cause of dementia and a significant cause of mortality [22]. When Alois Alzheimer firstly met Auguste Deter in 1901,

he had no way of knowing that her tragic tale would one day become his name a familiar word all over the globe. Auguste was barely 50 years old when her husband became aware of her deteriorating memory. It was essential to admit her to a mental institution when she was 51 years old because she had become more afraid, paranoid, and violent. She remained there as an inpatient until she died there in 1906.

Ms. Deter's brain was microscopically examined via Dr. Alzheimer, who worked on the autopsy in his capacity as a neuropathologist. New stains were used to examine Ms. Deter's brain, when it was determined that she suffered from "cerebral atrophy" (brain degeneration), "senile plaques" (protein deposits), and "neurofibrillary tangles" (abnormal filaments in nerve cells), all of which are typical path Alzheimer's disease becomes a significant study topic only when this occurs [23]. The studies that followed have shown a great deal, including that Alzheimer's disease starts years ere Alzheimer's signs are present. However, there are also many to understand about the exact biological of AD changes that contribute to its symptoms, why the disease symptoms are progressing more rapidly in some cases than others, which and how areas responsible for language, reasoning, and social behavior are affected via Alzheimer's disease (see Figure 2.1) and how the AD can slow down, halted, or reversed [4].

Alzheimer's and other kinds of dementia are now among the world's top ten causes of death, ranking 3ed in 2019 in both the USA of America and Europe. Men are less susceptible to this disease than women. Almost 2-thirds of Americans with Alzheimer's are women. A woman's lifetime chance of acquiring Alzheimer's disease is 1 in 6 at age 65, which corresponded with almost 1 in 11 for a man. Moreover, women have been disproportionately affected: women account for 65% of deaths from Alzheimer's and other forms of dementia globally[24, 25](Figure 2.2).

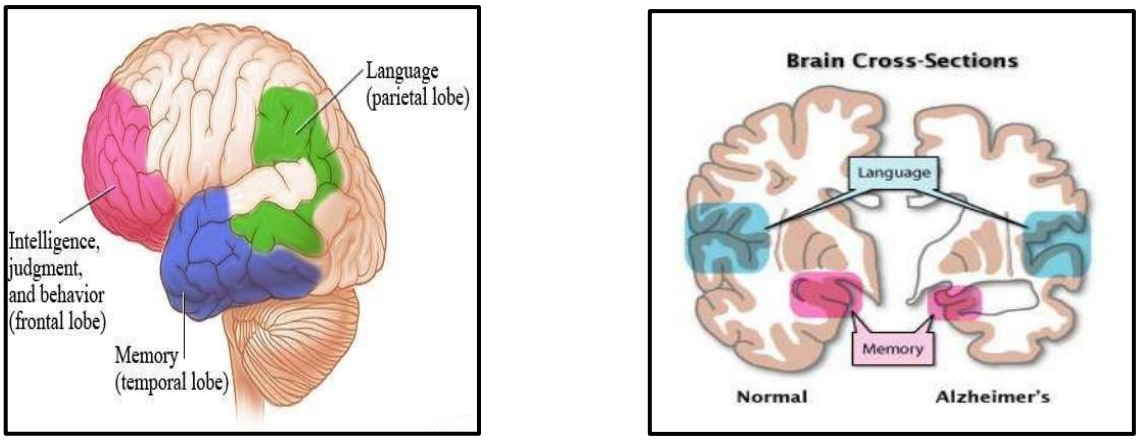

Figure 2. 1 Areas of brain affected by Alzheimer's

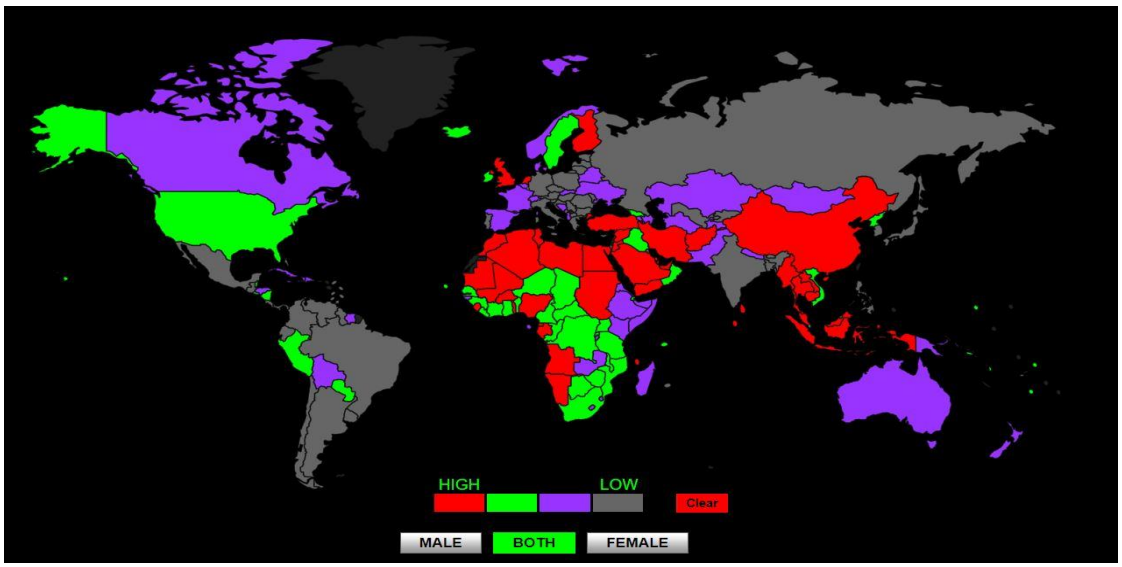

Figure 2. 2 Alzheimer and Dementia death rate per 100,00

2.3 "Alzheimer's Dementia" what is it?

Dementia is a condition characterized via disturbance in the brain's different functions, including memory, perception, orientation, understanding, calculation, ability to learn, language, and judgment. Consciousness is not overcast[26]. The impairments in cognitive function are generally followed via regression of emotional regulation, social activity, or motivation, and sometimes preceded via it. The common prevalent kind of dementia is AD, likely leading to 60-70% of states and still today an incurable degenerative disease that is incurable today [27, 28]. The progression of the disease is categorized into five stages (preclinical AD, mild cognitive impairment (MCI) may be classified into three levels: mild,

moderate, and severe, with a progressive pattern of cognitive and functional dysfunction [29] (Figure 2.3). Mild cognitive impairment (MCI) was described as a stage of cognitive decline between normal aging and Alzheimer's disease (AD) (MCI). Patients with MCI have a higher degree of memory loss than would be anticipated for their age, but do not satisfy the currently recognized clinically probable Alzheimer's disease criteria [30]. Biomarkers that identify the presence or absence of the disease may assist clinical diagnosis. In the future, this will become much more important as new Alzheimer's disease drugs become available.

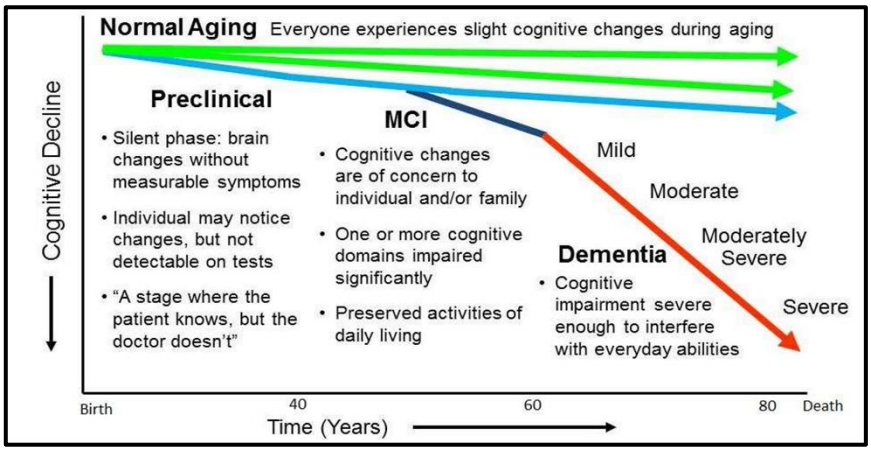

Figure 2. 3 Alzheimer's disease (AD) continuum. *MCI: mild cognitive impairment

AD is a developing global healthcare illness, and it is a sort of brain disease like coronary arteries is a type of heart failure disease. It is also a degenerative condition, which means that it gets worse over time [4]. AD is a progressive neurodegenerative illness (neurodegeneration is the growing loss of structure or function of neurons, including their death) that typically begins slowly and steadily worsens over time as the global population ages [31]. AD affects a patient's cognitive ability, especially the episodic memory system (see Figure 2.4). The episodic and semantic memories are information retrieval systems. *Episodic* memory is the term used to describe the ability to recall events and circumstances that have occurred in one's own life consciously. It is one of the most important mental (cognitive) abilities made possible via the brain's wiring [32].

It is the memory of everyday events (such as location geography, time, associated sentiments, and other contextual information) that can be explicitly declared or conjured. Episodic memory helps us learn about specific personal events that occur in our everyday lives and recall knowledge [33]. Patients may forget these events when episodic memory deteriorates due to AD or fail to remember them later [22]. It is another kind of declarative memory that relates to broad world knowledge that we have acquired throughout our lives and that is known as semantic memory. It is based on cultural traditions and interwoven with experience to form this broad knowledge (facts, ideas, meaning, and concepts)[34].

The medial temporal lobe (MTL), an area of the brain that includes the hippocampus, supports episodic memory. The hippocampus makes it possible for us to encode, store, and recover events in our daily lives. Unfortunately, in patients with AD, this brain area experiences significant damage caused via an aggregation of beta-amyloid plaques andneurofibrillary tangles[35].

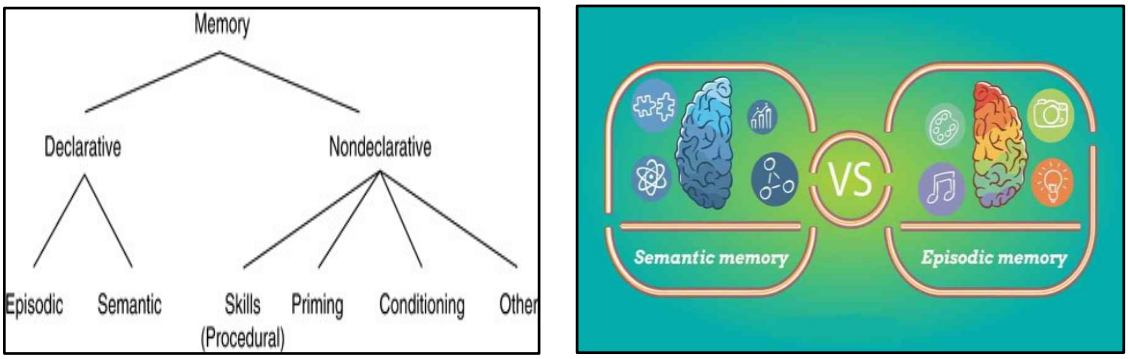

Figure 2. 4 Comparison of episodic vs semantic memory

2.4 Alzheimer's Disease Signs

Scientists are currently unraveling the complex brain alterations involved with the onset and progression of Alzheimer's disease. While individuals seem to stay symptom-free throughout the preclinical stage of Alzheimer's disease, catastrophic changes in the brain are happening. Individuals with Alzheimer's disease have a broad variety of symptoms, and there may be subtle distinctions between normal cognitive changes associated with aging and early signs of Alzheimer's dementia

that vary with time. These symptoms [30] provide insight into the degree to which neurons in various areas of the brain have been damaged.

- **Signs of Mild AD:** It is possible for someone to look healthy at this stage, but he or she will have increasing difficulties making sense of the world around him or her. Memory difficulties, poor decision-making, loss of spontaneity and feeling of initiative, taking longer to accomplish regular daily chores, asking the same questions over and again, and other issues are all possible. Through this stage of the illness, Alzheimer's disease is often discovered.
- **Signs of Moderate AD:** Through this period, more intense monitoring and care are required, which may be difficult for many spouses and families to provide. Progressive memory loss and disruption, frustration with regulating thoughts and thinking logically, difficulties realizing family and friends, failure to learn new things, difficulties with language, reading, writing, and working with numbers, hallucinations, delusions, paranoia, and occasional muscle twitches are some of the signs and symptoms of Alzheimer's disease.
- **Signs of Severe AD:** People suffering from severe Alzheimer's disease are unable to communicate and are completely reliant on others to provide for their basic needs and requirements. The individual may spend the most of their time in bed while their body shuts down. The following are some of their most frequent symptoms: loss of bowel and bladder control, inability to talk, weight loss, convulsions, skin illnesses, difficulty chewing, moaning and grunting, and an inability to sleep longer periods.

Individuals' rates of progression from mild to moderate to severe symptoms vary (see Table 2.1)[31].

Table 2. 1 Signs of Alzheimer's compared with typical age-related changes

Signs of Alzheimer's or other dementias	Typical age-related changes
❖ **Memory loss that disrupts daily life:** One of the most common signs of Alzheimer's is memory loss, especially forgetting recently learned information. Others include forgetting important dates or events, asking for the same information over and over, and increasingly needing to rely on memory aids (for example, reminder notes or electronic devices) or family members for things that used to be handled on one's own.	Sometimes forgetting names or appointments, but remembering them later.
❖ **Challenges in planning or solving problems:** Some people experience changes in their ability to develop and follow a plan or work with numbers. They may have trouble following a familiar recipe, keeping track of monthly bills or counting change. They may have difficulty concentrating and take much longer to do things than they did before.	Making occasional errors when balancing a checkbook.
❖ **Difficulty completing familiar tasks at home, at work or at leisure:** People with Alzheimer's often find it hard to complete daily tasks. Sometimes, people have trouble driving to a familiar location, managing a budget at work or remembering the rules of a favorite game.	Occasionally needing help to use the settings on a microwave or record a television show.
❖ **Confusion with time or place:** People with Alzheimer's can lose track of dates, seasons and the passage of time. They may have trouble understanding something if it is not happening immediately. Sometimes they forget where they are or how they got there.	Getting confused about the day of the week but figuring it out later.
❖ **Trouble understanding visual images and spatial relationships:** For some people, having vision problems is a sign of Alzheimer's. They may have difficulty reading, judging distance and determining color or contrast, which may cause problems with driving.	Vision changes related to cataracts, glaucoma or age-related macular degeneration.
❖ **New problems with words in speaking or writing:** People with Alzheimer's may have trouble following or joining a conversation. They may stop in the middle of a conversation and have no idea how to continue or they may repeat themselves. They may struggle with vocabulary, have problems finding the right word or call things by the wrong name (e.g., calling a watch a "hand clock").	Sometimes having trouble finding the right word.
❖ **Misplacing things and losing the ability to retrace steps:** People with Alzheimer's may put things in unusual places, and lose things and be unable to go back over their steps to find them again. Sometimes, they accuse others of stealing. This may occur more frequently over time.	Misplacing things from time to time and retracing steps to find them.

Table 2. 2 Signs of Alzheimer's compared with typical age-related changes (continued)

❖ **Decreased or poor judgment:** People with Alzheimer's may experience changes in judgment or decision-making. For example, they may use poor judgment when dealing with money, giving large amounts to telemarketers. They may pay less attention to grooming or keeping themselves clean.	Making a bad decision once in a while.
❖ **Withdrawal from work or social activities:** People with Alzheimer's may start to remove themselves from hobbies, social activities, work projects or sports. They may have trouble keeping up with a favorite sports team or remembering how to complete a favorite hobby. They may also avoid being social because of the changes they have experienced.	Sometimes feeling weary of work, family and social obligations.
❖ **Changes in mood and personality:** The mood and personalities of people with Alzheimer's can change. They can become confused, suspicious, depressed, fearful or anxious. They may be easily upset at home, at work, with friends or in places where they are out of their comfort zones.	Developing very specific ways of doing things and becoming irritable when a routine is disrupted.

2.5 Causes of Alzheimer's Disease

Till now, scientists could not predict what the actual causes (exact etiology) behind Alzheimer's disease are; however, the disease exhibit some associations with a combination of factors related to genetics, environment, and lifestyle[5]. There are multiple conflicting theories attempting to understand the disease causes:

- Genetic Hypothesis
- Cholinergic Hypothesis
- Amyloid Cascade Hypothesis
- The Tau Hypothesis
- Inflammatory Hypothesis
- Other Hypothesis

2.5.1 Genetic Hypothesis

Alzheimer's disease (including memory components) has a genetic heritability of between 49 and 79%, according to twin and family studies. Around 0.1 percent of cases are familial autosomal dominant inheritance variations (not sex-related) that manifest before the age of 65. Knowledge epistemic relationships may be critical for improving our understanding of complicated illnesses such as Alzheimer's disease, diabetes, and cardiovascular disease., and cancer. Numerous scientists discovered in the early 1990s that a gene called apolipoprotein E4 was linked with an increased chance of developing Alzheimer's disease. However, scientists observed that possessing one or 2 copies of apolipoprotein E4 significantly enhances one's chance of developing Alzheimer's disease. Not all carriers of apolipoprotein E4 acquire this illness, suggesting that other genes or gene-gene interactions were involved in the disease's genesis. Alzheimer's disease is classified into 2 types: early-onset and late-onset. Both kinds include genetic material.

Early-onset Alzheimer's disease occurs in individuals between the ages of 30 and 60. While some instances of early-onset Alzheimer's disease are unknown, the majority are inherited, a condition known as Familial Alzheimer's Disease (FAD). The majority of autosomal dominant FADs are caused via mutations in one of three genes: the amyloid precursor protein (APP) or the presenilins PSEN1 and PSEN2[4, 35, 36]. Multiple single-gene mutations on chromosomes 1, 14, and 21 cause FAD. All of these mutations result in the formation of aberrant proteins (see Table 2.2). A kid whose parents have the FAD gene mutation has a 50/50 chance of acquiring it, and the child will almost certainly acquire FAD [22].

Late-onset Alzheimer's disease the majority of cases are of late onset, occurring beyond the age of 60. The reasons of late-onset Alzheimer's disease remain unknown. They very certainly involve a mix of genetic, environmental, and behavioral variables that contribute to an individual's chance of getting the illness [22].

Table 2. 3 Genetic factors associated with Alzheimer's disease

Chromosome	Defective gene	Onset	Putative mechanisms
1	PSEN-2	Early	Altered Aβ metabolism
14	PSEN-1	Early	Increased production of Aβ
19	APOE 4	Late	Tau hyperphosphorylation Impaired production/ polymerization/ clearance of Aβ
21	APP	Early	Increased production of Aβ

Note: APP: amyloid precursor protein; **Aβ:** beta amyloid protein; **APOE:** apolipoprotein; **PSEN:** presenilins.

2.5.2 Cholinergic Hypothesis

The oldest hypothesis proposes that AD is generally characterized via a deficiency in the amount of neurotransmitter acetylcholine (ACh) in the brain; therefore, cholinesterase inhibitors (ChE) are the 1st-line pharmacological agents used to treat this disease. The damage of the cholinergic neurotransmitter produces Ach, which is relevant to memory disorders in AD patients. Several of the cognitive habits were correlated with ACh existing in the brain cortex (see Figure 2.5)[37, 38]. After signaling, acetylcholine is released from receptors and broken down by acetylcholinesterase to be recycled in a continuous process.

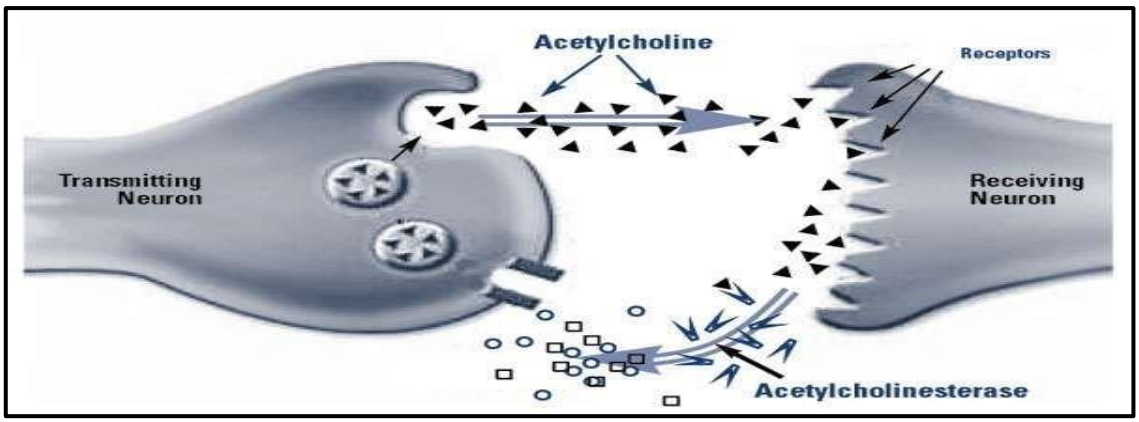

Figure 2. 5 Principle of cholinergic hypothesis

2.5.3 Amyloid Cascade Hypothesis

In 1991, the amyloid hypothesis proposed that plaques consisting of a peptide called beta-amyloid (Aβ) are primary brain characteristics with AD [39](Figure 2.6). Neurological changes due to sedimentation of abnormal, stable, and insoluble protein in the brain associated with Alzheimer's disease force healthy neurons to cease functioning, lose connections, and die in association with other neurons (Figure 2.7). Numerous additional complicated brain alterations are also believed to have a role in Alzheimer's[40, 41].

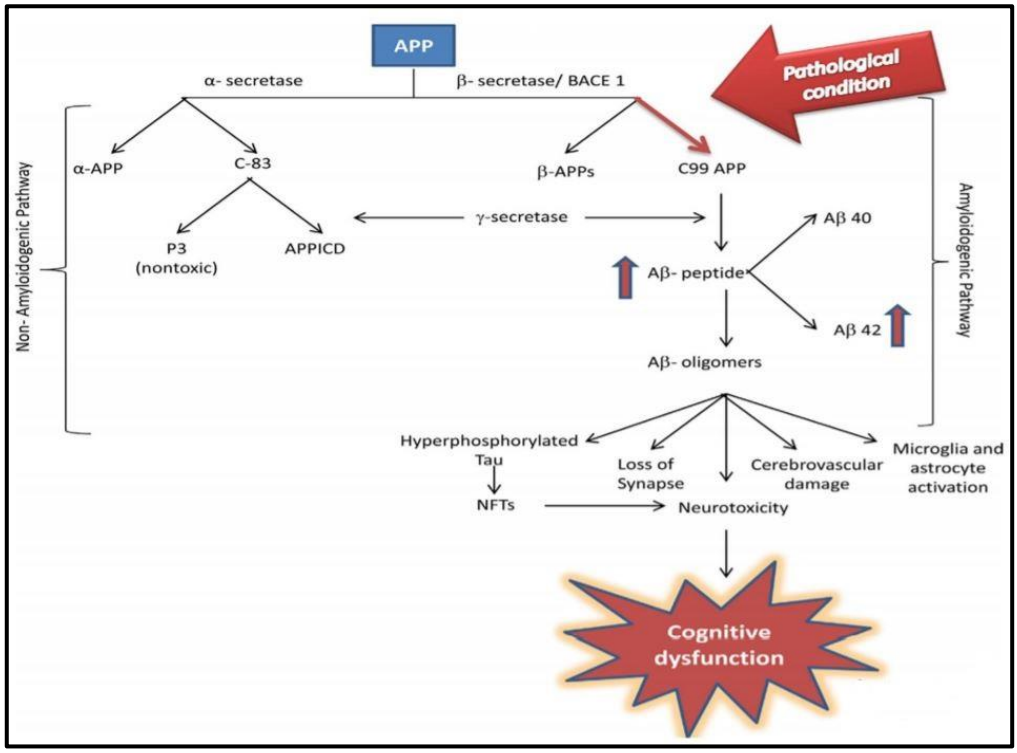

Figure 2. 6 Beta-amyloid aggregation as the cause of AD

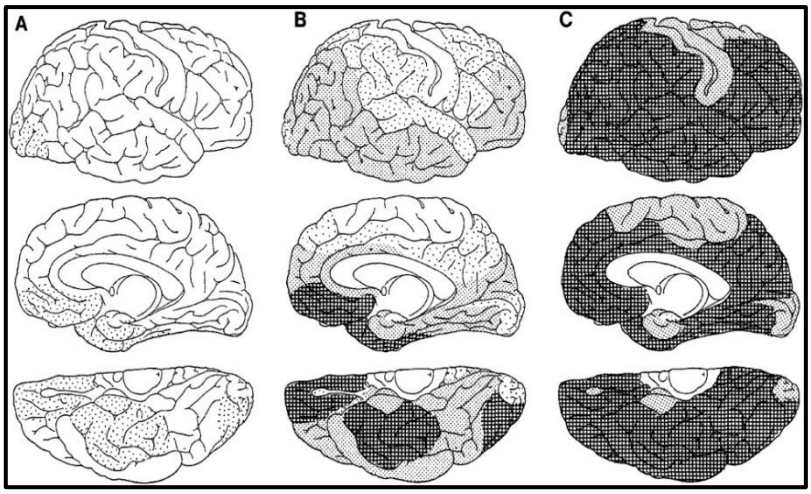

Figure 2. 7 Distribution pattern of amyloid deposits

Stage A: Initial deposits can be found in basal portions of the isocortex; **Stage B:** The next stage shows amyloid in virtually all isocortical association areas. **Stage C:** In the end-stage deposits can be seen in all areas of the isocortex including sensory and motor core fields. Increasing density of shading indicates increasing numbers of amyloid deposits[42].

2.5.4 The Tau Hypothesis

In Alzheimer's, tau protein abnormalities, according to the tau hypothesis, start the disease cascade [43]. Hyperphosphorylated tau has 7-10 moles of phosphate per mole of protein, whereas normal tau has 3 moles of phosphate per mole of protein. Hyperphosphorylated τ can cause to detach from microtubules, resulting in the development of soluble tau aggregates and insoluble paired helical filaments, which eventually form neurofibrillary tangles within nerve cell bodies. When this happens, the microtubules disintegrate, weakening the cytoskeleton's structure and causing the neuron's transport mechanism to fail. This could lead to problems with biochemical communication between neurons and, eventually, cell death. The aim of anti-phosphorylated strategies (kinase inhibitors) is to stop these processes from happening. Aggregation inhibitors may be able to prevent the formation of soluble tau aggregates and tangles (see Figures 2.8 and 2.9)[44].

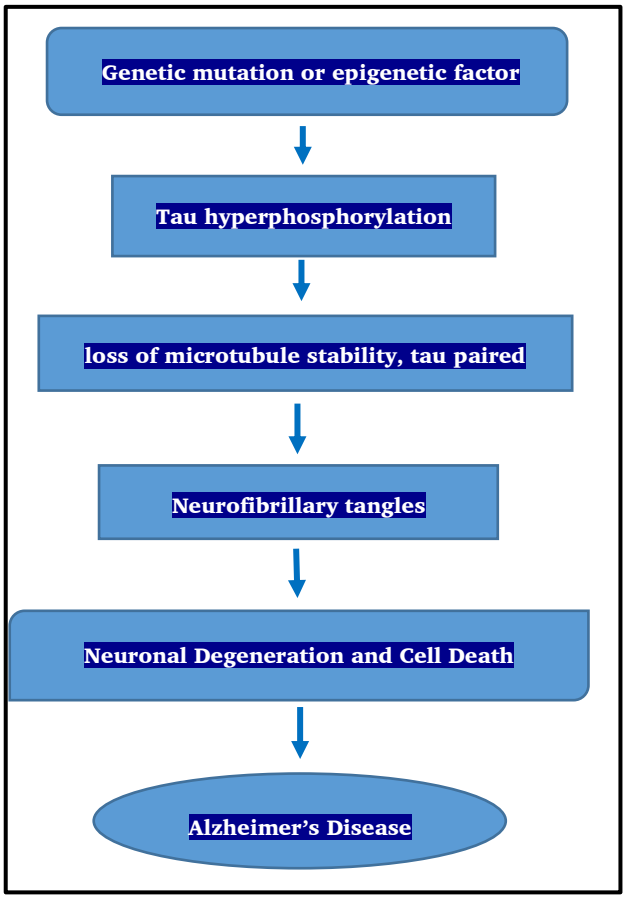

Figure 2. 8 Schematic of the tau hypothesis as the cause of AD

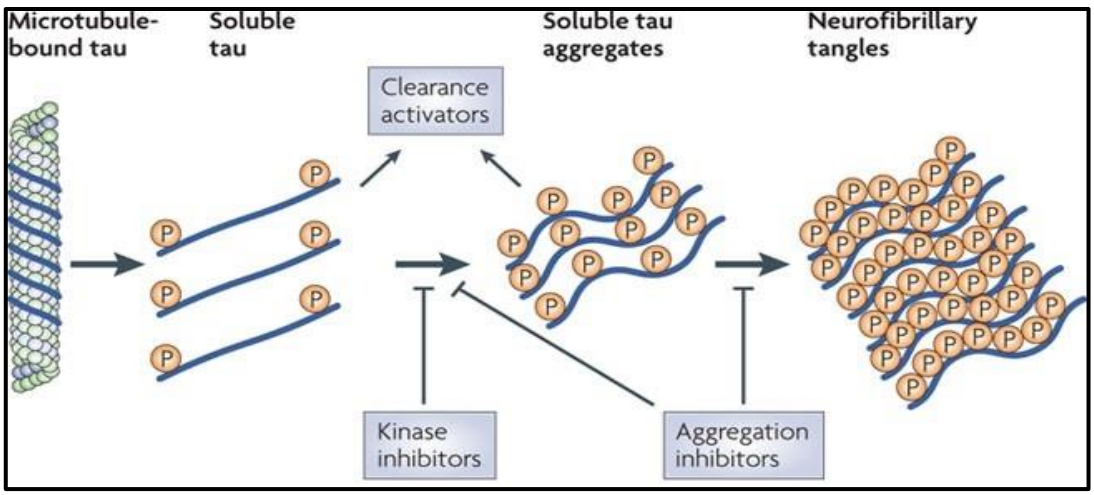

Figure 2. 9 Alzheimer's disease (AD) hyperphosphorylated tau protein in the brain forms neurofibrillary tangles

2.5.5 The Inflammatory Hypothesis of Alzheimer's

Inflammatory stimuli (beta-amyloid, neurofibrillary tangles (NFTs), and neuron fragments) stimulate glial cells, resulting in the production of pro-inflammatory mediators and inflammatory response proteins. These products may activate glial cells, which in turn promotes the synthesis of P-tau, A42, and other pro-inflammatory cytokines, thus perpetuating the cycle. The cycle increases neurodegeneration and other diseases associated with Alzheimer's disease. persistent inflammation as a result of oxidative stress [45]. Oxidative stress is likely to develop in the brain, since the brain consumes up to 20% of the body's inspired oxygen. Additionally, the brain contains high quantities of polyunsaturated fatty acids, which are susceptible to lipid peroxidation. Amorphous proteins such as beta-amyloid and tau proteins function as free radicals, causing further damage (see Figure 2.10)[46, 47].

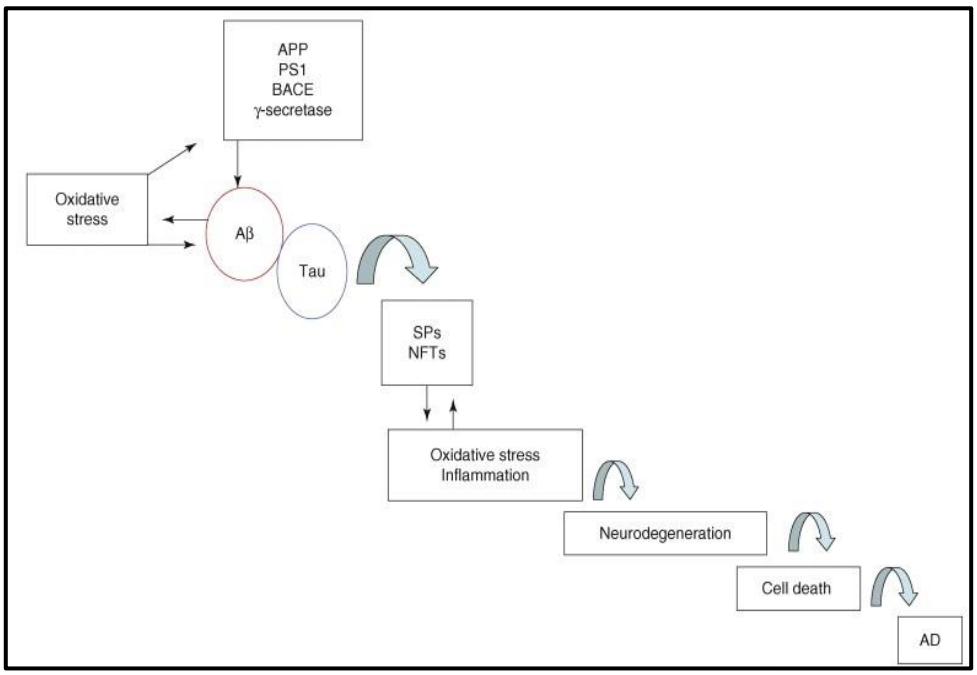

Figure 2. 10 Inflammatory hypothesis of AD

2.5.6 Other Hypothesis

With the exception of 1-2 percent of instances in which deterministic genetic variants have been identified, the etiology of the majority of Alzheimer's illnesses remains unclear [36]. There are several conflicting theories attempting to explain the disease's cause:

- **A neurovascular theory** It has been hypothesized that a dysfunctional blood–brain barrier may be involved [46].
- **Smoking** is a significant risk factor for Alzheimer's disease[48].
- **Innate immune system markers** are associated with an increased chance of developing late-onset Alzheimer's disease [49].
- **Glucose hypometabolism** is the prodromal stage of AD's early pathogenic case and is associated with cognitive and functional deterioration. Early therapeutic intervention before to irreversible deterioration has become a condition of consent in the treatment of Alzheimer's disease. As a result, alleviating glucose hypometabolism became an appealing approach for treating AD [50, 51].
- There is some indirect evidence that **air pollution** can play a role in developing Alzheimer's disease [52, 53].
- In 2019, a report found no increase in dementia overall in people with **celiac disease**, but 2018 research discovered a link to a variety of types of dementia, including Alzheimer's disease [54, 55].
- **Mutation by Osaka:** Since 2008, when the Osaka mutation was originally discovered, it has been related to Alzheimer's disease [56]. A deletion mutation at codon 693 of the amyloid precursor protein (APP) was associated with familial Alzheimer's disease in a Japanese pedigree. Only homozygous bearers of this mutation are affected via AD[57]. This mutation accelerates Å oligomerization, but does not result in the formation of amyloid fibrils, suggesting that Å oligomerization, rather than fibrils, may be the source of disease [58].

2.6 Clinical Criteria for Alzheimer': Labeling and Imaging

The clinical examination of AD is presented in a sequential fashion:

- The 1st stage involves obtaining the patient's history and pertinent information about prior illnesses from an informant.
- The 2nd stage includes a mental state examination and a confirmatory cognitive function test.
- The 3rd and most critical stage is a physical examination, which should emphasize vascular and neurological symptoms and should be accompanied via investigation [59].

Dementia assessment is a two-steps procedure. To begin, it is critical to distinguish dementia syndromes from other diseases that mimic them: depression, delirium, and moderate cognitive impairment. 2nd, once the dementia syndrome is recognized, the identification of the dementia subtype is critical because it aids in the selection of potential treatments for the illness. A timely and correct identification of AD is critical for the advancement of dementia research. Numerous diagnostic procedures must be undertaken in order to diagnose AD:

- A complete medical history.
- Mental status examinations.
- A comprehensive physical and neurological examination, as well as CT (computed tomography) and MRI (magnetic resonance imaging) may all be used to diagnose AD.
- Blood tests and MRI images of the brain [60].

A biomarker is a biological component that may be used to determine the presence or absence of a disease, a person's likelihood of contracting an illness, or the development of a disease. It is essential to identify reliable biomarkers for pre-symptomatic Alzheimer's disease in order to determine the exact etiology of the disease. Several Alzheimer's disease-related biomarkers, including the levels of beta-amyloid and abnormal tau in the brain as determined via positron emission tomography (PET) imaging, the levels of specific proteins in fluid (for example,

beta-amyloid and tau levels in cerebrospinal fluid and specific protein groups in the blood), and the level of glucose metabolism in the brain are all being investigated.. A novel blood test has been developed that may correctly predict whether an otherwise healthy person will develop MCI or AD three years before cognitive impairment begins[61]. The test is based on the identification of 10 lipid biomarkers in the blood that are predictive of both diseases.

Changes in the breakdown of brain cell membranes result in the circulation of 10 distinct lipids, or metabolites. Two of the ten metabolites in particular show significant associations with the neuropathology of AD, suggesting the possibility of developing early treatment options for AD, when medication may be more successful at delaying or even avoiding disease onset. Ten proteins have been identified in the blood that may signal the beginning of Alzheimer's disease. A simple blood test may be able to predict whether a patient may develop AD even before symptoms manifest. The test was reported to be capable of predicting AD with an accuracy of 87 percent. It was discovered that 26 proteins are associated with Alzheimer's disease, 10 of which may be used to predict the illness. If those protein levels were examined, it could be predicted correctly in almost 9 out of 10 cases[62] whether a patient will acquire AD (see Figure 2.11). For patients, doctors, and scientists, developing a reliable and accurate test, such as a blood test, to identify AD would be ideal. A study is being conducted to create such a test.

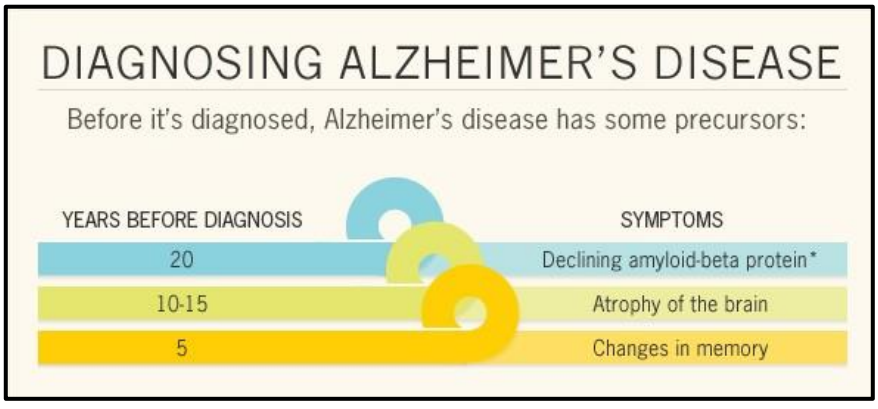

Figure 2. 11 Diagnosing of Alzheimer's disease

2.7 Changes in the Brain

The brain shrinks somewhat with healthy aging but, surprisingly, does not lose a substantial number of neurons. Alzheimer's disease impairs neuronal connections, metabolism, and repair processes. Numerous neurons cease to function and lose contact with neighboring neurons, resulting in extensive damage [63]. The loss of mass has a profound effect on almost all of the brain's functions:

- The brain shrinks, impairing cognition, planning, and memory.
- The shrinkage of the hippocampus has an effect on the development of new memories.
- Ventricles have grown in size when they are filled with cerebrospinal fluid. Alzheimer's disease progressively erodes a person's capacity to live and function independently.

At the end of the day, the illness is fatal over time, a person with Alzheimer's gradually loses his or her ability to live and function independently[64] (see Figure 2.12).

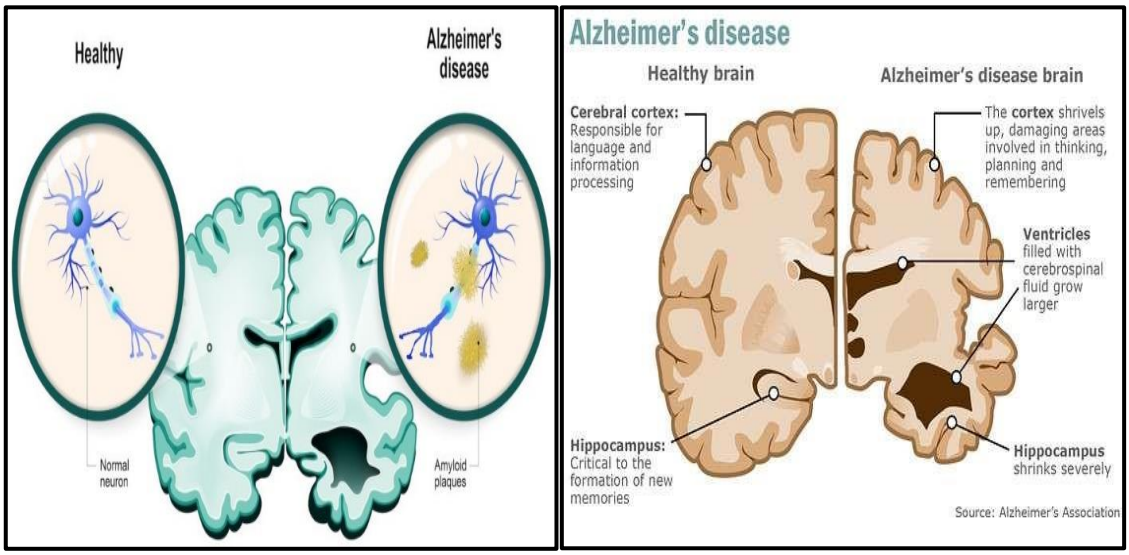

Figure 2. 12 Comparison of Alzheimer's affected brain and normal brain

2.8 Pathophysiology of Alzheimer's Disease

Various histological and molecular alterations characterize AD. The pathophysiology of AD has been largely hypothesized based on evidence produced via (immune) chemical analysis of the disease's most prominent brain hallmarks (amyloid plaques and neurofibrillary tangles). AD is usually regarded as a disease characterized via progressive neuronal loss, and synapses occur in various anatomical locations, resulting in distinct phenotypes [65]. AD may be classified into 2 subtypes: those with an early start and those with a late onset. Early-onset AD, also known as familial AD (FAD), affects people under the age of 65 and accounts for only 3–10% of overall AD cases. This kind of AD is caused via mutations in amyloid precursor protein (APP), presenilins 1 (PSEN1), and presenilins 2 (PSEN2) (PSEN2). Although late-onset AD is considered sporadic (SAD), genetic risk factors, notably the apolipoprotein E gene (APOE), have been identified [66, 67]. Regardless of the form of AD, this illness is associated with distinct pathologies, including extracellular plaques composed of insoluble amyloid beta peptides (A) and neurofibrillary tangles (NFTs). Recently, AD has been linked to mitochondrial dysfunction, decreased energy metabolism, synaptic loss, altered Wnt signaling, and inflammation [68]. The pathophysiology of AD is summarized in (Figure 2.13).

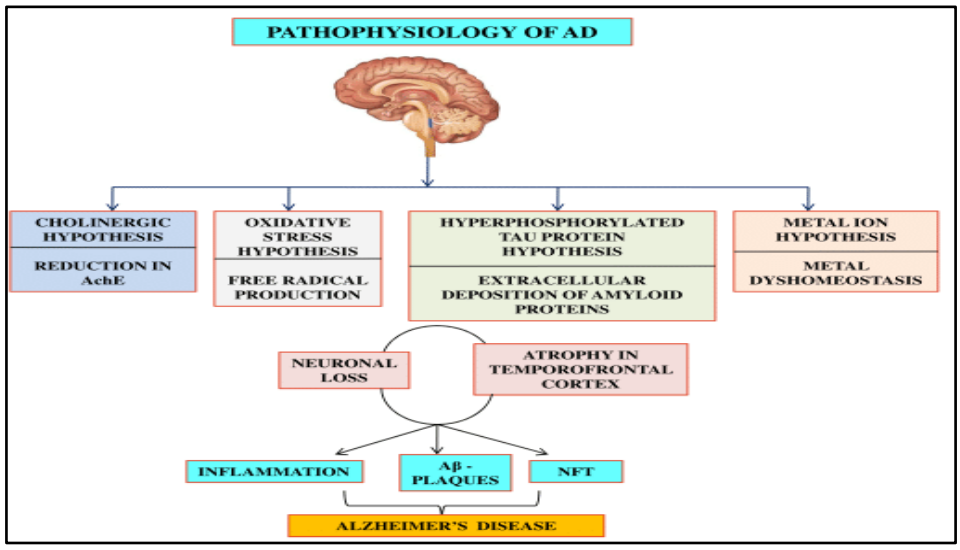

Figure 2. 13 Hypothesis for pathophysiology of Alzheimer's disease

2.8.1 Neuropathology of Alzheimer’s Disease

The loss of neurons is a key pathogenic feature of Alzheimer's disease's neuropathology. Because Alzheimer's disease is classified as a neurodegenerative disease, its clinical manifestations are associated with neuronal loss and atrophy in the temporal and frontal cortex, resulting in an increase in the appearance of monocytes and macrophages in the cerebral cortex, as well as activation of microglial cells in the parenchyma [69](Figure 2.14).

A variety of variables may play a role in the neuronal degeneration that occurs in Alzheimer's disease. For example, investigations have shown that A is linked with the development of Alzheimer's disease (AD) as a result of its cytotoxicity. Additionally, mitochondrial dysfunction and oxidative stress have been shown to substantially contribute to neuronal death. Neuronal death, regardless of the source, is a key characteristic of Alzheimer's disease [70, 71].

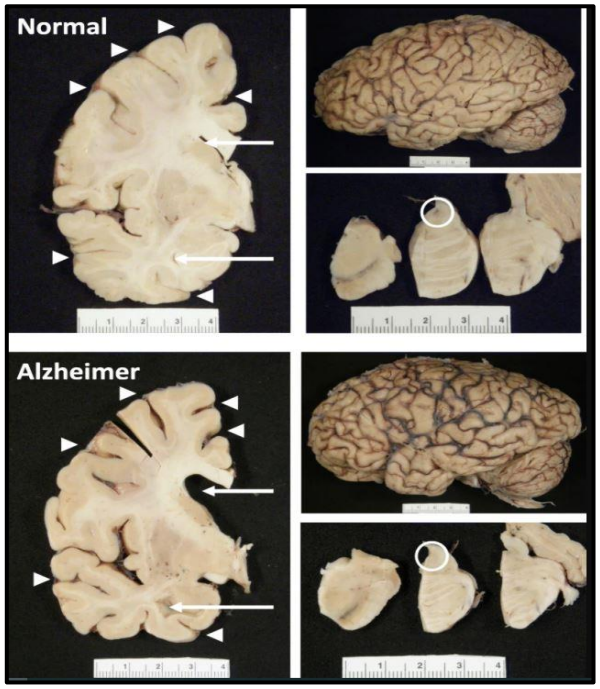

Figure 2. 14 The neuropathological diagnosis of Alzheimer’s disease

2.8.2 Biochemistry of Alzheimer's Disease

2.8.2.1 Amyloid Precursor Protein

The amyloid βprotein (Aβ) accumulation in plaques and the walls of cerebral blood vessels is the primary characteristic of AD pathogenesis. Numerous genetic and environmental variables may result in the deposition of Aβ. Aβ is a 39–43 amino acid peptide that was synthesized through proteolysis from a more important and essential precursor molecule known as the amyloid precursor protein (APP) (see Figure 2.15) [72].

APP is a type I transmembrane glycoprotein that has 695-770 amino acids and is found in a variety of cells. It is encoded via a gene on chromosome 21. Proteolytic processing of APP may occur in 2 ways: through a non-amyloidogenic route (normal state, which prevents the production of Aβ) or via an amyloidogenic pathway (diseased state). The physiological functions of APP are yet unknown. APP has been shown to regulate cell survival, growth, and motility, as well as neurite outgrowth and other activities associated with the release of soluble ectodomain following proper APP cleavage. It produces a variety of polypeptides through alternate splicing, glycosylation, phosphorylation, or complicated proteolysis. APP produces amyloidogenic fragments in a sick state through differential cleavage via enzymes [73].

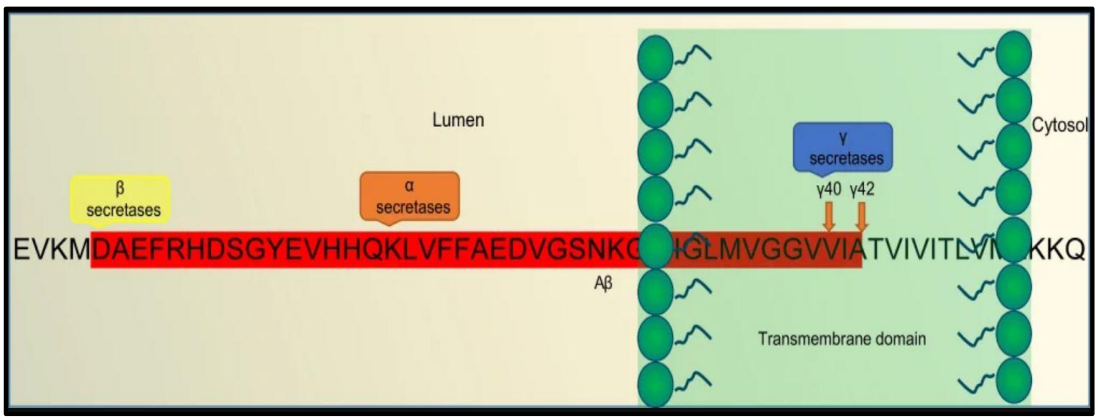

Figure 2. 15 An overview of the Aβ-pathogenesis hypothesis

Note: Amino-acid sequence of the Aβ fragment and location of action of α-, β-, and γ-secretases in diseased neurons within a diseased amyloid genic pathway.

The α-secretase cleaves APP between residues 16–17 of the Aβ domain and secretes wide soluble ectodomain nonpathogenic precursors APPs into the media near the cleavage site. Simultaneously, the C-terminal fragment C83 is maintained in the membrane and cleaved at residue 711 via -secretase, releasing P3 peptide. P3 peptide is soluble and plays a part in normal synaptic transmission, although its precise activities remain unknown [74]. The α processing of the -secretase results in the release of large soluble ectodomain APPsα, which serve as a neuroprotective factor and play a role in cell–substrate adhesion (see Figure 2.16).

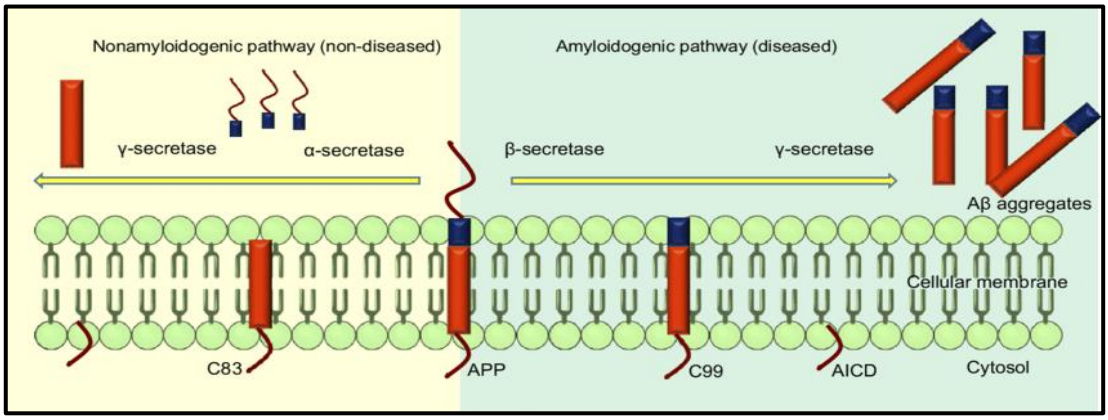

Figure 2. 16 Formation of βeta-amyloid plaque

Note: Cleavage of APP by α- and γ-secretases in normal state and alternative cleavage by β- and γ- secretases in diseased state. The Aβ fragment is crucial in the formation of amyloid plaques in AD.

APPs are required for biological synaptic signaling and plasticity, as well as for learning, memory, emotional activity, and neuronal survival. Additionally, sequential processing liberates the APP intracellular domain, which translocates into nuclei and promotes nuclear signaling, as well as gene expression and control.

In a sick condition, APP is cleaved differentially; -βsecretase conducts irregular cleavage, releasing shortened APPsβ, while the C-terminal fragment C99 stays in the membrane and is subsequently cleaved via -secretase, resulting in the release of insoluble Aβ peptides. The intracellular domain of APP is released into the cytoplasm upon cleavage of both C83 and C99 via soluble -secretase and translocates to nuclei for subsequent gene expression operation [75, 76]. The 1st and most important step is the cleavage of β-secretase, which cuts the N-terminus

of Aβ. It removes the bulk of the extracellular component of the protein, leaving just the

C-terminus of APP, which is subsequently cleaved at the C-terminus of Aβ, leading in the production of Aβ oligomers, which eventually polymerize to form aggregated plaques (see Figure 2.17)[77].

$A\beta_{40}$ and $A\beta_{42}$ are the 2 major Aβ polymer types that have a substantial effect on plaque development and neurotoxicity. $A\beta_{40}$ is more plentiful and less neurotoxic than $A\beta_{42}$, which is less abundant, extremely insoluble, neurotoxic, and resistant to accumulation, and functions as a hazardous building component of Aβ assembly. Aggregation of $A\beta_{40}$/$A\beta_{42}$ results in blocked ion channels, disrupted calcium homeostasis, increased mitochondrial oxidative stress, and decreased energy metabolism and glucose regulation, all of which contribute to the degeneration of neuronal health and ultimately, neuronal cell death[78].

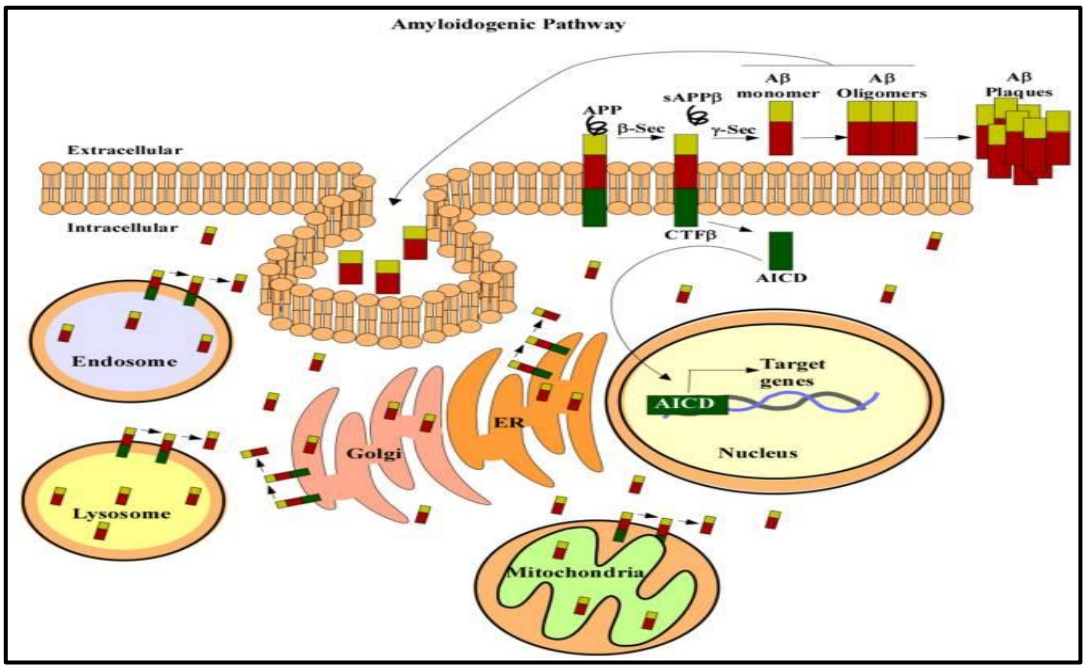

Figure 2. 17 Amyloid precursor protein (APP) processing

Abbreviations: amyloid precursor protein **(APP)**, secreted APP derivative **(sAPPβ)**, amyloid beta **(Aβ)**, β-Secretase-Derived C-Terminal Fragment **(CTFβ)**, APP intracellular domain **(AICD)**, β-APP-site cleaving enzyme **(β-Sec)**, γ-Secretase **(γ-Sec)**, **ER** (endoplasmic reticulum).

Increased neuronal synthesis of Aβ, reduced activity of Aβ degrading enzymes, or alterations in the transport mechanisms that transport Aβ over the blood-brain barrier may all contribute to Aβ aggregating and accumulating in the brain. Amyloid fibrils obliterate and alter neural circuits, while Aβ oligomers impair synaptic function[79]. Aβ oligomer interacts with the membranes and receptors on the surface of cells, modifying signaling pathways, affecting neuronal activity, and triggering microglia to produce neurotoxic mediators (resident immune cells). Vascular abnormalities impede the delivery of nutrients and metabolic wastes, induce micro-infarcts, and increase astrocyte and microglia activation. The lipid-carrier protein apoE4 increases the amount of Aβ produced while reducing its clearance. Similar to intracellular Aβ, when apoE4 is produced in stressed neurons, it is cleaved into neurotoxic fragments that disrupt the cytoskeleton and impair mitochondrial function [80].

2.8.2.2 Hyperphosphorylation of Tau (τ) and Alzheimer's Disease

The AD area is dominated via studies focused on plaques. Numerous studies have focused on neurofibrillary tangles (NFTs). AD is defined via the presence of NFTs. Tau is usually unphosphorylated in differentiated cells and interacts with microtubule cytoskeleton components. This is in contrast to undifferentiated cells, which lack a persistent cytoskeleton composed of microtubules and tau and are phosphorylated tau. Tangles form as a consequence of hyperphosphorylation of the tau protein linked with microtubules[81]. Tau is mostly expressed in neurons and its unphosphorylated form is present exclusively in axons. Previous study on tau has shown that certain forms of phosphorylation may alter the protein's structure, impairing its capacity to polymerize tubulin [82](Figure 2.18). Tau, for instance, dissociates from microtubules as a result of phosphorylation at Thr231, Thr214, and Ser235 [83, 84]. Additionally, tau self-aggregation is induced via C-terminal phosphorylation. Phosphorylated tau may have a role in the development of NFTs. NFTs are a subset of protein filaments that are paired and helically coiled in the cytoplasm of neurons and their processes [85].

Tau is a microtubule-binding protein that interacts with tubulin to create matured and stable microtubules. It has the ability to stabilize microtubules and create

linking bridges between adjacent microtubules, thus forming a stable ne2rk and tethering them together. Due to the excess of Aβ in the environment, when the tau protein comes into touch with the released kinases, it becomes hyperphosphorylated.

It has been shown that soluble Aβ regulates the cleavage and phosphorylation of to produce NFTs. It is oligomerized as a result of its hyperphosphorylation[86]. As a consequence of the dissociation of tubule subunits, the tubule becomes unstable, converting into large pieces of filaments that cluster and include improperly configured, overly phosphorylated NFTs. These NFTs are straight, fibrillary, and extremely insoluble patches inside the neuronal cytoplasm that disrupt communication and signal processing between neurons, resulting in neuronal death (Figure 2.19). Additionally, tau gene mutations are linked with familial frontotemporal dementia, particularly when parkinsonism and tangle histology coexist[87]. Additionally, many kinases, notably Glycogen Synthase Kinase 3 (GSK3) and cyclin-dependent kinase 5 (CDK5) triggered via extracellular A, control the phosphorylation of τ [88].

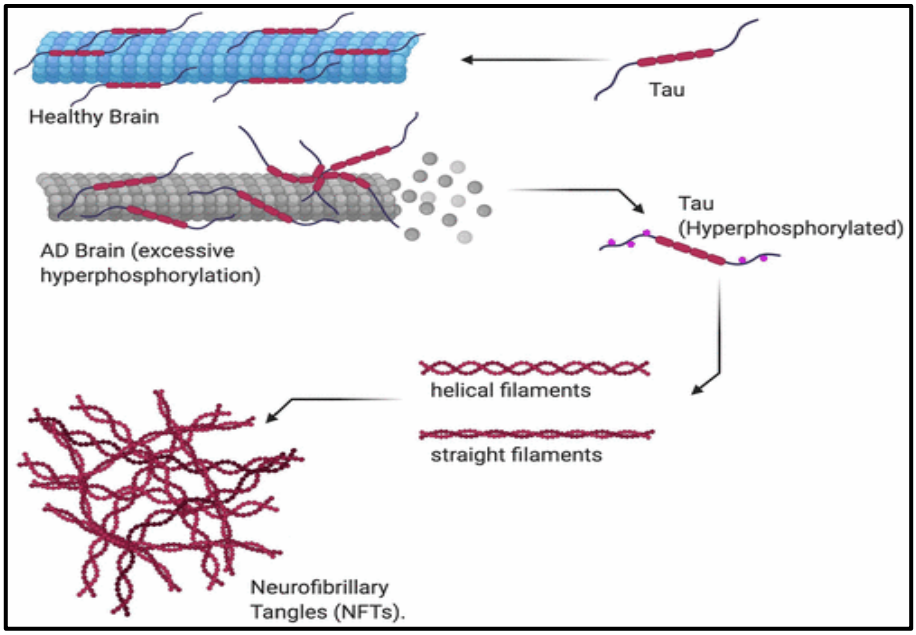

Figure 2. 18 Transmission of tau pathology in the brain of Alzheimer's disease (AD)[89]

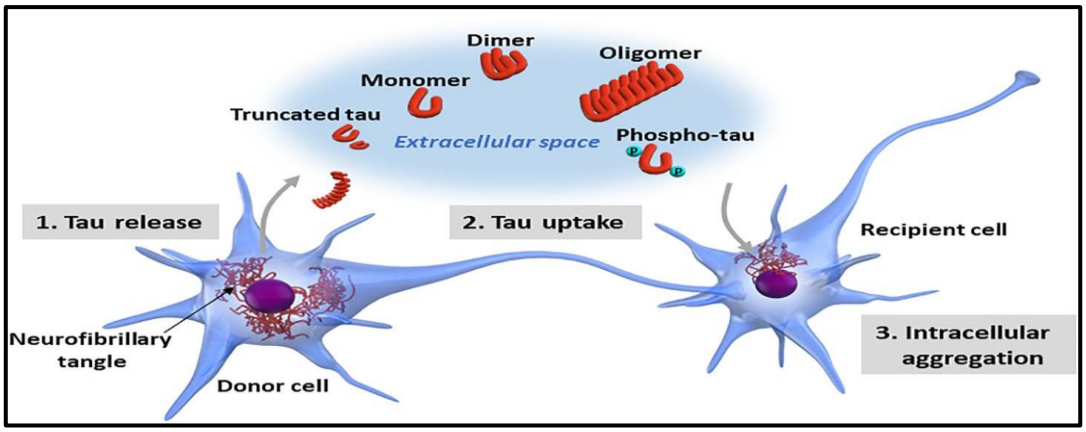

Figure 2. 19 Neuron-to-neuron transfer of tau

Note: The processes involved in tau propagation can be divided into three basic steps: (1) the pathological form of tau is released into the extracellular space from the donor cell; (2) the pathological tau released into the extracellular space is taken up by recipient cells; and (3) the pathological tau taken up into the recipient cells forms new intracellular aggregates.

2.8.2.3 Oxidative Stress and Alzheimer's disease

Oxidative stress is a condition produced via an imbalance between pro-oxidants and antioxidants, which results in an increase in reactive oxygen and nitrogen species (ROS and RNS)[90]. The electron transport chain (ETC) is composed of complexes I, II, III, IV, and V that catalyze the conversion of adenosine diphosphate (ADP) to adenosine triphosphate (ATP) [91]. The proton gradient from complexes I, III, and IV through complex V generates ATP. This decrease of O_2 sometimes results in the formation of a small number of superoxides. These superoxides are among of the most powerful oxidants known as reactive oxygen species (ROS) (Figure 2.20) [91, 92].

Mitochondria are the main source of potentially harmful free radicals, which are produced Through normal cellular respiration. Neurons are high-energy cells that rely on mitochondria to perform a variety of tasks, including action potential generation, neural transmission, and axonal transport. Mitochondria generate more than 90% of all ATP generated[93]. Numerous studies demonstrate that mitochondrial dysfunction is a critical factor in the development of AD (Figure 2.21). For example, cells treated with Aβ accumulate Aβ in the mitochondria, resulting in cell death. Additionally, research has shown that APP accumulates in

mitochondrial import channels, resulting in an increase in H_2O_2 [94]. Under typical circumstances, about 1–5% of oxygen is transformed to reactive oxygen species (ROS). The main causes of mitochondrial ROS are 2 factors: a high NADH/NAD ratio in the matrix and a substantially reduced coenzyme Q in the presence of a strong proton gradient and no ATP synthesis [95]. Significantly, although different enzymes may neutralize ROS, if the number of free radicals produced exceeds the capacity of neurons, oxidative stress, mitochondrial damage, and neuronal damage can result [96]. Additionally, protein oxidation and nitration are oxidative stress-induced changes. These modifications may have an effect on metabolic enzymes found inside the ETC [92]. These changes in enzymes may impair the function of neurons and result in neurodegeneration. The buildup of Aβ and NFTs is linked with oxidative damage in AD. Lipids are well-studied oxidative stress targets. Aβ has been found to promote lipid peroxidation in cells [97, 98]. Apart from lipid oxidation, AD has investigated protein oxidation. Proteins that have been oxidized may undergo conformational changes, resulting in the loss of structural and functional activity. Specifically, Aβ has been shown to enhance protein oxidation [99]. A proteomic study revealed that glyceraldehyde-3-phosphate dehydrogenase is oxidized in neurons treated with Aβ.

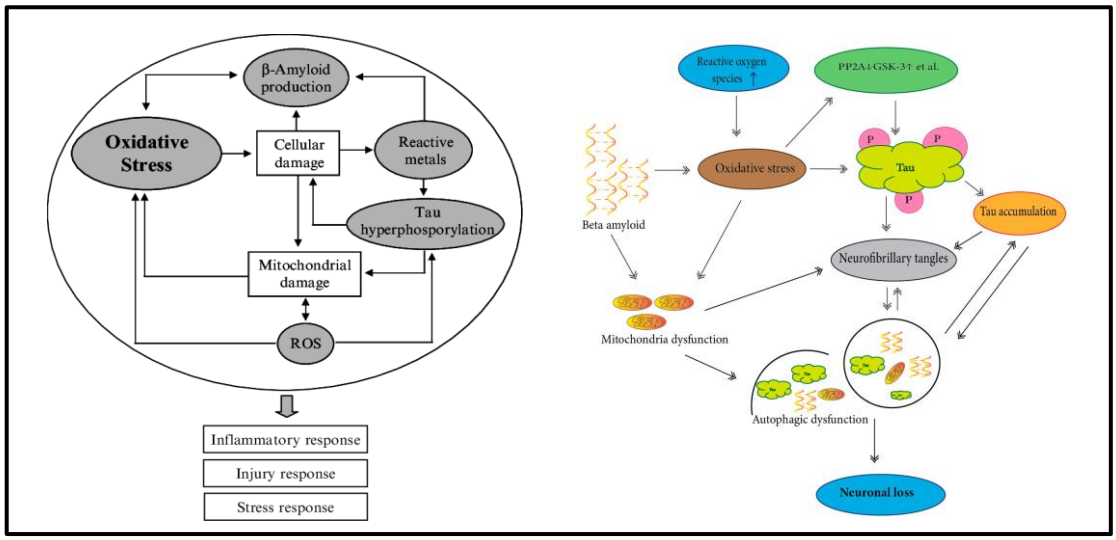

Figure 2. 20 Oxidative stress in Alzheimer's disease

Note: Oligomeric Aβ induced ROS production results in oxidative damage and mitochondrial dysfunction, in which hyperphosphorylated tau protein and NFTs produce through an imbalance of various protein kinases and phosphatases. The accruing of oxidative stress may, in turn, promote cellular dysfunction, injury, and inflammatory responses[100, 101].

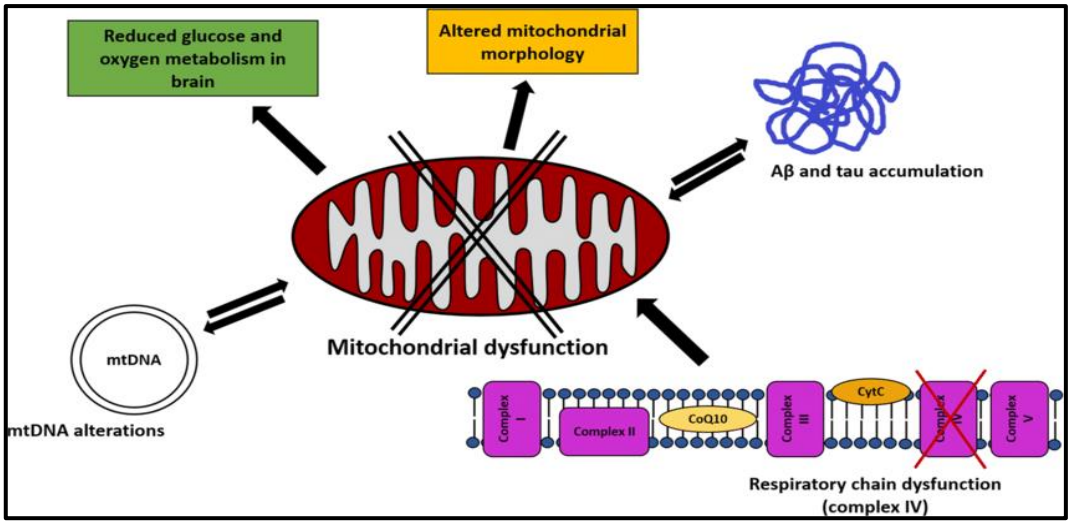

Figure 2. 21 Mitochondrial dysfunction in Alzheimer's disease

Note: The main mitochondria-related mechanisms proposed to be involved in the pathogenesis of AD. A defective mitochondrial functioning is supported by various findings, including altered mitochondrial morphology and reduced glucose and oxygen consumption in patients' brains. Impairment of respiratory chain activity, in particular complex IV, has been detected in the disease. Extracellular Aβ and intracellular tau protein accumulation, prominent neuropathological findings in AD, have been proposed to be bi-directionally linked to mitochondrial dysfunction. Mitochondrial DNA alterations have also been detected in the disease [102].

Oxidation of these proteins may result in many of the most well-known AD changes, including NFTs and glucose hypometabolism [103]. In the resting awake state, the brain uses about 25% of total body glucose [104]. Carbohydrates are a predominant substrate for oxidative metabolism in the brain. In the brain, carbohydrates constitute the primary substrate for oxidative metabolism. Glucose is often regarded as the brain's primary energy substrate [105] (Figure 2.22). Glucose transport and intracellular oxidative catabolism both contribute to the total glucose metabolism in the cerebral cortex. The blood-brain barrier (BBB) and glucose transporters are required for glucose transfer [106].

Alzheimer's disease is known to cause a decrease in the brain metabolic rate of glucose. Reduced glucose levels may lead to a decrease in mitochondrial ATP production. The decrease in glucose metabolic rate in the brain is also seen in pre-symptomatic patients who have autosomal dominant FAD mutations [107, 108].

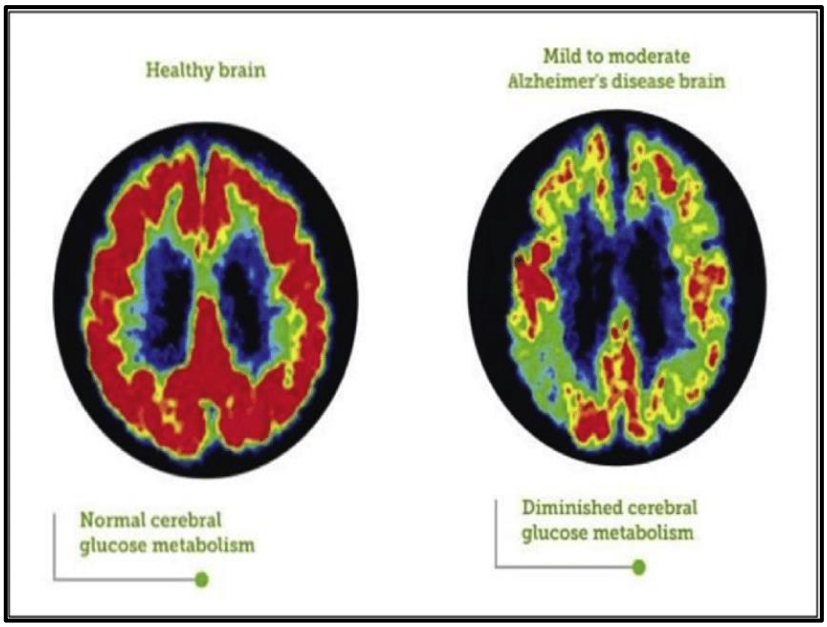

Figure 2. 22 Carbohydrate metabolism in the healthy brain (on the left) and a Alzheimer's brain (on the right)

The healthy brain on the left shows strong glucose availability and metabolism, while the impaired brain on the right reflects the characteristic hypometabolism state induced initiated in the peripheral tissues leading to excess insulin and declining glucose transport across the BBB [109].

2.8.2.4 Dysregulated Homeostasis of Metals and Heme with Alzheimer's Disease

Significant evidence indicates that (iron (Fe), copper (Cu), and zinc (Zn)) were involved in a dysregulated metal brain homeostasis and accelerated oxidative stress in both AD and PD [110]. The BBB maintains a strict control on the concentrations of Fe, Cu, and Zn. However, it has been shown that AD brains have elevated levels of these trace components. Recent meta-analyses of reported AD (compared to age-matched controls) revealed considerable disagreement over whether Fe and Cu are substantially elevated, although many studies highlighted metals' uncontrolled homeostasis in AD. Numerous studies demonstrate that particular A plaques include copper, iron, and zinc, and that individual intracellular metal levels in the brain may vary [111].

Additionally, Aβ may convert Fe(III) or Cu(II) to form H_2O_2, adding to the oxidative stress associated with AD [112] (Figure 2.23). Zinc does not, but has been linked to being a perfect aggregator of A plaques and an inducer of tau hyperphosphorylation. Zinc may also impede the iron-export ferroxidase activity of APP. Heme is another iron-containing molecule that has been linked to AD. Heme, also known as iron-protoporphyrin IX, is a necessary nutrient that plays a role in a variety of physiological and pathological processes [113]. According to Faux et al. [114] individuals with AD had significantly lower hemoglobin levels, mean cell hemoglobin concentrations, and packed cell volume than healthy controls. This study's participants demonstrated a significant correlation between anemia and AD, suggesting that hemoglobin production may be impaired in AD patients. Similarly, a research published in 2013 showed that anemia is linked with an increased risk of acquiring dementia among 2552 older people[115].

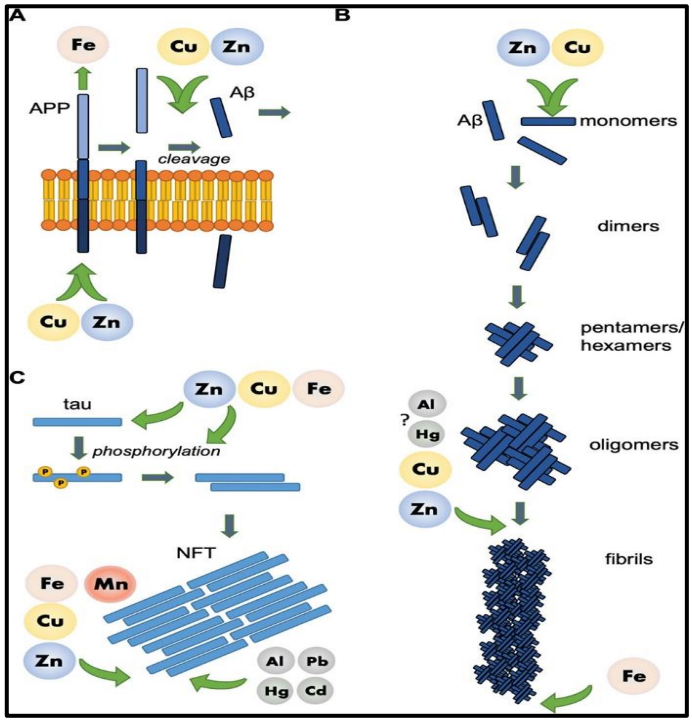

Figure 2. 23 Trace metals interactions with APP, Aβ, and tau

2.9 Pharmacologic and Nonpharmacologic Therapies for Alzheimer's Disease

There is currently no cure for AD, and medical treatment for the illness is in its infancy. The medications prescribed for the treatment of AD provide control over the disease's symptoms, but they do not slow or reverse the disease's development. Thus, complete AD treatment requires both nonpharmacologic and pharmacologic interventions [116](Figure 2.24).

Figure 2. 24 Pharmacologic and nonpharmacologic therapies for Alzheimer's disease [1]

In most cases, nonpharmacological interventions are used to address behavioral difficulties (such as task simplification, environmental modification, and minimal excess stimulation) and cognitive impairment (such as treating comorbid medical conditions, minimizing or eliminating the use of drugs with adverse mental side effects) [117]. Individuals suffering from Alzheimer's disease may benefit from nonpharmacological therapies that assist them enhance their quality of life (QOL). A large number of well-conducted randomized controlled studies have demonstrated that various nonpharmacological treatments for individuals with Alzheimer's disease, such as cognitive training, cognitive rehabilitation, and cognitive stimulation therapy, provide small but significant benefits in the treatment of cognitive symptoms[118]. Additionally, when taken with cholinesterase inhibitors, there may be additional advantages. For instance, many age-related sleep and wakefulness issues may be the result of a dampening of circadian rhythm amplitudes.

On the other hand, nonpharmacological modulation of circadian rhythms through a variety of external cues (such as physical exercise and music) significantly improves sleep and cognitive performance in older adults and Alzheimer's disease patients[119].

Pharmacologic treatments have mostly focused on modulating neurotransmitters that are associated with disease. When it comes to clinical trial outcomes, although both asymptomatic and neuroprotective pharmacologic therapies may have similar features, the most important difference is that neuroprotective medicine has a cumulative impact that lasts even after therapy has been discontinued [120]. As of right now, symptomatic therapy options include medications such as cholinesterase inhibitors (ChEIs) and N-Methyl-D-Aspartate (NMDA) receptor antagonists, which have been shown to reduce clinical development symptoms across cognitive, behavioral, and functional domains [120]. The initial pharmacological treatment for Alzheimer's disease was based on the "cholinergic hypothesis," which suggested that increasing cholinergic transition in the brain would be beneficial. Preventing acetylcholine breakdown via reducing acetylcholinesterase (AChE) activity has been proven to be the most effective strategy for increasing synaptic acetylcholine (ACh) levels among the many methods tested too far. Because of the presence of plaques and tangles in the brains of Alzheimer's patients, it may be possible to improve cholinergic transmission via inhibiting the enzyme butyrylcholinesterase (BuChE), which is present in minimal quantities in normal brains but increased in the brains of Alzheimer's patients. Current pharmacological treatments for Alzheimer's disease (AD) are effective in alleviating symptoms but do not change the illness's main clinical characteristics. As a consequence, it is essential to develop medicines that are both efficacious and innovative [121].

There are currently just four medications that are approved and available for the treatment of Alzheimer's disease-associated dementia, and their effectiveness is limited. Three of these medications, donepezil, galantamine, and rivastigmine, act on cholinergic pathways in the central nervous system (CNS) to produce their effects [122]. Each of the three medicines inhibits cholinesterase, while

galantamine, a natural product alkaloid, acts as an allosteric modulator of nicotinic acetylcholine receptors. These medications are currently available in generic forms and are authorized for the treatment of moderate to severe dementia, but they are often prescribed for patients in early pre-dementia stages who have substantial progressive memory deterioration on cognitive tests.

Memantine is the most recently authorized AD medication in the USA, and it is notable for being the 1st AD medication to specifically target the N-methyl-d-aspartate (NMDA) receptor and glutaminergic pathways. Both medications, memantine and donepezil, are authorized for monotherapy. They are impacted because to their authorized indications for treating AD symptoms. Both Memantine and donepezil have distinct and complementary modes of action, and when used in combination, they provide extra and beneficial effects to the patient. Clinical trial results in healthy volunteers established the possibility of safely combining memantine and donepezil. When memantine is used in conjunction with a steady ChEI treatment, it has a favorable safety profile in individuals with AD [121, 123].

3

CHOLINESTERASE ENZYMES

3.1 Esterase Enzymes

In biochemistry, a cholinesterase enzyme family is a form of esterase enzyme that lysis choline-based esters, some of which are neurotransmitters. Cholinesterases differ in terms of substrate selectivity and sensitivity to different inhibitor classes [26]. They were classified into 2 kinds as a result of these variances:

- Acetylcholinesterase (AChE, E.C. 3.1.1.7), also referred to as choline esterase I or erythrocyte cholinesterase, is more abundant in chemical synapses and red blood cell membranes. AChE catalyzes the hydrolysis of acetylcholine (ACh), and it is the most prevalent type of this enzyme [124](Figure 3.1).
- Butyrylcholinesterase (BuChE, E.C. 3.1.1.8), also known as choline esterase II or plasma cholinesterase, is the other form that is often present in blood plasma which can hydrolyze larger molecules, such as butyrylcholine [125](Figure 3.1).

Both cholinesterase enzymes belong to a large protein family containing the α/β hydrolase fold.

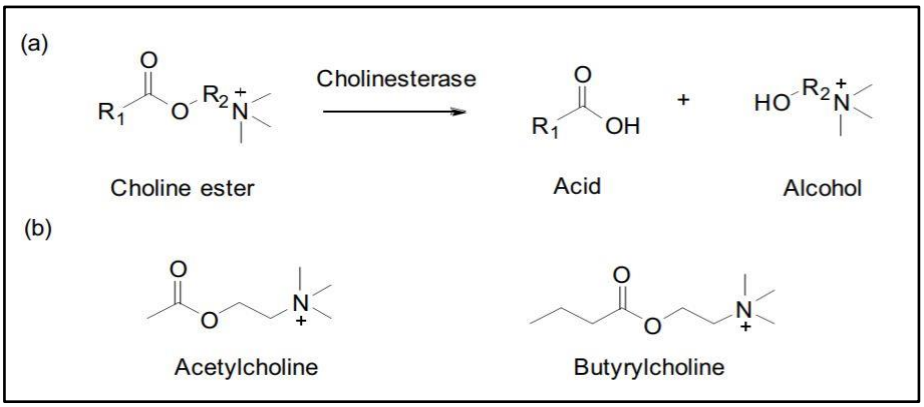

Figure 3. 1 Breakdown of different substrate by cholinesterase enzymes[126]

3.2 Acetylcholine (ACh) as Neurotransmitter

Acetylcholine (ACh) is a neurotransmitter that is extensively distributed throughout the central nervous system (CNS) and peripheral nervous system (PNS) of a variety of species, including humans [127]. It was the 1st identified neurotransmitter. It was discovered in 1914 via Henry Hallett Dale, and Otto Loewi subsequently confirmed its existence. The term acetylcholine derives from the structure of the compound. It is a chemical compound composed of choline and acetic acid. Acetylcholine is transmitted via cholinergic synapses [128]. ACh is a critical neurotransmitter that the brain and body need to function properly. As a result, changes in the release and action of this neurotransmitter may result in serious problems with memory and movement[129](Figure 3.2).

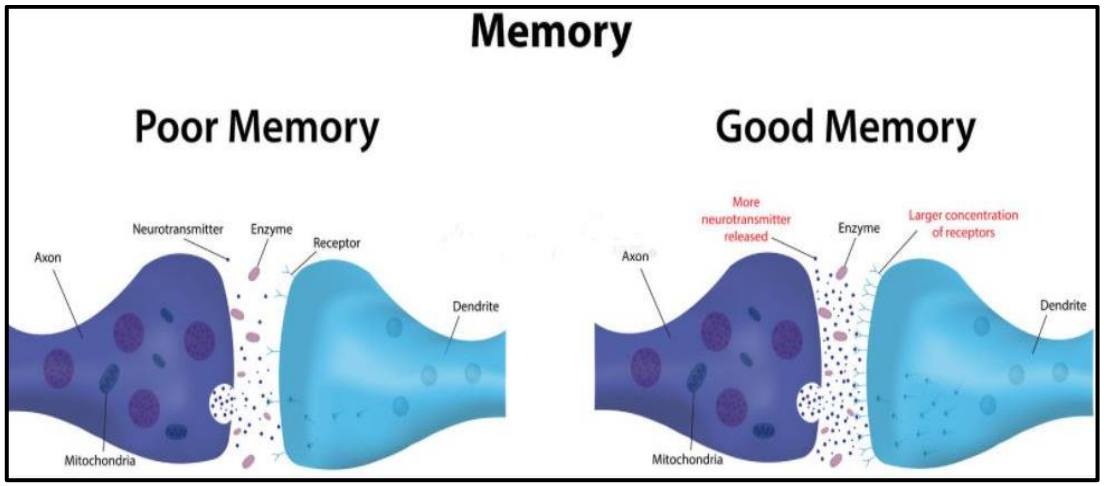

Figure 3. 2 Acetylcholine (ACh) is a neurotransmitter that helps nerve functions such as memory and muscle control

Ach is generated via neurons that contain the choline acetyltransferase enzyme (ChAT). This enzyme is responsible for converting Acetyl-CoA to choline via transferring an acetyl group. Acetyl CoA is synthesized from pyruvate produced through glycolysis, while choline enters the terminals through a Na^{+}dependent transporter. This enzyme has 2 binding sites: one for the choline molecule is located inside the enzyme, while the other for the Acetyl-CoA molecule is located on the surface (Figure 3.3).

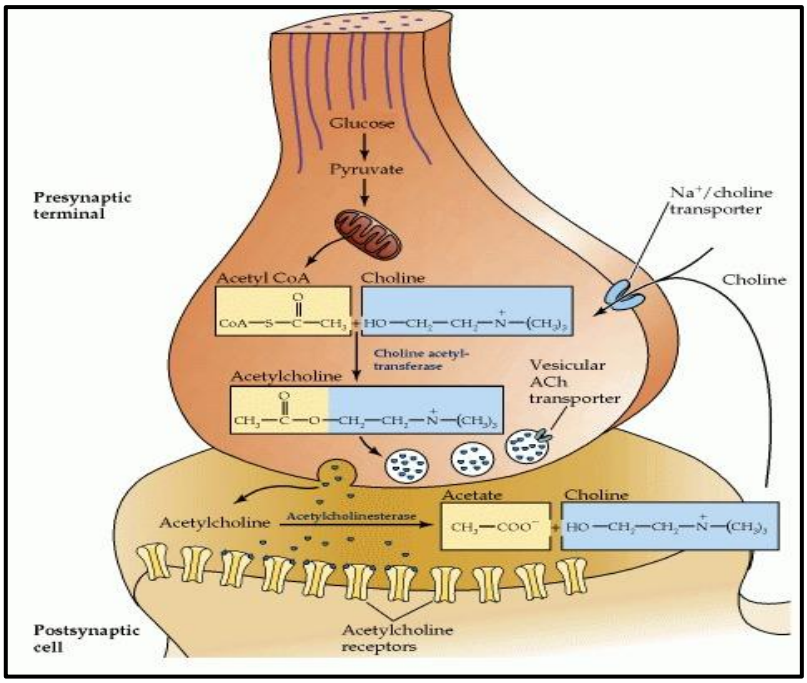

Figure 3. 3 Synthesis and breakdown of acetylcholine by cholinesterase[130]

When ACh is released at a neuromuscular junction, a cholinergic neuron has been activated and causes a muscle contraction. After a cholinergic neuron has been activated, these reactions are required to enable it to return to its resting state. Therefore, in order for the muscle to relax afterward rather than remain stressed, the acetylcholine must be broken down via a choline esterase. AChE enzyme catalyzes the hydrolysis of these ACh and breaking into choline and acetic acid (weak organic acid).

The membrane protein choline transporter then transports the breakdown product choline back into the presynaptic terminal [131, 132](Figure 3.3). It was not until years later those further studies were performed to discern the function of acetylcholine in the body entirely and precisely how it is recycled. Through this time, acetylcholinesterase was discovered, and their role in the function of ACh was more elucidated. More extensive work has been completed in more recent years to look at the medical implications of acetylcholinesterase and, more importantly, how inhibitors of it could be used as a symptomatic treatment in some diseases and significantly have an essential function in the treatment of AD[133].

3.3 Acetylcholinesterase (AChE)

Acetylcholinesterase (AChE, EC 3.1.1.7) is an essential enzyme involved in the cholinergic nervous system, including the PNS and the CNS [134]. Serum cholinesterase has a half-life of about eight days, while erythrocytes have a half-life of between 2 and three months. AChE is a serine hydrolase with an ellipsoidal structure. AChE is the primary enzyme responsible for the metabolization of acetylcholine. The enzyme is present on both nerve terminals and the post-junction or post-synaptic membrane at cholinergic synapses or junctions, according to electron microscope investigations using histochemical techniques. This enzyme, also known as substantial cholinesterase, hydrolyzes ACh the quickest of all the choline esters. Additionally, it may hydrolyze methacholine but not benzoylcholine[134]. J. Sussman 1st characterized the structure of AChE in 1991, after successfully crystallizing it from the electric ray device Torpedo californica (TcAChE) [135]. AChE is a glycoprotein that may take on a variety of forms. Due to the chemical structural difference, certain types of AChE are hydrophobic, while others are hydrophilic. Generally, the hydrophilic species act inside the cell to degrade excessive intracellular ACh concentrations. However, the lipid-linked (hydrophobic) variants are the main agents of ACh inactivation, acting at the neuromuscular junction's synaptic cleft to break ACh. To guarantee rapid inactivation of ACh, hydrophobic species of AChE are buried inside the post-synaptic membrane and positioned strategically near to post-synaptic receptor molecules [136].

3.3.1 Acetylcholinesterase Functions

AChE is the primary enzyme responsible for acetylcholine metabolism and has an AChE has an extremely high catalytic activity; one molecule of AChE may degrade 25000 molecules of ACh per second [137](Figure 3.4). Additionally, it has been shown to be beneficial in modulating cerebral blood flow, β-amyloid aggregation, activation, and production of the APP protein, τ protein phosphorylation, and inflammatory processes. Additionally, it interacts with β-amyloid, forming permanent complexes and senile plaques[130].

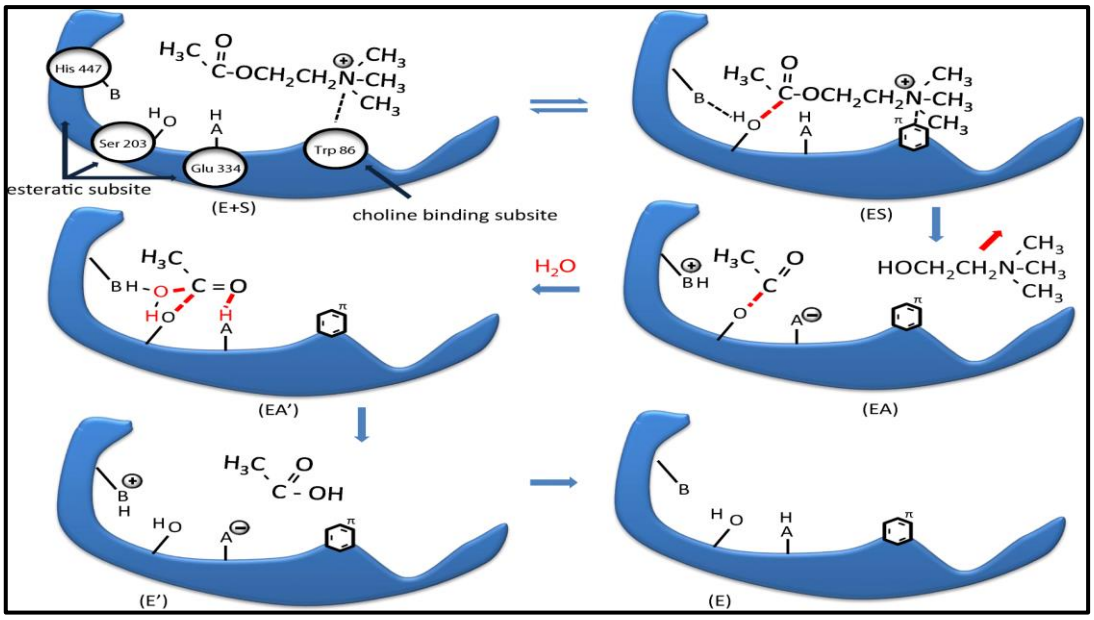

Figure 3. 4 Schematic diagram of the AChE active site canyon interaction, where acetylcholine hydrolysis catalyzed by the enzyme occurs[138]

3.3.2 Acetylcholinesterase Structure

A monomer of the enzyme is formed of 531 amino acids and contains 12 mixed β-sheets encircled via 14 α-helices [137](Figure3.5). The active site of AChE is a substantial hydrophobic cavity and consists of 2 subsites: i) the anionic substrate binding site (AS) and ii) The esteratic subsite (ES); both subsites are significant in the function of the enzyme[137]. The peripheral anionic site of AChE is liable for allosteric inhibition in the catalytic site via cationic ligand interactions. Changeux et al., in 1966 who suggested this area as a possible connection between agents such as propidium and leftovers along the gorge's brink. Additionally, this peripheral anionic area may contribute to the catalytic process via inhibiting substrates. The enzyme contains one somewhat remarkable feature, a deep and narrow gorge that is ~20Å long and ~5Å wide penetrating halfway into the enzyme called the catalytic triad (CT), consisting of Ser203, Glu334, and His447. The hydrolysis reaction takes place in the CT site of the enzyme. As a part of the CT, Ser203 is effective for the hydrolysis of choline esters via proton transfer [139].

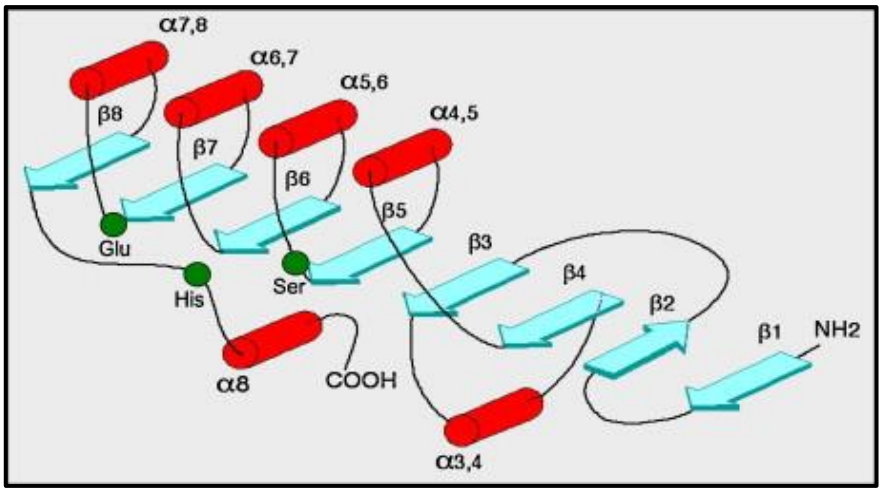

Figure 3. 5 Schematic diagram of the topological secondary structure of the α/β hydrolase folding

Note: The α-helices are shown as red cylinders, the β-strands as turquoise arrows, and the three residues making up the active site are shown as green circles (the labels of Ser, Glu and His correspond to the catalytic-triad residues found in the AChE active site).

There are 14 aromatic residues made up of phenylalanine (Phe), tyrosine (Tyr), or tryptophan (Trp), and several anionic residues near the bottom of the gorge that leads to the active site. These residues are critical in AChE operations since they are highly conserved across all species that rely on them[137](Figure 3.6).

The cation-π interaction is present between these aromatic amino acids and the positively charged of quaternary ammonium of Ach and the acceleration of binding of the cationic ligands. Trp86 is the essential aromatic amino acid for the AChE-ACh interaction is inhibited when alanine is substituted, resulting in a 3,000-fold reduction in reactivity. Apart from these locations, AChE has a (acyl pocket) that imparts substrate selectivity, as well as a (oxyanion hole) that interacts with negative oxygen ions Through catalysis, thus increasing AChE's catalytic effectiveness. There is an additional peripheral binding site within AChE which is distinct from the primary acetylcholine binding site. This additional site serves as a binding site for uncompetitive inhibitors separate from the site occupied via competitive inhibitors. Therefore, this is the additional binding site thoroughly studied via pharmaceutical companies developing AChE inhibitors to treat several diseases[140](Figure 3.7) and (Figure 3.8).

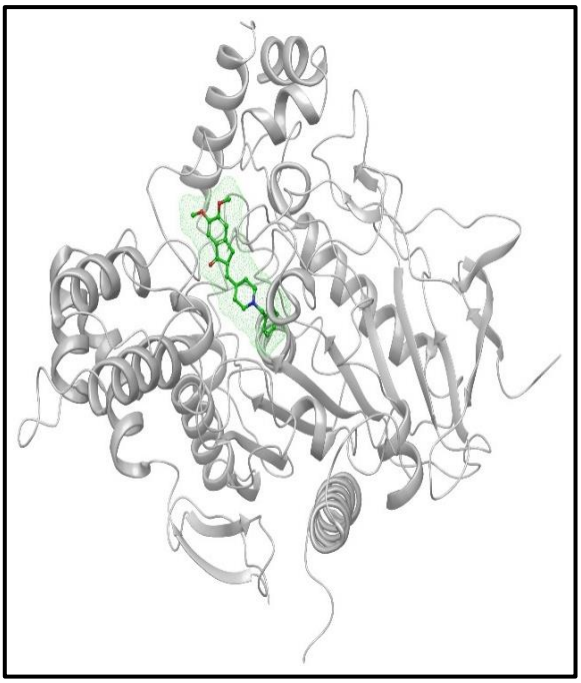

Figure 3. 6 The 3D structure of AChE (PDB:4EY7) is displayed as a ribbon diagram

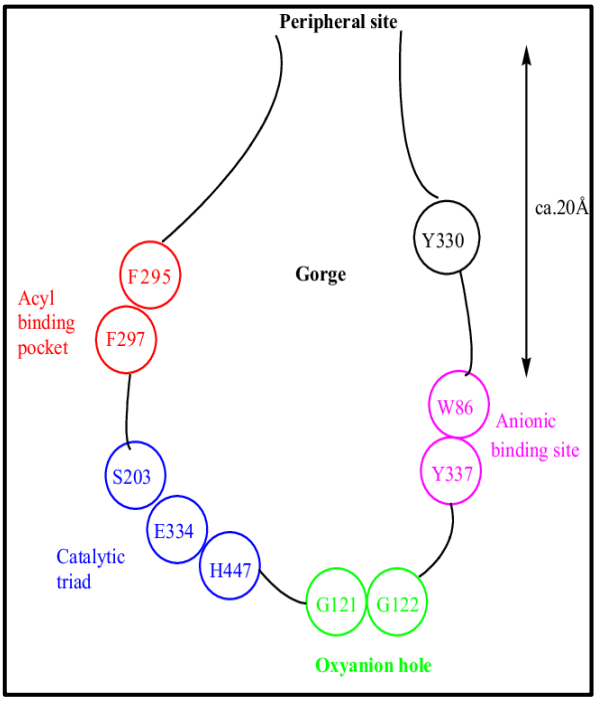

Figure 3. 7 Schematic diagram of active sites in AChE canyon [141]

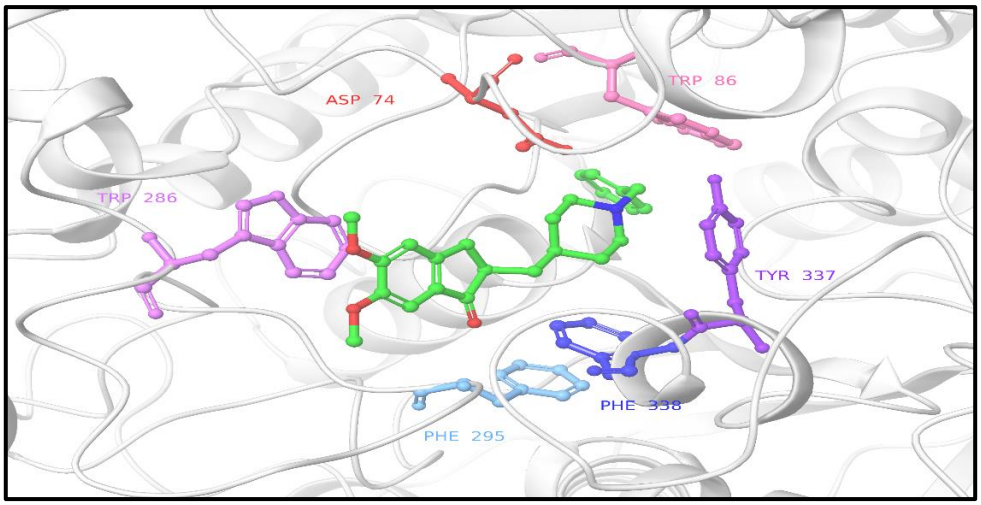

Figure 3. 8 The active site gorges of human acetylcholinesterase (hAChE)[142]

3.3.3 Acetylcholinesterase Inhibitors (AChE-Is)

Alzheimer's disease (AD) is the most common kind of adult-onset dementia and is characterized via a progressive decline in cognitive skills and behavioral features. Because cholinergic deficits are a constant and early finding in AD, acetylcholinesterase has been validated as the most promising treatment target for symptomatic improvement in AD [140].

The most often used medicines to treat AD are acetylcholinesterase (AChE)/cholinesterase inhibitors (ChE-Is). The ChE-I mechanism entails an increase in cholinergic transmission across the central nervous system, with impairments affecting memory and cognitive disorders (Figure 3.9). Tacrine was the 1st ChE-I agent to get FDA approval for the symptomatic treatment of Alzheimer's disease. Only cholinesterase inhibitors, such as donepezil, rivastigmine, and galantamine, and N-Methyl-D-aspartate (NMDA) antagonists, such as memantine, have been authorized and are available. Due to tacrine's hepatotoxicity, it is no longer used[143]. AChE-Is or anti-cholinesterases block the ChE enzyme from degrading ACh, thus enhancing the amount and duration of neurotransmitter activity.

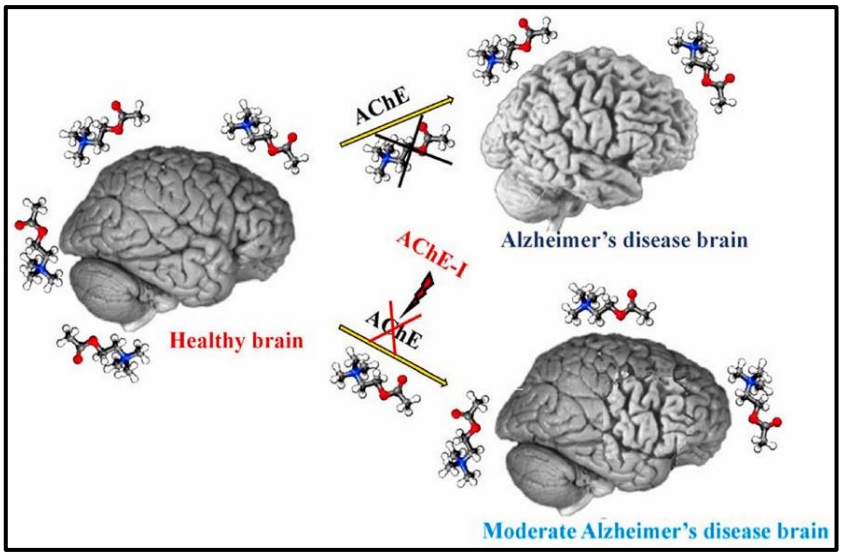

Figure 3. 9 Efficacy of acetylcholinesterase inhibitors in AD[143]

AChE-Is may be classified into 2 classes based on their mechanism of action [11] (Figure 3.10):

- **Reversible inhibitors:** They are categorized as either competitive or non-competitive inhibitors, with the majority of them having therapeutic use. Reversible AChE-Is are critical for manipulating the enzyme's activity pharmacologically. These inhibitors are composed of several functional groups (carbamate, quaternary, or tertiary ammonium) and have been used to diagnose and treat a variety of illnesses, including AD[144].
- **Irreversible inhibitors:** The hazardous consequences are associated with irreversible inhibitors of AChE activity. AChE-Is that being irreversible are organophosphorus chemicals (OPs). They are phosphoric, phosphonic, phosphinic, or phosphor amide acid thiols or esters. The OPs primarily exert their toxicological effects in the CNS through irreversible phosphorylation of esterases. The acute toxicity is due to AChE's irreversible inactivation. OPs are substrate analogs of ACh that, like natural substrate, covalently attach to the serine –OH group in the active site. As with acetylation, OP is divided into 2 molecules and the enzyme is phosphorylated[145, 146].

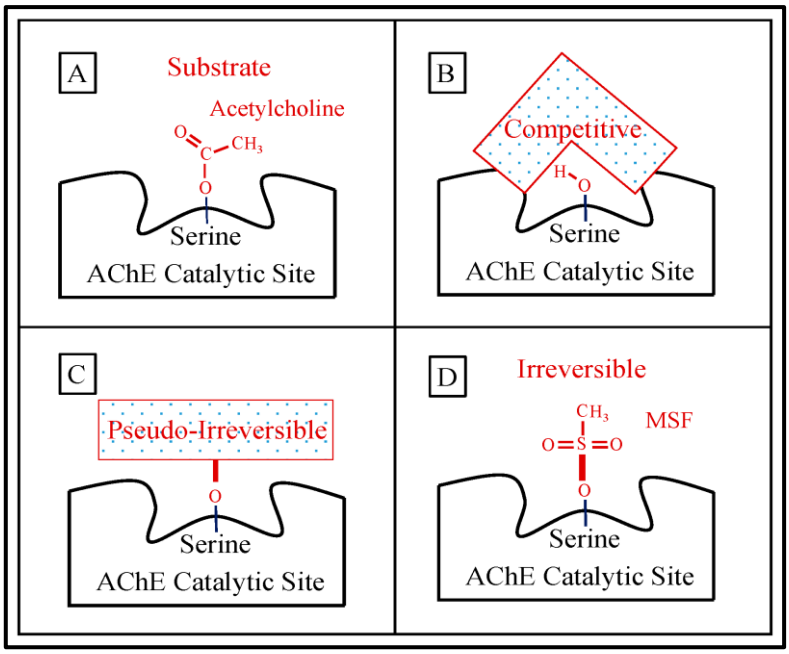

Figure 3. 10 Mechanisms actions of AChE-Is

(**A**) the normal ephemeral (microseconds) covalent acetyl-enzyme complex formed as an intermediate step in the hydrolysis of acetylcholine. (**B**) A schematic of a competitive inhibitor binding reversibly the catalytic site (**C**) The longer-lasting covalent bond formed between pseudo-irreversible inhibitors and the enzyme (**D**) Example of the irreversible sulfonyl-enzyme covalent complex (no spontaneous hydrolysis, no recovery) permanently excluding acetylcholine binding and hydrolysis[147].

Tacrine, donepezil, and galantamine are categorized as intermediate-acting and rivastigmine as pseudo-irreversible agents. Overall, the efficiency of the three ChE-Is available in the market is similar, and the benefit of administering these compounds is mild. Their therapeutic effect is based on maintaining ACh level through slowing down its hydrolysis rate. Because of these medications' gastrointestinal adverse and other side effects, medicinal chemistry and pharmaceutical delivery research has investigated many solutions to develop the pharmacological activity of these compounds. However, it has been shown in recent years that cholinesterases may affect a variety of other processes, including -amyloid aggregation, owing to the presence of a peripheral anionic site (PAS) structure [135]. These findings rekindled interest in cholinesterases as a critical target for Alzheimer's disease treatment, and many research organizations have conducted studies on the design and manufacture of novel inhibitors. Despite their limited effectiveness, ChE-Is remain a pharmaco-therapeutic option for treating

Alzheimer's disease while more effective techniques are developed[140, 143]. AChE-Is have been studied extensively as a treatment medication for AD. In the USA, all of the current 1st-line therapies are AChE-Is. Natural AChE-Is is also a potential field of research. In China, HupA is the medicine of choice[148]. Many hybrids are also being formed. Some hybrids are made wholly of new materials, while others improve on the older AChE-I. Because these AChE-Is are proven, symptomatic treatment with a known target, these medication's class will continue to be developed. The drugs in this class have a track record of CNS permeability, a well-known side effect profile, and demonstrated efficacy (Figure 3.11). Because the FDA has already authorized donepezil, rivastigmine, and galantamine, the risk of developing novel ChE-Is will need to be more effective. The focus of future research in this class should be on whether ChE-Is directly impact the pathogenesis of AD[149].

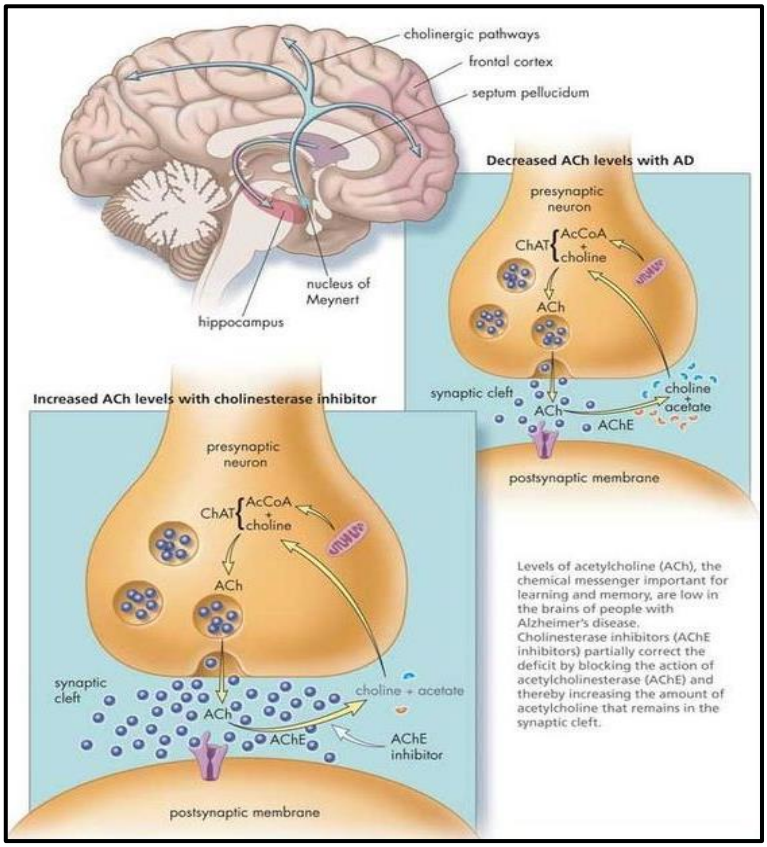

Figure 3. 11 The use of cholinesterase inhibitors in patients with Alzheimer's disease

3.4 Butyrylcholinesterase (BuChE)

Butyrylcholinesterase (BuChE, E.C. 3.1.1.8) is a serine hydrolase that is structurally similar to acetylcholinesterase (AChE). This enzyme is the 2nd kind of cholinesterase., also called pseudocholinesterase. BuChE is also an α-glycoprotein with a biological half-life of about 12 days (human) and can be found in central and peripheral tissues. BuChE is present in plasma and numerous vertebrate tissues, and it is essential because of its ability to hydrolyze choline esters molecules[150]. BuChE is not found in synapses; therefore, unlike AChE that plays a crucial role in terminating the action of ACh in the cholinergic system, no direct involvement of BuChE in the cholinergic system has been demonstrated (breaks down ACh more slowly). However, BuChE may be a surrogate for AChE in deficiency of this enzyme[151](Figure 3.12).

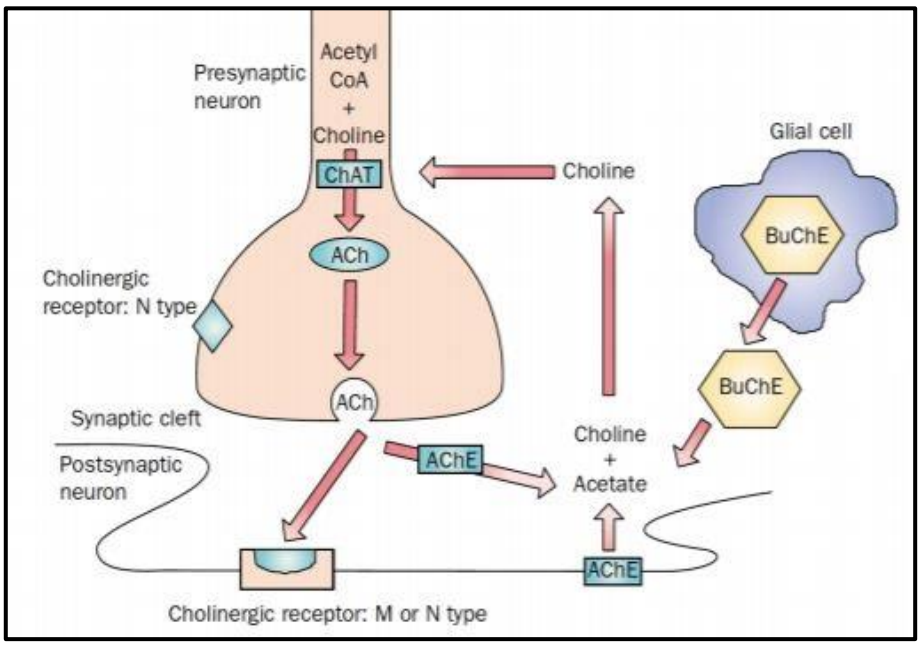

Figure 3. 12 Hydrolysis of acetylcholine by AChE and BuChE

BuChE is the enzyme that degrades the choline ester butyrylcholine the quickest; therefore, it is called BuChE. The 1st research on BuChE shown that inhibiting the enzyme resulted in an increase in brain ACh levels. Additional gene investigations indicated that it is involved in the control of -amyloid, a harmful brain protein, and its amount rises in AD patients (Figure 3.13). As such, it is an intriguing target for neurological diseases such as Alzheimer's disease. BuChE's substrate range was

recently expanded to include cocaine and ghrelin, the "hunger hormone"[152]. It is noted that BuChE's pharmacological effect evolved in lockstep with each published result. Thus, not only is the enzyme now regarded as a critical pharmaceutical target, but it is also emerging as a critical tool for studying the molecular processes involved in a variety of diseases [153].

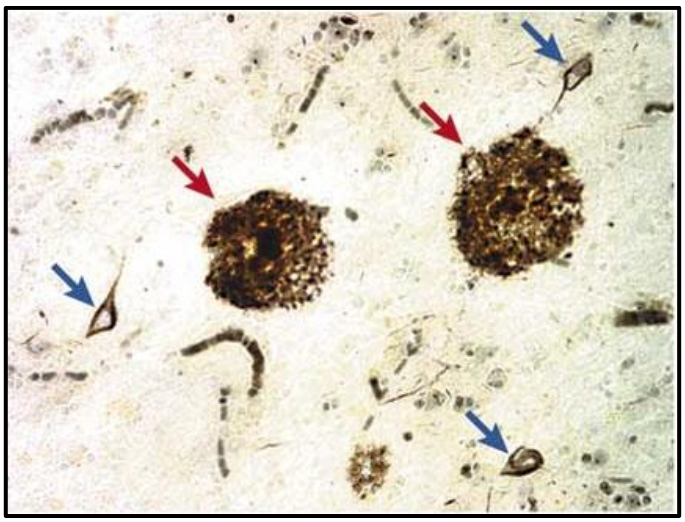

Figure 3. 13 Butyrylcholinesterase and Alzheimer's disease

Note: BuChE in plaques (red arrows) and tangles (blue arrows) in the cerebral cortex of a patient with Alzheimer's disease (AD). Many tangles and plaques in the brains of AD patients contain BuChE activity[154].

3.4.1 Butyrylcholinesterase Functions

BuChE's function act as a natural scavenger in the bloodstream. It is utilized to catalyze the hydrolysis of choline esters such as butyrylcholine, succinylcholine, and acetylcholine, albeit with a lower efficiency than AChE [155].

Additionally, it has been shown that it catalyzes the hydrolysis of various esters, including cocaine, acetylsalicylic acid, and heroin [156, 157]. Additionally, BuChE is involved in the scavenging of naturally occurring (physostigmine) and manufactured anticholinesterases (organophosphate) [155].

The implications of BuChE in AD, as well as supporting research, were discussed:

- The modulator of β-amyloid plaques in the positive direction:

Accumulation of BuChE in plaque deposits in post-mortem human AD brain tissues and an induced AD mouse model [158, 159]. Plaque formation is reduced in male BuChE-deficient mice [160].

- Acetylcholine is hydrolyzed, resulting in cholinergic depression:

BuChE-deficient animals have enhanced cognitive capacity and cholinergic activity [161].

- Inhibitor of the production of amyloid-beta fibrils:

In vitro experiments with recombinant BuChE, fibril formation was suppressed. In vitro, it was discovered that a synthetic C-terminal peptide from BuChE inhibits fibril formation [162]. According to genotyping research, the BuChE-K mutation at the C-terminal of BuChE may confer risk for AD [163].

3.4.2 Butyrylcholinesterase Structure

Human BuChE is a glycoprotein constituted of four analogous subunits and each with 574 amino acid residues and nine polysaccharide chains [164]. Between the 2 human cholinesterases, AChE and BuChE, there is an 84 percent amino acid sequence homology. As a result, they are structurally and functionally linked. AChE and BuChE are members of the -fold family of proteins due to the presence of a core -sheet surrounded via -helices (Figure 3.14). BuChE is similarly ellipsoidal in form, with a 20-deep gouge that contains a peripheral anionic site, a choline-binding site, an oxyanion hole, an acyl-binding site, and a catalytic triad site, as shown in several studies[153](Figure 3.15).

In-depth investigations using site-directed mutagenesis of the cholinesterase enzymes showed the critical role of particular amino acids in the active core, highlighting the distinction between the 2 cholinesterase enzymes. These structural studies explain the molecular basis for the selectivity between the active center and the ligand, as illustrated in Table 3.1[165].

In hBuChE, the catalytic triad consists of three conserved residues: Ser198, Glu325, and His438; in hAChE, the catalytic triad consists of Ser203, Glu334 and His447[18].

At the molecular level, the primary distinction is the acyl-binding pocket, which is one of the component domains in the gorge responsible for accommodating the acyl moiety of substrates Through hydrolysis. BuChE has six less aromatic amino acids than AChE in the gorge. Additionally, one important distinction between AChE and BuChE is the substitution of aromatic residues in the active region of AChE for aliphatic residues in BuChE, resulting in enzyme selectivity.

Radić et al. [166] used site-directed mutagenesis to identify three domains: the peripheral anionic site, the choline-binding site, and the acyl pocket that imparts selectivity on AChE and BuChE. The main substrate difference between AChE and BuChE was found via replacing six of the fourteen aromatic amino acids that surround the active site gorge in AChE with aliphatic residues. Due to the presence of these aromatic amino acid residues (Tyr72, Tyr124, Phe295, Phe297, and Tyr337) in AChE, they have been replaced with aliphatic amino acid residues (Asn72, Gln124, Leu286, Val288, and Ala337) to provide a less structurally restricted pocket in BuChE (Figure 3.16). (Table 3.1).

As a consequence, it lacks - solid bonding, which allows for the binding of bigger inhibitor molecules and substrates such as butyrylcholine and succinylcholine to BuChE. Both enzymes have the same catalytic triad of amino acids, which classifies them as serine hydrolases. Serine is activated via the adjacent histidine, forming a nucleophile that attacks the substrate's electrophilic carbon, forming an acyl-enzyme intermediate and cleaving the ester link. The cleaved substrate is then released through nucleophilic substitution via the hydroxyl group of water, forming an acid [167].

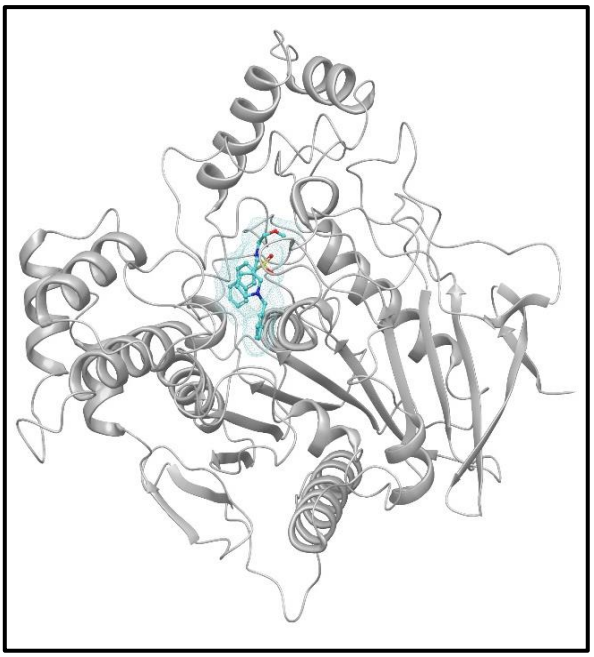

Figure 3. 14 3D structure of BuChE (PDB:5DWY) displayed as a ribbon diagram

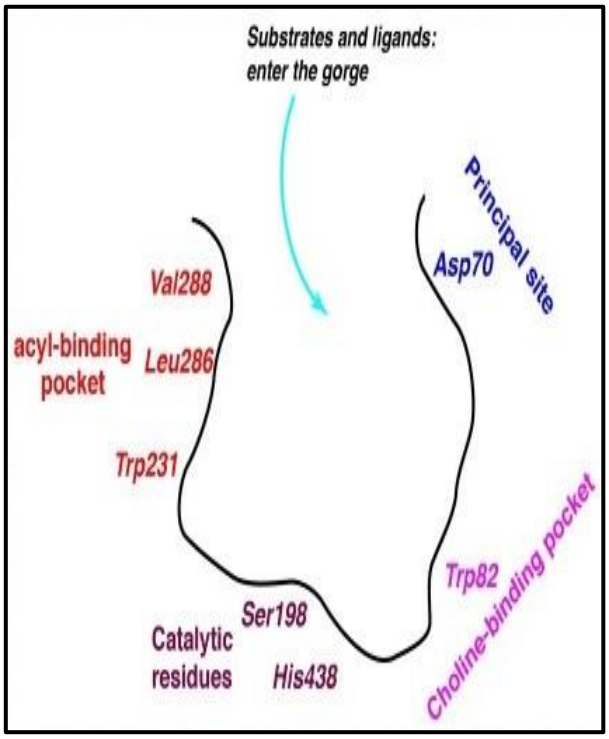

Figure 3. 15 Schematic view of the active site of gorge of BuChE[154]

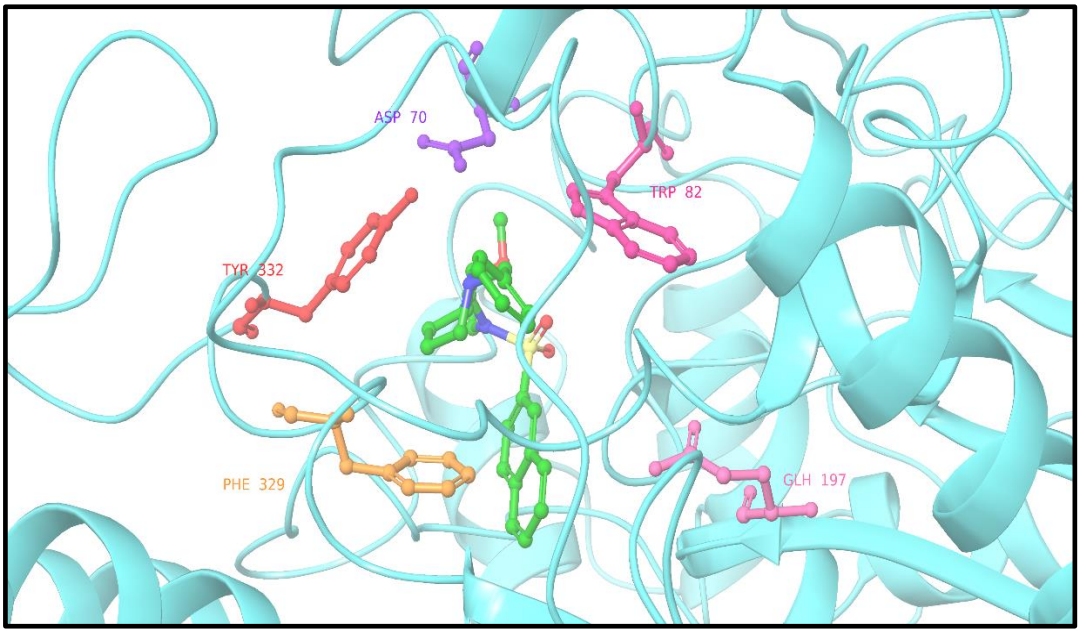

Figure 3. 16 Active site gorges of human butyrylcholinesterase (hBuChE)[142]

Table 3. 1 Tabulation of the key amino acids in the active center of AChE and BuChE

Sites in Active Center	**Amino Acid Residues Involved**	
	AChE	**BuChE**
Peripheral anionic site	Tyr72, Asp74, Tyr124, Trp286	Asp70, Asn72, Gln124
Choline-binding site	Trp86, Tyr337	Trp86, Ala337
Oxyanion hole	Gly121, Gly122, Ala201	Gly116, Gly117, Ala199
Acyl-binding site	Phe295, Phe297	Leu286, Val288
Catalytic triad	Ser203, Glu327, His447	Ser198, Glu325, His438

3.4.3 Butyrylcholinesterase Inhibitors (BuChE-Is)

For a lengthy period of time, researchers concentrated their efforts on the development of AChE inhibitors for the treatment of AD. However, a small number of BuChE-targeted compounds have been identified on purpose. Existing BuChE inhibitors were discovered mostly as a result of the research of AChE inhibitors. As a result, these drugs exhibit dual-target inhibitory activity.

In recent years, as research into AD pathogenesis has progressed, the critical function of BuChE has become more clear. As a result, the efficacy of BuChE inhibitors in the treatment of AD has already gained widespread recognition[168]. Numerous good reviews have examined a variety of nonselective and selective ChEs inhibitors. BuChE is considered a potential therapeutic target due to its increased levels and activity in the late stages of AD [154].

Additionally, the literature has many research demonstrating that BuChE may restore the cholinesterase function in the absence of AChE. This result is consistent with previous studies indicating that the relative expressions of AChE and BuChE invert Through AD development. Furthermore, BuChE knockout animals have no physiological detriment, while human patients with silent BuChE mutations exhibit a slower rate of cognitive decline [153].

As a result, inhibiting BuChE is anticipated to help AD patients in the same manner as AChE inhibition does. In vivo evidence supporting this hypothesis includes the observation that specific BuChE inhibitors can restore ACh levels in mice and improve cognitive performance in mice treated with the amyloid-peptide while avoiding peripheral (para-sympathomimetic) adverse effects that have been shown to limit the dosing of AChE inhibitors [150](Figure 3.17).

BuChE inhibition may be divided into 2 types according to its mechanism of action:

- **Reversible inhibition:** BuChE is capable of binding a broad range of amine and quaternary ammonium compounds. Monofunctional ligands temporarily attach to the peripheral anionic site (PAS) and then glide down the gorge to interact with the cation binding site. These ligands are either competitive inhibitors, non-competitive inhibitors, or inhibitors of mixed kind. Bifunctional ligands, such as decamethonium, may bind to both the PAS and the cation site concurrently. The interaction of the PAS and the active center may result in complicated inhibitory kinetics, such as partial nonlinear inhibition; in certain instances, an inhibitor may convert to an activator, depending on the substrate type and concentration range [169, 170]. Medical researchers are interested in specific reversible inhibitors of BuChE.

- **Irreversible or progressive inhibition:** Via interacting with the catalytic serine (Ser198), carbamyl, organosulfonyl, and organophosphorus-esters induce gradual inhibition of BuChE. The mechanism via which these chemicals inhibit cholinesterase has been extensively investigated [171].

  Rivastigmine, a carbamate, has been approved as an anti-Alzheimer medication; it has a similar IC50 for human BuChE and AChE. Cymserine and its derivatives, such as tetrahydrofurobenzofuran cymserine (THFBFC), boost acetylcholine and improve cognition in rats without the adverse effects associated with AChE inhibitors. As a result, targeted carbamylation of BuChE may offer a novel therapeutic strategy for AD [172].

  Numerous organophosphates (Ops) have been extensively employed as pesticides (coumaphos, paraoxon, and so forth) and pharmaceuticals (echothiophate, cyclophosphamide). Additionally, certain OPs are very effective chemical warfare agents (tabun, sarin, soman, VX). Nucleophilic chemicals may be used to reactivate phosphorylated cholinesterases.

As a result, a number of selective BuChE inhibitors have been discovered, the most powerful of which are the carbamate analogs of cymserine and isosorbide, which block the enzyme irreversibly[173, 174].

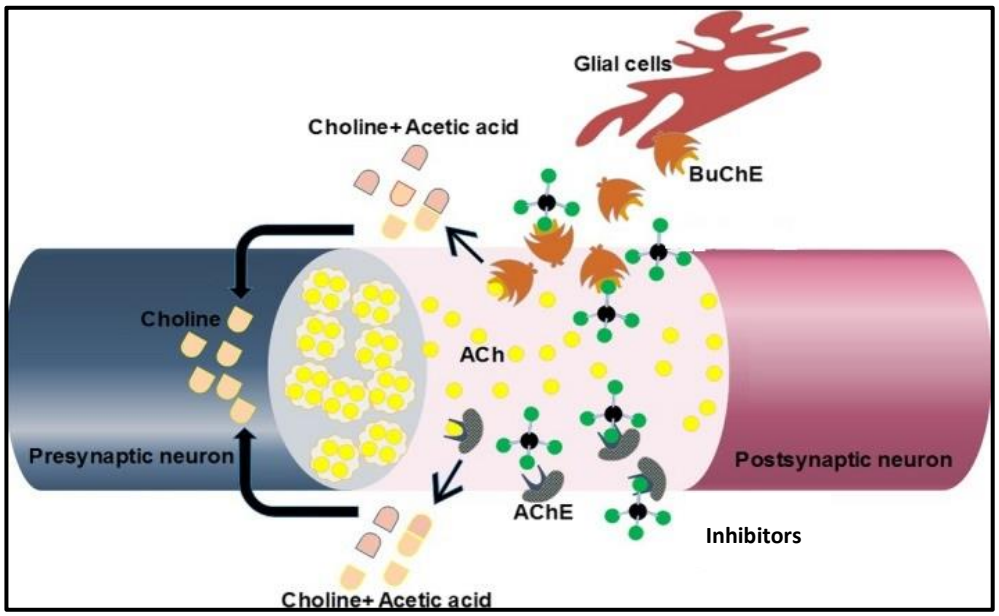

Figure 3. 17 Cartoon image depicting possible mode of inhibitors action on cholinesterase enzymes[175]

4

COMPUTER-AIDED DRUG DESIGN

4.1 Theoretical Background of Computer-Aided Drug Design (CADD)

Hypothetically, a drug is used to cure a specific disease. A drug is considered to be the ligand, replacing the natural substrate of a protein. Launching a new drug to the market is a costly affair that involves considerable time and money. The underlying reason may be that the process of finding a suitable, relatively non-toxic drug for a specific disease is a time-consuming, arduous, and costly process. It has been estimated that the average research and development investment needed to get a new drug approved and on the market would cost approximately 10-14 years and $2.7 billion USD on average[176]. Ever since the development of Viracept in 1997, derived from the target structure HIV protease, computational tools for drug design have become a pillar in drug discovery. To assist the discovery process, a mix of sophisticated computer methods, biological research, and chemical synthesis was developed, and this combined approach increased the size of discovery [177].

The term computer-aided drug design (CADD) was eventually used to refer to the use of computers in drug development. CADD has substantially shortened the time required to advance a drug candidate from more than 10 years to a few years [178]. Additionally, it has been shown that via using CADD methods, we may decrease the cost of drug discovery and development via up to 50%. CADD is any method that utilizes a computer program to create a standard for relating activity to structure [179](Figure 4.1). Advanced computational applications are useful tools, and they have resulted in noteworthy achievements. CADD is a specific field of study in which various computational techniques are used to model the interactions of receptors and medicines in order to estimate binding affinities. However, the technique is not limited to the study of chemical interactions and

the prediction of binding affinity; it has a plethora of other applications, ranging from the design of compounds with desired physicochemical properties to the management of compound digital repositories [180].

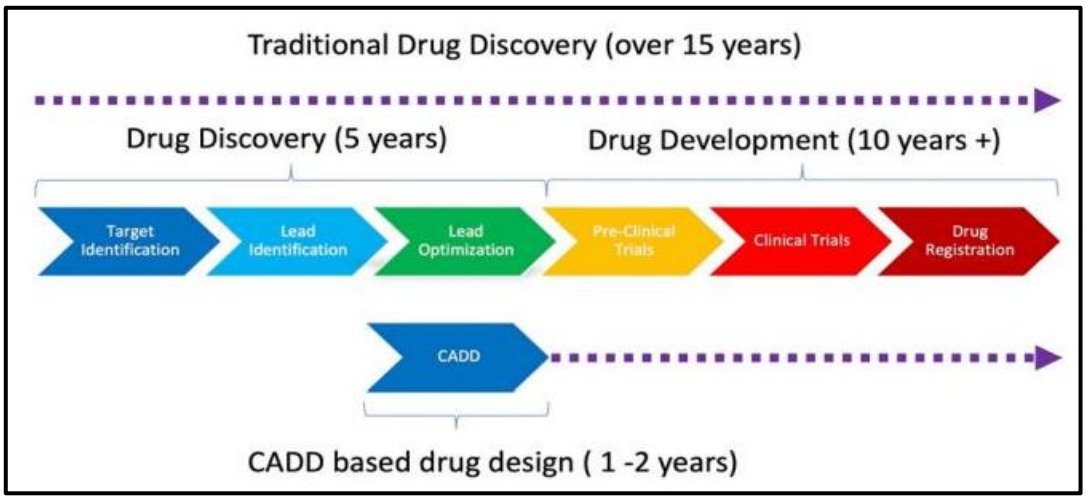

Figure 4. 1 Traditional process of drug discovery and development versus CADD timeline

Via displaying the three-dimensional structures of proteins, ligands, and protein-ligand interactions, computational techniques may offer the most useful information (Figure 4.2). Finding an active leading molecule is the cornerstone of the new medication development process (Figure 4.3). As a result, the advantages of CADD screening bioactive chemicals become the jumping-off point and critical stage in novel drug development. CADD has recently been widely used to the creation and identification of novel pharmacological drugs because to its better hit rate of novel compounds when compared to conventional high-throughput screening (HTS) and combinatorial chemistry [181].

CADD is often used for three main objectives in practice:

1. Filter large compound libraries into smaller sets of predicted active compounds, which can reduce experimental workloads.
2. Optimize lead compounds via increasing their affinity or optimizing their drug metabolism and pharmacokinetics (DMPK) characteristics.
3. Create new compounds via "growing" functional groups on beginning molecules or putting together pieces.

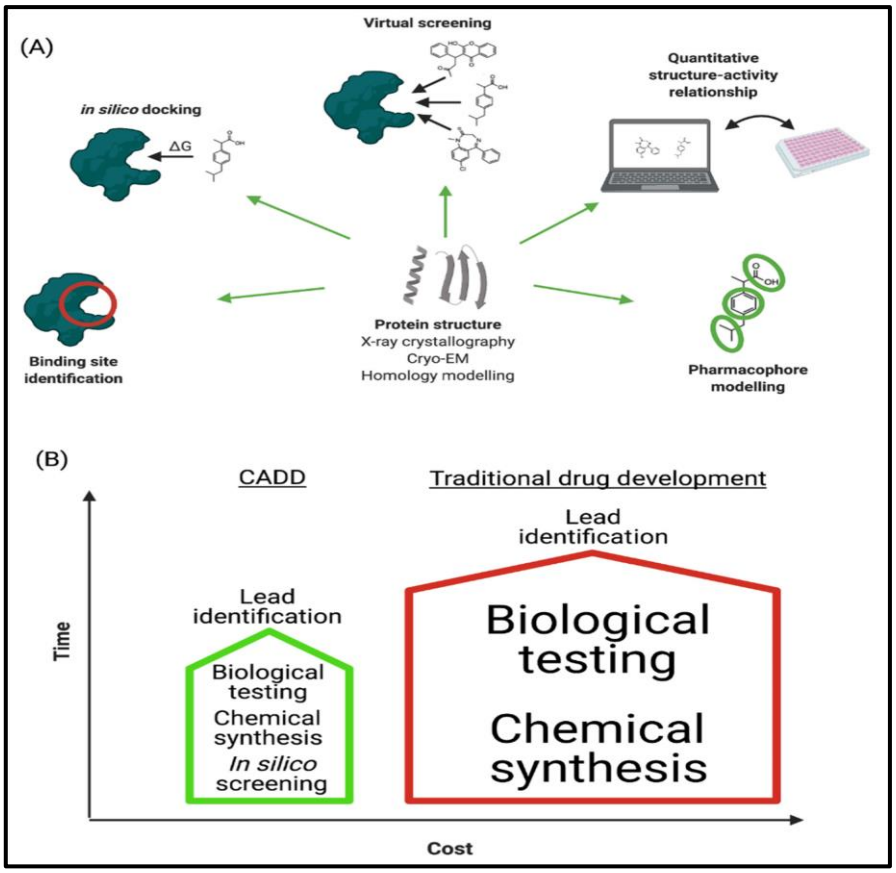

Figure 4. 2 (A) Schematic diagram of CADD process. (B) Comparison of traditional and computer-aided drug development in terms of time and cost investment[182]

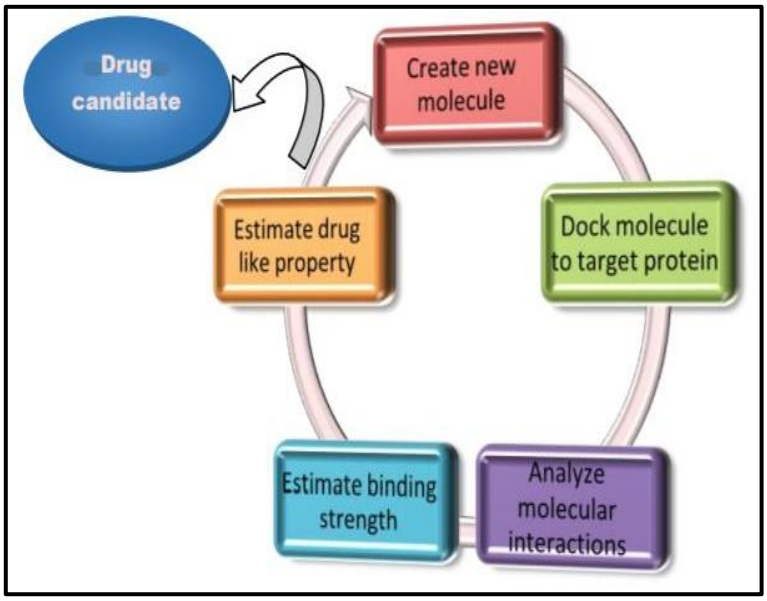

Figure 4. 3 General principle for drug design through CADD[176]

Computer-Aided Drug Design (CADD) is an effective technique for discovering new medicines to prevent or cure Alzheimer's disease. There are primarily 2 methods. for drug design through CADD as following[42] (Figure 4.4):

- The direct approach to drug design, or structure-based drug design (SBDD).
- The indirect method, often referred to as ligand-based drug design (LBDD).

The 1st approach, which incorporates Molecular Dynamics (MD), Quantum Mechanics (QM), and Linear Interaction Energy (LIE), is conceptually similar to high-throughput screening (HTS) in that structure information for the protein and ligand is required to identify novel hit chemicals from virtual compound libraries using docking simulation tools [182].

The 2nd approach, which includes pharmacophore modeling, quantitative structure-activity relationship (QSAR) analysis, and matched molecular pairs (MMP) search, among others, uses only ligand information to predict activity based on its similarity/dissimilarity to previously known active ligands [182] (Figure 4.4).

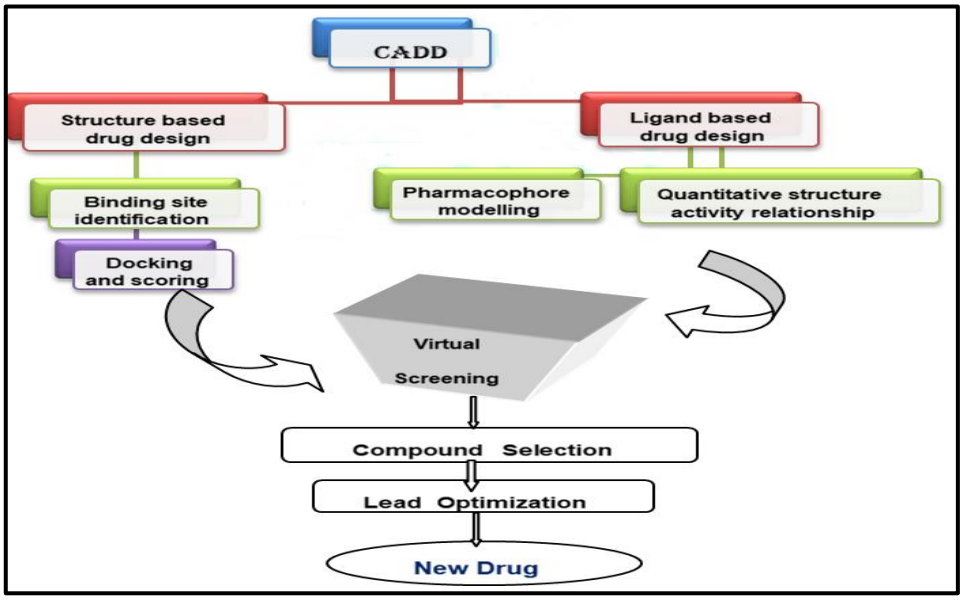

Figure 4. 4 Overview of computer-aided drug design (CADD) process[183]

Recently, CADD has become an increasingly essential technique in the identification of new AD drugs, allowing for substantial cost savings and accelerated development cycles in drug research [184]. Numerous research groups have successfully used CADD to produce inhibitors of the cholinesterase enzyme, beta secretases, and gamma secretases, as well as additional AD treatment and diagnostic compounds [182, 184-186]. In (CADD), the energy of the systems is calculated using either Molecular Mechanics (MM) or Quantum Mechanics (QM). Since each particle is referred to as a wave function or a function of the state, the state of each particle is determined using Schrödinger's time-dependent wave function. Although QM may predict molecular orbital energies, it is not utilized for docking or MD simulations, since this would contradict CADD's "convenience" approach[187].

For large systems, MM computations offer rapid, empirical energy calculations. However, MM employs straightforward equations based on classical physics, and atoms are regarded as harmonic spheres. As a result, MM methods may be used to compute non-electronic molecule characteristics. Force fields are MM energy functions that are used to determine the system's potential energies. This potential energy function entails a number of parameters, including inter- and intramolecular forces, bond lengths, bond angles, bond torsions, and non-bonded interactions such as the Lennard-Jones potential (van der Waals interactions) and the Coulombic potential (electrostatic interactions)[188]:

$$\vartheta(r^N)=\sum_{bonds}\frac{Ki}{2}(l_i - l_{i,0})^2 + \sum_{angels}\frac{Ki}{2}(\theta_i - \theta_{i,0})^2 + \sum_{torsions}\frac{Vn}{2}(1+\cos(n\omega-\gamma)) + \sum_{i=1}^{N}\sum_{j=i+1}^{N}(4\varepsilon ij\left[\left(\frac{\sigma ij}{rij}\right)^{12} - \left(\frac{\sigma ij}{rij}\right)^{6}\right] + \frac{q1q2}{4\pi\varepsilon 0 rij}) \quad \textbf{(4.1)}$$

Such that $\vartheta(r^N)$ is the potential energy function, as the function of position (r) and of number of particles (N). $\sum_{bonds}\frac{Ki}{2}(l_i - l_{i,0})$ is the energy function for bonded atoms, where (l) is the length of the bonds. $\sum_{angels}\frac{Ki}{2}(\theta_i - \theta_{i,0})$ is the function for the potential energy related to the deviations of the bond angles, and $\sum_{torsions}\frac{Vn}{2}(1+\cos(n\omega-\gamma))$ is the rotational potential energy of a bond. The last term accounts for non-bonded interactions between atoms, such as van der Waals and

electrostatic interactions. Thus, CADD may be divided into 2 broad categories: structure-based and ligand-based drug design. When combined with the increased availability of various chemical databases, these cost-effective structure- or ligand-based methods substantially enhance drug discovery efficiency and provide new vistas and potential pathways for the treatment of life-threatening illnesses. The process for CADD is shown in Figure 4.5.

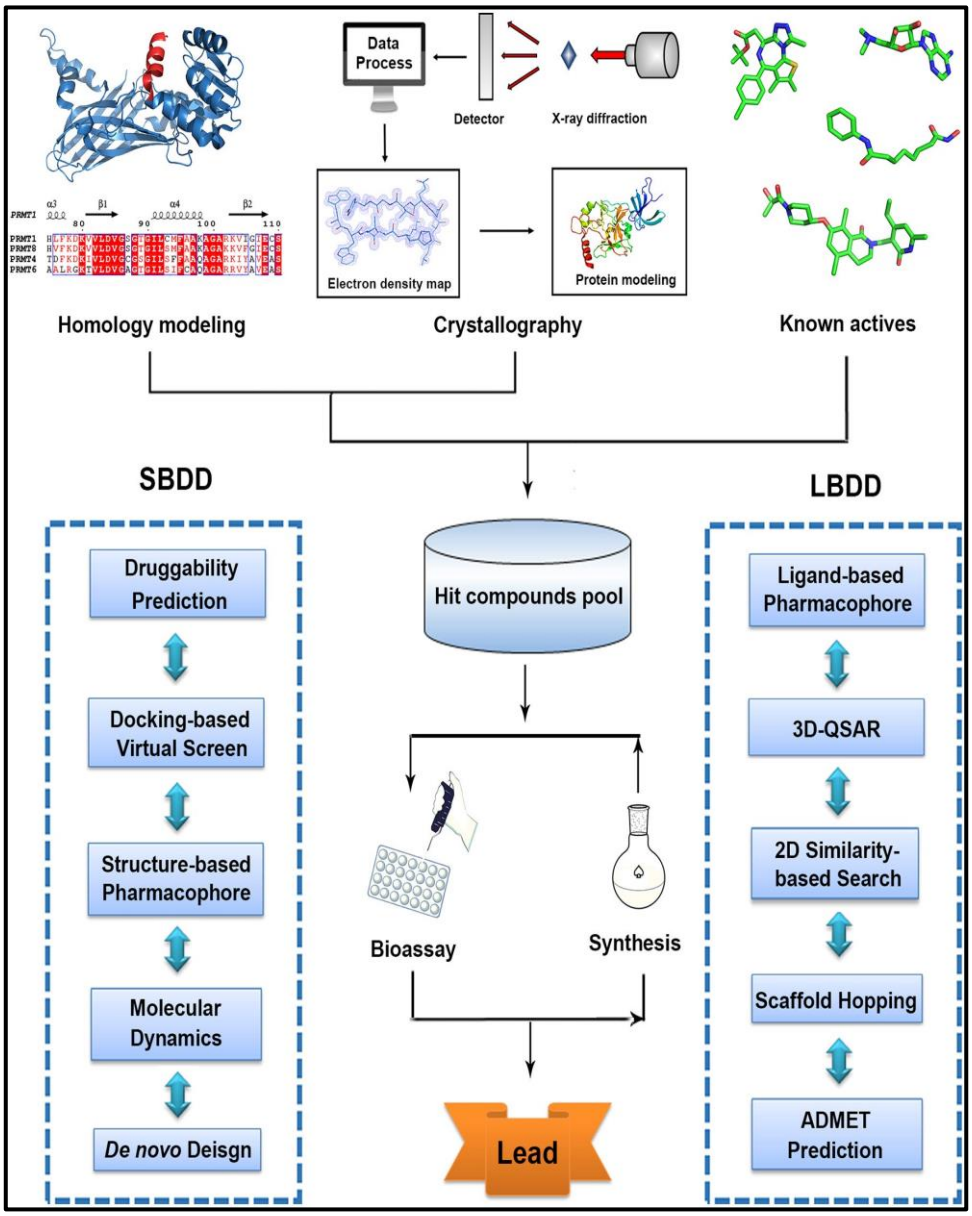

Figure 4. 5 Traditional workflow of structure-based drug design (SBDD) and ligand-based drug design (LBDD)

4.1.1 Structure – Based Drug Design (SBDD)

Structure-based drug design is a technique that makes use of three-dimensional (3D) structural information from proteins to create novel biologically active compounds. Thus, the main 1st step in SBDD is selecting a target molecule and determining its structure. When the 3D structure is known, it is possible to carefully analyze the binding site and its topology and steric and electronic properties[189](Figure 4.6). Applications such as molecular docking (MD) simulations are used in SBDD to examine the conformational changes acquired in the binding pocket of the target and to inspect how the protein and ligand behave together when both are allowed to move, respectively. For example, the specified target may be an enzyme associated with a disease of interest. Then, based on binding affinity determinations, potential compounds are determined, which attenuates the activity of the target via its inhibition[190]. Thus, SBDD utilizes information about a biological target and identifies possible new medications; therefore, SBDD constitutes a marked advancement in the computational techniques used in biophysics, medicinal chemistry, statistics, biochemistry, and other fields. In addition, scientific advances have resulted in a large number of methods for predicting protein structures. These state-of-the-art technologies enable the determination of the forms of large numbers of proteins via using Cryo-electron microscopy (CryoEM), nuclear magnetic resonance (NMR), X-ray crystallography, and computational methods like homology modeling and molecular dynamic (MD) simulation[191](Figure 4.7).

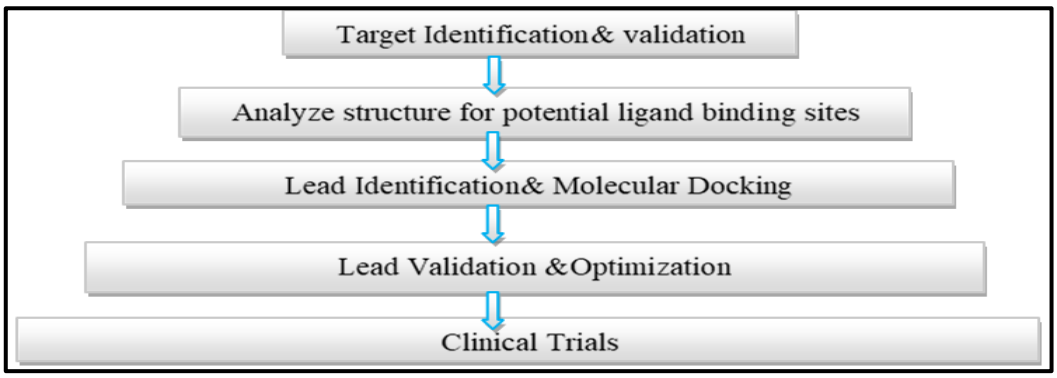

Figure 4. 6 Steps involved in structure – based drug design (SBDD)

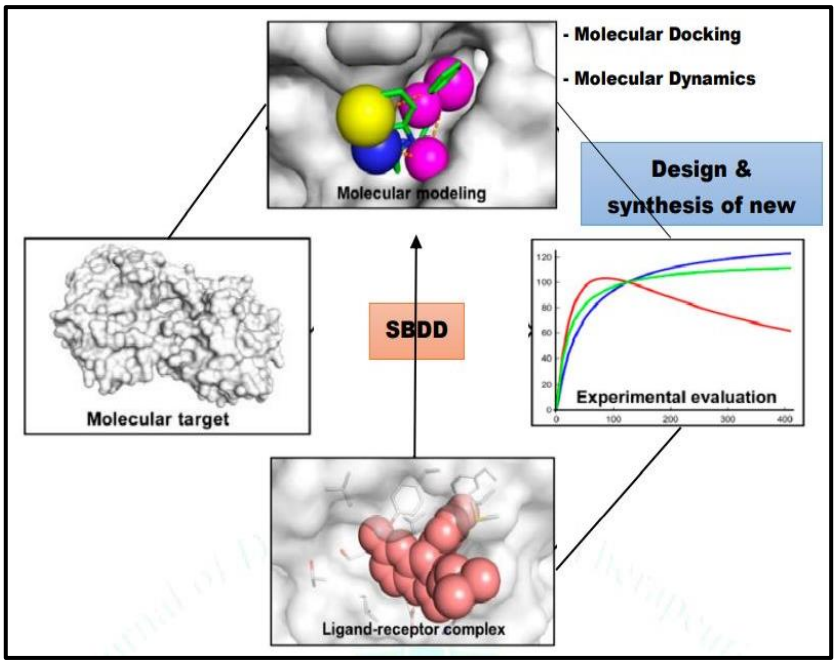

Figure 4. 7 Layout of structure – based drug design (SBDD)[176]

4.1.1.1 Molecular Docking (MD)

Molecular docking is a computational technique for predicting the location of tiny molecules or ligands inside the active region of a target protein (receptor) (Figure 4.8). It is mostly utilized to determine the most advantageous binding mechanisms and bioaffinities of ligands for their receptor. At the moment, it is widely used in virtual screening for the optimization of lead compounds. The technique of molecular docking is primarily concerned with three interrelated objectives:

- Prediction of the entanglement posture
- Biological affinity
- Virtual examination

The search algorithm and scoring algorithms used in molecular docking are critical tools for generating and evaluating ligand conformations [192]. For novel drug molecule discovery, molecular docking is used to predict the spatial arrangements of the drug molecule in question within the vicinity of the binding cavity of the target structure. The primary yield of molecular docking is the 'docking score' and a 'docking pose,' which aids with predicting the biologically active or bioactive conformation the molecule will most likely adapt when in physiological

conditions. In many molecular docking simulation algorithms, the ligand is exclusively given conformational flexibility, while only some residues in the binding pocket are allowed restricted flexibility. The reason behind this lies in the fact that if both the ligand and protein were allowed flexibility, excessive computational resources would be needed.

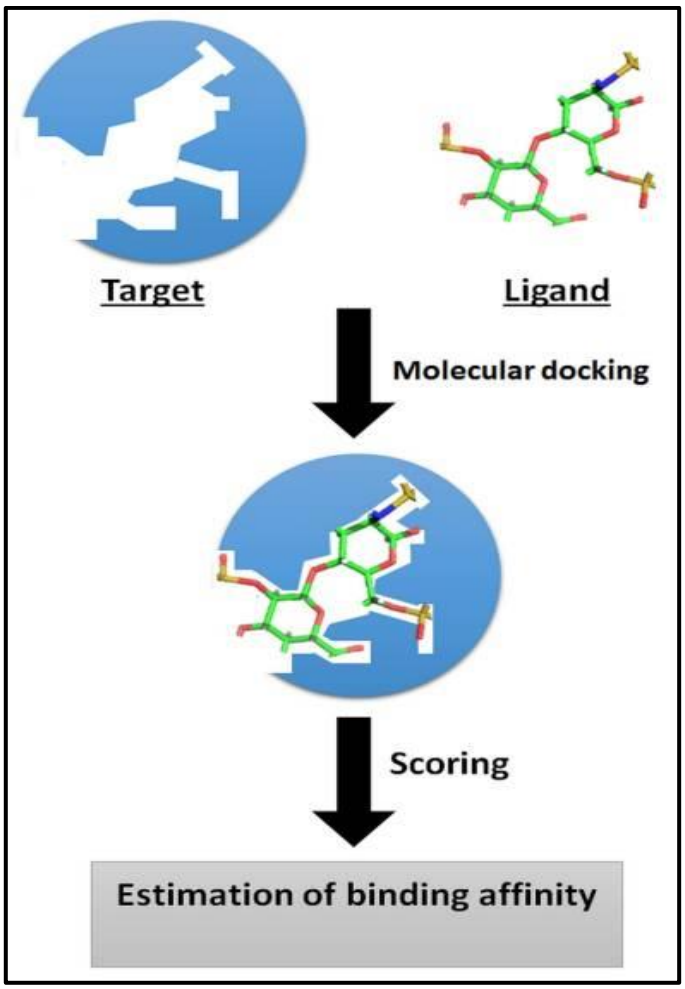

Figure 4. 8 Process of docking[183]

Molecular docking predicts free energy of binding ΔG (Gibbs free energy-docking score), which corresponds to the sum of all these non-bonded terms. Low docking score (i.e., high ΔG values) corresponds to the unfavorable binding pose, and low ΔG corresponds to the favorable binding conformation at the binding pocket. Due to computational costs, most docking programs only take ligand flexibility into account while neglecting protein flexibility[193].

When calculating the binding free energy of a ligand, the following approximations are taken into consideration;

1stly,

$$\Delta G = \Delta H - T\Delta S \quad \textbf{(4.2)}$$

As it is considered, the change in entropy (ΔS) is assumed zero since the addition of a ligand relatively very small compared to the protein may not cause a substantial change in entropy,

$$\Delta G = \Delta H - \cancel{T\Delta S} \quad \textbf{(4.3)}$$

2ndly;

$$\Delta U = \Delta H + P\Delta V \quad \textbf{(4.4)}$$

As it is considered, the volume change, again, is assumed not to be affected via adding a ligand that is considerably smaller than the protein itself,

$$\Delta U = \Delta H + \cancel{P\Delta V} \quad \textbf{(4.5)}$$

Therefore, since;

$$\Delta H = \Delta U \quad \textbf{(4.6)}$$

then

$$\Delta G = \Delta U \quad \textbf{(4.7)}$$

This indicates that the binding free energy can be estimated from internal energy [194]. The internal energy consists of:

A) Bonded Energies

- 2-body covalently bonded atoms
- 3-body covalently bonded atoms
- 4-body covalently bonded atoms

B) Non-bonded energies

- van Der Waals (Lennard Jones)
- Electrostatic Potential

These components are included in the experimental docking function;

$$\Delta G_{bind} = \Delta G_0 + \Delta G_{H\text{-}bonds} \sum_{H-bonds} f(\Delta r, \Delta\alpha) + \Delta G_{ionic} \sum_{ionic} f(\Delta r, \Delta\alpha) + \Delta G_{arom} \sum_{arom} f(\Delta r, \Delta\alpha) + \Delta G_{lipo} \sum_{lipo} |Alipo| + \Delta GrotNrot \quad \textbf{(4.8)}$$

where ΔG_0 is a constant term, not dependent of the system. The terms $\Delta G_{H\text{-bonds}}$, ΔG_{ionic}, ΔG_{arom}, and ΔG_{lipo} are the contributions from ideal hydrogen bonds, ionic interactions, aromatic interactions and lipophilic interactions, respectively. These terms are multiplied via f (Δr, Δα), which is a penalty function. ΔG_{rot} accounts for the loss of free energy that occurs when a rotatable bond in the ligand is frozen for binding, and it is multiplied via N_{rot}, which is the number of rotatable bonds in the ligand[194]. Various docking algorithms and programs are available like DOCK, AutoDock, Auto-Dock Vina, FlexX, GOLD, HADDOCK, Glide, etc.[195-198]. Each of these programs has its algorithm to search different conformations of ligands at the binding site and to score functions to rank molecules according to their binding affinities. In Maestro molecular modeling package, a Glide docking algorithm with different precisions is available, namely, starting from the most complicated one quantum-polarized ligand docking (QPLD), induced-fit docking (IFD), extra precision (XP), standard precision (SP), and high throughput virtual screening (HTVS). Millions of compounds can be screened against a specific target in silico using HTVS (Schrödinger, 2010). The main differences between SP and XP algorithms are their scoring functions and penalties like de-solvation and charge. XP uses more complicated scoring functions and applies charge and de-solvation penalties. In this thesis, the Glide SP docking, IFD, and QPLD algorithm were considered, using a hierarchical filter to predict bioactive ligands conformations at the binding pocket.

In the IFD algorithm, initial docking is performed using SP or XP mode, then generated poses are refined using the Prime module of Maestro to provide flexibility to the surrounding residues at the binding pocket. This enables active site residues to adopt more favorable orientations to maximize ligand-protein interactions. Finally, refined protein-ligand complexes are used to re-dock ligands back to the binding pocket and scored.

Although QPLD is the algorithm that provides one of the most reliable bioactive poses and docking scores, it is one of the most time-consuming docking protocols compared to the others. This algorithm combines quantum mechanics QM calculations which provide high-level accuracy, and molecular mechanics (MM), which enables speed. Docking algorithms and programs provide the static picture of protein-ligand complexes and do not contain physiological conditions such as temperature. Since all biological processes are dynamic and occur in physiological conditions, these conditions are required to represent the nature of dynamical cellular processes correctly. Therefore, this can be acquired via using molecular dynamic (MD) simulations.

4.1.1.2 Molecular Dynamic (MD) Simulations

In order to study the conformations and dynamic behaviors of biomolecules on a long-timescale, molecular dynamics (MD) simulation is a suitable theoretical method that offers atomic-level insight into the regulating mechanism[199]. MD simulation uses Newton's law of motion to calculate the potential energy of each atom. Potential energy term calculated via considering non-bonded interactions, bond angles and lengths, and dihedral angles (Figure 4.9). MD method enables to calculate of atomic positions and give insights into the dynamic nature of protein-ligand complexes within a specific time, yielding MD trajectories.

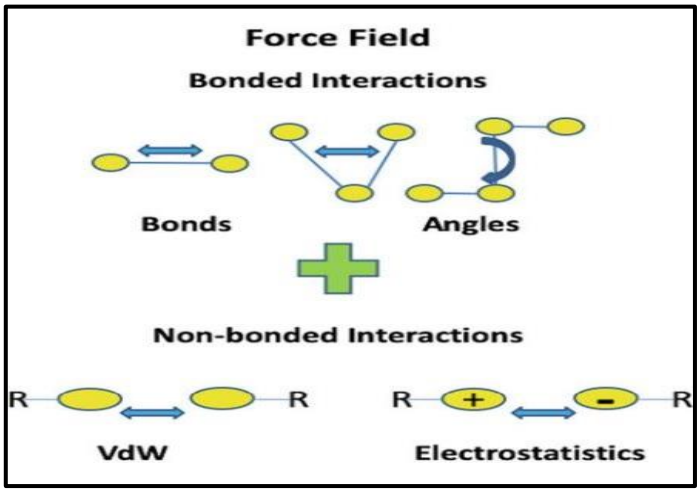

Figure 4. 9 The components of the force field, representing bonded and non-bonded interactions [200]

MD simulations start with an equilibrium phase, where the whole system is relaxed to a more lifelike arrangement. Temperature is kept near zero for the equilibrium run and is increased at the production run step of the MD simulation[201]. To keep the system progressing, numerical integration of Newton's 2nd law of motion is done via a set of algorithms known as "integrators." Solving the Newtonian equation for each particle will provide the system with physical attributes, such as volume and energy. However, additional attributes or variables termed "extended degrees of freedom" can improve the system[202]. The calculations are broken down into a sequence of equations for short time steps denoted via δt, which are generally determined via the fastest action in the system. This is generally the vibration of bonds, which are at femtosecond frequency. A trajectory file can be collected at the end of an MD simulation, interpreting all the dynamic variables and their change with time. The trajectory includes Every parameter that was generated Through each step movement of atoms is listed here. The following are some of the structural parameters that may be utilized to evaluate the findings.

- RMSD
- RMSF
- Radius of Gyration
- Protein–Ligand Contacts
- SASA
- Particle Swarm Optimization (PSO) or Essential Dynamics (ED)
- The Analysis of secondary Structures

The root mean square deviation (RMSD) is the most important ad first metric to consider while analyzing the MD trajectory's trajectory. The root mean square deviation (RMSD) of a protein is used to quantify the variance between its backbones from its initial structural conformation to its final location. The variations generated through the MD modeling process [203] may be used to specify the stability of the protein in relation to its conformation.

The relative mean squared deviation (RMSD) is computed in relation to the reference native conformation rref using the following formula:

$$\mathrm{RMSD}(t) = \left[\frac{1}{M}\sum_{i=1}^{N} m_i \left| r_i(t) - r_i^{\mathrm{ref}} \right|^2\right]^{1/2}$$

Where $M=\sum_i m_i$ and $r_i(t)$ represent the atom, i position at the time t after least square fitting the structure to a reference structure. It is possible to compute the root mean square deviation (RMSD) for all residues, the backbone, the side chains, and the C atoms. The root mean square fluctuation (RMSF) method is the most effective method for analyzing the residue-wise fluctuation of the protein derived from the MD trajectory of the protein. The variation of each residue or domain in a protein is represented via this value. The RMSF may be displayed as RMSF (nm) vs residue number[203] which is a linear function. The RMSF of a protein is defined as the difference between the location of particle i and its reference position, where T denotes the passage of time and *riref* denotes the position of particle i in the reference position.

$$\mathrm{RMSF}_i = \left[\frac{1}{T}\sum_{t_j=1}^{T} \left| r_i(t_j) - r_i^{\mathrm{ref}} \right|^2\right]^{1/2}$$

The RMSF of well-organized and rigid structures, such as helix and sheets, is low, while the RMSF of loosely organized and flexible structures, such as bends and coils, is high. This is because atoms may cause more fluctuation in bends and coils than in helix and sheet.

4.1.1.3 Molecular Mechanics / the Generalized Born Solvent Accessible Surface Area (MM/GBSA) Calculation

MM/GBSA calculation is a popular approach used to predict free-energy changes upon binding ligands to biological molecules such as proteins. Free energy calculations of biomolecular systems hold great importance since free energy is associated with all molecular operations, namely protein folding and molecular catabolism, and anabolism. MD simulations are currently one of the most advanced techniques in simulating biomolecular systems[204].

End-point free energy calculations are used to calculate the binding energies since they are computationally more efficient. End-point free energy calculations take into account the “final state” of the system, just like docking algorithms. However, they are more accurate than the latter[205]. The MM/GBSA calculation approach 1st considers the protein and ligand individually and then as a complex. The individual free energies are subtracted from the free energy of the complex. There are 2 parts involved in the computation of a MM/GBSA score, the MM approaches and the implicit solvation approaches that calculate the polar and non-polar contributors. MM/GBSA calculations can be expressed as basically. As a rule, ligand-based methods are based on the pharmacophore approach and quantitative-structure activity connections, respectively (QSARs). In LBDD, it is believed that molecules with structural similarities also have biological activities and interactions with the target protein that are similar[206].

4.1.2 Ligand – Based Drug Design (LBDD)

Although the 3D structure of the target protein is unknown (either because it has not been crystallized or due to the inability of homology modeling to accurately represent it), the knowledge of ligands that bind to the desired target location is known [207]. It is possible to enhance a pharmacophore model or a molecule that already has all of the necessary structural properties for binding to a target active site with the help of these ligands. Generally speaking, ligand-based methods are as follows:

- pharmacophore-based approach
- quantitative-structure activity relationships (QSARs).

According to LBDD, substances that are structurally similar to one another also have the same biological activity and interact with the same target protein [208] see (Figure 4.10). In this method, functional groups on each ligand set are aligned on a template molecule to obtain a universal pharmacophore model. Further, the generated pharmacophore model can be validated using another set of ligands with known experimental binding data. Where the 3D structure of the protein is

not revealed, this method allows the discovery of new molecules capable of binding on the same target.

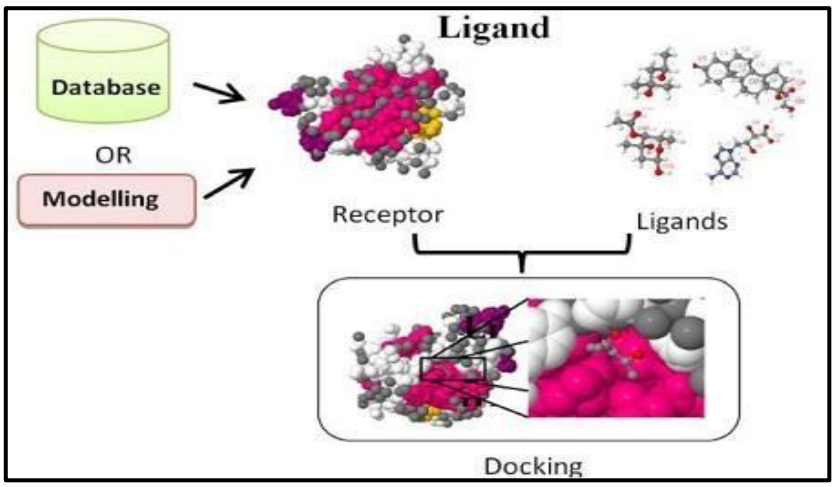

Figure 4. 10 Outline of process involved in ligand-based drug design[209]

4.1.2.1 Pharmacophore Modelling

After a century of researches, pharmacophore methods have become one of the most potent tools in drug creation. For better pharmacophore modeling, a variety of ligand-based and structure-based methods have been developed. They have been used in 3D chemical databases, virtual screening, ligand profiling, de novo design, and biological activity prediction for lead optimization with great success. Each atom or group in a molecule that shows specific properties linked to molecular recognition can be reduced to a pharmacophore trait[210]. Ligands with the best fitness to the model will identify as having higher biological activity. The six different pharmacophore characteristics are used to define functional groups of studied molecules:

- Hydrogen bond donors
- Hydrogen bond acceptors
- Cationic group
- Anionic group
- Aromatic rings
- Hydrophobic sites, and any possible combinations.

Different compounds may be compared at the pharmacophore level; this method is referred to as “pharmacophore fingerprints”[211] and is often used.

4.1.2.2 Quantitative Structure – Activity Relationship (QSAR)

Hansch and Fujita 1st coined the term QSAR in 1964 to describe the correlation between biological activity and chemical structure [212]. Molecular descriptors are the essence of QSAR, and they can range from 1D (molecular formula), 2D (structure), 3D (conformational spatial arrangements), and more.

QSAR investigations are widely used in contemporary chemistry and biochemistry, and they have a wide range of applications. Quasi-static regression (QSAR) models are developed to provide an understanding of the relationship between the chemical structure and biological activity, to aid in the design of novel compounds with enhanced biological activity profiles, and to predict the biological activity of compounds *in silico*[213] (Figure 4.11).

It is necessary to examine physicochemical parameters such as partition coefficient and the presence or absence of certain chemical characteristics. QSAR may be binary or categorical in nature, in which case they specify a variable such as harmful or not toxic, active or not active, and so on. Furthermore, they may be statistical and continuous in nature [214] depending on the pIC_{50}, Ki, or other factors. QSAR directs the process of lead optimization, and it is also used as a screening and enrichment technique to eliminate compounds that do not exhibit drug-like characteristics or those are anticipated to be hazardous from the pool of compounds.

For QSAR analysis, a variety of techniques are developed that are dependent on the following criteria or variables relevant to the study [215]:

- Molecular structural characteristics or parameters that are generated from a sequence of molecules
- The mathematical approach that was utilized to determine the connection between the structural characteristics and biological activity was described in detail below.

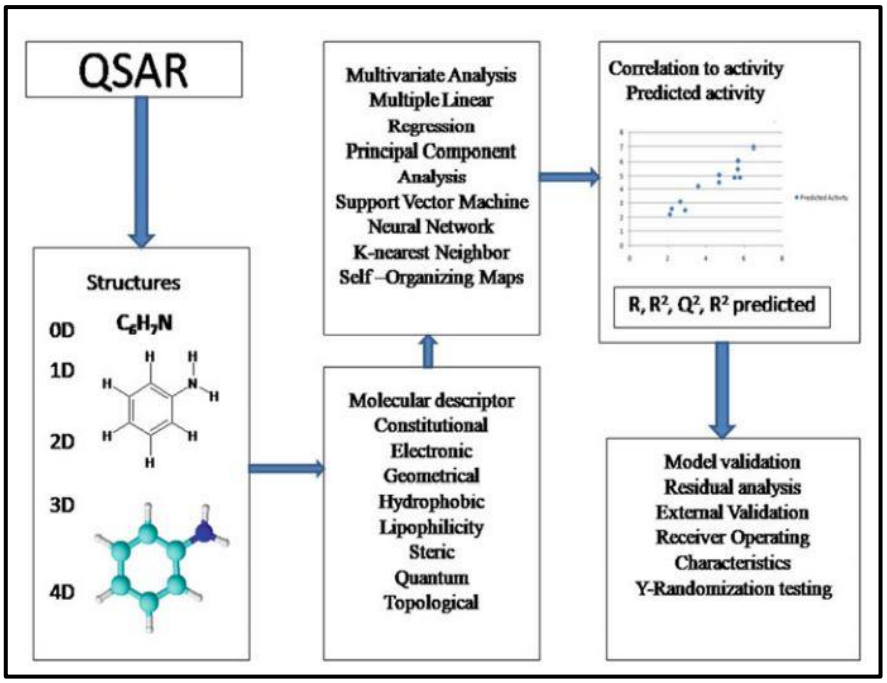

Figure 4. 11 QSAR methodology, mathematical models, and validation procedures[215]

4.1.2.3 MetaCore™/MetaDrug™

The MetaCore™ /MetaDrug™ platform is an online tool provided via Clarivate Analytics to obtain an extensive profile of the pharmacokinetics and pharmacodynamic properties for a selected compound or a set of compounds. Mainly, there are 25 common diseases binary QSAR models and 26 toxicities binary QSAR models, which can give the Tanimoto Prioritization (TP) value of a compound depending on how similar it is to the training and test set of the QSAR models. In the "therapeutic activity prediction" function, it is possible to forecast whether or not a chemical has therapeutic action[216].

Indications of possible therapeutic action are shown via a projected QSAR value (between 0 and 1) higher than 0.5. The Cooper statistics parameters (specificity, sensitivity, accuracy, and Matthews Correlation Coefficient) are used via the MetaCore platform to assess the model's performance on the MetaCore platform (MCC). Sensitivity, specificity, and accuracy are measures of the proportion of properly predicted positives, correctly predicted negatives, and the degree to which anticipated characteristics (such as the inhibition constant value, IC_{50}) are near to the actual values of expected attributes [70].

The closer the value of these coefficients is to one hundred percent, the higher the quality of the model is considered to be. MCC is a correlation coefficient between observed and predicted values, with values ranging from -1.00 to +1.00 (+1.00 representing perfect prediction and -1.00 representing inverse prediction).

Model with the greatest values of those parameters was chosen as the winner. Tanimoto prioritization [217] is used to identify the applicability scope of a model.

- Sensitivity $= \frac{TP}{(TP+FN)}$ **(4.9)**
- Specificity $= \frac{TN}{(TN+FP)}$ **(4.10)**
- Accuracy $= \frac{(TP+TN)}{(TP+FN+TN+FP)}$ **(4.11)**
- MCC $= \frac{(TP*TN-FP*FN)}{\sqrt{(TP+FN)*(TP+FP)*(TN+FN)*(TN+FP)}}$ **(4.12)**

where

- TP – true positive,
- FN – false negative,
- TN – true negative,
- FP – false positive.

4.1.3 Virtual Screening

Virtual screening has evolved as a key technique in the search for new drug-like compounds, and it has become one of the most widely used. Virtual screening has been shown to be the most convenient method available today for identifying the most promising bioactive compounds with the assistance of information about the protein target or known active ligands, among other things (Figure 4.12).

Since its inception, virtual screening has gained widespread recognition as a revolutionary alternative to high-throughput screening, primarily in terms of cost-effectiveness and the likelihood of identifying the most suitable new hit via filtering through huge libraries of compounds [218]. Virtual screening methods may be divided into 2 categories: structure-based virtual screening (SBVS) and

ligand-based virtual screening (LBVS) (LBVS). In contrast to the SBVS technique, which is based on the structure of the target protein active site, the LBVS method is based on an estimate of computed similarity between the known active and compound sites that are derived from databases of known active sites. According to the lead–target interaction, i.e., binding free energy and interacting amino acid residues through non-covalent bonding (hydrogen and hydrophobic bond) for further validation [219], it makes it easier for researchers to select appropriate molecule(s) as a lead from the available chemical compounds database for further validation.

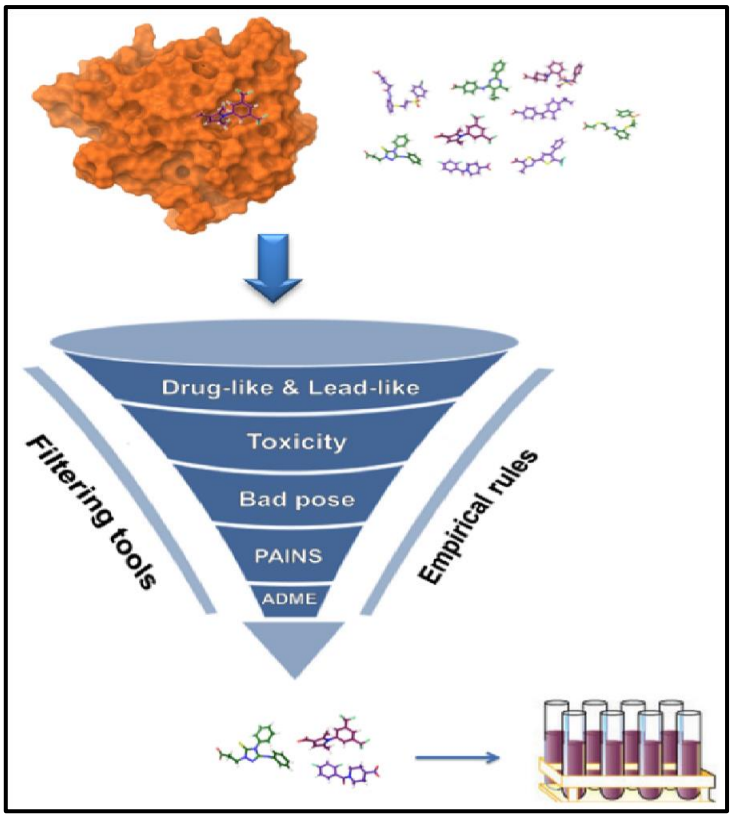

Figure 4. 12 Overview of virtual screening process[220]

4.2 Advantages of Computer-Aided Drug Design

We can identify the most promising drug candidate in the shortest amount of time and at the lowest possible cost using computer-aided drug design (CADD), which is an efficient technique in drug discovery and development. It always offers a ray of optimism for progress in the field of drug development. With the present accomplishments, there is a bright future for CADD in terms of assisting in the

development of many more curative drugs in the near future. Through CADD, we can reduce synthetic and biological testing efforts. Through CADD, we can reduce synthetic and biological testing efforts[221].

- Via using *in silico* filters, it is possible to identify the most promising medication candidate via removing molecules with undesirable characteristics (such as low effectiveness, weak ADMET, and so on) [222].
- A cost-effective, time-saving, rapid, and automated method is used.
- We can learn about the pattern of drug-receptor interactions via CADD.
- When compared to conventional high throughput screening, it provides compounds with high success rates via exploring large libraries of compounds in silico [223].
- These methods help to reduce the likelihood of failures at the final phase.

4.3 Computer-Aided Drug Design for Identifying Anti-Alzheimer's Disease Drug Candidates

Without a question, Alzheimer's disease (AD) is one of the most difficult human illnesses to cure, not only because of its widespread prevalence among older people throughout the globe, but also because there is presently no effective therapy available. Several symptomatic medicines have been approved for use, but there is still a significant need to identify chemicals that target the complex processes that impact the brain and contribute to Alzheimer's disease (AD). Computational methods have shown to be helpful in the search for novel medicines, and the use of in silico methodology is common in many drugs discovery programs, particularly those conducted via businesses seeking to introduce new products to the pharmaceutical market.

The relevance of CADD methods to drug development is becoming more apparent with each passing day (Figure 4.13). As a result of recent advances in drug design, it is now possible to rationally develop powerful treatments with multi-targeting effects, increased efficacies, and reduced side effects, particularly in terms of toxicity (Figure 4.13).

The use of computer algorithms was used in this research to analyze a large collection of medicines (about 7900 small molecules) in order to discover compounds that have potential therapeutic effectiveness in the treatment of Alzheimer's disease (AD).

We have concentrated our efforts on 2 enzymes that are prospective targets and have a particular role in the treatment of Alzheimer's disease, namely, acetylcholinesterase (AChE) and butyrylcholinesterase (BuChE).

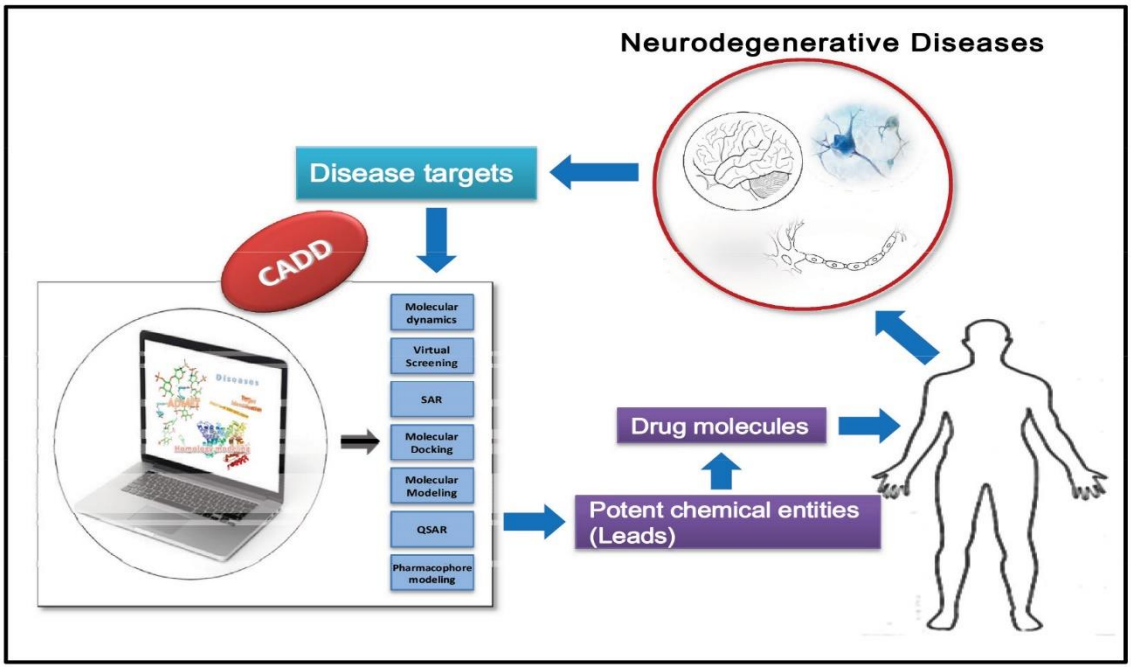

Figure 4. 13 Neurodegenerative disease drug development based on computer-aided drug design[180]

5

MATERIALS AND METHODS

5.1 Screening of Anti-Alzheimer's Disease Molecules from Databases

Small-molecule complexes that have been authorized for use as medicines may be "repurposed" to serve new purposes, and their mechanisms of action can be investigated to determine the reasons of their positive and harmful effects. The pharmaceutical database (NPC) of the National Institutes of Health Chemical Genomics Center (NCGC) [224] (retrieved on July 2018 from https://tripod.nih.gov/npc) contains an assembly of recognized and registered medicines (about 7922 small molecules) that has been assembled. The NCGC Pharmaceutical Collection (NPC) is an extensive, publicly available collection of approved and investigational drugs for high-throughput screening that serves as a valuable resource for validating new disease models and better understanding disease pathology and intervention. The NCGC Pharmaceutical Collection (NPC) is a valuable resource for validating new disease models and better understanding disease pathology and intervention. Systemic human disease repurposing would be made possible via NPC's extensive collection of all human-approved small-molecule drugs, which would be especially beneficial for rare and neglected diseases, for which the cost and time required to develop a new chemical entity are often prohibitively expensive [224].

5.2 MetaCore™/MetaDrug™ Analysis

In order to determine if the structures have therapeutic efficacy against Alzheimer's disease, the clarivate analytics MetaCore™/MetaDrug™ platforms were used to screen the structures. This integrated platform integrates quantitative structural analysis and systems biology techniques to predict pharmacokinetics and pharmacodynamics profiles of small molecules. This feature lets you predict the probability of anti-Alzheimer's activity a compound might

have. The input compounds are screened based on how similar they are to compounds with known high anti-Alzheimer's activity. The "The "Therapeutic Action Prediction" function predicts whether or not a chemical will have potential therapeutic activity. The anticipated QSAR values (between 0 and 1) are in the range of 0.5 to 1.0, with values less than 0.5 indicating inactivity and higher than 0.5 indicating possible therapeutic action. In our analysis, the AD QSAR model was used with a cut-off TAV of ≥ 0.75 to screen molecules. 1338 out of 7900 molecules were found to have a larger TAV of 0.75 in the QSAR model. The toxicity QSAR models for these compounds were then tested using 26 different MetaCore™/MetaDrug™. Each toxicity model has a threshold value, and the toxicity of compounds is determined based on how different they are from the threshold value. We observed that only ten molecules out of 1338 showed no toxicity, and these compounds were selected for structure-based studies. The model performance in MetaCore™/MetaDrug™ was evaluated using Cooper statistics parameters: training set: N=261, test set: N=44, specificity: 0.82, sensitivity: 0.91, accuracy: 0.86, and Matthews Correlation Coefficient (MCC): 0.73 [216].

5.3 *In Silico* Studies

5.3.1 Ligand Preparation

In order to optimize the geometrical properties of the ten selected hit small molecules, the LigPrep module of maestro was used in conjunction with the OPLS 2005 force field (OPLS_2005)[216]. This process generates a large number of ligand molecules from each drug, each with a unique set of stereochemical features, ionization states, ring conformations, and tautomeric properties. Molecular states in aqueous solution at pH 7.4 were generated using the Schrodinger Epik module; a wide pH range was considered due to the activity range of AChE and BuChE enzymes[11, 225], which allowed for the generation of ionization and tautomeric states for molecules in aqueous solution at pH 7.4. The optimized potentials for the OPLS_2005 force field liquid simulations were utilized for the optimization, which resulted in the formation of the ligands' low-energy conformer.

OPLS_2005 force field liquid simulations following the synthesis of the ligands, a total of 120 compounds were produced. Finally, these 120 bioactive and nontoxic ligands have been docked into the binding pocket of the AChE and BuChE enzymes[226, 227].

5.3.2 Protein Preparation

First, the crystal structure of enzymes was retrieved from the protein data bank (PDB) server, AChE (ID: 4EY7), and the resolution of the structure is 2.35 Å [228], and BuChE (ID: 5DYW) and its resolution of the structure is 2.5 Å [229]. The amino acid sequences of AChE and BuChE were obtained from UniProt in order to cross-check and repair the incomplete residues in the crystal structures, which were discovered throughout the research.

The Crosslink Proteins method developed via Maestro was used in an imagined solvent environment to fill in the amino acid residues that were lacking. Next that, the "A" chain of each crystal structure was used in the following steps: When it comes to protein synthesis, the three critical stages are preprocessing, optimization, and minimization. The protein is first preprocessed, and then bond orders are given to the various amino acids. Crosslink proteins, a tool from the Biologics Suite [230] that is implemented in the Schrodinger molecular modeling program, was used to replace the missing residues in the protein (for example, hydrogen atoms and missing atoms) of the third intracellular loop. Water particles in the vicinity of 5 of the ligands were maintained, while other water particles were removed from the solution. Secondly, at pH (7.4), the protonation state and protonation constant (pKa) of ligands were predicted [230, 231]. To modify amino acid protonation states, PROPKA [232] was utilized, and Epik [233] was used to predict the ionization and tautomeric states of the co-crystallized ligand at the physiological pH of the solution (7.4). For systems including an OPLS_2005 (Optimized Potentials for Liquid Simulations 2005) force field, it was possible to accomplish limited minimization with 0.30 root mean square deviation heavy atom convergence [234]. The new AChE and BuChE structures were created with the help of the Protein Preparation Wizard, which is included in the Schrodinger software suite.

We have taken into account the various protonation states of binding pocket residues in this study since the formation of the protein-ligand complex may result in variations in the protonation states of the ionizable groups in the protein.

5.3.3 Receptor Grid Generation

Prepared protein structures were used in grid generation for molecular docking. Grid centers were -14.07, -43.93, and 27.92 and -5.33, 10.63, and -12.73 for x, y, and z coordinates, for AChE (4EY7) and BuChE (5DYW) respectively. Glide sets inner box to 10x10x10 and outer box respect to the ligand size. The outer box dimensions were 27.82x27.82x27.82 and 25.18x25.18x25.18 for AChE (4EY7) and BuChE (5DYW) respectively.

5.3.4 Re-Docked Pose in Docking Models

The effectiveness of molecular docking procedures in predicting the optimum binding mode of ligands in the binding pocket of the receptor is determined via re-docking co-crystallized molecules (E20) and (5HF) into the binding site of the AChE and BuChE crystal structures, respectively. The E20 and 5HF molecules are withdrawn from the binding pocket of their targets, and docking is conducted with no constraints. The docking poses obtained via various docking methods are compared to the hole complex structure (i.e., the conformer of E20 and 5HF small molecules at the AChE and BuChE X-ray structures), and the root mean square deviation (RMSD) values are calculated (Table 6.8). Values less than 2.0 usually suggest that the bioactive conformation of the ligand was properly identified throughout the experimental process. All docking values obtained were less than 2.0 for both AChE and BuChE[235]. These findings demonstrate that docking algorithms may accurately anticipate the bioactivity of ligands in the E20 and 5HF binding sites. The ligand’s calculated binding posture is well matched with the X-ray structural conformation in all docking methods employed (Glide/SP, IFD, and QPLD) (Figure 5.1). RMSD values less than 2 may suggest that the used methodology is capable of accurately predicting the ligand’s bioactive confirmation at the protein's binding site. Thus, docking algorithms may be

utilized to predict the bioactive conformation of ligands inside the AChE and BuChE receptor binding pockets[235].

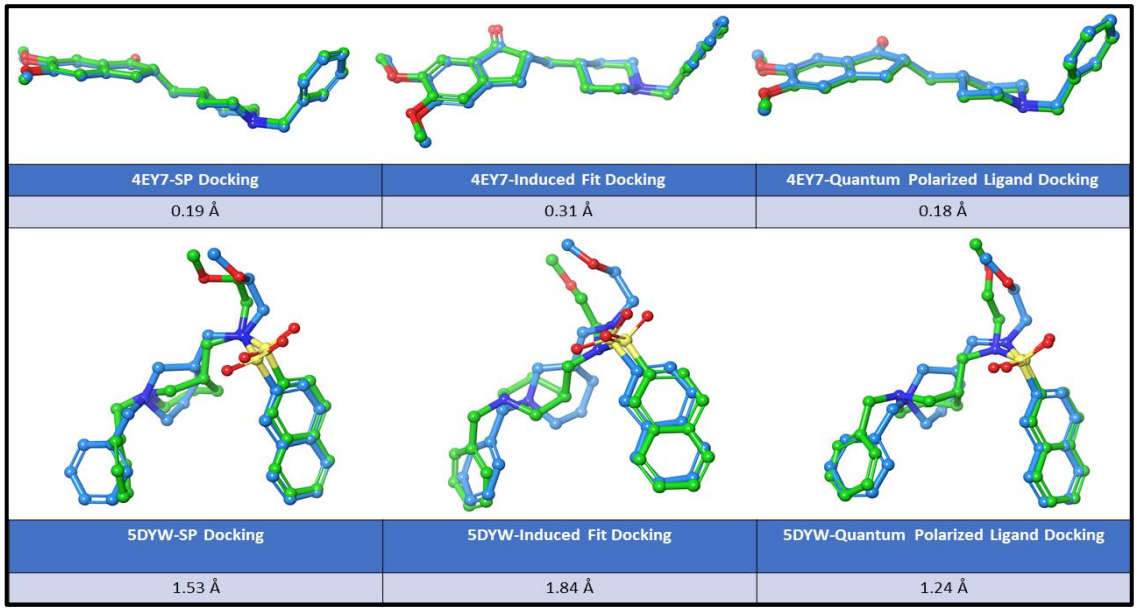

Figure 5. 1 Redocked poses of the native ligand with three protocols, SP, IFD, and QPLD, respectively

5.3.5 Docking Analysis of Selected Molecules

Three distinct docking methods (Glide/Standard Precision (SP), Glide/Induced Fit Docking (IFD), and Quantum Mechanics-Polarized Ligand Docking (QPLD)) were used using Maestro Glide docking tools to chosen active and benign compounds from MetaCore™/MetaDrug™. Glide SP docking software was first used to establish the predicted binding poses of the studied ligands to AChE and BuChE proteins [236, 237]. Utilization of computational techniques, the docking procedure predicts the preferred conformational matching of ligands in the binding site of target proteins[233, 234].

The goal of molecular docking is to predict the optimum binding orientation as well as the structural stability of complexes of interacting molecules. The docking software usually consists of three parts: (1) Illustration of a protein structure; (2) Compound poses are created using a scanning algorithm; (3) A scoring method for evaluating the binding interactions of the docking complexes that have been produced[238]. All ligands were docked into the AChE and BuChE binding

pockets using the Maestro molecular modeling program's grid-based docking method (Glide), and 20 docking poses were required for each ligand.

Secondly, the IFD method contributes to increased conformational sampling of both target and ligand structures. While conventional virtual docking studies assume a rigid receptor, many receptors change their binding location to the shape and binding mode of the ligand. This is referred to as induced-fit docking, and it is one of the most important aspects challenging product design that is structure-dependent. It is in charge of the following protocols: I) using Glide/SP, all inhibitors were docked into the catalytic domains of AChE and BuChE, and then complexes with high docking scores were chosen for the following stage; II) utilizing the Maestro's Prime module, the amino acids of the complexes containing five docked ligands were refined. III) Finally, utilizing the Glide/XP docking technique, all ligands were re-docked into the improved receptor [238, 239]. All ligands were docked into the AChE and BuChE binding pockets, and each ligand needed a minimum of 20 docking poses.

Thirdly, the QM-Polarized Ligand Docking procedure attempts to enhance the partial charges on the ligand atoms in the receptor area of a Glide docking run via substituting quantum mechanical charges. Thus, the receptor takes into consideration the polarization of the ligand’s charges, and redocking the ligands with these new charges contributes to improved docking accuracy [240]. The method works via selecting a subset of the highest-scoring postures for each ligand, measuring charges using QSite, redocking each of these positions, and selecting the best poses from the list. All ligands were docked into the AChE and BuChE binding pockets, and each ligand needed a minimum of 20 docking poses.

5.3.6 Molecular Dynamics (MD) Simulations and Molecular Mechanics Generalized Born Surface Area (MM/GBSA) Free Energy Calculations

MD simulations at short (50-ns) and long (100-ns) time scales were performed using the Desmond force field and OPLS_2005 to examine the structural and functional properties of ligands in the target protein binding pocket for top-

induced fit docking poses based on ChemScore [241] (i.e., for eight compounds in the binding pockets of AChE and BuChE, totaling 2400 ns MD simulations). Top-IFD poses were submerged in an orthorhombic water box (with a minimum distance of 10 between the box of edges and the complex). Initially, the systems were all specific water molecule (SPC) models; subsequently, the systems were all neutralized, and the solvent systems' concentrations were adjusted using an ionic concentration of 0.15 M NaCl solution[241]. Prior to initiating the MD simulations for manufacturing, relaxation methods for equilibration of the enzyme-ligand complexes were employed. Through development simulations, the starting temperature was set to 310 K and controlled using the Nose-Hoover thermostat [242, 243]. The pressure was set at 1.01325 bar and was originally constrained via the Martyna–Tobias–Klein system [244] The systems were modeled using an isothermal–isobaric (NPT) ensemble. Other default values were utilized.

MD simulations of chosen chemicals were run for 50 ns. Post-process analysis was performed on the trajectory frames acquired from MD simulations. We determined the root mean square deviation (RMSD) of selected structures. RMSD measures the average shift in the modification of chosen atoms in the studied structure through simulations using a reference trajectory system. This cycle is repeated for each frame's stored trajectories throughout the simulation phase. When complex structure swings between well-defined mean locations, RMSD may be called RMSF. Because the amount of this variation is quantifiable, it may be used to characterize changes in the local protein chain. The binding free energies of chosen ligands were calculated using the MM/GBSA method implemented in Schrodinger's Prime module[245] (i.e., eight compounds). Throughout the MD simulations in MM/GBSA, derivative trajectory frames were used. The primary advantage of the MM/GBSA method is that it allows for the analysis of the protein-ligand complex's conformational stability via the use of a collection of configurations (snapshots or frames). Several performance characteristics of the MM/GBSA have been examined in recent experiments, including the length of MD simulations [246, 247]. The MM/GBSA system is widely used in the measurement of free energy, and it outperforms docking [248]. The MM/GBSA system finds

extensive use in the measurement of free energy, and MM/GBSA produces better performance than docking [249]. For the MM/GBSA tests, eight impact compounds were utilized. The rescoring of ligand-protein interactions was performed using MM/GBSA, which has been shown to be the most accurate technique for rescoring hits after docking in many articles.

5.4 *In Vitro* Studies

5.4.1 Chemicals and Devices

For the measurement the activity of AChE and BuChE enzymes, chemicals used in the present study are listed below in Table 5.1.

Table 5. 1 Chemicals, solutions, and kits used

Name	GAS Number	Company
Acetylcholinesterase from Electrophorus electricus (electric eel)	C3389-500UN	SIGMA
Butyrylcholinesterase from equine serum	C1057-1KU	SIGMA
5, 5'-Dithiobis (2-nitrobenzoi acid) (DTNB)	D21,820-0	ALDRICH
Acetylthiocholine iodide	A5751-5G	SIGMA
S-butyrylthiocholine iodide	B3253-5G	ALDRICH
DimethylSulfoxide(DMSO)	67-68-5	Thermo Scientific
Nelfinavir	A128893-001	AmBeed
Ocaperidone	A367930-002	AmBeed
Risperidone	AALH021148	BioFarma

Devices used in the present study are listed below (Table 5.2):

Table 5. 2 Experimental devices

Name	Company	Series/Code
Multiskan Go Spectrophotometer	ThermoScientific / Japan	51119200
Automatic pipettes	Eppendorf	1.0µl/2.5μl/20μl/200μl/1000μl

5.4.2 Biological Activity Test for Cholinesterase Enzymes

Since we found that 5 out of 10 selected hit compounds show promising binding free energy results at both AChE and BuChE targets, *in vitro* tests were considered for these compounds. Two of the selected compounds (cafedrine and isosulpride) were not considered, that they were too expensive to purchase. Thus, we ordered three identified hits in silico drug repurposing study (i.e., ocaperidone, risperidone, and nelfinavir) from the available small molecule library.

Selected three hit compounds were used in *in vitro* tests against AChE and BuChE targets. The inhibitory activities were calculated according to Ellman's method [250] (Figure 5.2). For this study, donepezil, neostigmine, and rivastigmine, as reference compounds, AChE inhibitors were utilized. The stock solutions for the compounds used in this research were produced via dissolving 1 milligram of each drug in one ml dimethyl sulfoxide (DMSO) to a concentration of 1 mg/ml and then diluting with clean water to get the desired concentrations. The inhibitors' cholinesterase inhibitory activity was determined using six consecutive dilutions. The reaction system consisted of 10–60 μL inhibitor, 200 μL buffer (1 M, pH 8.0: Tris-HCl buffer for the AChE assay and phosphate buffer for the BuChE assay), 50 μL DTNB (0.5 μM), 50 μL acetylthiocholine iodide/S-butyrylthiocholine iodide (10 µM), and 2 μL enzyme (0.28 units μL for the AChE assay and 0.32 units μL for the BuChE assay) (Table 5.3 and 5.4).

The reaction had begun with the addition of the enzyme, and the reaction system was constructed in a quartz cuvette at room temperature. The blank reading

consisted all of substances other than the inhibitor. Within three minutes of initiating the reaction, the absorbance of the reaction mixture at 412 nm was measured using a Thermo Scientific Multiskan GO spectrophotometer (Thermo Fischer Scientific, Japan). Three times within 3 minutes after enzyme application, the absorbance of each reaction mixture was measured, and the findings are expressed as mean standard deviation (SD). Additionally, inhibitory properties such as IC_{50} values are given, which were determined visually using log inhibitor concentration vs percent inhibition (percent%) curves.

As a consequence, the IC_{50} values represent the inhibitor concentration required to block 50% of the enzyme for a certain amount of time was calculated [14, 251, 252]. Figure 5.3 summarizes all of the virtual screening procedures used in this study.

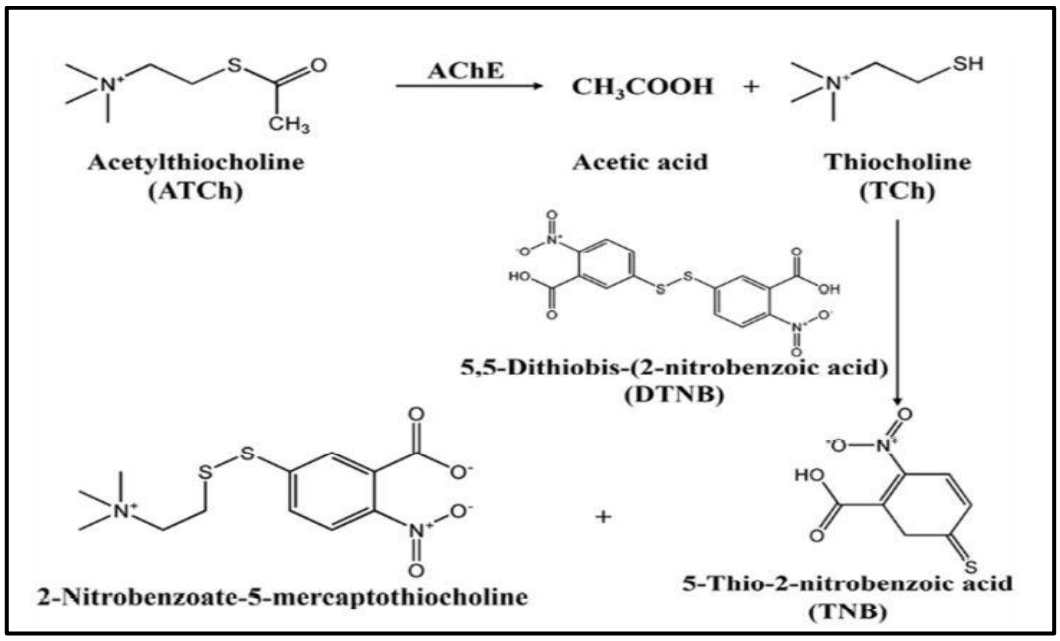

Figure 5. 2 Schematic illustration of the principle of Ellman's method

Table 5. 3 Cuvette ingredient that used for measuring the effect of investigated drugs on esterase activity of AChE

Distilled water µl	Substrate1 µl	Substrate2 µl	Buffer µl	AChE µl	Inhibitor µl	Total volume µl
645	50	50	200	2	0	947
645	50	50	200	2	10	957
645	50	50	200	2	20	967
645	50	50	200	2	30	977
645	50	50	200	2	40	987
645	50	50	200	2	50	997
645	50	50	200	2	60	1007

Table 5. 4 Cuvette ingredient that used for measuring the effect of investigated drugs on esterase activity of BuChE

Distilled water µl	Substrate1 µl	Substrate2 µl	Buffer µl	BuChE µl	Inhibitor µl	Total volume µl
645	50	50	200	2	0	947
645	50	50	200	2	10	957
645	50	50	200	2	20	967
645	50	50	200	2	30	977
645	50	50	200	2	40	987
645	50	50	200	2	50	997
645	50	50	200	2	60	1007

All applied procedure for virtual screening in this study has been summarized in (Figure 5.3).

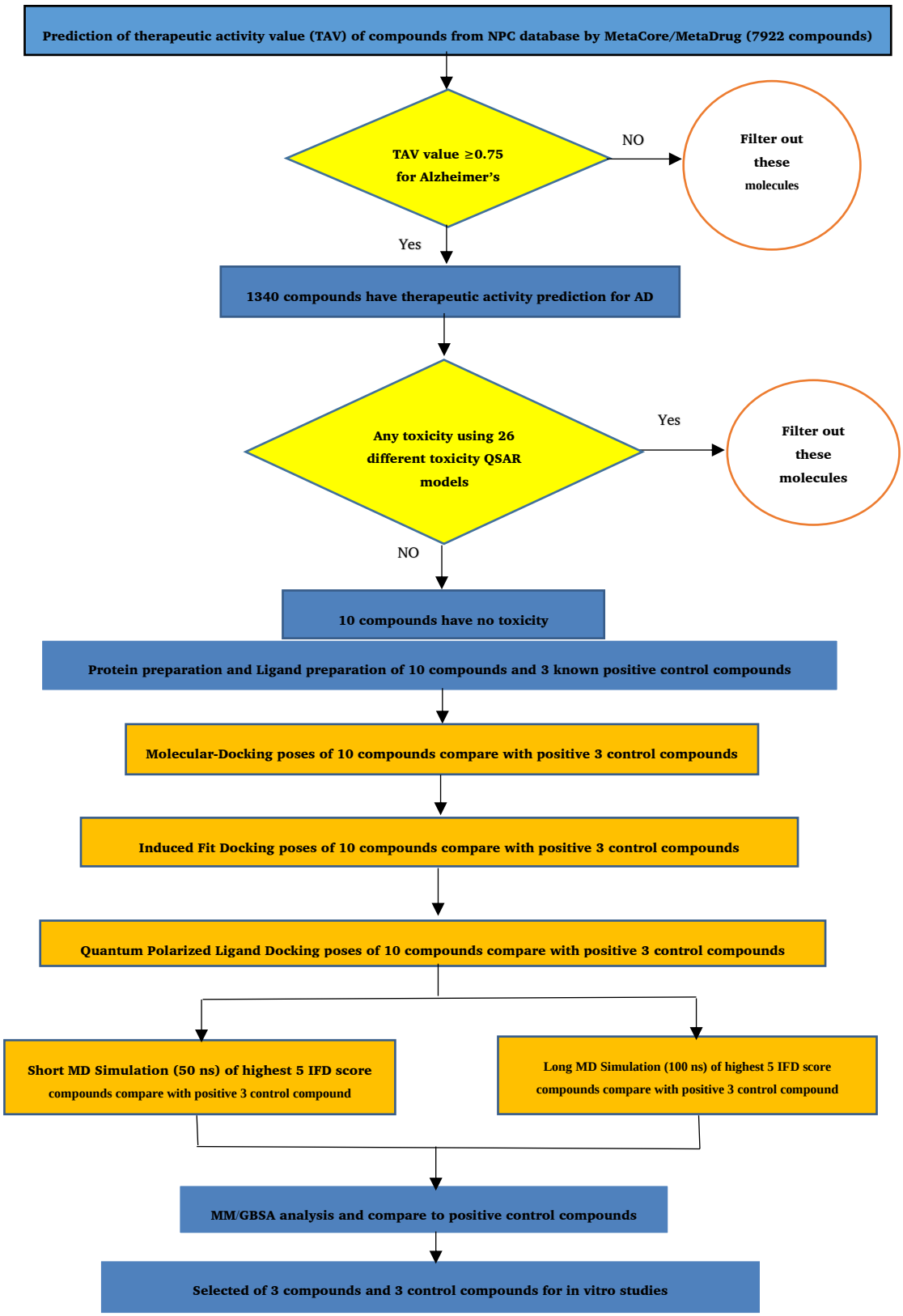

Figure 5. 3 Conducted virtual screening workflow

6

RESULTS AND DISCUSSION

Although the pathophysiology of Alzheimer's disease has not been entirely explained, the reduced rates of acetylcholine and butyrylcholine found in Alzheimer's patients' brains are one of the most significant hypotheses. As a result, inhibiting the enzymes AChE and BuChE, which hydrolyze the neurotransmitters ACh and BuCh, can be used as a therapeutic strategy. Of this cause, the inhibitory function for certain enzymes implicated in Alzheimer's pathogenesis has been studied via several study groupings [13, 252]. Repurposing/repositioning medicines has become more frequent in recent years, since developing new therapies requires time and money. We evaluated substances that have previously been authorized via the FDA as well as compounds that are now undergoing clinical trials in this study. We purchased the NPC small molecule library, which included 7922 compounds [224]. Along with identifying new hit compounds from the FDA-approved small molecule library, our objective was to discover and evaluate small hit ligands with novel scaffolds for AChE and BuChE inhibition.

6.1 *In Silico* Results and Discussion

6.1.1 MetaCore™/MetaDrug™ Analysis

MetaCore™/MetaDrug™ is an integrated software package that is used to predict the pharmacokinetic and toxicity properties of the molecules under investigation using a comprehensive system biology analysis package with the help of existing ADME, disease, and toxicity-QSAR models. After the screening of the NPC database with MetaCore™/MetaDrug™, 1340 compounds where potential therapeutic molecules against Alzheimer's disease have predicted activity values of equal or higher than (0.75). These selected compounds were then subjected to MetaCore™/MetaDrug™ for toxicity test QSAR models in which we observed that only ten compounds pass the 26-different toxicity test, (within these 10 molecules [251], 2 of them was found as approved drugs, nelfinavir used for HIV and

risperidone is a second-generation antipsychotic (SGA) medication). (Table 6.1) shows these selected compounds.

Table 6. 1 MetaCore™/MetaDrug™ predicted therapeutic activity and 2D structure for top ten nontoxic selected molecules against AD

Name	Formula	2D Structure	Prediction of therapeutic activity with AD
Nelfinavir	$C_{32}H_{45}N_3O_4S$	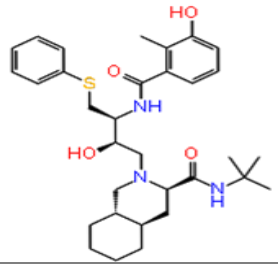	0.89
Montirelin	$C_{17}H_{24}N_6O_4S$	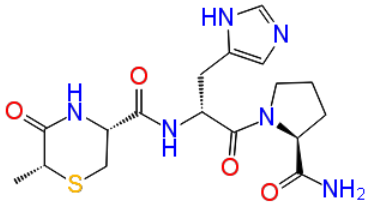	0.88
Tubulozole R 46846	$C_{23}H_{23}Cl_2N_3O_4S$	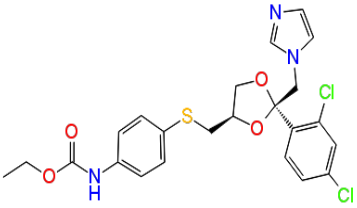	0.88
Zolasartan	$C_{24}H_{20}BrClN_6O_3$	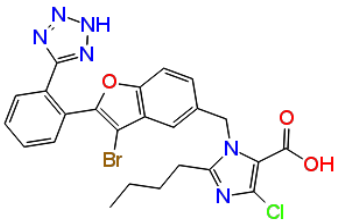	0.82
Risperidone	$C_{23}H_{27}FN_4O_2$	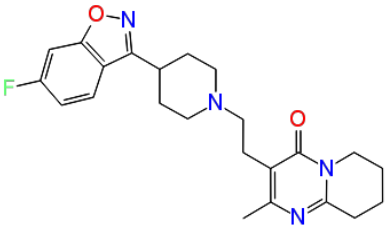	0.82

Table 6. 1 MetaCore™/MetaDrug™ predicted therapeutic activity and 2D structure for top ten nontoxic selected molecules against AD (continued)

Ocaperidone	$C_{24}H_{25}FN_4O_2$	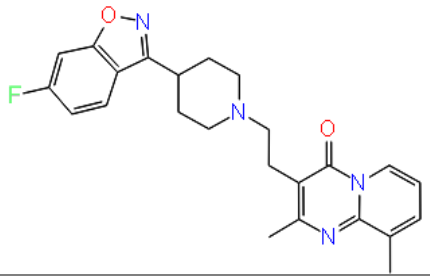	0.81
Podilfen	$C_{18}H_{23}N_3O_2S$	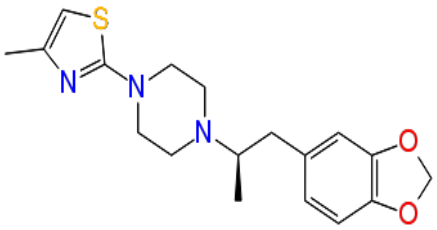	0.78
Mafoprazine	$C_{22}H_{28}FN_3O_3$	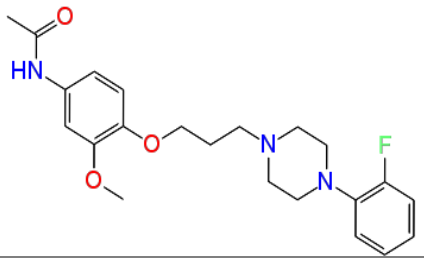	0.77
Isosulpride	$C_{15}H_{23}N_3O_4S$	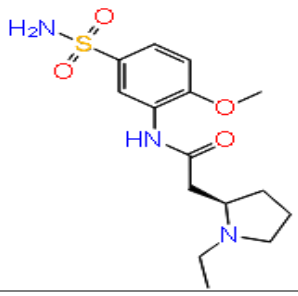	0.76
Cafedrine	$C_{18}H_{23}N_5O_3$	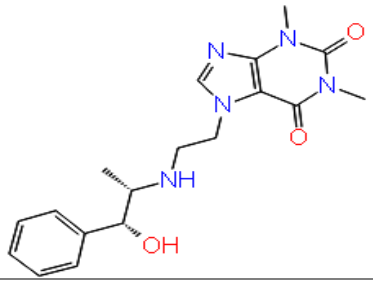	0.76

Note: Potential activity against Alzheimer's disease. Cutoff is 0.5. Values higher than 0.5 indicate potentially active compounds. Training set consists of approved drugs, drug candidates in clinical trials and preclinical compounds with in vivo activity. Model description: Training set N=261, Test set N=44, Sensitivity= 0.91, Specificity=0.82, Accuracy=0.86, MCC=0.73. Reference: Clarivate Analytics.

While (Table 6.2) shows toxicity properties of 5 compounds were studied with 26-different toxicity QSAR models compare with references molecules (donepezil, neostigmine, and rivastigmine). All five compounds did not show any high toxicity risks. Correspondingly the toxicity data for donepezil were found in five models (cardiotoxicity, genotoxicity, liver cholestasis, liver necrosis, and liver weight increase). Table 6.3 compares predicted pharmacokinetic profiles (ADME QSAR and Protein Binding QSAR Models) of five compounds with permitted drugs donepezil, neostigmine and rivastigmine. Three molecules (isosulpride, ocaperidone and risperidone) pass the BBB while 2 molecules (nelfinavir and cafedrine) did not pass comparison with donepezil. The compounds show high Lipophilicity, and they do not obstruct the hERG (human ether a-go-go-related gene) channel. They also show moderate human serum protein binding profiles, while nelfinavir and cafedrine showed lower binding profiles. The calculated criteria are all believed to be pivotal to explore the drug-like properties of these ligands. The data suggested that the ligands can be studied as hit molecules with low side effects in the human body.

Table 6. 2 Prediction of toxicity values using MetaCore™/MetaDrug™ results are compared with positive control molecules

Property	Donepezil	Neostigmine	Rivastigmine	Ocaperidone	Cafedrine	Isosulpride	Risperidone	Nelfinavir
AMES [1]	0.35	0.44	0.42	0.29	0.31	0.29	0.34	0.32
Anemia [2]	0.17	0.29	0.17	0.27	0.13	0.50	0.27	0.23
Carcinogenicity [3]	0.08	0.38	0.33	0.02	0.04	0.27	0.02	0.03
Carcinogenicity Mouse Female [4]	0.11	**0.61**	0.23	0.05	0.08	0.24	0.05	0.06
Carcinogenicity Mouse Male [5]	0.12	**0.61**	0.20	0.04	0.07	0.27	0.05	0.09
Carcinogenicity Rat Female [6]	0.02	**0.72**	0.22	0.02	0.09	0.25	0.02	0.03
Carcinogenicity Rat Male [7]	0.03	**0.81**	0.16	0.08	0.03	0.28	0.05	0.04
Cardiotoxicity [8]	**0.75**	**0.78**	**0.78**	0.15	0.24	0.20	0.15	0.27
Cytotoxicity Model, -log GI50 (M) [9]	5.21	4.88	5.29	4.80	4.94	4.97	4.84	5.85
Epididymis Toxicity [10]	0.04	0.41	0.14	0.05	0.09	0.21	0.05	0.02
Genotoxicity [11]	**0.58**	**0.72**	**0.62**	0.21	0.31	0.44	0.29	0.31
Hepatotoxicity [12]	0.14	**0.78**	0.27	0.18	0.19	0.29	0.18	0.40
Kidney Necrosis [13]	0.06	**0.70**	0.14	0.04	0.15	0.19	0.04	0.15

Table 6. 2 Prediction of toxicity values using MetaCore™/MetaDrug™ results are compared with positive control molecules (continued)

Kidney Weight Gain [14]	0.09	**0.62**	0.19	0.01	0.18	0.09	0.01	0.04
Liver Cholestasis [15]	**0.62**	**0.57**	**0.56**	0.19	0.27	0.41	0.20	0.34
Liver Lipid Accumulation [16]	0.29	**0.57**	0.38	0.21	0.28	0.15	0.25	0.37
Liver Necrosis [17]	**0.78**	**0.97**	0.31	0.24	0.16	0.34	0.27	0.12
Liver Weight Gain [18]	**0.54**	**0.94**	0.35	0.08	0.11	0.14	0.10	0.04
MRTD [19]	0.22	**0.69**	0.37	-0.13	0.34	0.46	0.07	0.39
Nasal Pathology [20]	0.04	**0.37**	0.22	0.06	0.11	0.26	0.06	0.15
Nephron Injury [21]	0.38	**0.79**	0.33	0.07	0.11	0.24	0.04	0.04
Nephrotoxicity [22]	0.12	**0.27**	0.08	0.05	0.23	0.20	0.05	0.27
Neurotoxicity [23]	0.18	**0.92**	0.38	0.10	0.18	0.41	0.14	0.15
Pulmonary Toxicity [24]	0.37	**0.55**	0.46	0.04	0.10	0.18	0.04	0.09
Skin Sens, EC3 [25]	21.85	**3.46**	32.04	42.96	12.56	24.76	34.58	39.15
Testicular Toxicity [26]	0.04	0.48	0.03	0.04	0.08	0.25	0.05	0.05

1. Potential to be mutagenic (AMES positive), range from 0 to 1. A value of 1 is AMES positive (mutagenic), and a value of 0 is AMES negative (non-mutagenic). Cutoff is 0.5. Values close to zero are preferable. The AMES assay is based upon the reversion of mutations in the histidine operon in the bacterium Salmonella enterica vs. Typhimurium.

2. Potential for causing anemia. Cutoff is 0.5. Values higher than 0.5 indicate potentially toxic compounds. Training set consists of chemicals and drugs causing anemia in vivo. Model organisms: human. Model description: Training set N=324, Test set N=51, Sensitivity= 0.82, Specificity=0.90, Accuracy=0.86, MCC=0.72.

3. Potential for inducing carcinogenicity in rats and mice. Cutoff is 0.5. Values higher than 0.5 indicate potentially toxic compounds. Training set consists of chemicals and drugs causing carcinogenicity in vivo. Model organisms: mouse, rat. Model description: Training set N=1210, Test set N=185, Sensitivity= 0.96, Specificity=0.90, Accuracy=0.93, MCC=0.86.

4. Potential for inducing carcinogenicity in female mice. Cutoff is 0.5. Values higher than 0.5 indicate potentially toxic compounds. Training set consists of chemicals and drugs causing carcinogenicity in vivo. Model organisms: female mice. Model description: Training set N=640, Test set N=94, Sensitivity= 0.90, Specificity=0.93, Accuracy=0.92, MCC=0.83.

5. Potential for inducing carcinogenicity in male mice. Cutoff is 0.5. Values higher than 0.5 indicate potentially toxic compounds. Training set consists of chemicals and drugs causing carcinogenicity in vivo. Model organisms: mouse male. Model description: Training set N=584, Test set N=93, Sensitivity= 0.91, Specificity=0.88, Accuracy=0.89, MCC=0.78.

6. Potential for inducing carcinogenicity in female rats. Cutoff is 0.5. Values higher than 0.5 indicate potentially toxic compounds. Training set consists of chemicals and drugs causing carcinogenicity in vivo. Model organisms: female rat. Model description: Training set N=667, Test set N=120, Sensitivity= 0.90, Specificity=0.96, Accuracy=0.93, MCC=0.86.

7. Potential for inducing carcinogenicity in male rats. Cutoff is 0.5. Values higher than 0.5 indicate potentially toxic compounds. Training set consists of chemicals and drugs causing carcinogenicity in vivo. Model organisms: male rat. Model description: Training set N=715, Test set N=117, Sensitivity= 0.92, Specificity=0.88, Accuracy=0.90, MCC=0.79.

8. Potential for inducing cardiotoxicity. Cutoff is 0.5. Values higher than 0.5 indicate potentially toxic compounds. Training set consists of chemicals and drugs causing cardiotoxicity in vivo. Model organisms: mouse, rat, human. Model description: Training set N=143, Test set N=30, Sensitivity= 0.80, Specificity=1.00, Accuracy=0.90, MCC=0.82.

9. Growth inhibition of MCF7 cell line (human caucasian breast adenocarcinoma), pGI50. Cutoff is 6. Values from 6 to 8 correspond to a toxic metabolite, values less than 6 are preferable, values less than 3 are more preferable and less toxic. Model description: N=1474, R2=0.9, RMSE=0.05.

10. Potential for inducing epididymis toxicity. Training set consists of chemicals and drugs causing epididymis toxicity in vivo. Model organisms: mouse, rat, human. Cutoff is 0.5. Values higher than 0.5 indicate potentially toxic compounds. Model description: Training set N=252, Test set N=42, Sensitivity= 0.90, Specificity=0.86, Accuracy=0.88, MCC=0.76.

11. Potential for inducing genotoxicity. Cutoff is 0.5. Values higher than 0.5 indicate potentially toxic compounds. Training set consists of chemicals and drugs causing genotoxicity in vivo. Model organisms: mouse, rat. Model description: Training set N=372, Test set N=86, Sensitivity= 0.75, Specificity=0.84, Accuracy=0.79, MCC=0.59.

12. Potential for inducing hepatotoxicity. Cutoff is 0.5. Values higher than 0.5 indicate potentially toxic compounds. Training set consists of chemicals and drugs causing hepatotoxicity in vivo. Model organisms: mouse, rat, human. Model description: Training set N=1380, Test set N=231, Sensitivity= 0.73, Specificity=0.88, Accuracy=0.81, MCC=0.62.

13. Potential for inducing kidney necrosis. Cutoff is 0.5. Values higher than 0.5 indicate potentially toxic compounds. Training set consists of chemicals and drugs causing renal necrosis in vivo. Model organisms: mouse, rat, human. Model description: Training set N=221, Test set N=42, Sensitivity= 0.96, Specificity=1.00, Accuracy=0.98, MCC=0.95.

14. Potential for inducing kidney weight gain. Cutoff is 0.5. The values higher than 0.5 indicate potentially toxic compounds. Training set consists of chemicals and drugs causing kidney weight gain in vivo. Model organisms: mouse, rat. Model description: Training set N=240, Test set N=49, Sensitivity= 0.95, Specificity=1.00, Accuracy=0.98, MCC=0.96.

15. Potential for inducing liver cholestasis. Cutoff is 0.5. Values higher than 0.5 indicate potentially toxic compounds. Training set consists of chemicals and drugs causing cholestasis in vivo. Model organisms: mouse, rat, human. Model description: Training set N=218, Test set N=35, Sensitivity= 0.79, Specificity=0.67, Accuracy=0.74, MCC=0.46.

16. Potential for inducing liver lipid accumulation. Cutoff is 0.5. Values higher than 0.5 indicate potentially toxic compounds. Training set consists of chemicals and drugs causing lipid accumulation in vivo. Model organisms: mouse, rat, human. Model description: Training set N=172, Test set N=28, Sensitivity= 0.80, Specificity=0.85, Accuracy=0.82, MCC=0.64.

17. Potential for inducing liver necrosis. Cutoff is 0.5. Values higher than 0.5 indicate potentially toxic compounds. Training set consists of chemicals and drugs causing hepatic necrosis in vivo. Model organisms: mouse, rat, human. Model description: Training set N=300, Test set N=57, Sensitivity= 0.91, Specificity=0.91, Accuracy=0.91, MCC=0.82.

18. Potential for inducing liver weight gain. Cutoff is 0.5. Values higher than 0.5 indicate potential liver weight changing compounds. Training set consists of chemicals and drugs causing liver weight gain in vivo. Model organisms: mouse, rat. Model description: Training set N=292, Test set N=52, Sensitivity= 1.00, Specificity=1.00, Accuracy=1.00, MCC=1.00.

19. Maximum Recommended Therapeutic Dose, log mg/kg-bm/day, range is from -5 to 3. Cutoff is 0.5. Chemicals with high log MRTDs can be classified as mildly toxic compounds, chemicals with low log MRTDs as highly toxic compounds. Model description: N=1209, R2= 0.86, RMSE=0.42.

20. Potential for causing nasal pathology. Training set consists of chemicals and drugs causing nasal pathology in vivo. Model organisms: mouse, rat, human. Cutoff is 0.5. Values higher than 0.5 indicate potentially toxic compounds. Model description: Training set N=246, Test set N=47, Sensitivity= 1.00, Specificity=0.93, Accuracy=0.96, MCC=0.92.

21. Potential for inducing nephron injury. Cutoff is 0.5. Values higher than 0.5 indicate potentially toxic compounds. Training set consists of chemicals and drugs causing nephron injury in vivo. Model organisms: mouse, rat, human. Model description: Training set N=598, Test set N=109, Sensitivity= 0.91, Specificity=1.00, Accuracy=0.96, MCC=0.93.

22. Potential for inducing nephrotoxicity. Cutoff is 0.5. Values higher than 0.5 indicate potentially toxic compounds. Training set consists of chemicals and drugs causing nephrotoxicity in vivo. Model organisms: mouse, rat, human. Model description: Training set N=847, Test set N=154, Sensitivity= 0.90, Specificity=0.84, Accuracy=0.87, MCC=0.74.

23. Potential for inducing neurotoxicity. Training set consists of chemicals and drugs causing neurotoxicity in vivo. Model organisms: mouse, rat, human. Cutoff is 0.5. Values higher than 0.5 indicate potentially toxic compounds. Model description: Training set N=175, Test set N=34, Sensitivity= 0.94, Specificity=0.94, Accuracy=0.94, MCC=0.88.

24. Potential for inducing pulmonary toxicity. Training set consists of chemicals and drugs causing pulmonary toxicity in vivo. Model organisms: mouse, rat, human. Cutoff is 0.5. Values higher than 0.5 indicate potentially toxic compounds. Model description: Training set N=482, Test set N=87, Sensitivity= 0.89, Specificity=0.88, Accuracy=0.89, MCC=0.77.

25. Skin sensitization potential expressed as effective concentration 3, EC3 %. Values higher than 10 indicate weak and moderate sensitizers. Model description: N=89, R2=0.67, RMSE=22.56.

26. It consists of chemicals and drugs causing testicular toxicity in vivo. Model organisms: mouse, rat, human. Cutoff is 0.5. Values higher than 0.5 indicate potentially toxic compounds. Model description: Training set N=439, Test set N=88, Sensitivity= 0.81, Specificity=0.85, Accuracy=0.83, MCC=0.66.

Table 6. 3 ADME-QSAR and protein binding QSAR models predictions using MetaCoreTM/MetaDrugTM Results are compared with positive control molecules

Property	Donepezil	Neostigmine	Rivastigmine	Ocaperidone	Cafedrine	Isosulpride	Risperidone	Nelfinavir
BBB, log ratio (1)	0.05	0.17	0.22	0.01	-0.57	0.05	-0.02	-0.50
G-LogP (2)	4.10	-2.29	1.81	4.23	1.12	2.36	3.78	2.38
Prot-bind, % (3)	79.13	39.00	45.45	91.39	43.76	65.44	90.93	85.23
Prot-bind, Log t (4)	0.24	-0.44	-0.12	0.23	-0.26	0.01	0.22	-0.06
W Sol, log mg/L (5)	1.03	4.19	2.83	1.5	2.71	2.48	1.48	1.83
hERG-inh, pKi (6)	0.42	-0.51	-0.42	0.01	-0.07	-0.05	-0.05	0.01

1. Blood brain barrier penetration model. The data is expressed as log values of the ratio of the metabolite concentrations in brain and plasma. Cutoff is -0.3. Larger values indicate that the metabolite is more likely to enter the brain. Model description: N=107, R2=0.89, RMSE=0.26.

2. Lipophilicity, log of compound octanol water distribution. Cutoffs are -0.4 to 5.6. Values greater than 5.6 correspond to overly hydrophobic compounds. Model description: N=13474, R2=0.95, RMSE=0.21.

3. Human serum protein binding, %. Cutoff is 50%. A value of more than 95% is highly bound, less than 50% is a low binding metabolite. Model description: N=265, R2=0.909, RMSE=10.11.

4. Affinity to human serum albumin, log value of the retention time. Cutoff is 0. Positive values correspond to higher protein binding, negative values to lower protein binding. The model is based on retention times of compounds assayed by HPLC using an immobilized HSA column. Values are expressed as log values of the retention time. Model description: N=95, R2=0.904, RMSE=0.2.

5. Water solubility at 25°C, log mg/L. Cutoffs are from 2 to 4. An acceptable level of solubility is project dependent. Model description: N=2871, R2=0.91, RMSE=0.54.

6. Human hERG (human ether a-go-go-related gene) channel inhibition, pKi (uM). Cutoff is -1.7. The higher the value, the higher the inhibition activity. Lower values are preferable. Model description: N=196, R2=0.93, RMSE=0.23.

6.1.2 Ligand Binding Domain Analysis and MM/GBSA Results

Ten bioactive and nontoxic compounds were collected to identify the potential ligand-bound poses of implied AChE and BuChE inhibitors. Three-dimensional structures were created using these chemicals (using the Ligand Preparation module of the Maestro molecular modeling package). After ligand synthesis, the total number of compounds reached 120 due to the stereochemistry, tautomer, and different protonation states of the studied ligands. These ligands were docked using three different molecular docking techniques, Glide/SP, Glide/IFD, and QPLD, to determine the potential AChE and BuChE inhibitors' likely ligand binding poses, and the top docking poses of five molecules with higher scores than the reference molecules were presented in (Table 6.4).

We examined the lowest binding energies (kcal/mol) of 120 AChE and BuChE complex ligands, as well as chemical interactions with known key binding pocket amino acids of enzymes. When five compounds' top docking postures were compared to the reference molecule, the top docking postures scored higher. In this section, we examined Glide/IFD. Donepezil's lowest binding G score indicates stronger binding interactions with AChE, while nelfinavir was shown to be the most effective inhibitor of BuChE. Additionally, the investigated compounds' ligand efficiency scores (LIE) are shown (ligand efficiency: GlideScore/number of heavy atoms). Rather than considering the affinity of the entire compound, it was recommended to consider the affinity of the heavy atoms in a molecule and to coin the term ligand efficiency (the average affinity contribution per atom is considered) in order to avoid affinity-based selection and optimization toward larger ligands. This enables the comparison of the affinity of molecules that have been adjusted for their size. In this instance, we calculated ligand efficiency scores using Glide/IFD scores. The isosulpride molecule exhibited the greatest LIE values in both AChE and BuChE (-0.747 and -0.487, respectively).

Table 6. 4 Glide SP, IFD, QPLD and ligand efficiency of selected 10 molecules and references compounds with AChE and BuChE

Molecules Names	AChE				BuChE			
	Glide/SP Kcal/mol	Glide/IFD Kcal/mol	QPLD Kcal/mol	Ligand Efficiency	Glide/SP Kcal/mol	Glide/IFD Kcal/mol	QPLD Kcal/mol	Ligand Efficiency
Donepezil	-14.101	-18.645	-19.797	-0.665	-7.882	-11.712	-9.962	-0.418
Ocaperidone	-12.312	-17.763	-15.260	-0.573	-8.722	-10.704	-8.719	-0.345
Cafedrine	-12.370	-17.593	-16.489	-0.676	-8.806	-9.266	-8.440	-0.356
Isosulpride	-11.202	-17.203	-15.207	-0.747	-7.603	-11.205	-8.997	-0.487
Risperidone	-10.225	-17.043	-17.253	-0.568	-8.938	-11.484	-9.113	-0.383
Nelfinavir	-9.773	-12.601	-11.783	-0.315	-9.801	-13.424	-10.757	-0.336
Tubulozole	-7.210	-12.372	-8.902	-0.375	-6.479	-9.232	-8.002	-0.280
Zolasartan	-5.116	-11.347	-6.075	-0.324	-7.059	-8.417	-8.518	-0.240
Montirelin	-6.051	-10.933	-8.822	-0.390	-7.896	-9.823	-8.458	-0.351
Podilfen	-9.098	-11.134	-9.312	-0.464	-7.160	-9.156	-7.465	-0.381
Mafoprazine	-7.791	-9.378	-9.731	-0.323	-6.703	-8.947	-8.455	-0.308
Neostigmine	-8.839	-12.029	-12.631	-0.752	-6.120	-6.371	-7.250	-0.400
Rivastigmine	-8.538	-10.980	-11.536	-0.610	-5.421	-6.566	-6.415	-0.365

The structure of AChE-ligand complexes determined via IFD computations was subjected to short (50-ns) and long (100-ns) molecular dynamics (MD) simulations to determine their structural stability on the nanosecond time scale. We assessed the 50-ns simulation and MM/GBSA techniques for five ligands and compared the findings to those obtained from reference medications, followed via 100-ns MD simulations on the hit compounds (Table 6.5). When average MM/GBSA scores were compared, cafedrine and risperidone were found to be the most potent ones, for AChE, while cafedrine and nelfinavir for BuChE, respectively. However, when ligand efficiency scores were evaluated, cafedrine and nelfinavir were found to be the most potent ones for AChE and BuChE, respectively. Using MM/GBSA, the free binding energies were recalculated (Figure 6.1, 6.2, 6.5 and 6.6). Consequently, the five hits found have comparable or even better average MM/GBSA scores than the FDA known drugs.

Average MM/GBSA calculations in 50-ns and 100-ns with standard deviation, maximum and minimum values are given in Table 6.6 and 6.7, respectively. These values were used to construct a Box and Whisker plot of MM/GBSA scores that can be seen in (Figures 6.3, 6.4, 6.7, and 6.8). Outliers are given as dots above and below the average boxes. Among all hit compounds, cafedrine has the lowest average MM/GBSA score Through short and long simulations (-102.60 kcal/mol and -99.940 kcal/mol) for AChE and (-105.95 kcal/mol and -99.852 kcal/mol) for BuChE, respectively.

Table 6. 5 MM/GBSA scores for the 50 and 100 ns simulations and the averages of the studied ligands

Molecules Names	AChE		BuChE	
	MM/GBSA ΔG Kcal/mol	Ligand Efficiency Score	MM/GBSA ΔG Kcal/mol	Ligand Efficiency Score
Donepezil 50-ns	-79.196	-2.828	-78.126	-2.790
Donepezil 100-ns	-81.122	-2.900	-70.153	-2.505
Average	**-80.159**	**-2.864**	**-74.140**	**-2.647**
Ocaperidone 50-ns	-79.178	-2.045	-65.842	-2.124
Ocaperidone 100-ns	-80.614	-2.600	-63.203	-2.038
Average	**-79.896**	**-2.322**	**-64.522**	**-2.079**
Cafedrine 50-ns	-89.031	-3.424	-91.314	-3.512
Cafedrine 100-ns	-83.570	-3.214	-70.674	-2.720
Average	**-86.300**	**-3.319**	**-80.994**	**-3.116**
Isosulpride 50-ns	-60.021	-2.610	-57.466	-2.500
Isosulpride 100-ns	-64.815	-2.818	-60.542	-2.632
Average	**-62.418**	**-2.714**	**-59.004**	**-2.566**
Risperidone 50-ns	-86.920	-2.900	-69.652	-2.322
Risperidone 100-ns	-86.653	-2.888	-74.535	-2.485
Average	**-86.786**	**-2.894**	**-72.100**	**-2.402**
Nelfinavir 50-ns	-65.533	-1.632	-75.417	-1.885
Nelfinavir 100-ns	-71.043	-1.776	-72.933	-1.823
Average	**-68.288**	**-1.704**	**-74.175**	**-1.854**
Neostigmine 50-ns	-53.393	-3.337	-42.788	-2.674
Neostigmine 100-ns	-58.926	-3.683	-36.931	-2.308
Average	**-56.160**	**-3.510**	**-39.860**	**-2.491**
Rivastigmine 50-ns	-54.480	-3.026	-48.423	-2.690
Rivastigmine 100-ns	-59.182	-3.285	-49.101	-2.720
Average	**-56.831**	**-3.155**	**-48.762**	**-2.705**

Table 6. 6 Average MM/GBSA calculations in 50-ns with standard deviation, maximum and minimum values for AChE and BuChE

Molecules Names	AChE			BuChE		
	MM/GBSA ± STDEV (kcal/mol)	Max. MM/GBSA	Min. MM/GBSA	MM/GBSA ± STDEV (Kcal/mol)	Max. MM/GBSA	Min. MM/GBSA
Donepezil	-79.196 ± 4.698	-66.406	-87.051	-78.126 ± 9.538	-54.370	-95.224
Ocaperidone	-79.178 ± 5.614	-69.340	-94.242	-65.842 ± 8.531	-53.011	-93.266
Cafedrine	-89.031 ± 7,290	-71.908	-102.60	-91.314 ± 7.477	-70.716	-105.95
Isosulpride	-60.021 ± 4.462	-46.909	-70.030	-57.466 ± 5.775	-42.662	-70.957
Risperidone	-86.920 ± 3.545	-78.126	-94.388	-69.652 ± 6.452	-58.165	-88.801
Nelfinavir	-65.533 ±11.936	-36.562	-98.106	-75.417 ± 9.049	-54.621	-97.772
Neostigmine	-53.393 ± 3.164	-47.665	-64.906	-42.788 ± 2.545	-34.966	-48.858
Rivastigmine	-54.480 ± 3.419	-47.590	-62.655	-48.423 ± 4.425	-35.053	-59.046

Table 6. 7 Average MM/GBSA calculations in 100-ns with standard deviation, maximum and minimum values for AChE and BuChE

Molecules Names	AChE			BuChE		
	MM/GBSA ± STDEV (kcal/mol)	Max. MM/GBSA	Min. MM/GBSA	MM/GBSA ± STDEV (Kcal/mol)	Max. MM/GBSA	Min. MM/GBSA
Donepezil	-81.122 ± 6.900	-59.512	-93.272	-70.153 ± 13.115	-49.301	-98.734
Ocaperidone	-80.614 ± 5.135	-66.400	-91.232	-63.203 ± 6.541	-51.787	-91.482
Cafedrine	-83.570 ± 6.407	-59.462	-99.940	-70.674 ± 7.268	-52.340	-99.852
Isosulpride	-64.815 ± 9.021	-42.720	-82.872	-60.542 ± 5.219	-45.427	-76.057
Risperidone	-86.653 ± 5.536	-66.800	-98.991	-74.535 ± 6.872	-59.044	-92.526
Nelfinavir	-71.043 ± 10.344	-44.330	-91.050	-72.933 ± 4.687	-59.612	-86.276
Neostigmine	-58.926 ± 5.514	-38.487	-69.891	-36.931 ± 4.223	-25.406	-51.049
Rivastigmine	-59.182 ± 5.604	-46.250	-72.230	-49.101 ± 4.825	-32.216	-61.064

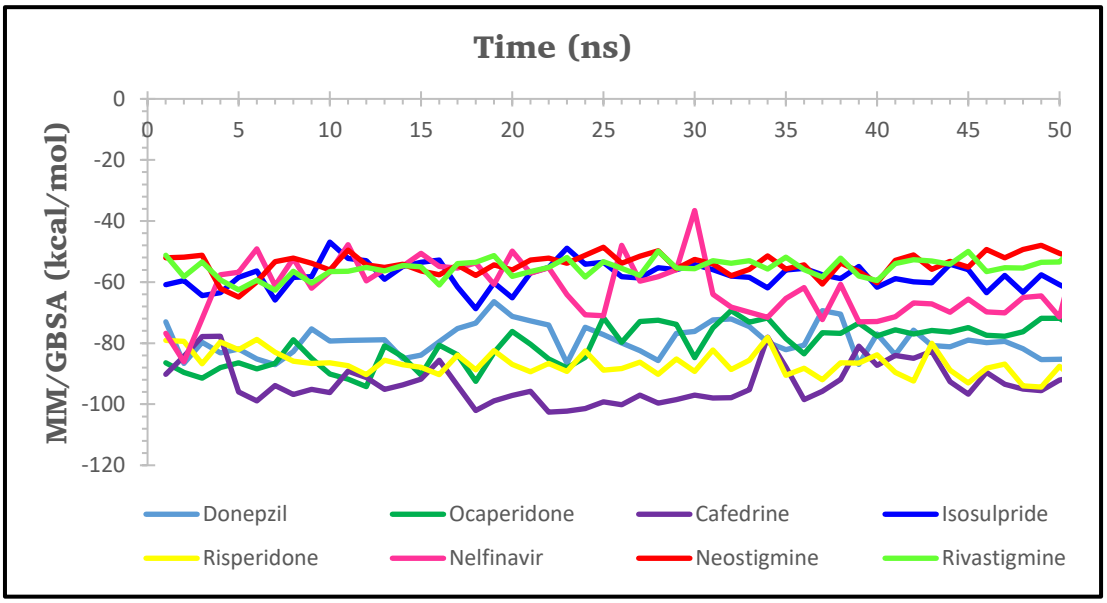

Figure 6. 1 MM/GBSA free energy analysis of the studied molecules at the AChE binding pocket in the entire 50-ns MD simulation (MM/GBSA binding energy value in kcal/mol)

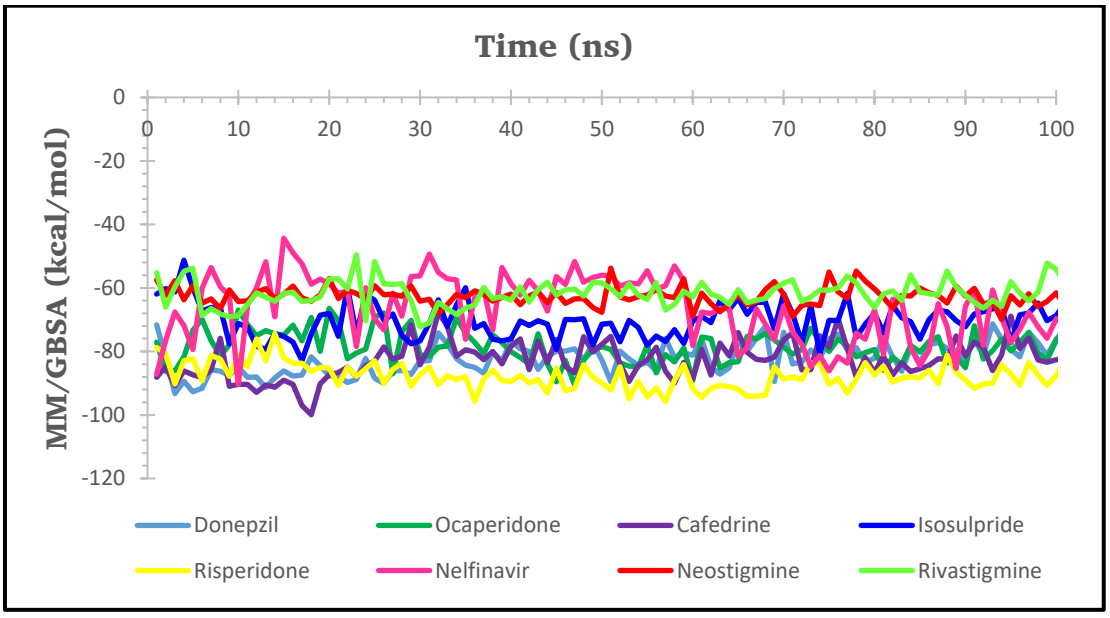

Figure 6. 2 MM/GBSA free energy analysis of the studied molecules at the AChE binding pocket in the entire 100-ns MD simulation (MM/GBSA binding energy value in kcal/mol)

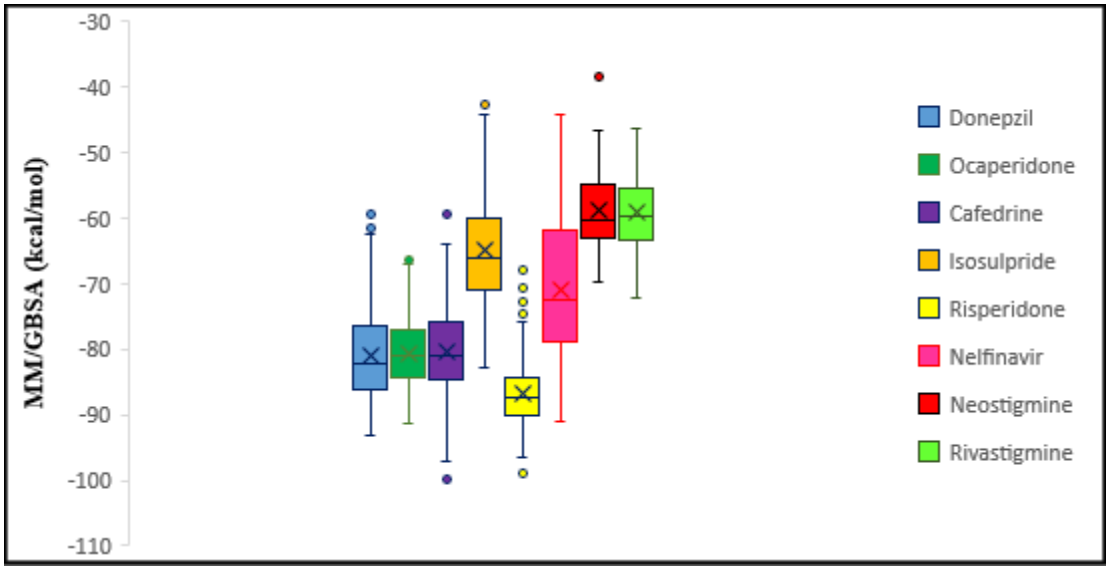

Figure 6. 3 Box and Whisker plot of AChE average MM/GBSA for 5 hit compounds and 3 references compounds for 50-ns

For the 50-ns MM/GBSA results, the biggest interquartile range was observed for the Nelfinavir, with two minimum outliers, and the smallest interquartile range, again with the two minimum outliers was observed in neostigmine.

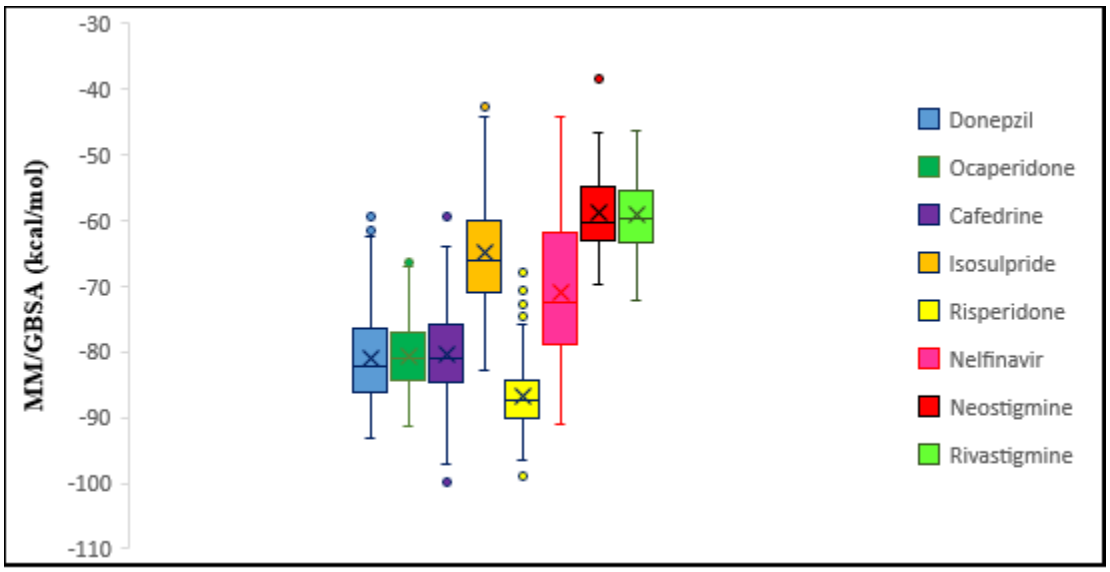

Figure 6. 4 Box and Whisker plot of AChE average MM/GBSA for 5 hit compounds and 3 references compounds for 100-ns

For the 100-ns MM/GBSA results, the biggest interquartile range was observed in nelfinavir. Interestingly, only nelfinavir and rivastigmine do not have any outliers compared to the other drugs. The smallest interquartile range was observed in risperidone with four maximums and one minimum outliers.

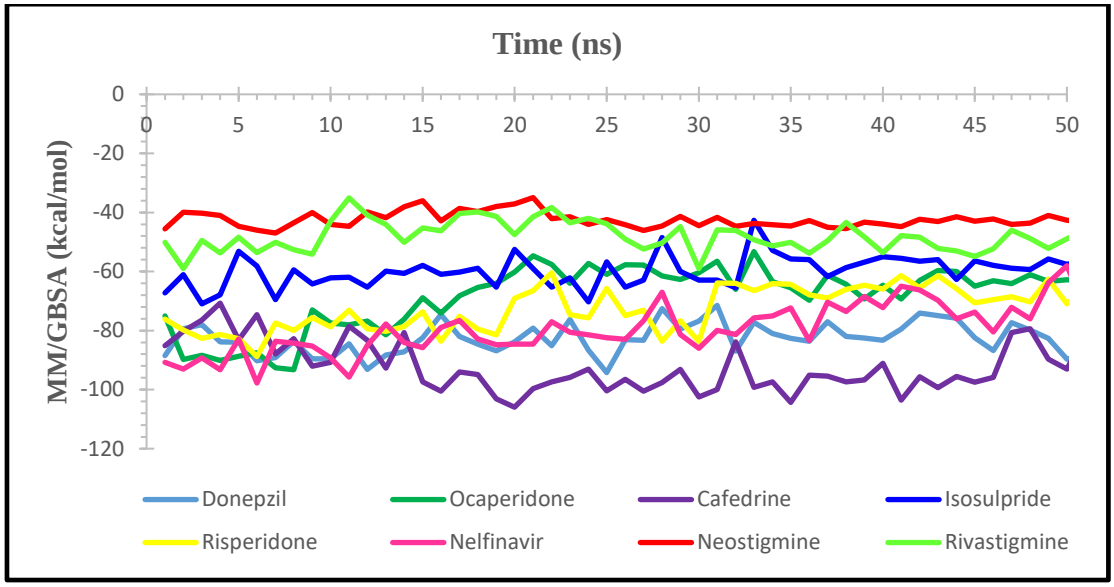

Figure 6. 5 MM/GBSA free energy analysis of the studied molecules at the BuChE binding pocket in the entire 50-ns MD simulation (MM/GBSA binding energy value in kcal/mol)

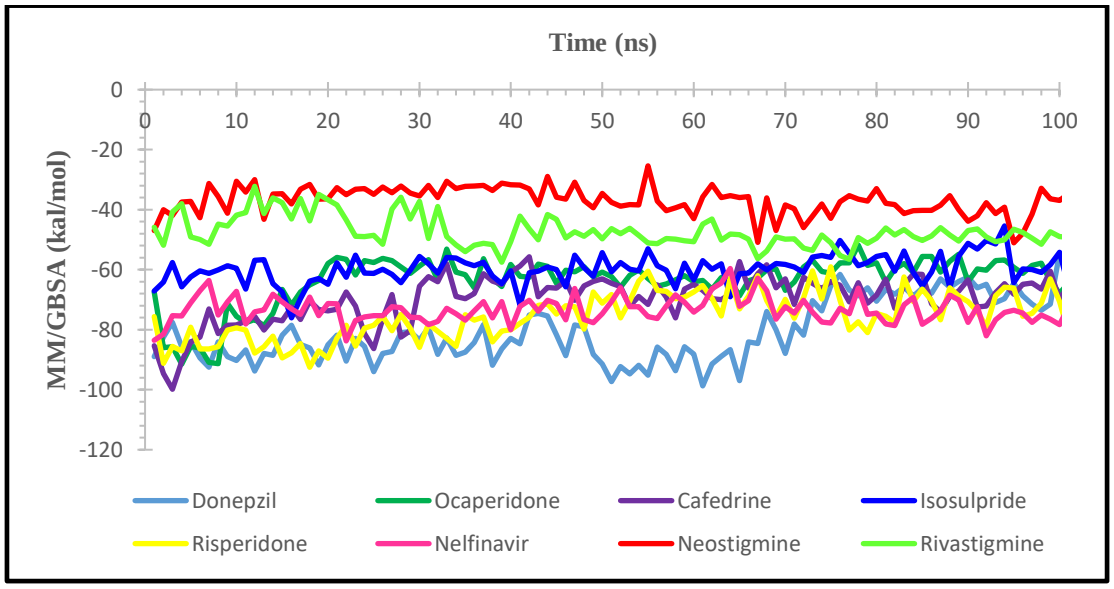

Figure 6. 6 MM/GBSA free energy analysis of the studied molecules at the BuChE binding pocket in the entire 100-ns MD simulation (MM/GBSA binding energy value in kcal/mol)

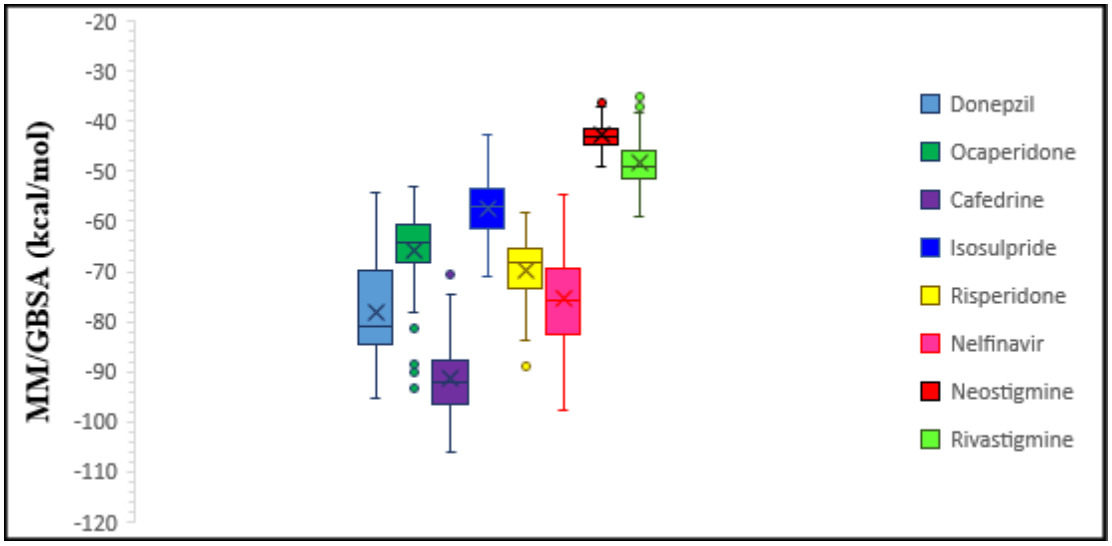

Figure 6. 7 Box and Whisker plot of BuChE average MM/GBSA for 5 hit compounds and 3 references compounds for 50-ns

For the BuChE 50-ns MM/GBSA scores, the biggest interquartile range was observed for the Donepezil with no outliers. The smallest interquartile range was observed for the neostigmine, with two maximum outliers.

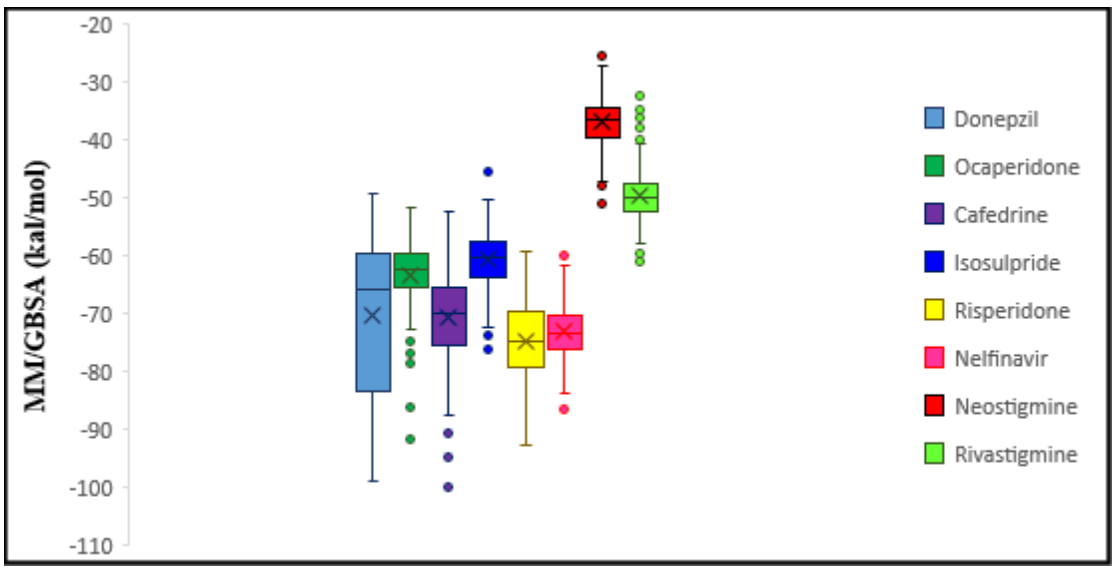

Figure 6. 8 Box and Whisker plot of BuChE average MM/GBSA for 5 hit compounds and 3 references compounds for 100-ns

For the 100-ns BuChE MM/GBSA scores, the biggest interquartile range was observed for the Donepezil with no outliers similarly as observed in 50-ns trajectory. The smallest interquartile range was observed for the rivastigmine with 5 maximums and 2 minimum outliers.

Protein-ligand complexes are stabilized via intermolecular hydrogen bonding and non-polar interactions between the protein and the investigated molecules. Figures 6.9 to 6.40 show 2D ligand interaction diagrams of top IF docking poses of 5 hit compounds and well-known inhibitors at the binding pocket of AChE and BuChE, as well as average interaction fractions and a timeline representation of contact residue interactions throughout MD simulations. All five compounds interact with AChE active site residues, including ASP74, TRP86, TRP286, PHE295, TYR337, and PHE338, as well as BuChE active site residues like TRP82, GLH197, PHE329, and TYR332. The protein-ligand complexes are stabilized via intermolecular hydrogen bonding and nonpolar interactions between the protein (enzyme) and the studied molecules. In IFD ligand interactions and MM/GBSA averages represent of top-docking poses of compounds ocaperidone, cafedrine and risperidone in addition well-known inhibitors at the binding pocket of AChE.

In IF docking of donepezil with AChE (Figure 6.9), Piperidine nitrogen of the donepezil formed three pi-cation interactions with TRP86, TYR337, and PHE338. Also, TRP86 contributed to binding of donepezil with 2 more hydrophobic interactions (pi-pi stacking) with the phenyl ring of the inhibitor. Through MD simulations, the interactions between TRP86 and donepezil conserved over 92% and 83% with short and long simulations. Similarly, the pi-cation interactions with the Piperidine nitrogen and side chains of the TYR337 and PHE338, were consumed (97% and 58%, respectively). ASP74 formed a salt bridge interaction with Piperidine nitrogen of the donepezil. Carboxy group of indanone ring of the donepezil formed a hydrogen bond with PHE295 (consumed over 63% and 41% through the 50-ns and 100-ns MD trajectory respectively), another hydrogen interaction bond was not observed in the docking formed via water bridge and expended 82% of the trajectory frames between nitrogen of the Piperidine ring of the donepezil and TYR341 through 100-ns simulations. Aromatic ring of the indanone interacted with side chain of the TRP286. Moreover, methoxy group of the donepezil was interacted with around water molecule.

In IFD ligand interactions and MM/GBSA averages represent of top-docking poses of compounds cafedrine, risperidone and nelfinavir beside well-known inhibitors at the binding pocket of BuChE. In IF docking of donepezil with BuChE (Figure 6.11), 2 pi-pi stacking interactions between the side chains of the TRP82 and TYR332 and the phenyl ring of the donepezil. However, TRP82 changed their interaction through simulations and formed pi-cation with the nitrogen of the Piperidine ring, which consumed (91% and 82%) of the trajectory frames through short and simulations, respectively. Similar to the docking interactions of the donepezil in AChE, nitrogen of the Piperidine ring of the donepezil, formed 2 pi-cation interactions with the side chains of the PHE329 and TYR332. Through MD simulations, we didn't recognize any interaction with TYR332, however PHE329 was conserved more than half of the trajectory frames through 50-ns simulation (54%) and about (43%) through 100-ns. One of the methoxy group of the indanone ring of the donepezil, formed hydrogen bond with GLU197. Carboxy group of the indanone ring formed another hydrogen bond via water bridge interaction with the 2 Glycine residues around, namely GLY116 and GLY117.

Other interactions that observed in molecular docking pose were lost through the MD simulations (note that if the interactions were not conserved over 20% of the trajectory frames, we did not take these interactions into account as essential interactions). 2 new hydrogen bond interactions were established between methoxy groups of the indanone ring of the donepezil and TYR128, and these 2 newly established interactions were conserved 47% and 61% through 50-ns. Whilst through 100-ns simulations, 2 hydrogen bond interactions were established between methoxy groups of the indanone ring and TYR128 and GLY115, and both of them depleted 31% of the trajectory frames. Another new hydrogen bond via water bridge was formed between ALA328 and nitrogen atom of Piperidine in the donepezil and consumed (46% and 37%) through short and long simulations, respectively.

The average interaction percentages of the contact residues diagram and a timeline depicting interactions and contacts (H-bonds, hydrophobic, ionic, and water bridges) through MD simulations of donepezil in the binding pocket of AChE

and BuChE are shown in Figures 6.10 and 6.12. The top panel displays the total number of unique interactions the protein has with the ligand, while the bottom panel displays which residues interact with the ligand throughout the simulations. Numerous residues allow for several direct contacts with the ligand, indicated on the map via a richer orange hue, according to the scale to the right of the picture. Donepezil constructs critical chemical interactions with residues TRP86, TRP286, TYR337, PHE338 and TYR341 which are stable throughout the simulation time. At the BuChE, TRP82, TYR128, ALA328, and PHE329 have corresponding interactions. Figures are also given for interactions that occur more than 30.0% of the time through the simulation.

Figure 6.13 represents the average interaction percentages of the contact residues diagram and a temporal depiction of interactions and contacts (H-bonds, hydrophobic, ionic, and water bridges) through MD simulations of ocaperidone in the AChE binding pocket. Ocaperidone constructs critical chemical interactions with residues TRP86, TYR337 and TYR341 which are stable throughout the simulation time. In IF docking of ocaperidone with AChE (Figure 6.13), TRP86 formed 2 pi-pi stacking interactions with benzoxazole of the inhibitor. Piperidine nitrogen of ocaperidone contributed to binding via three pi-cation interactions with TYR337, PHE338 and TYR341. ASP74 formed a salt bridge interaction with the nitrogen of Piperidine. Carboxy group of the pyrimidine ring of inhibitor formed a hydrogen bond with PHE295. Furthermore, one interaction formed via water molecule between TYR72 and the nitrogen of pyrimidine. Through molecular dynamics (MD) simulations (Figure 6.14), the interactions between TRP86 and benzoxazole ring of ocaperidone depleted 77% and 60% Through the 50 and 100-ns MD trajectory. TYR341 has formed 2 interactions, pi-cation with the Piperidine nitrogen which conserved 54% and 58% Through short and long simulation, the other pi-pi stacking with the pyrimidine that consumed 46% (this interaction that was not observed in the IFD docking). Another interaction that was not observed in the IF docking was formed between benzoxazole of ocaperidone and TYR337, which depleted 64% of the 50-ns trajectory frames. Hydrogen interaction bonds were observed in 100-ns MD simulation formed via

water bridge and expended 56% and 32% of the trajectory frames between PHE295 and SER125 with ocaperidone. Three new interactions were seen between ocaperidone and AChE Through long simulation TYR124(43%), TRP286(31%) and HIS447(31%).

In IF docking of cafedrine with AChE (Figure 6.17), TRP86 contributed to binding with hydrophobic interactions (pi-pi stacking) with the phenyl ring of the inhibitor (consumed 72%, 43% Through short and long simulations respectively). A new interaction between TRP86 and nitrogen of amine was observed and consumed 73% of the trajectory through 50-ns simulation (this interaction was not observed through IFD and long simulation). Nitrogen of amine in the cafedrine formed three pi-cation interactions through IFD with TYR337, PHE338 and TYR341. TYR337(60%, 76%) and TYR341 (63%, 82%) consumed through short and long simulations. PHE338 made a new interaction through 50-ns simulation with phenyl ring and expended 30% of the trajectory (we didn't recognize this interaction through IFD and long simulation). Purine ring of cafedrine formed three pi-pi stacking with TYR124, TRP286 and TYR341 through IFD. We didn't see all these interactions through simulation just TRP286 (31% of the trajectory through 50-ns) and TYR341(78% Through 100-ns). Carboxy group of purine ring of the cafedrine formed a hydrogen bond with PHE295, we were observed in the simulations this interaction formed via water bridge and expended of the trajectory frames (81% and 75%) through short and long simulations, respectively.

New interaction was observed between ASP74 and hydroxyl group of cafedrine through 50-ns simulations and consumed (38%). Furthermore, methoxy group and nitrogen of purine ring were interacted with around water molecules in IFD. Many hydrogen interaction bonds were observed in the simulations formed via water bridge and expended of the trajectory frames between water molecule (38%), ASP74 (47%) and ARG296 (44%) through 50-ns simulations, while through 100-ns, we recognized ASP74 (57% and 41%).

Through the IFD of the cafedrine with BuChE (Figure 6.19), three pi-pi stacking interactions between the TRP82 and purine ring of the ligand. These interactions

were reduced through 50-ns to one pi-pi stacking (68%), and 2 pi-pi interactions in 100-ns consumed (32% and 65%) of the trajectory frames. New pi-cation interaction was observed between TRP82 and nitrogen of amine through 100-ns (43%). Another 2 pi-pi stacking were seen through IFD among TRP231 and PHE329 with phenyl ring of cafedrine. This interaction was present through 50-ns and consumed (39% and 59%) of the trajectory (we lost these interactions in 100-ns). ASP70 being 2 different interactions with the nitrogen of amine in the ligand, in IFD formed a salt bridge and converted to hydrogen bond interaction Through 50-ns and consumed (40%) of the frame.

Two hydrogen bond interactions were observed between ligand and side-chain residues through IF docking and 50-ns simulation, the first PRO285 with the hydroxyl group of propan which depleted (97%) of the frame, second GLU197 with the carboxy group of purine cleanout (87%) from the trajectory. Moreover, through IFD, methoxy group of purine ring in cafedrine was interacted with around water molecule. New pi-cation interaction was observed through short and long simulations (we didn't catch in IFD) between TYR332 and the nitrogen of amine group, depleted (77% and 79%), respectively. Cafedrine via itself formed a hydrogen bond between the amine group's nitrogen and carboxy of purine ring Through 50-ns and 100-ns, which cleanout (74% and 35%) of the trajectory, respectively. Figures 6.18 and 6.20 show a schematic showing average interaction percentages of contact residues and a timeline description of interactions and contacts (H-bonds, hydrophobic, ionic, and water bridges) Through simulations of cafedrine at the binding pocket of AChE and BuChE. Cafedrine constructs critical chemical interactions with residues ASP74, TRP86, PHE295, TYR337, PHE338 and TYR341 which are stable throughout the simulation time. Corresponding interactions at BuChE were constructed with TRP82, GLU197, PHE329, and TYR332. Figures represent interactions that occur more than 30.0% of the time through the simulation.

In IF docking of risperidone with AChE (Figure 6.25), TRP86 formed three pi-pi stacking interactions with benzoxazole of the molecule. We didn't recognize this interaction Through 50-ns simulation but it observed Through long simulation

with pyrimidine ring and consumed 88% of the trajectory. Piperidine nitrogen of risperidone contributed to binding via three pi-cation interactions with TYR337, PHE338 and TYR341. Pi-pi stacking interaction of TYR341 with pyrimidine ring of molecule also observed. Through MD simulations, we observed that TYR337 made 2 interactions consumed through 50-ns (84% and 98%) and with 100-ns (36% and 94%) from the trajectory. TYR341 has showed interaction through short and long simulations (77% and 68%) respectively. Carboxy group of the pyrimidine ring of inhibitor formed a hydrogen bond with PHE295. Also, through simulations, we recognized the interaction between PHE295 and the oxygen of benzoxazole of risperidone, which consumed (60% and 71%). One hydrogen bond interaction formed via water molecule between TYR124 and the nitrogen of benzoxazole of the molecule. Four hydrogen interaction bonds were observed through 50-ns simulations formed via water bridge and expended of the trajectory frames between GLY82(47%), GLY121(43%), GLY122(56%) and SER203(61%), while through 100-ns, we recognized one bridge of water with SER125(30%). 2 new interactions were observed between risperidone and AChE through short and long simulation, ASP74(49% and 55%) and ARG296(52% and 30%).

In molecular docking of risperidone with BuChE (Figure 6.27), 2 pi-pi stacking interaction between the side chain of TRP430 and ring of benzoxazole was formed. The docking interaction of the nitrogen of Piperidine ring of the inhibitor formed pi-cation interactions with the side chains of the TRP82 and formed a salt bridge interaction with ASP70. Through long simulationsTRP82 changed their interaction (not recognized Through short simulation) and formed pi-pi stacking with the benzoxazole ring of molecule, which consumed (31%) of the trajectory frames. Carboxy group of the pyrimidine ring formed hydrogen bond via water bridge interaction with the 2 residues GLY116 and GLY117 respectively. These bridges were showed through 50-ns simulations and consumed (48% and 56%) of trajectory frames.

PHE329 residue formed pi-pi stacking interaction with the pyrimidine ring and kept this interaction Through simulations and consumed (39% and 42%) through 50 and 100-ns, respectively. New pi-cation interaction was observed through 50-

ns and 100-ns simulations between TYR332 and the nitrogen of piperidine, which expended (64% and 35%), respectively. 2 hydrogen bonds via water bridge were formed between the side chain PRO230 and ASN397 and nitrogen atom of Piperidine in the donepezil and consumed (36% and 34%) through 50-ns, respectively.

HIS438 residue formed water bridge with carboxy group of the pyrimidine ring through 100-ns (43%). The average interaction fractions of contact residues diagram and timeline representation throughout the simulations of risperidone at the bound pocket of AChE and BuChE were shown in Figures 6.26 and 6.28. Risperidone constructs critical chemical interactions with residues TRP86, PHE295, TYR337, PHE338 and TYR341 which are stable throughout the simulation time. Corresponding interactions were TRP82, PHE329 and TYR332 at BuChE.

Through IFD of nelfinavir with BuChE (Figure 6.31), four hydrogen bond interactions were detected between the side chain residues and ligand, SER287, and ASN289, with the hydroxyl group of methyl benzoyl, TYR332 to carboxy group of benzoyl and the fourth one with a water molecule. Through short MD simulations, TYR332 built pi-pi stacking with the phenyl ring, which expended 34% of the trajectory. GLU276 made a hydrogen bond with the hydroxyl of benzoyl (34%). We also observed three water bridges with GLN119, THR120, and SER198 depleted (60%, 35%, and 42%) of the trajectory, respectively. In long simulations, most hydrogen bond interactions have occurred across water molecules, ASP70 (40%), GLY116 (55%), THR120 (61%), SER198 (64%), LEU273 (75%) GLU276 (65%) and SER287 (84%). One direct H-bond interacted with ASN289 consumed (57%). The average interaction fractions of contact residues diagram and timeline representation of the interactions and contacts throughout the simulations of nelfinavir at the binding pocket of BuChE was shown in Figure 6.32. Nelfinavir constructs critical chemical interactions with residues ASP70, GLN119, THR120, GLU276, SER287 and TYR332 which are stable throughout the simulation time.

The top-docking poses and MD simulations of the complex systems showed that the ligands interacted properly with known critical residue interactions. Other groups have shown the significance of TRP86 in ligand binding in the literature [253-255]. Radic et al. conducted a mutational scan and revealed the importance of TRP86 and showed that TRP86 provides the ligands' alignment into the active binding pocket correctly [254]. The significance of these 2 adjacents (TYR337 and PHE338) residues were highlighted in other computational studies [256, 257]. Kaplan et al. argued that TYR337 is one of the essential residues and the 2 phenylalanine, namely PHE295 and PHE297 Cheung et al. have emphasized the importance of Tyr341 and Trp286 interactions for AChE inhibition in their research [228].

The residues ASP74, due to their significant interactions with the ligands, TRP86, TYR337, PHE338 PHE295 and TYR341 are recommended as possibilities for future experimental investigations of structure-function connections in drug creation. Through MD simulations, the pi-cation interaction between donepezil and PHE329 Gnatt et al. revealed that PHE329 mutations decreased inhibitor binding to the BuChE and highlighted its importance [258]. Biberoglu et al. conducted another mutation study., and successfully showed PHE329 is one of the critical residues residing active site of the BuChE [259, 260]. The importance of the TRP82 was shown successfully with experimental and computational studies [261-263]. Othman et al. investigated plant derivatives against inhibition of AChE and BuChE and identified TYR128 as an essential residue. The prominence of ALA328 was also shown via another experimental and modelling study [264].

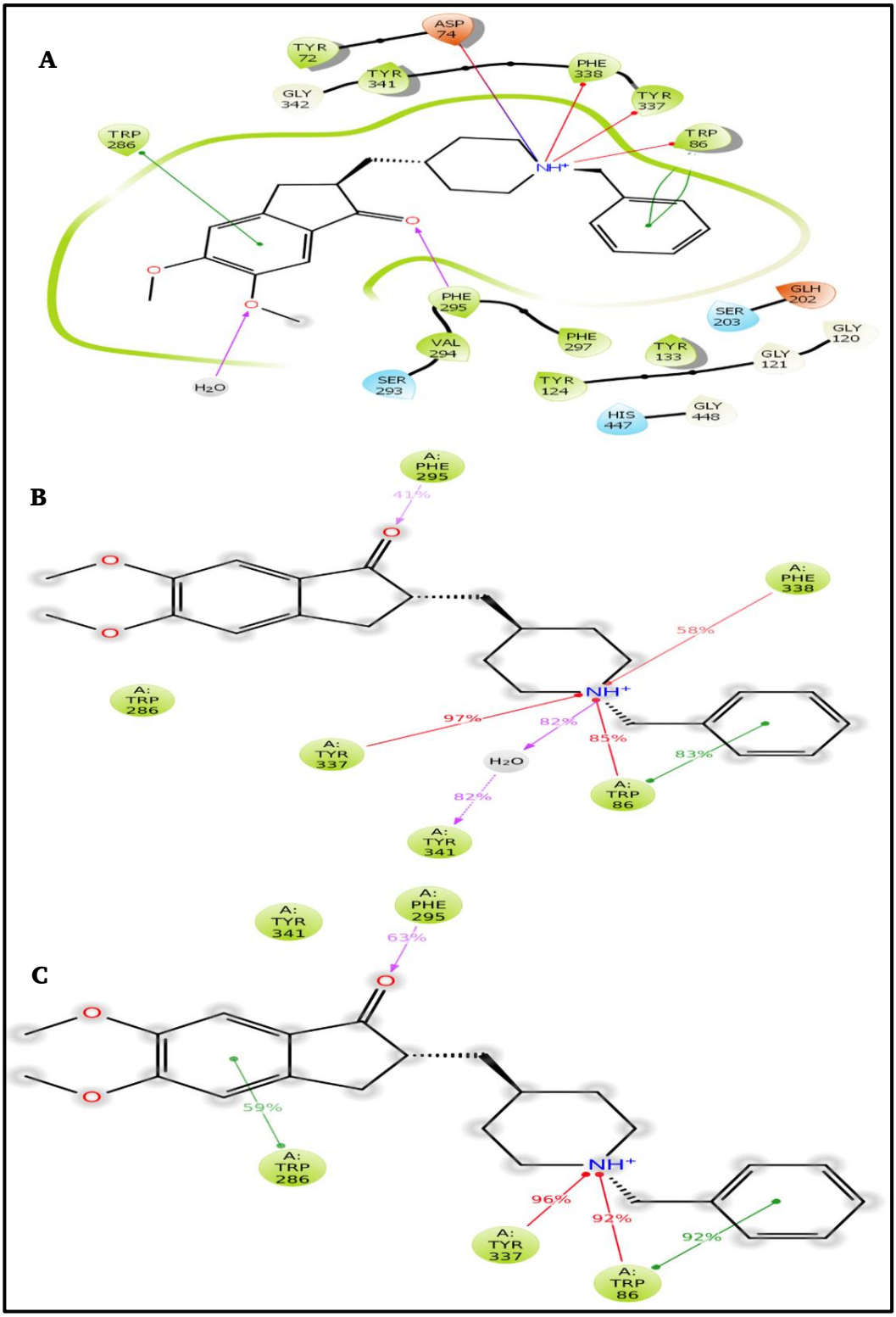

Figure 6. 9 (A) The two-dimensional IFD ligand interaction, and the average interaction score of contact residues diagram of donepezil throughout the MD simulation at the AChE binding pocket

((B)50-ns, (C)100-ns)

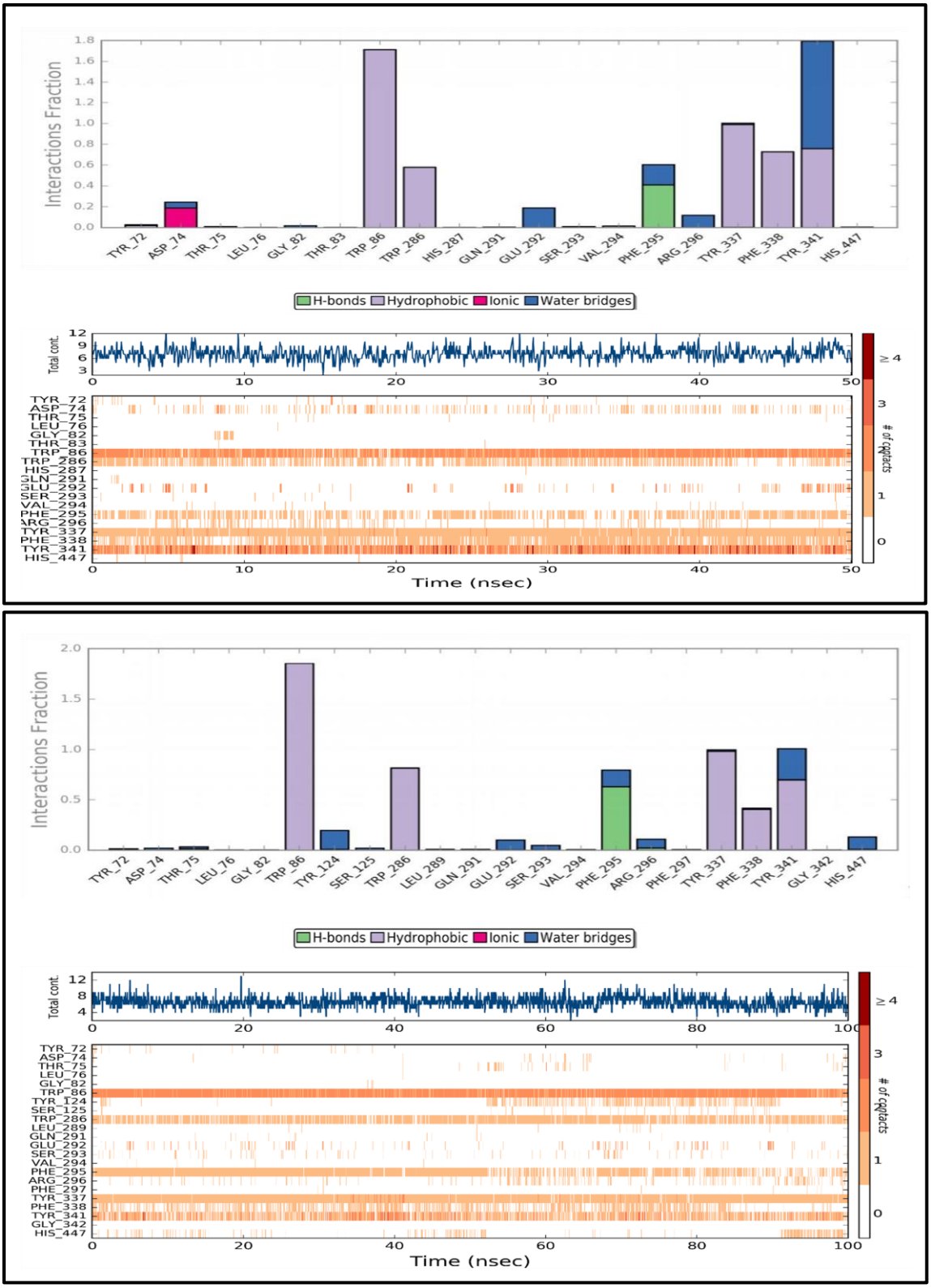

Figure 6. 10 The average interaction fractions of contact residues diagram and timeline representation of the interactions and contacts throughout the MD simulations of donepezil at the binding pocket of AChE

(top: 50-ns, bottom: 100-ns)

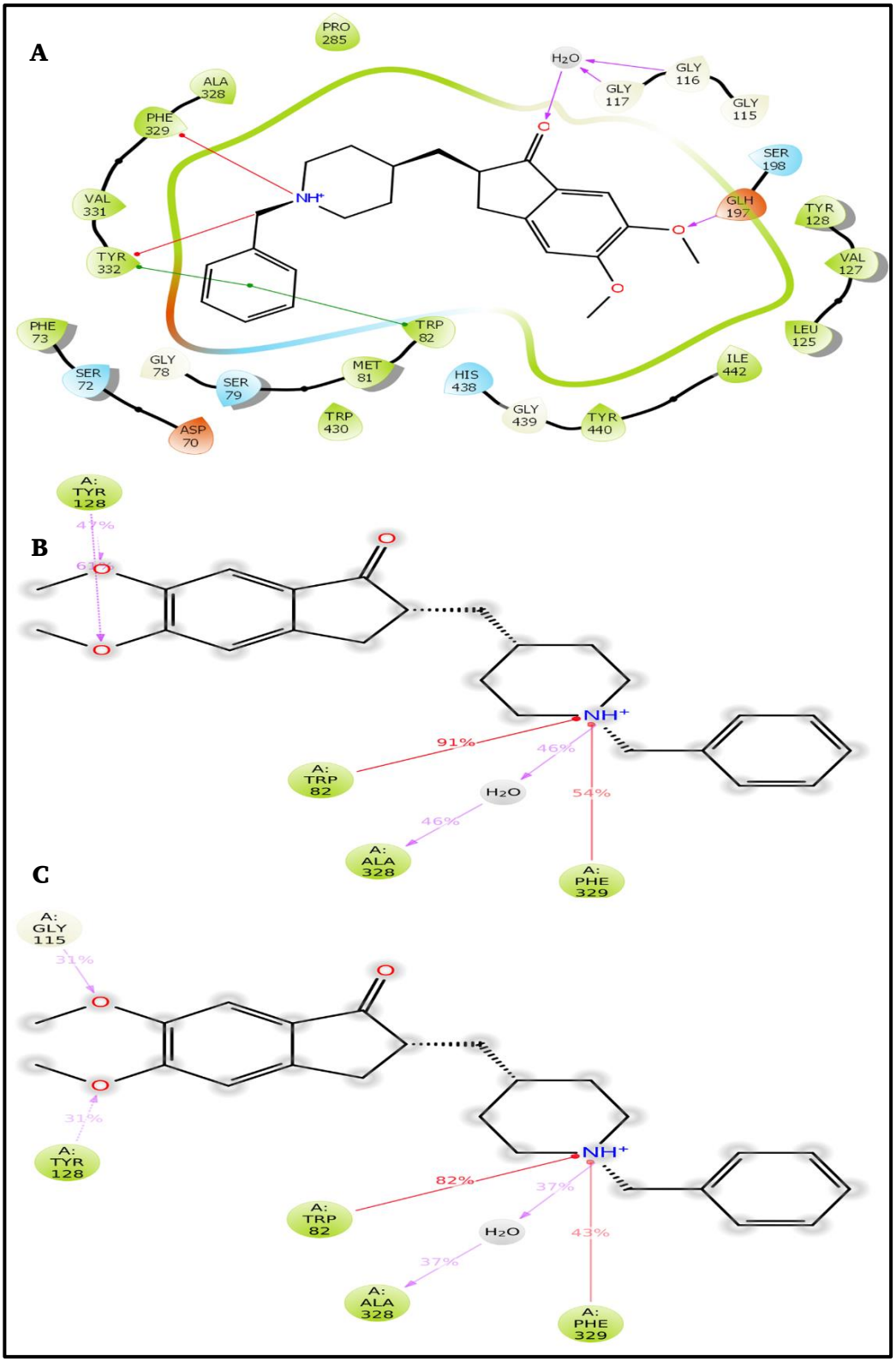

Figure 6. 11 (A) The two-dimensional IFD ligand interaction, and the average interaction scores of contact residues diagram of donepezil throughout the MD simulation at the BuChE binding pocket

((B)50-ns, (C)100-ns)

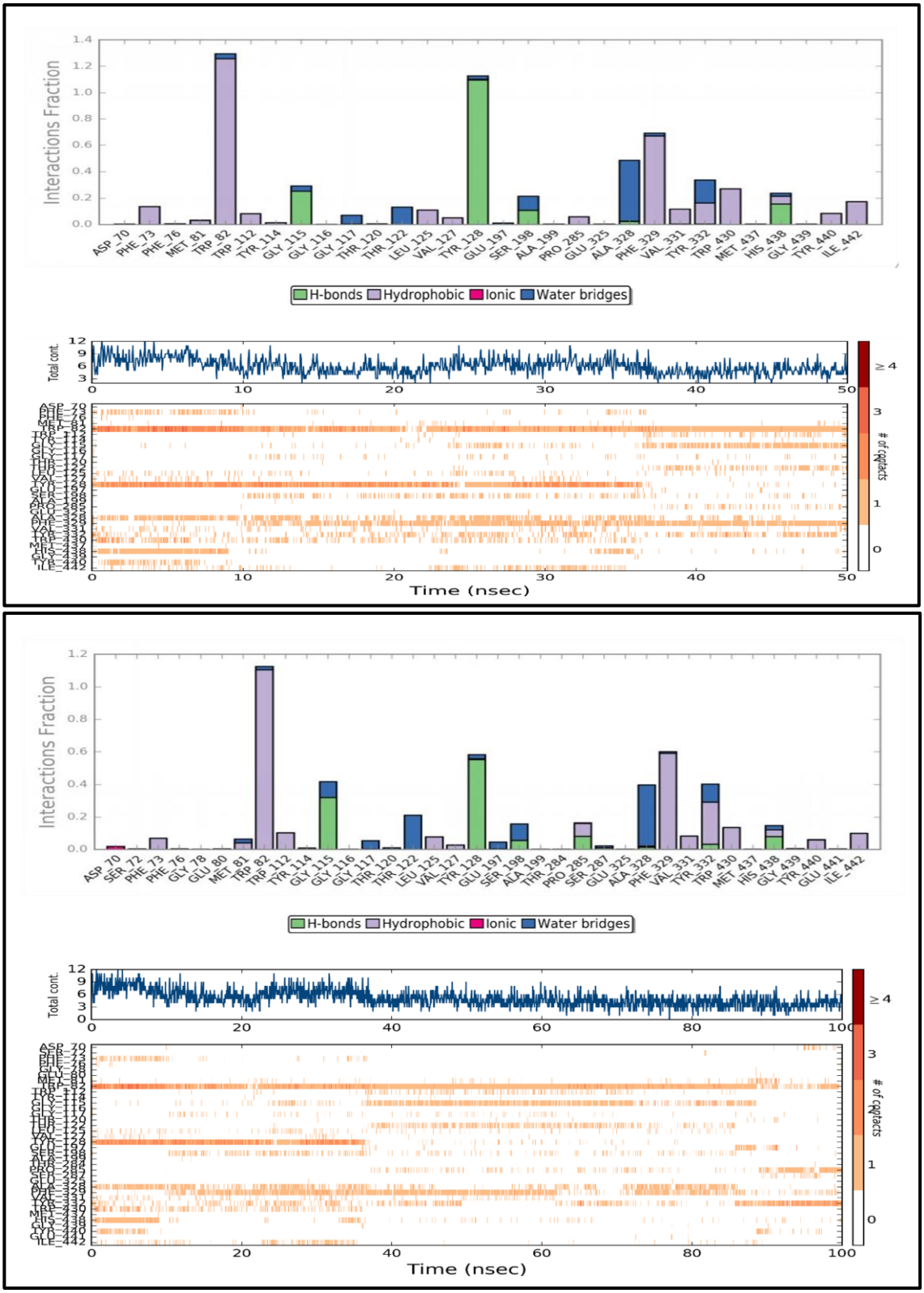

Figure 6. 12 The average interaction fractions of contact residues diagram and timeline representation of the interactions and contacts throughout the MD simulations of donepezil at the binding pocket of BuChE

(top: 50-ns, bottom: 100-ns)

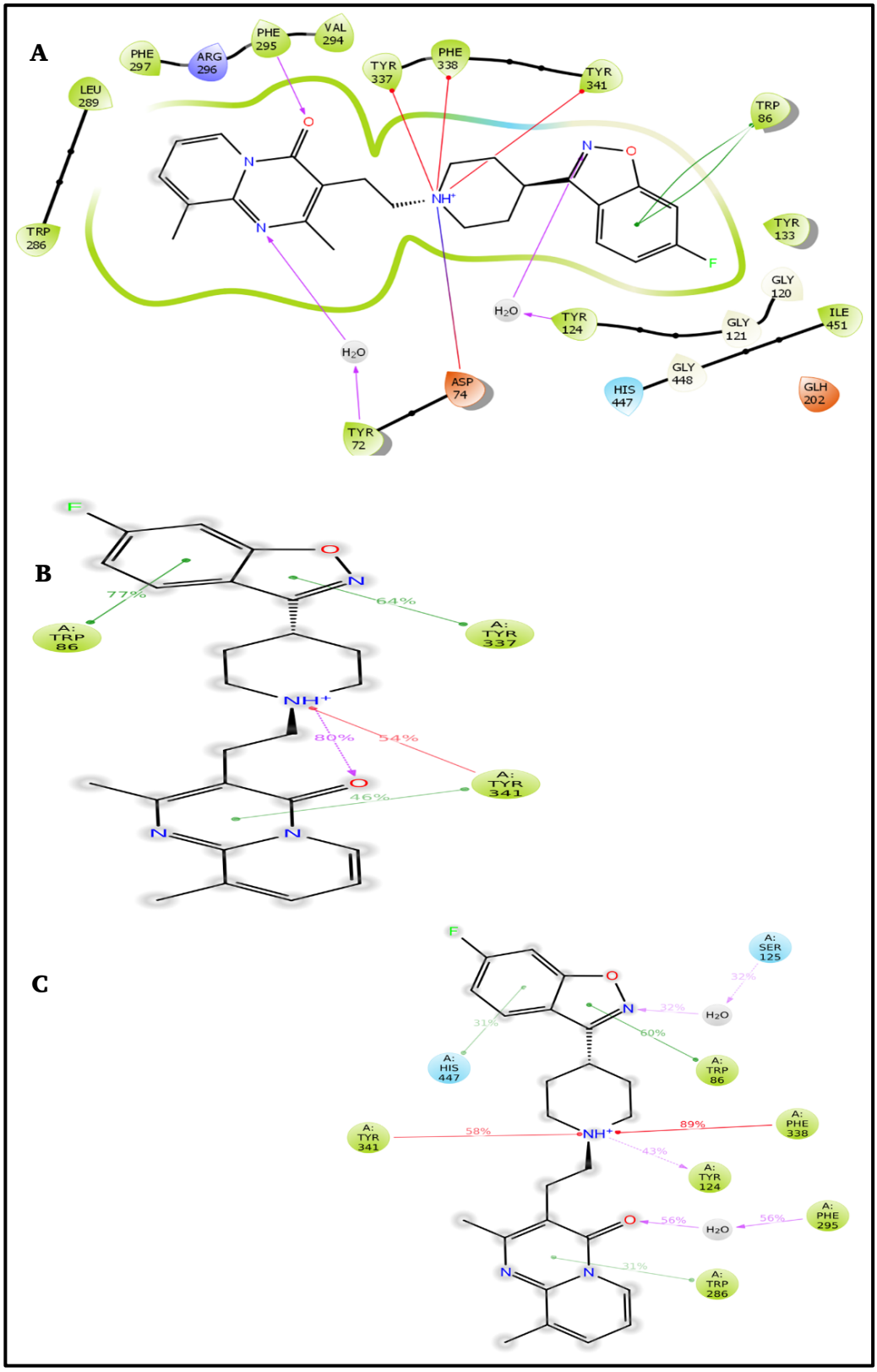

Figure 6. 13 (A) The two-dimensional IFD ligand interaction and average interaction scores of contact residues diagram throughout the MD simulations of ocaperidone at the AChE binding pocket

((B)50-ns, (C)100-ns)

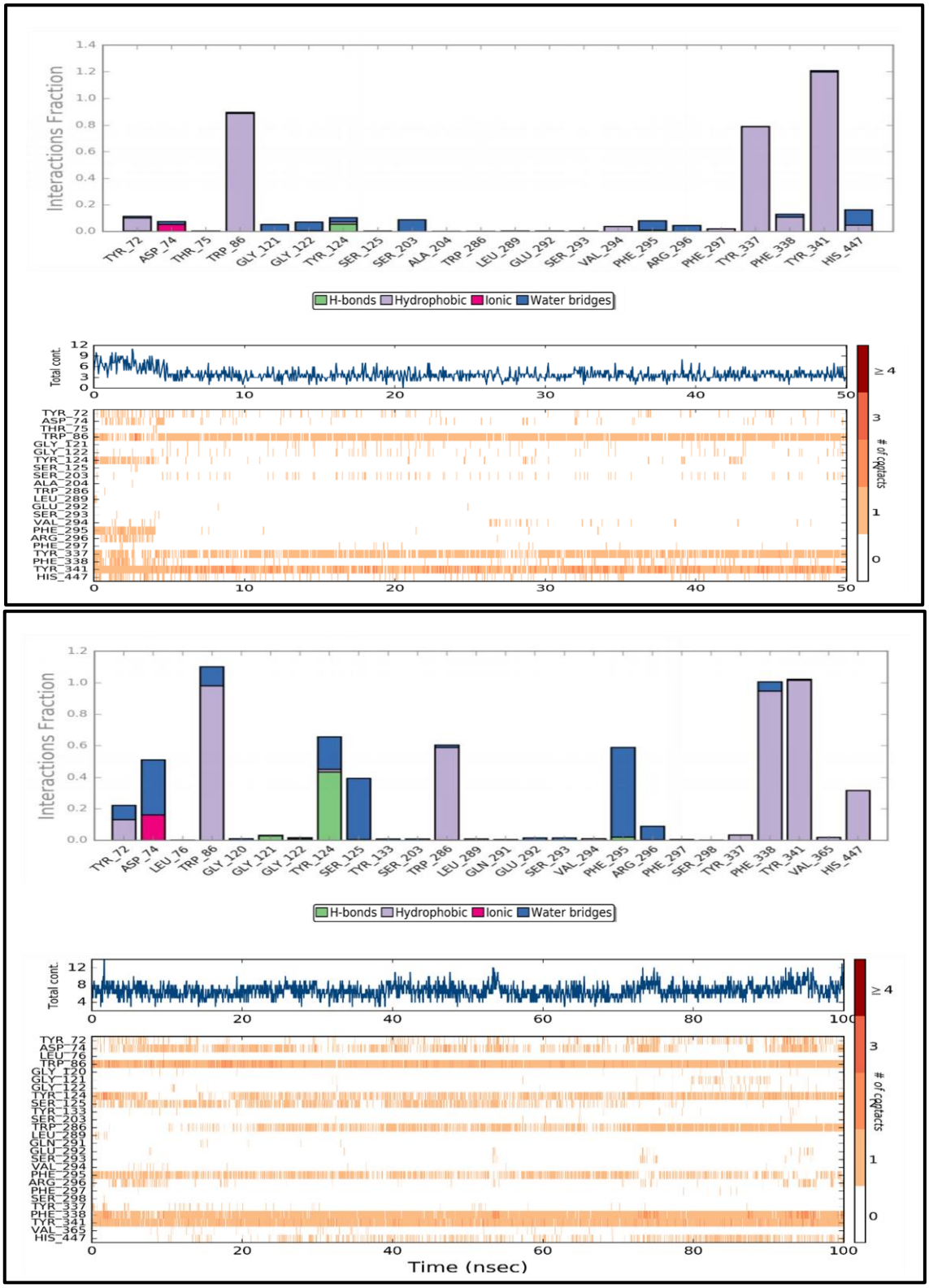

Figure 6. 14 The average interaction fractions of contact residues diagram and timeline representation of the interactions and contacts throughout the MD simulations of ocaperidone at the binding pocket of AChE

(top: 50-ns, bottom: 100-ns)

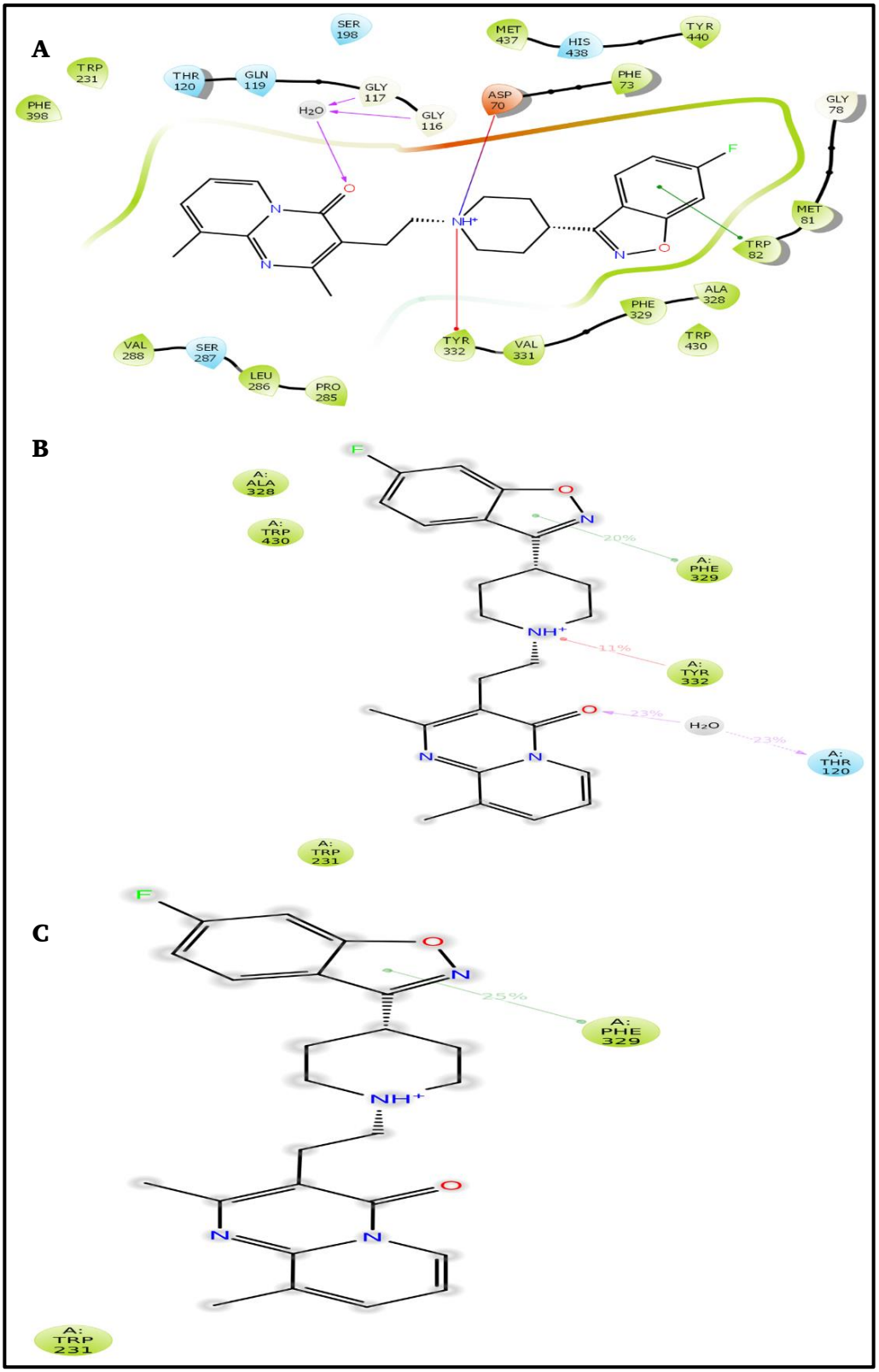

Figure 6. 15 The two-dimensional IFD ligand interaction and average interaction scores of contact residues diagram throughout the MD simulations of ocaperidone at the BuChE binding pocket

((B)50-ns, (C)100-ns

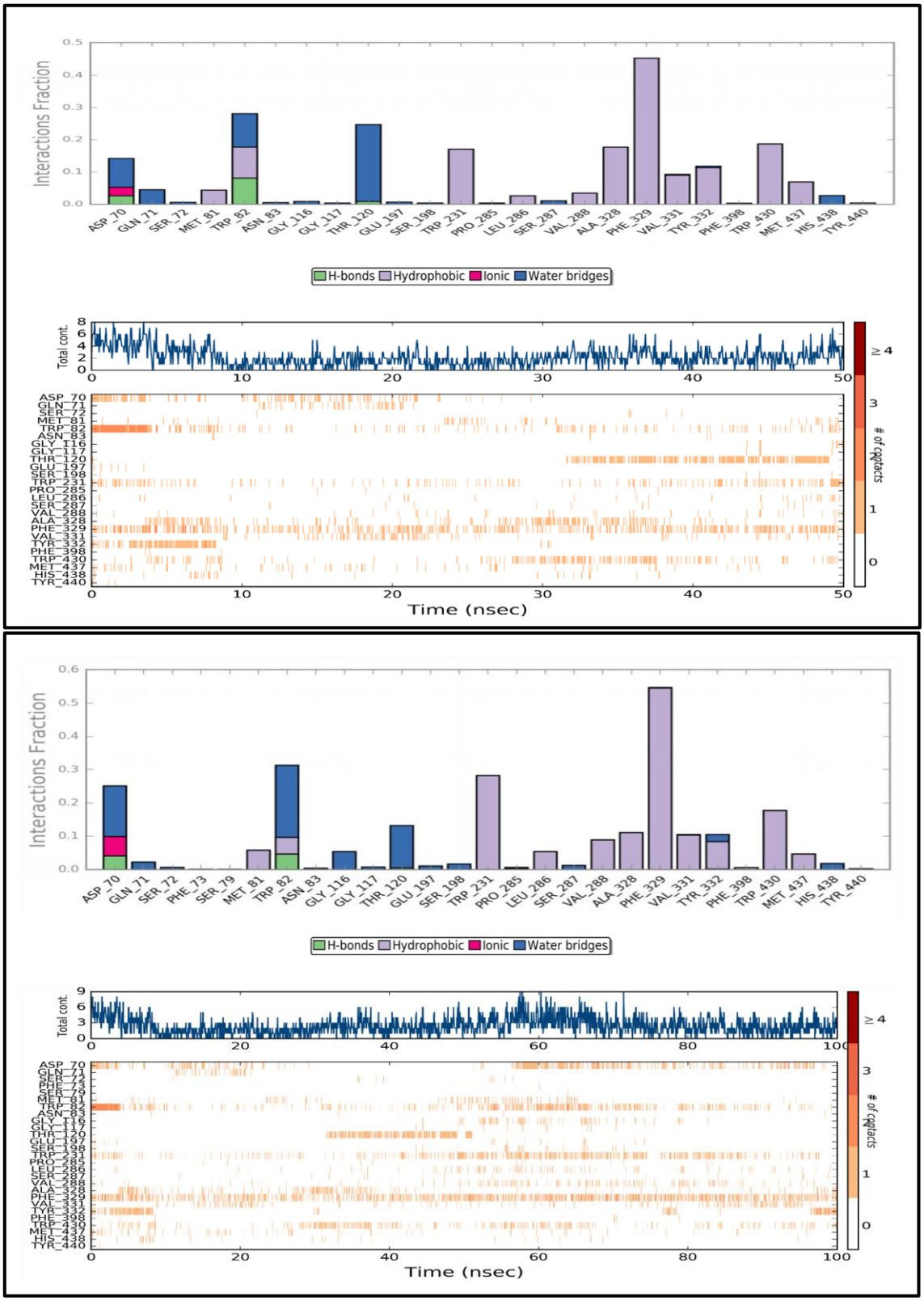

Figure 6. 16 The average interaction fractions of contact residues diagram and timeline representation of the interactions and contacts throughout the MD simulations of ocaperidone at the binding pocket of BuChE

(top: 50-ns, bottom: 100-ns)

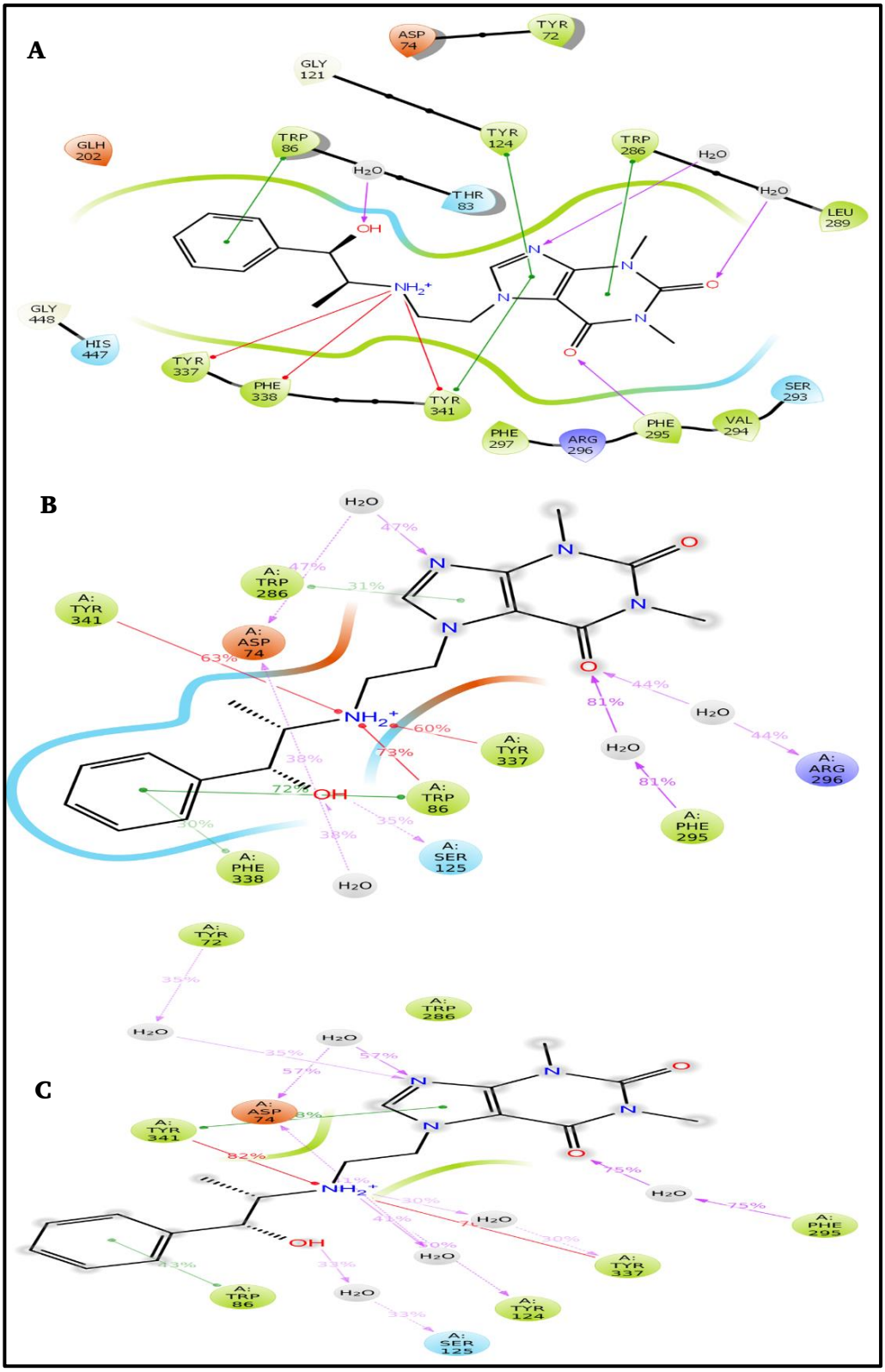

Figure 6. 17 (A) The two-dimensional IFD ligand interaction and average interaction scores of contact residues diagram throughout the MD simulations of cafedrine at the AChE binding pocket

((B)50-ns, (C)100-ns)

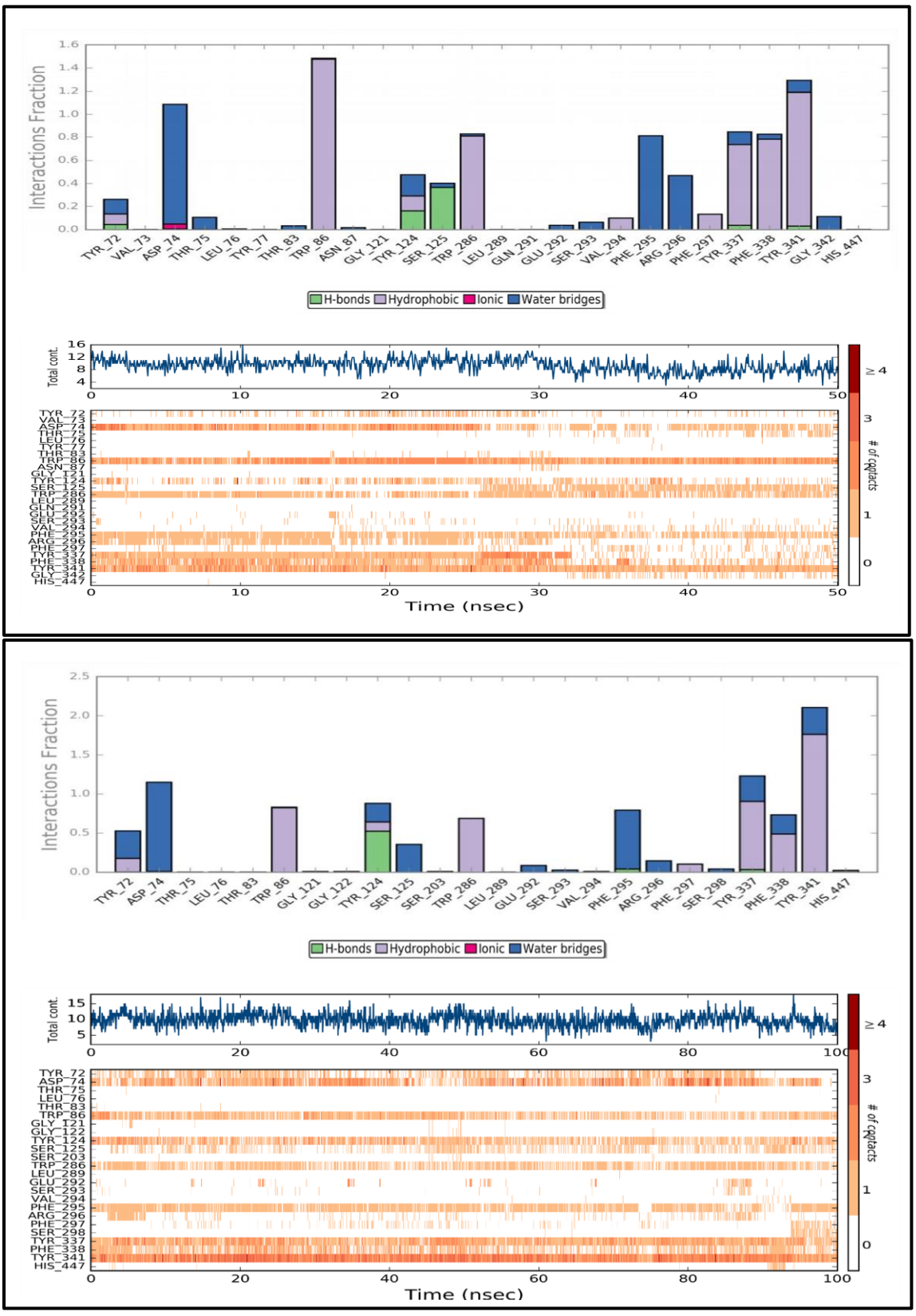

Figure 6. 18 The average interaction fractions of contact residues diagram and timeline representation of the interactions and contacts throughout the MD simulations of cafedrine at the binding pocket of AChE

(top: 50-ns, bottom: 100-ns)

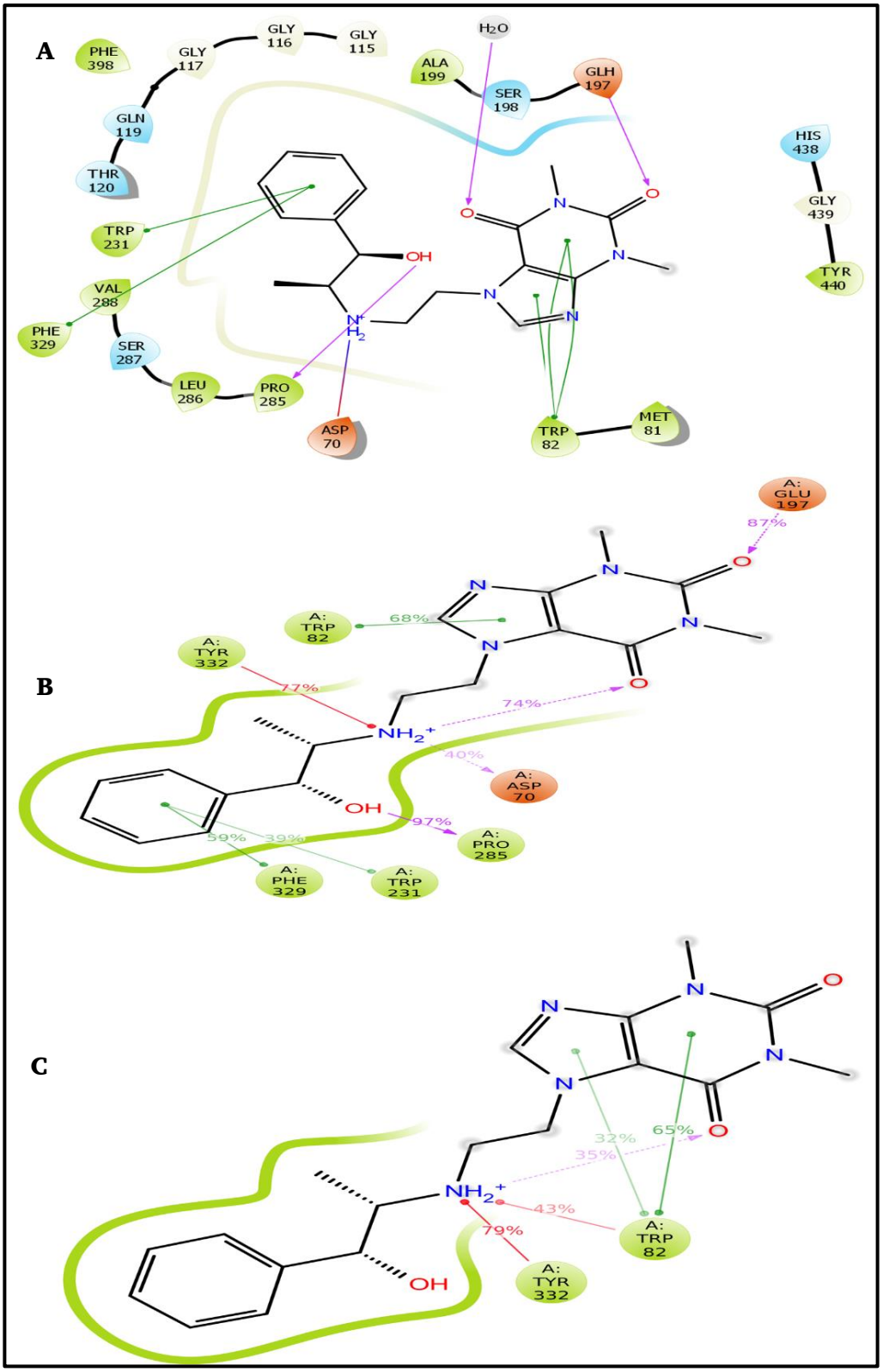

Figure 6. 19 (A) The two-dimensional IFD ligand interaction and average interaction scores of contact residues diagram throughout the MD simulations of cafedrine at the BuChE binding pocket

((B)50-ns, (C)100-ns)

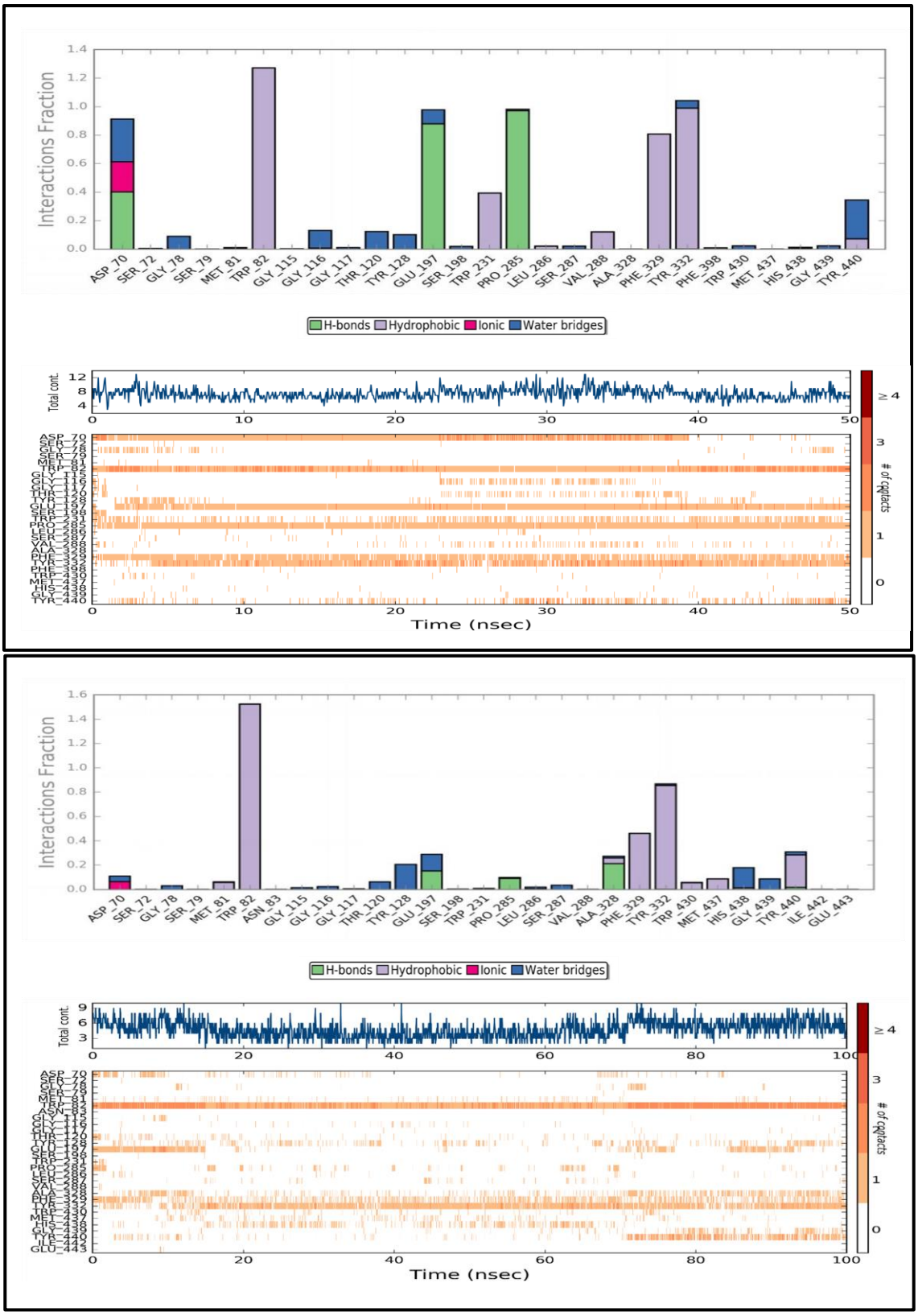

Figure 6. 20 The average interaction fractions of contact residues diagram and timeline representation of the interactions and contacts throughout the MD simulations of cafedrine at the binding pocket of BuChE

(top: 50-ns, bottom: 100-ns)

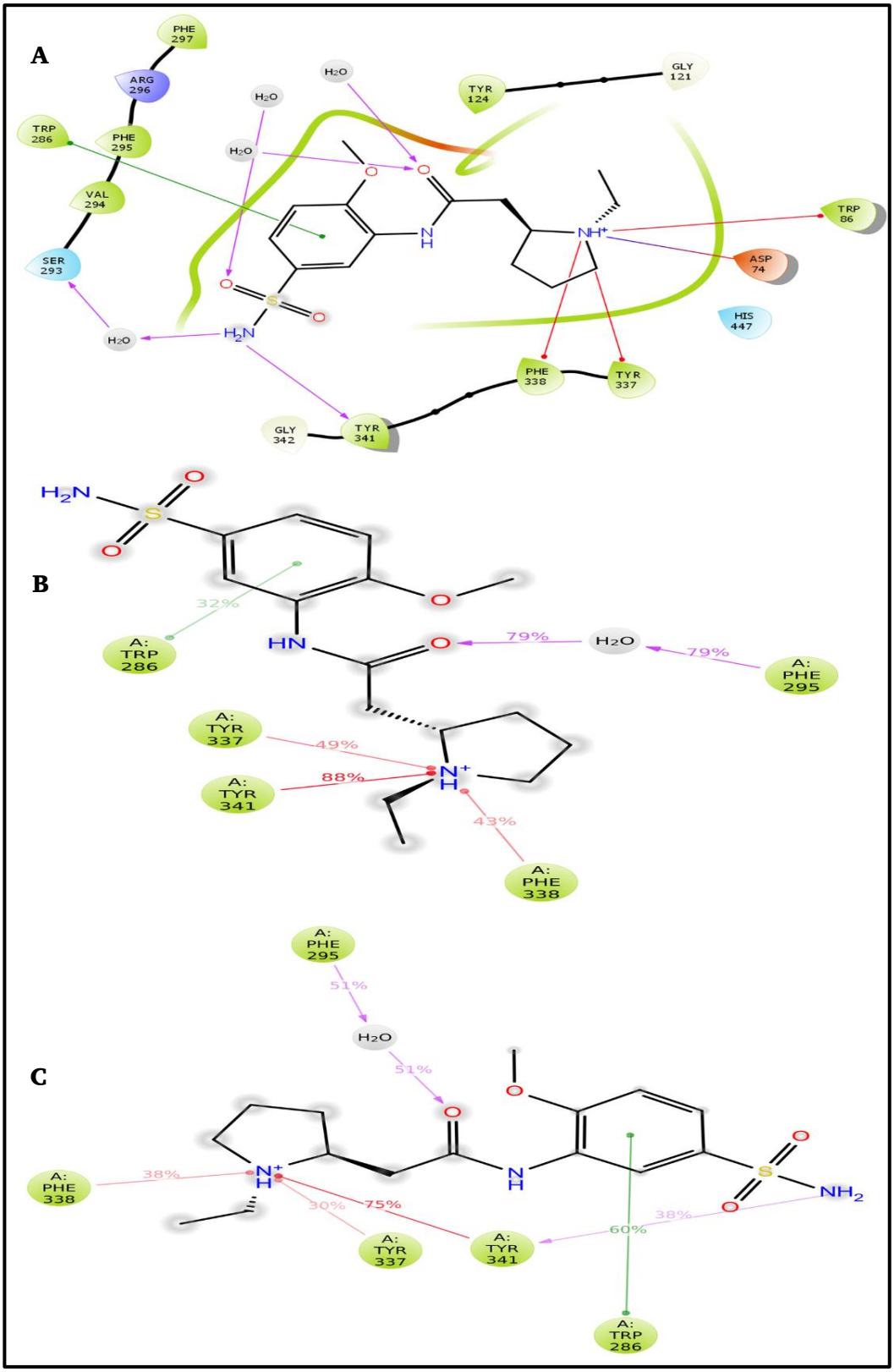

Figure 6. 21 (A) The two-dimensional IFD ligand interaction and average interaction scores of contact residues diagram throughout the MD simulations of isosulpride at the AChE binding pocket

((B)50-ns, (C)100-ns)

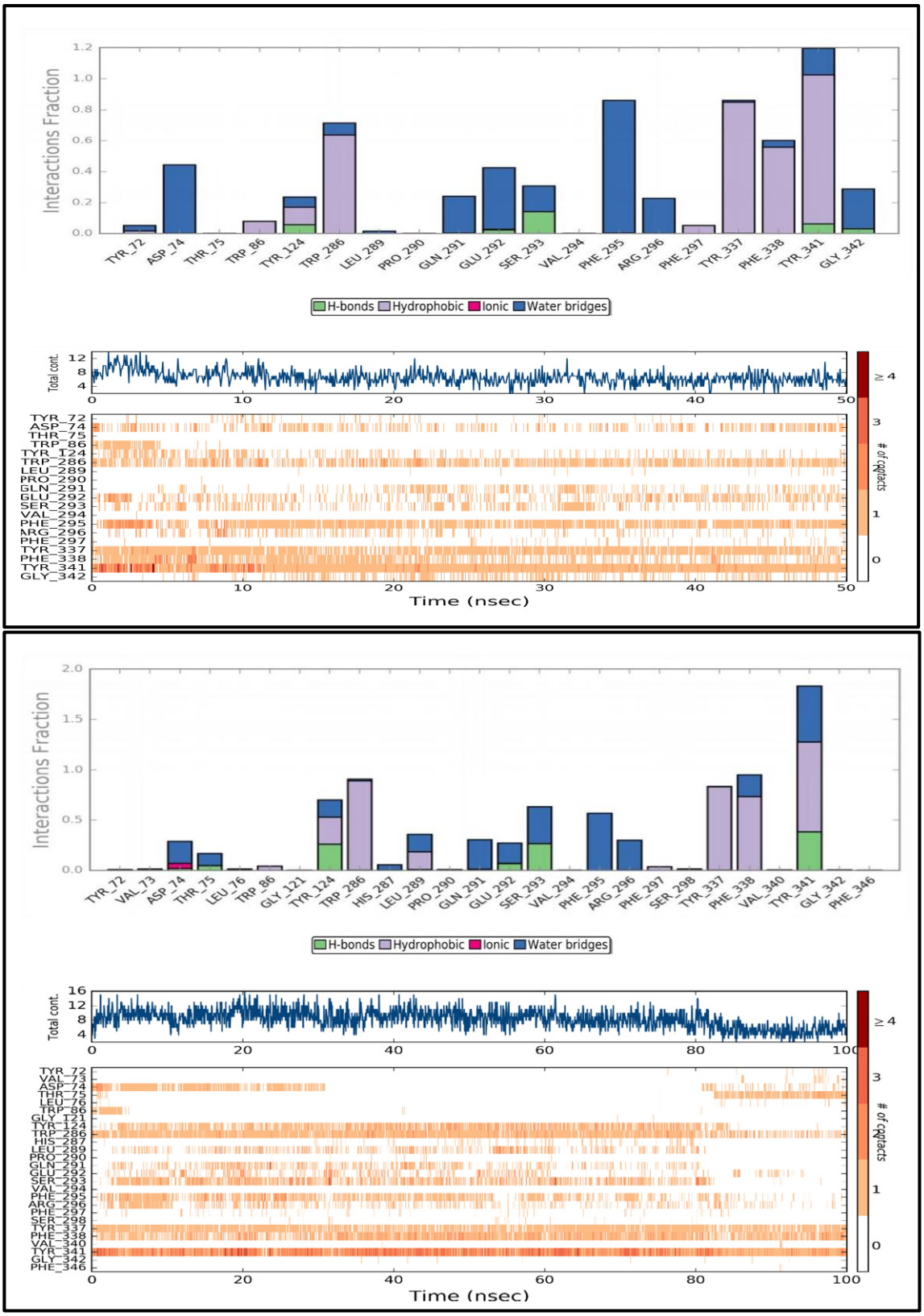

Figure 6. 22 The average interaction fractions of contact residues diagram and timeline representation of the interactions and contacts throughout the MD simulations of isosulpride at the binding pocket of AChE

(top: 50-ns, bottom: 100-ns)

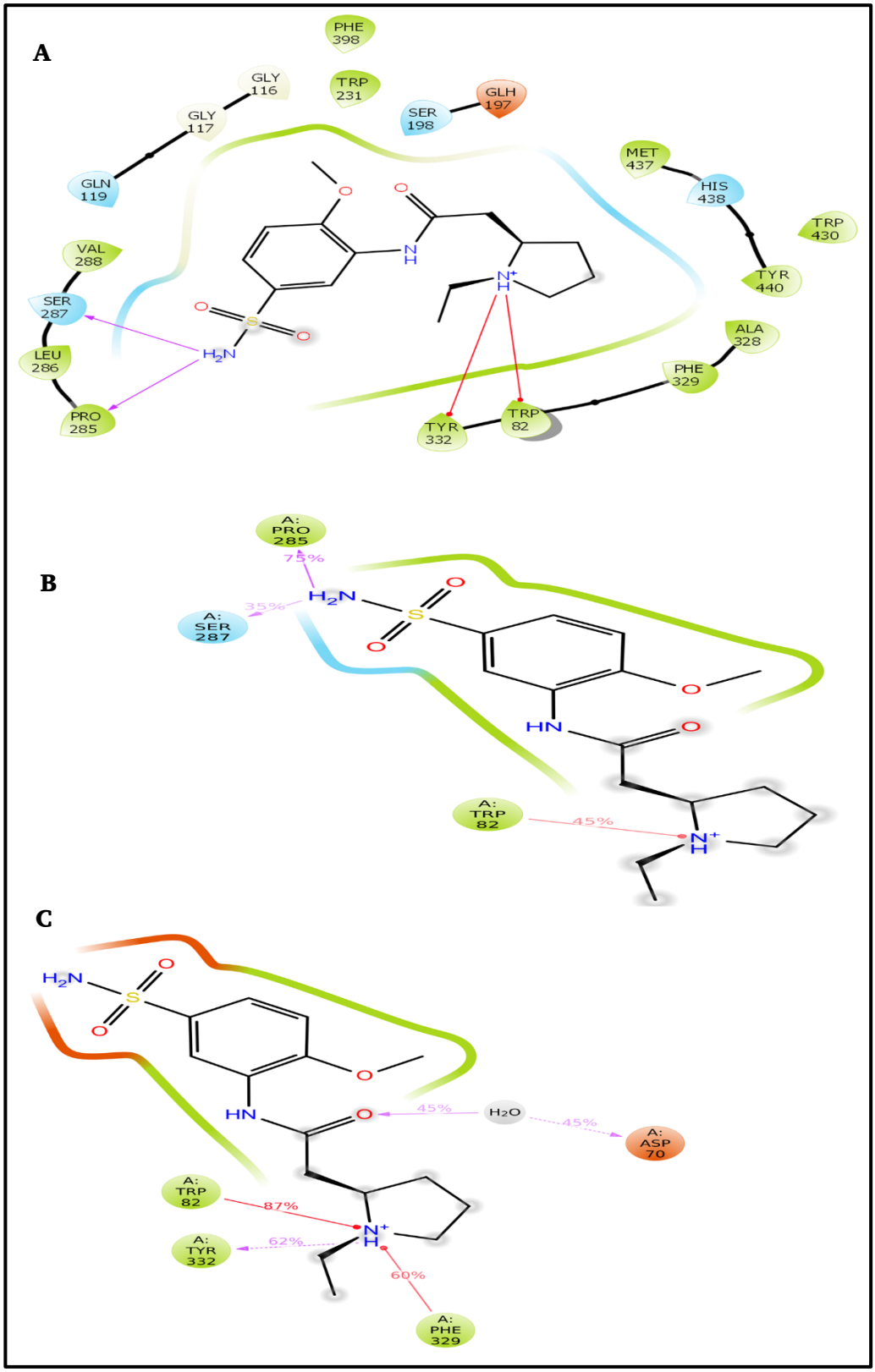

Figure 6. 23 (A) The two-dimensional IFD ligand interaction and average interaction scores of contact residues diagram throughout the MD simulations of isosulpride at the BuChE binding pocket

((B)50-ns, (C)100-ns)

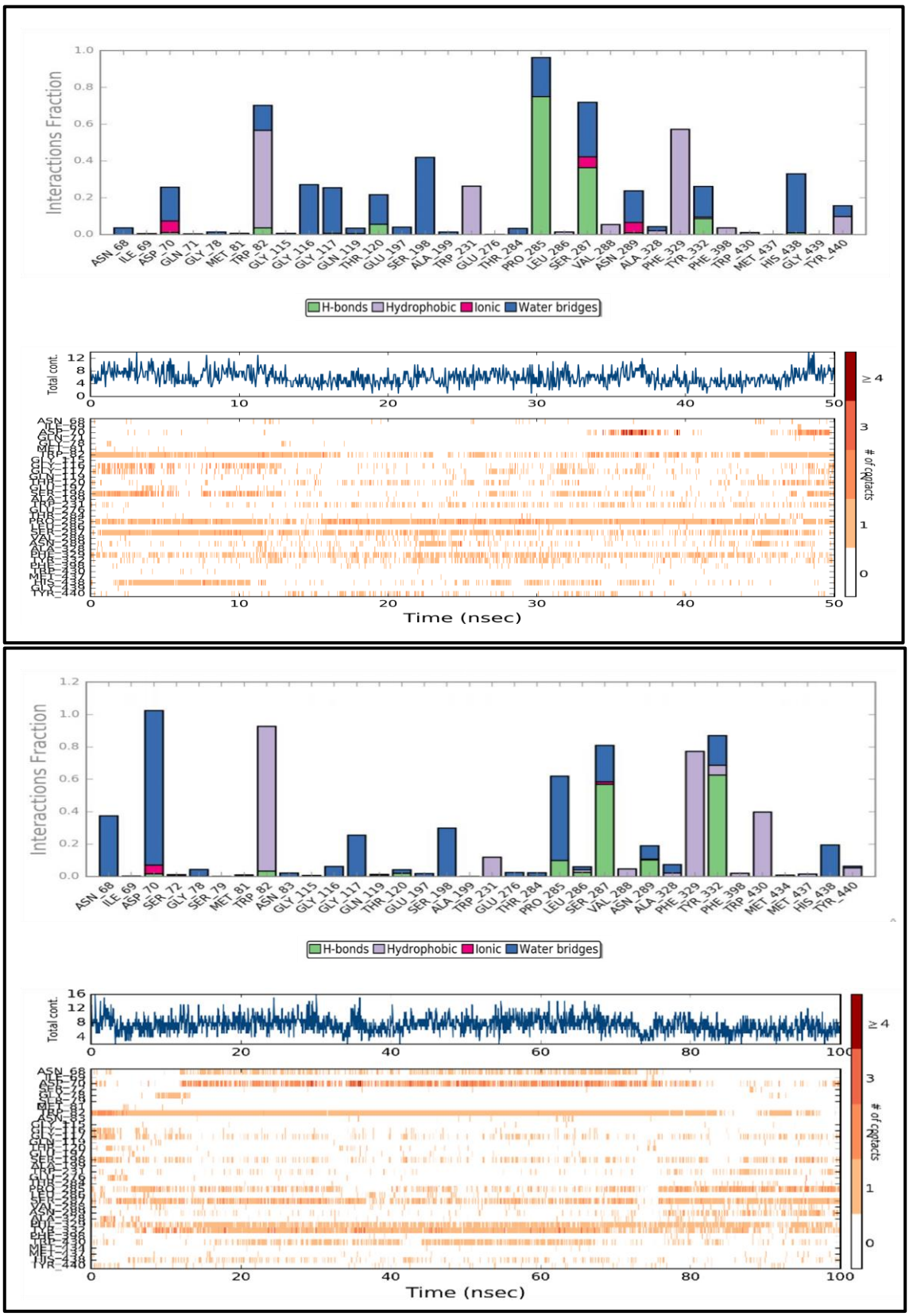

Figure 6. 24 : The average interaction fractions of contact residues diagram and timeline representation of the interactions and contacts throughout the MD simulations of isosulpride at the binding pocket of BuChE

(top: 50-ns, bottom: 100-ns)

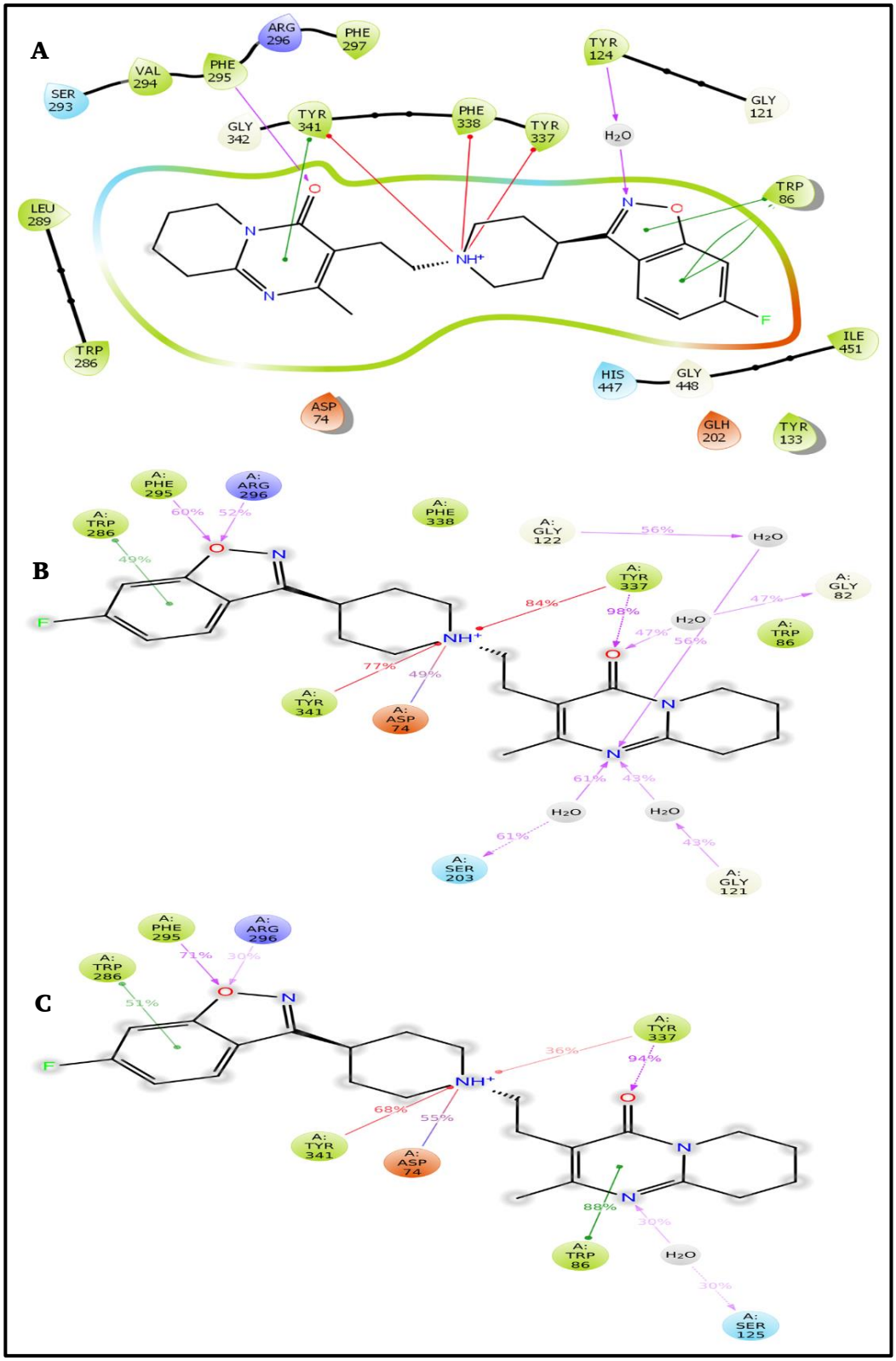

Figure 6. 25 (A) The two-dimensional IFD ligand interaction and average interaction scores of contact residues diagram throughout the MD simulations of risperidone at the AChE binding pocket

((B)50-ns, (C)100-ns)

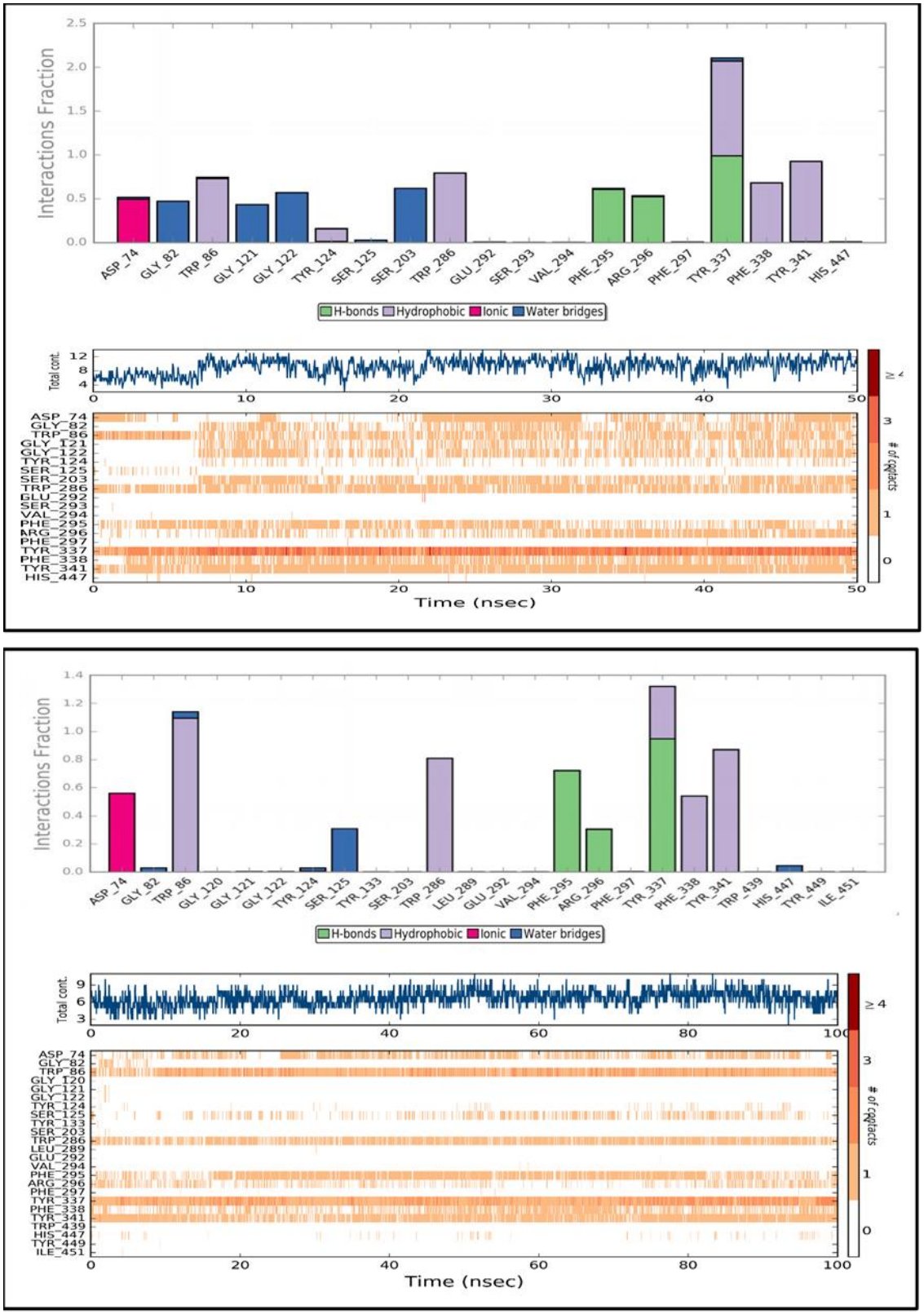

Figure 6. 26 The average interaction fractions of contact residues diagram and timeline representation of the interactions and contacts throughout the MD simulations of risperidone at the binding pocket of AChE

(top: 50-ns, bottom: 100-ns)

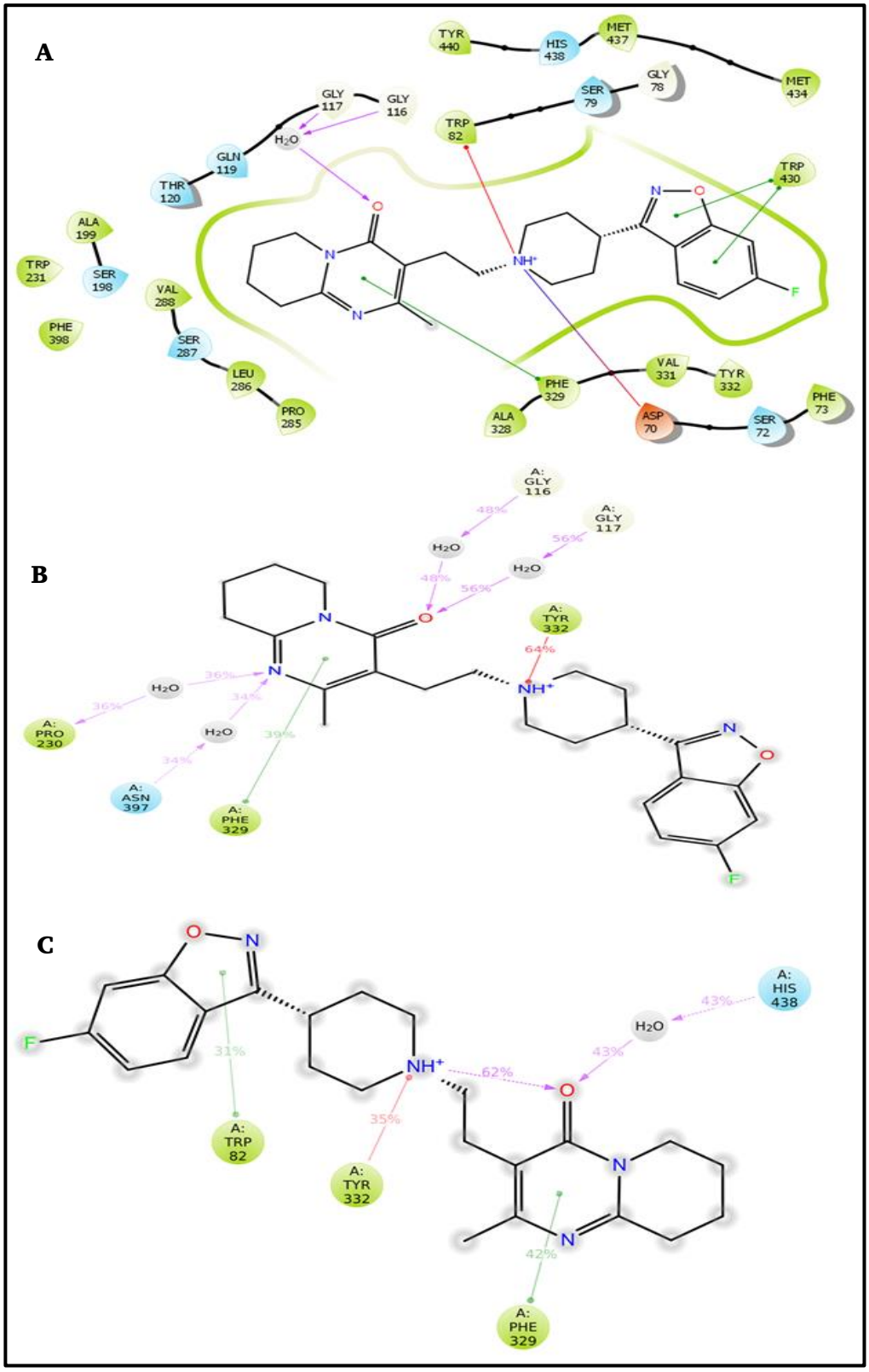

Figure 6. 27 (A) The two-dimensional IFD ligand interaction and average interaction scores of contact residues diagram throughout the MD simulations of risperidone at the BuChE binding pocket

((B)50-ns, (C)100-ns)

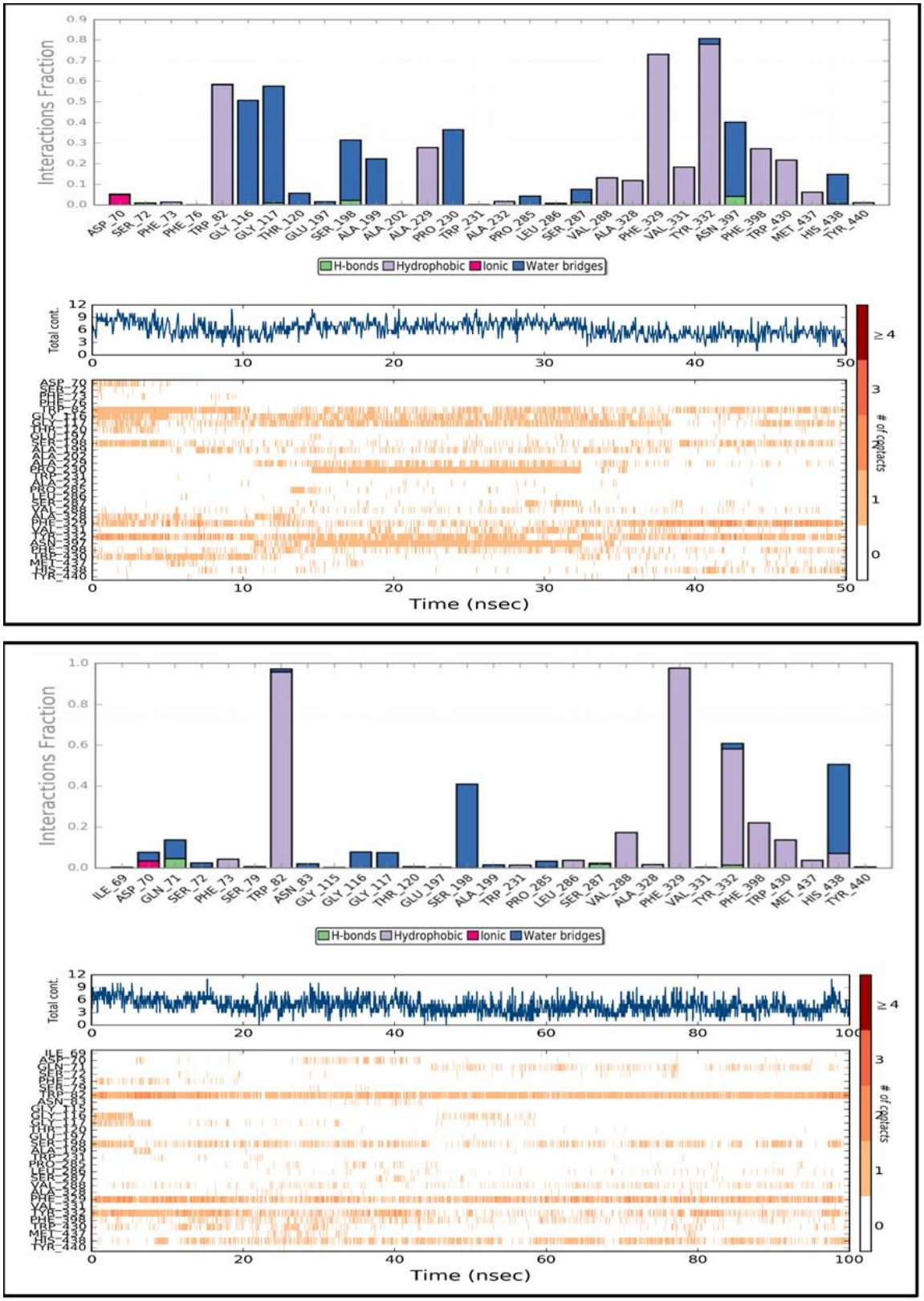

Figure 6. 28 The average interaction fractions of contact residues diagram and timeline representation of the interactions and contacts throughout the MD simulations of risperidone at the binding pocket of BuChE

(top: 50-ns, bottom: 100-ns)

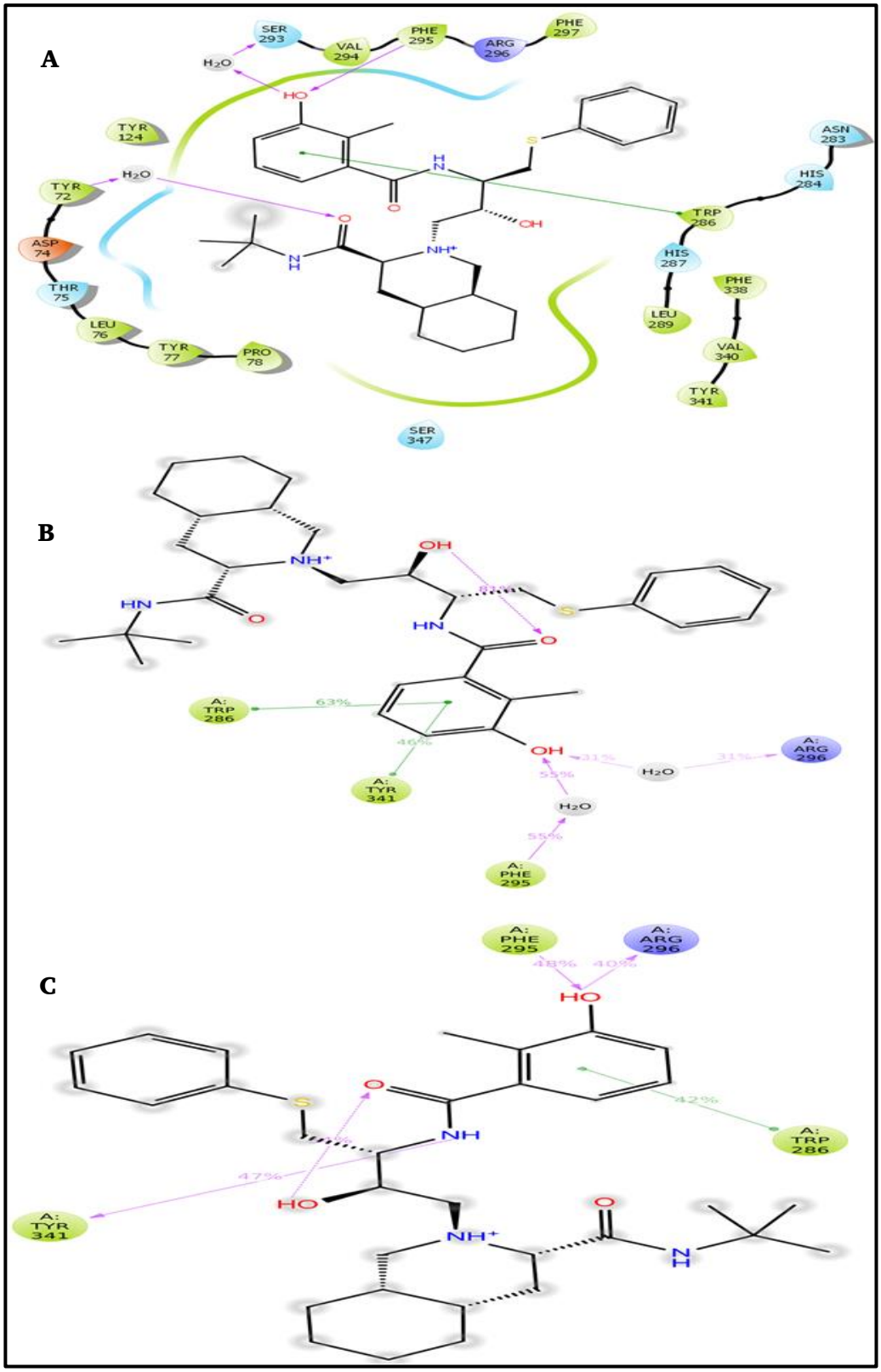

Figure 6. 29 (A) The two-dimensional IFD ligand interaction and average interaction scores of contact residues diagram throughout the MD simulations of nelfinavir at the AChE binding pocket

((B)50-ns, (C)100-ns)

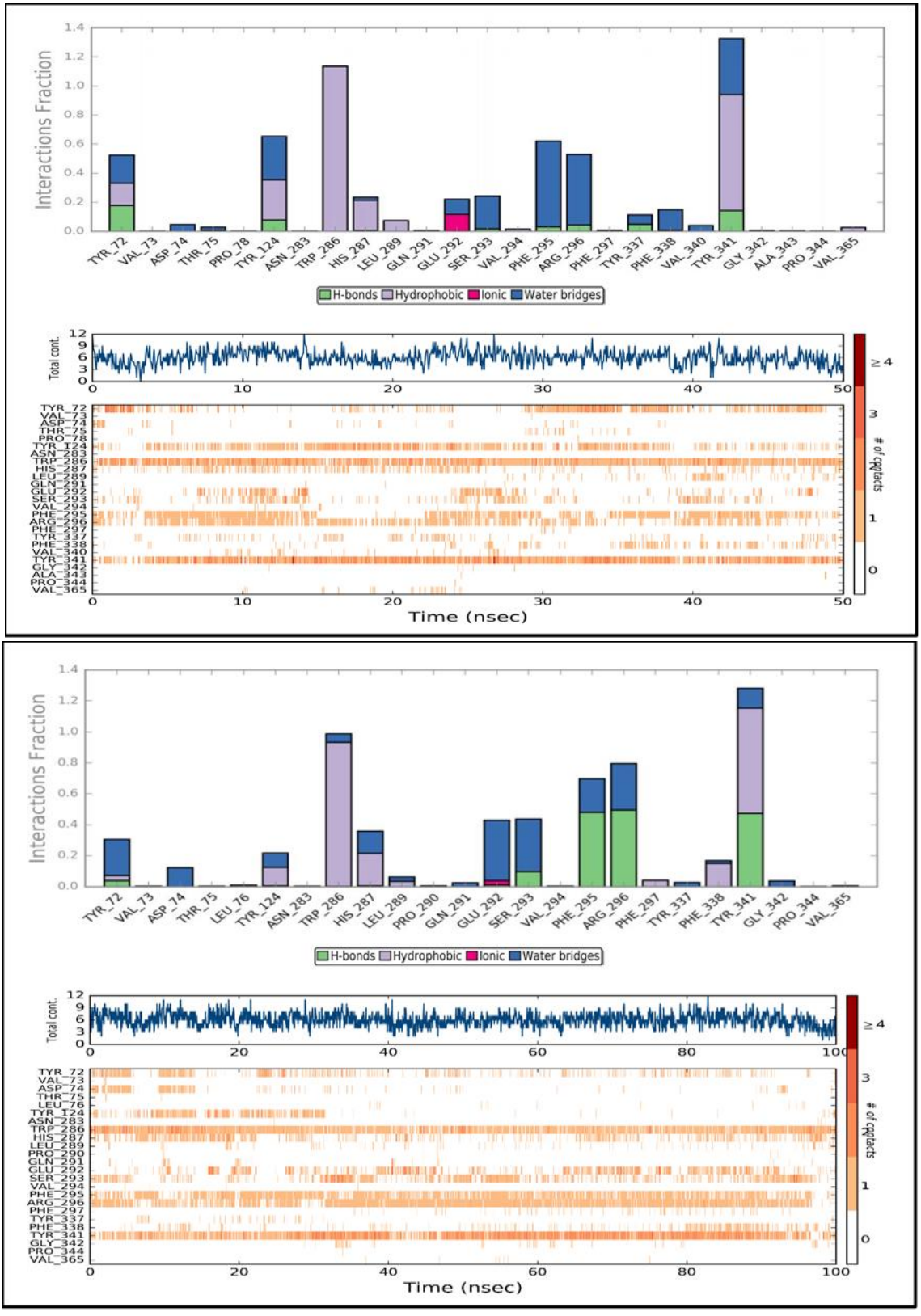

Figure 6. 30 The average interaction fractions of contact residues diagram and timeline representation of the interactions and contacts throughout the MD simulations of nelfinavir at the binding pocket of AChE

(top: 50-ns, bottom: 100-ns)

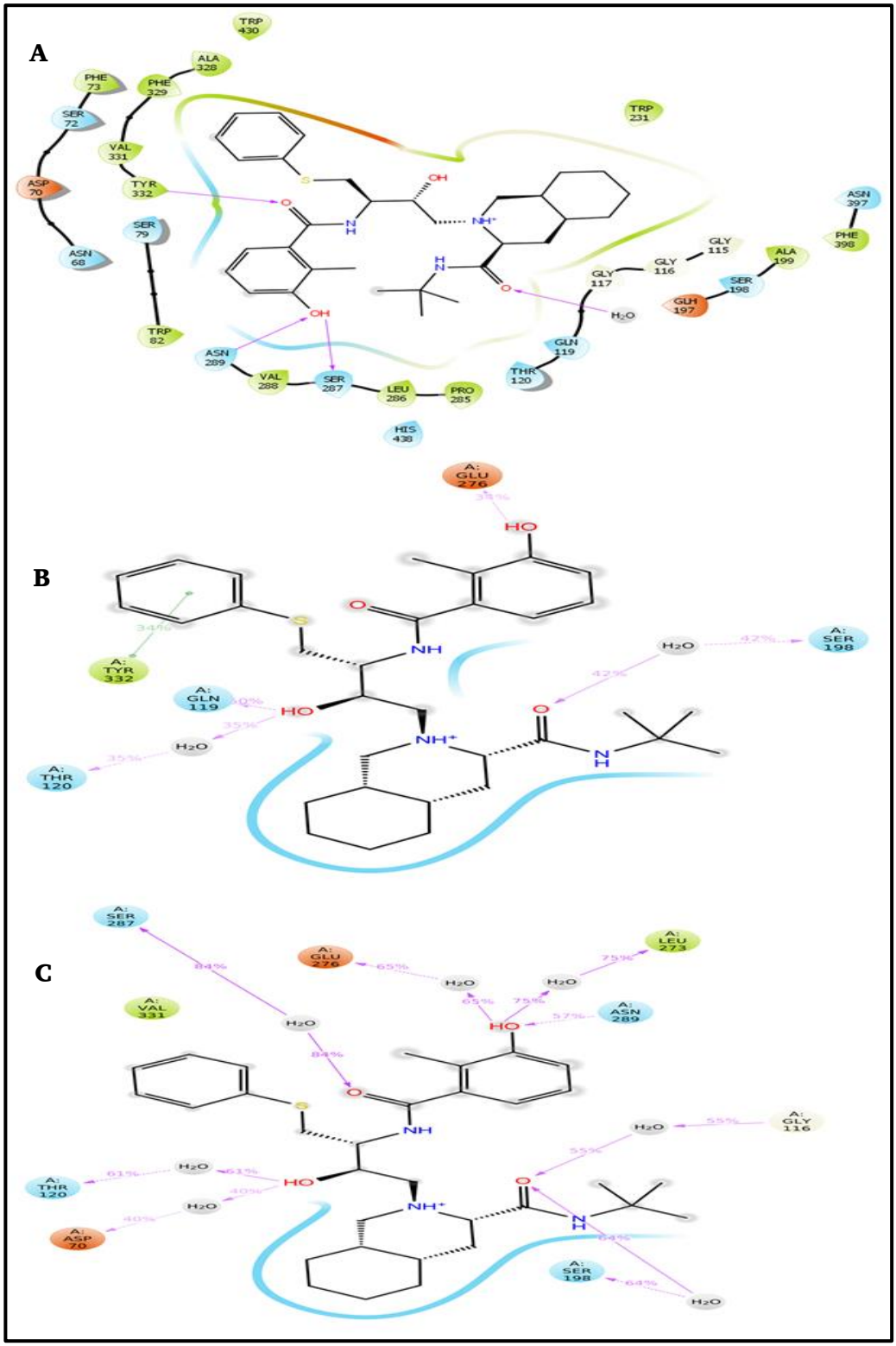

Figure 6. 31 (A) The two-dimensional IFD ligand interaction and average interaction scores of contact residues diagram throughout the MD simulations of nelfinavir at the BuChE binding pocket

((B)50-ns, (C)100-ns)

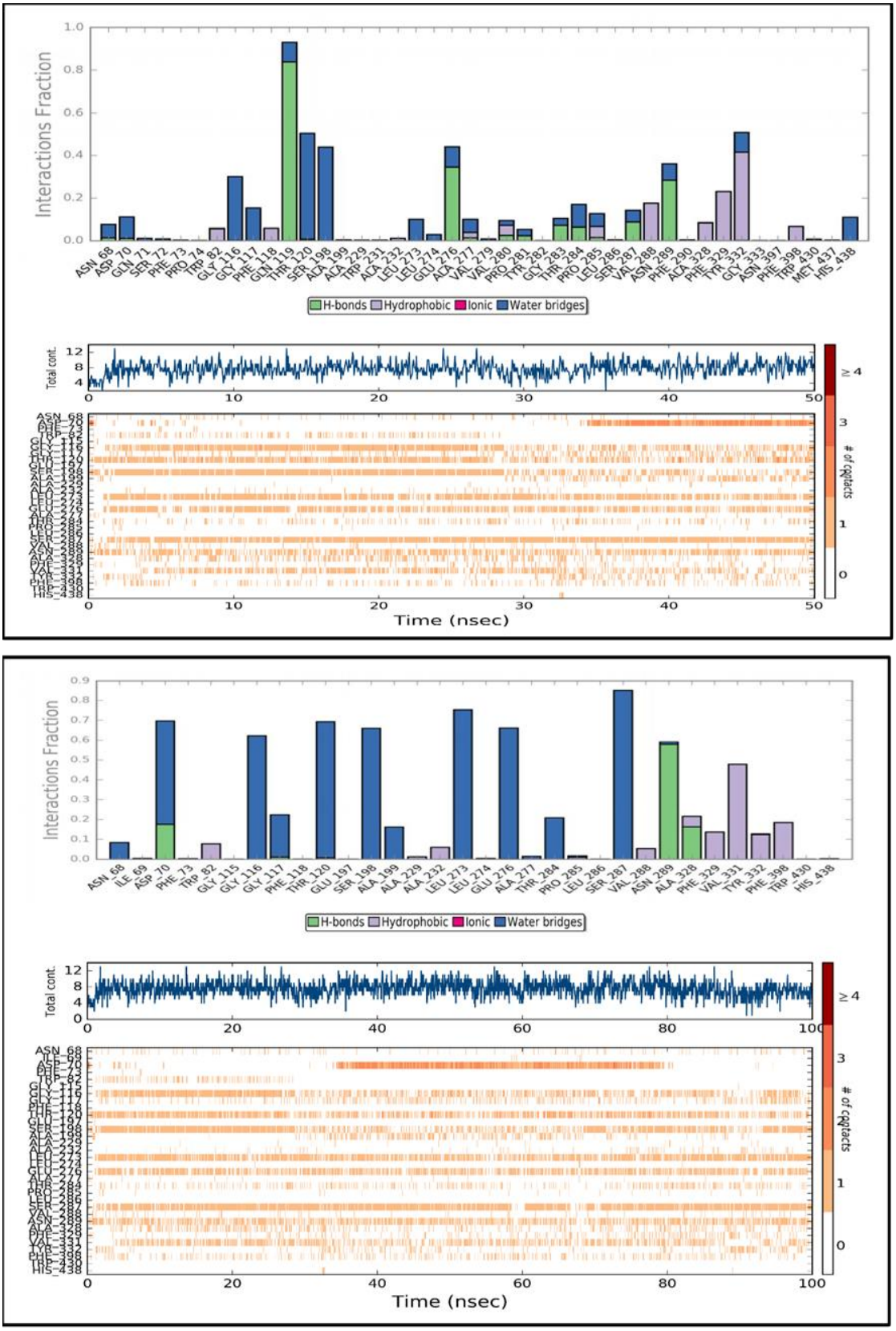

Figure 6. 32 The average interaction fractions of contact residues diagram and timeline representation of the interactions and contacts throughout the MD simulations of nelfinavir at the binding pocket of BuChE

(top: 50-ns, bottom: 100-ns)

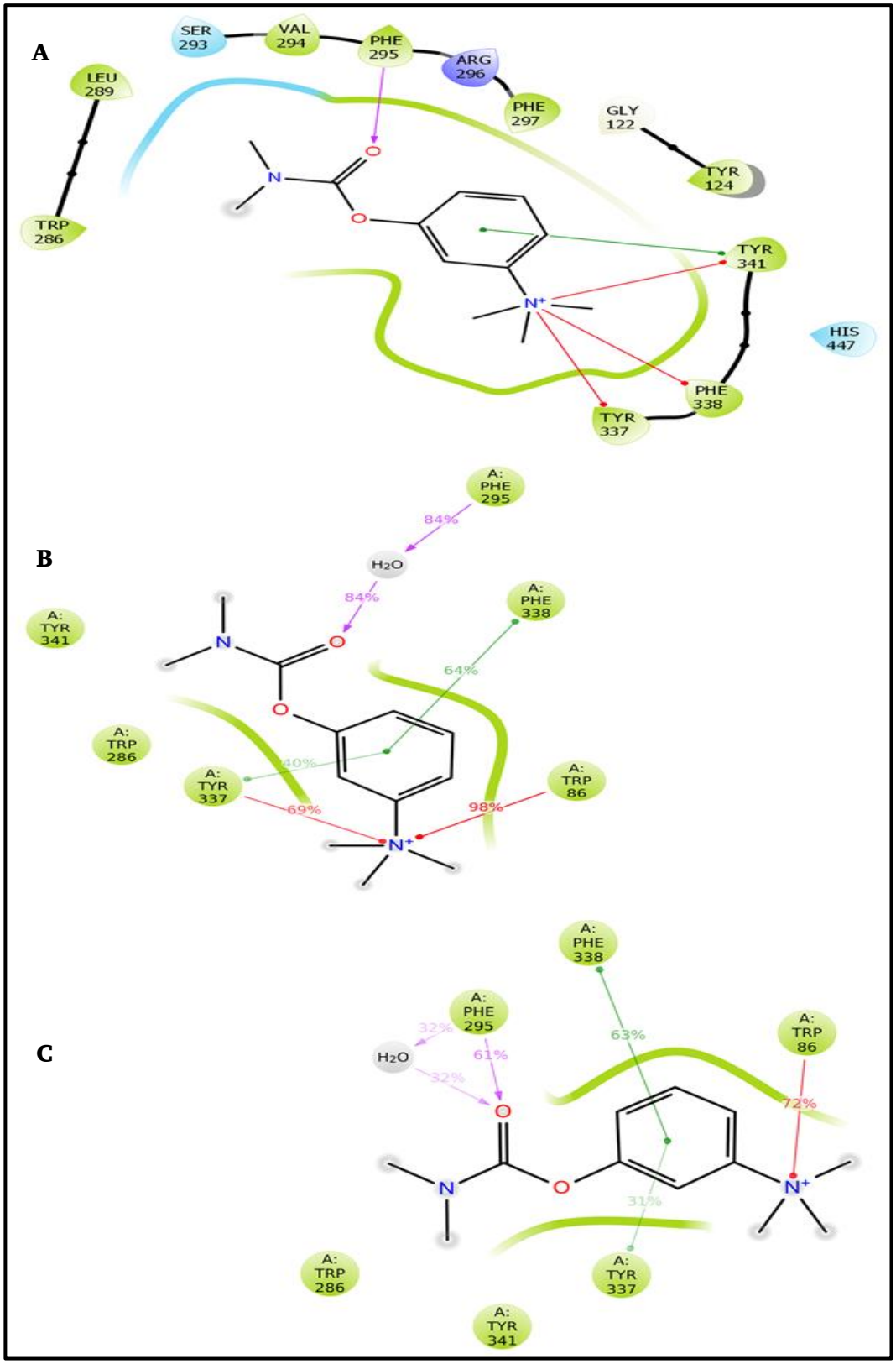

Figure 6. 33 (A) The two-dimensional IFD ligand interaction and average interaction scores of contact residues diagram throughout the MD simulations of neostigmine at the AChE binding pocket

((B)50-ns, (C)100-ns)

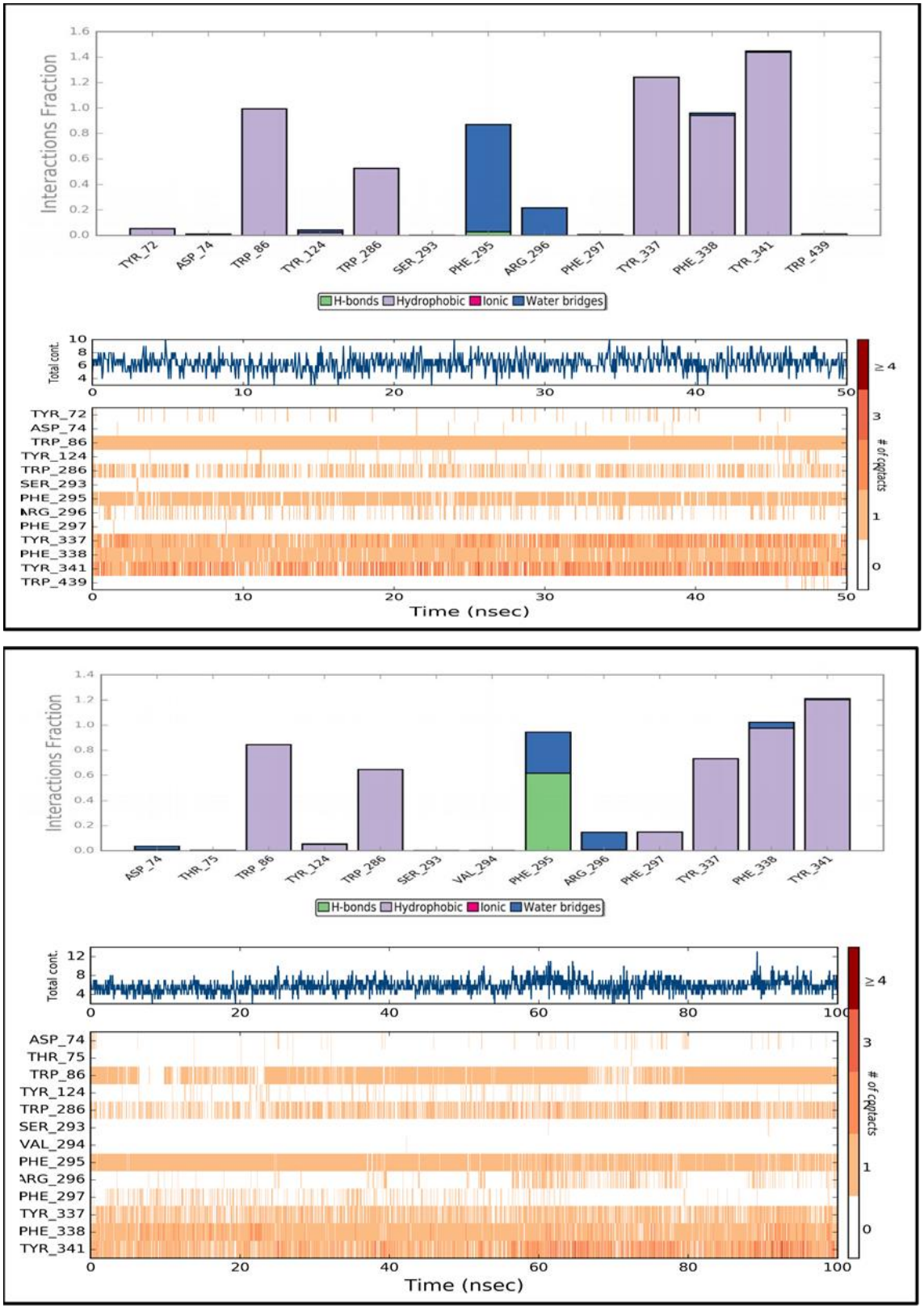

Figure 6. 34 The average interaction fractions of contact residues diagram and timeline representation of the interactions and contacts throughout the MD simulations of neostigmine at the binding pocket of AChE

(top: 50-ns, bottom: 100-ns)

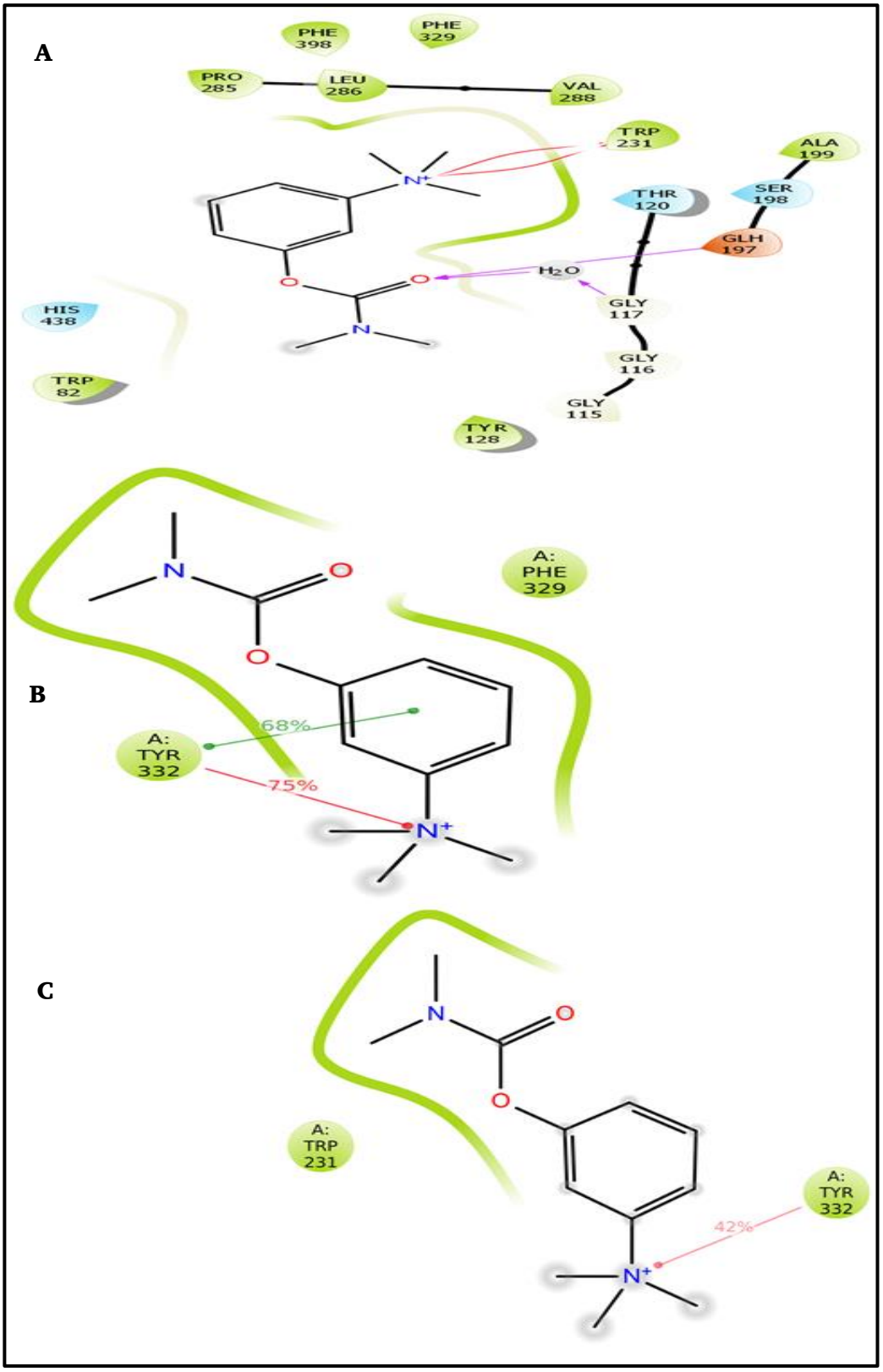

Figure 6. 35 (A) The two-dimensional IFD ligand interaction and average interaction scores of contact residues diagram throughout the MD simulations of neostigmine at the BuChE binding pocket

((B)50-ns, (C)100-ns)

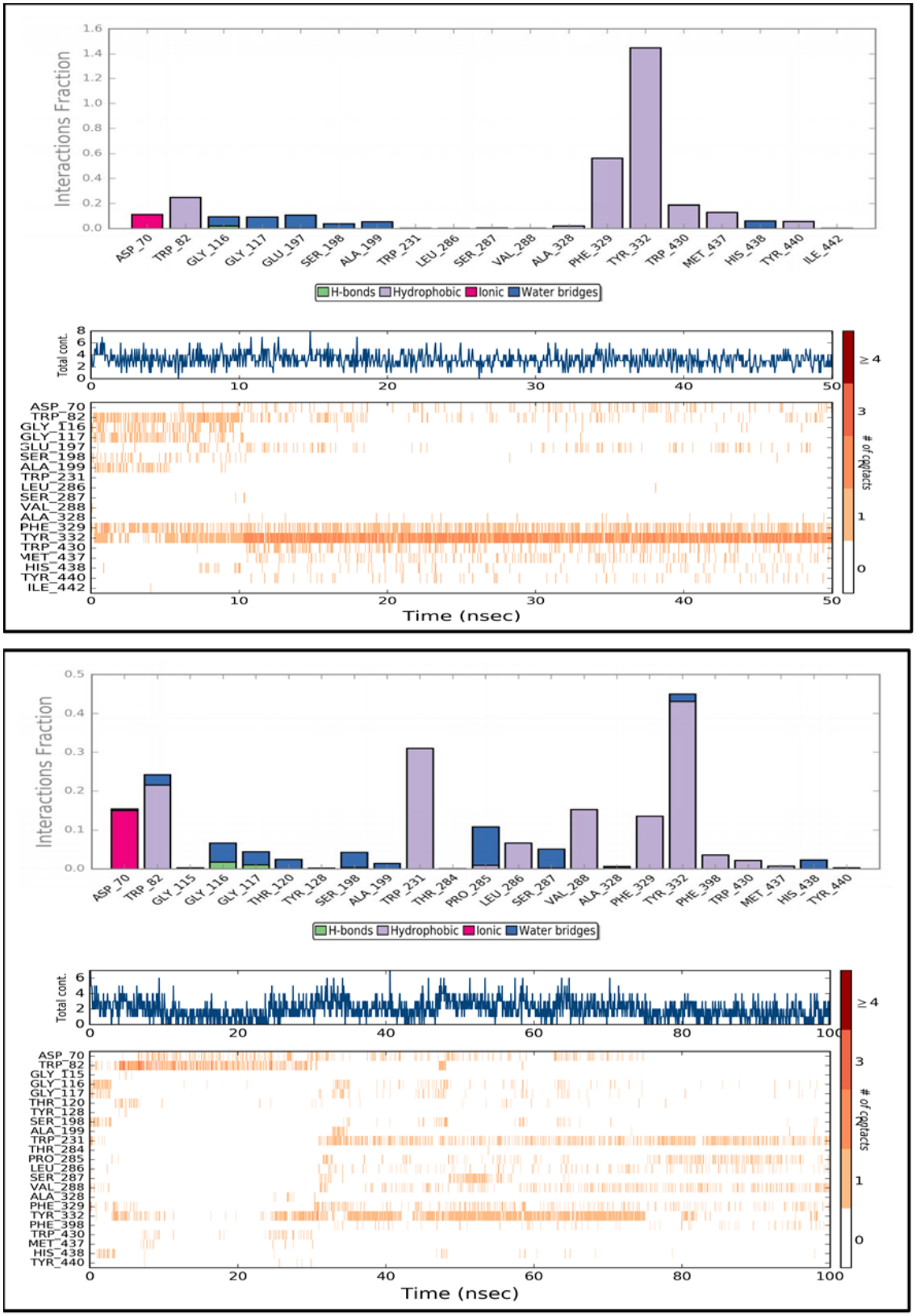

Figure 6. 36 The average interaction fractions of contact residues diagram and timeline representation of the interactions and contacts throughout the MD simulations of neostigmine at the binding pocket of BuChE

(top: 50-ns, bottom: 100-ns)

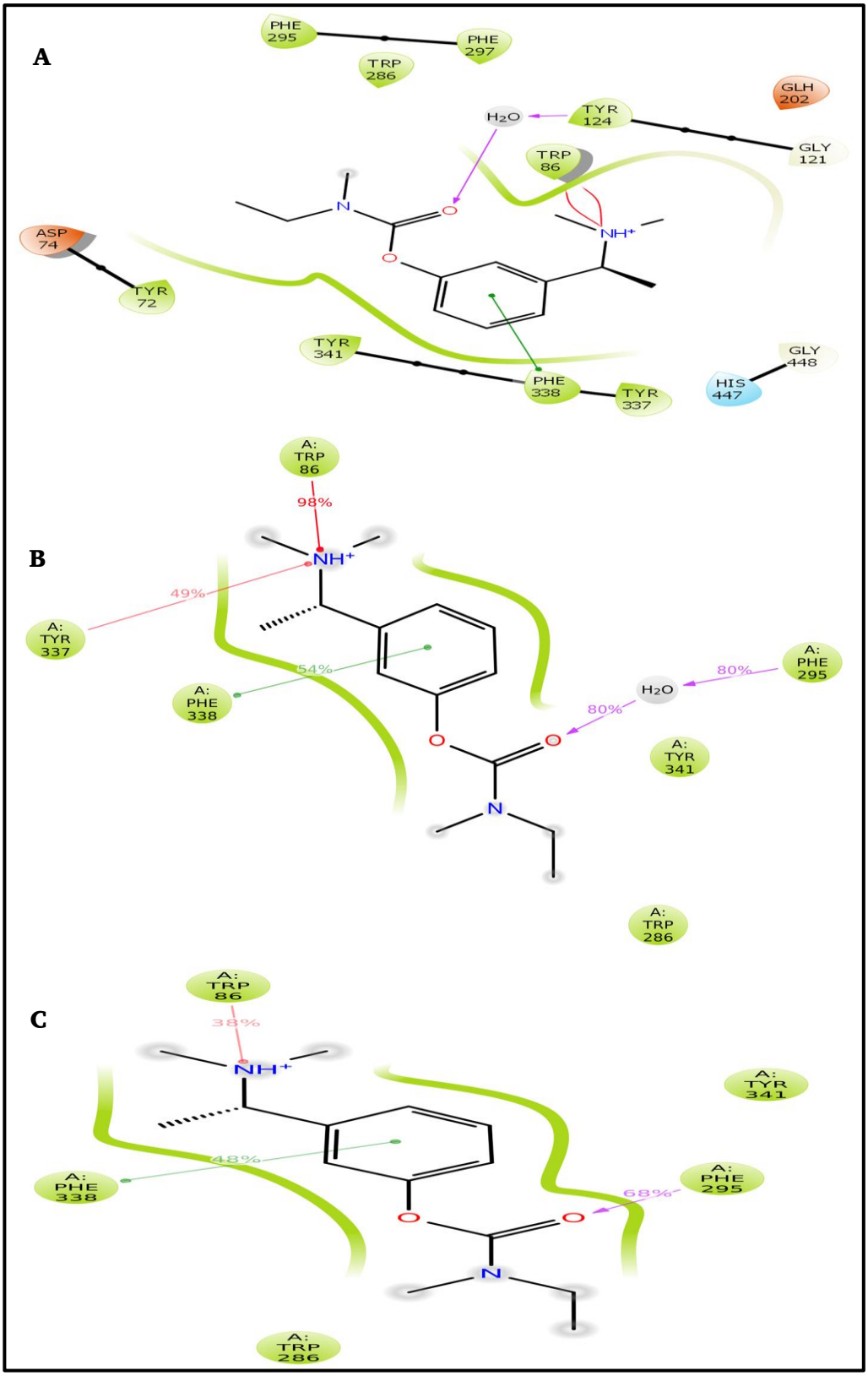

Figure 6. 37 (A) The two-dimensional IFD ligand interaction and average interaction scores of contact residues diagram throughout the MD simulations of rivastigmine at the AChE binding pocket

((B)50-ns, (C)100-ns)

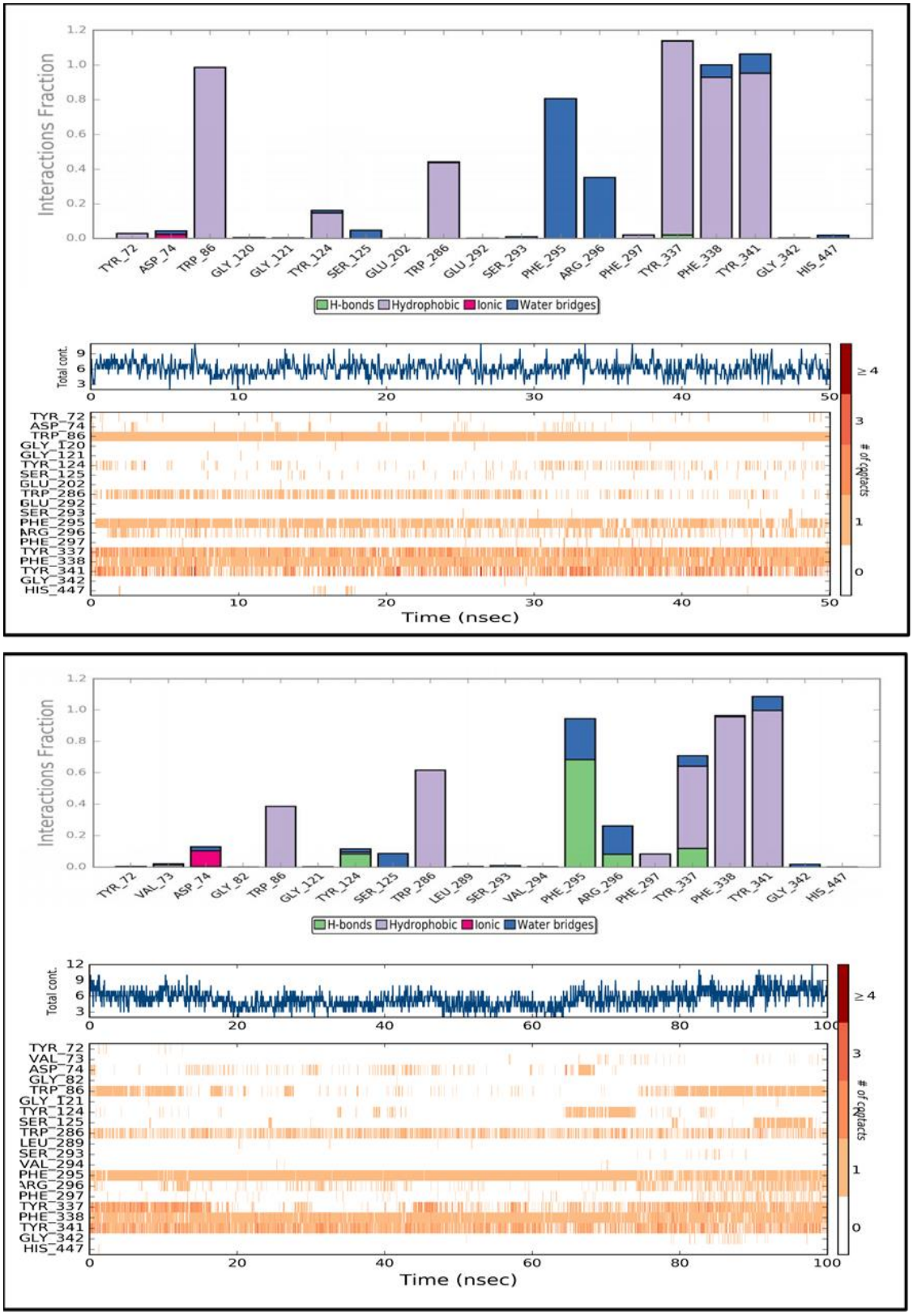

Figure 6. 38 The average interaction fractions of contact residues diagram and timeline representation of the interactions and contacts throughout the MD simulations of rivastigmine at the binding pocket of AChE

(top: 50-ns, bottom: 100-ns)

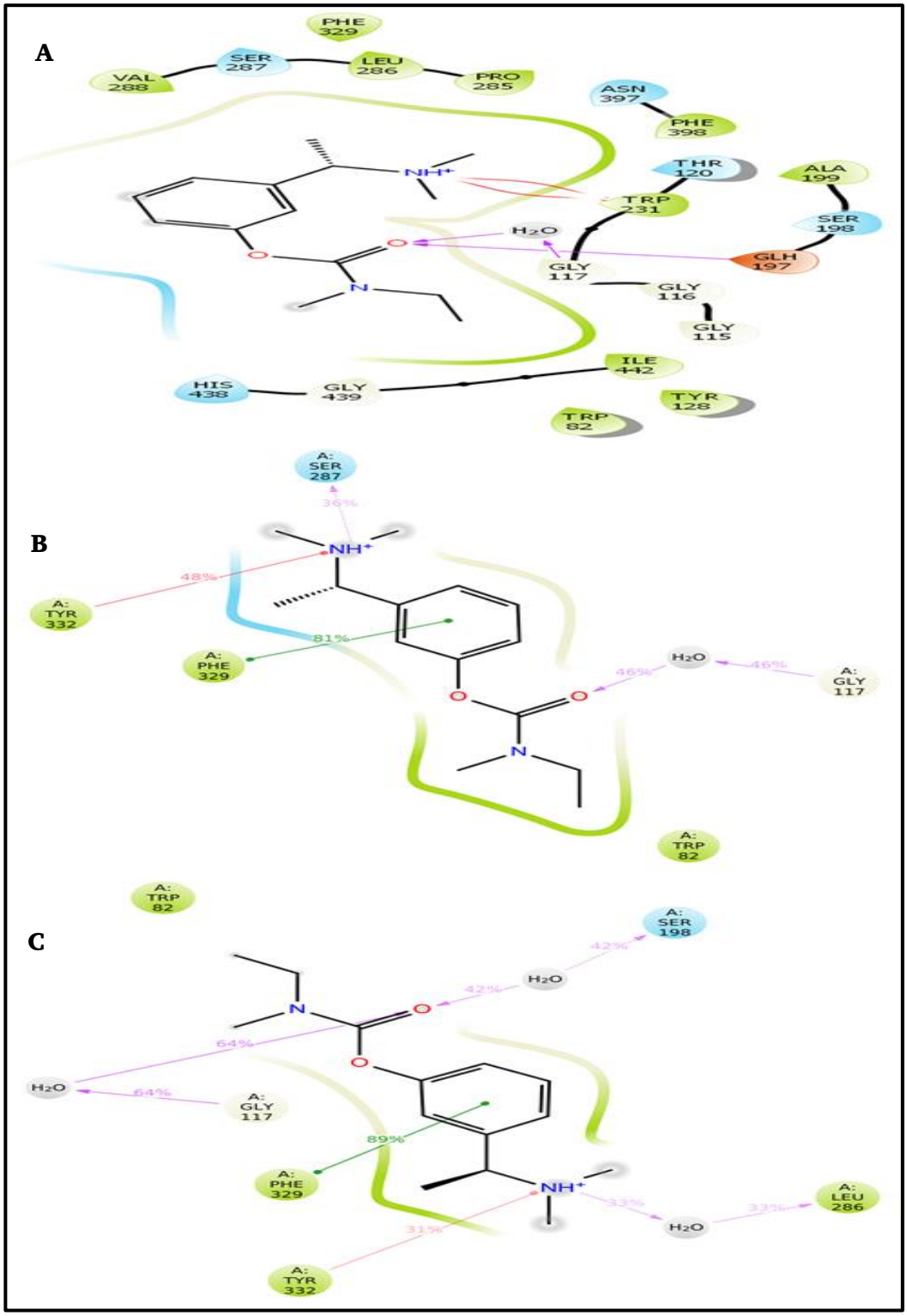

Figure 6. 39 (A) The two-dimensional IFD ligand interaction and average interaction scores of contact residues diagram throughout the MD simulations of rivastigmine at the BuChE binding pocket

((B)50-ns, (C)100-ns)

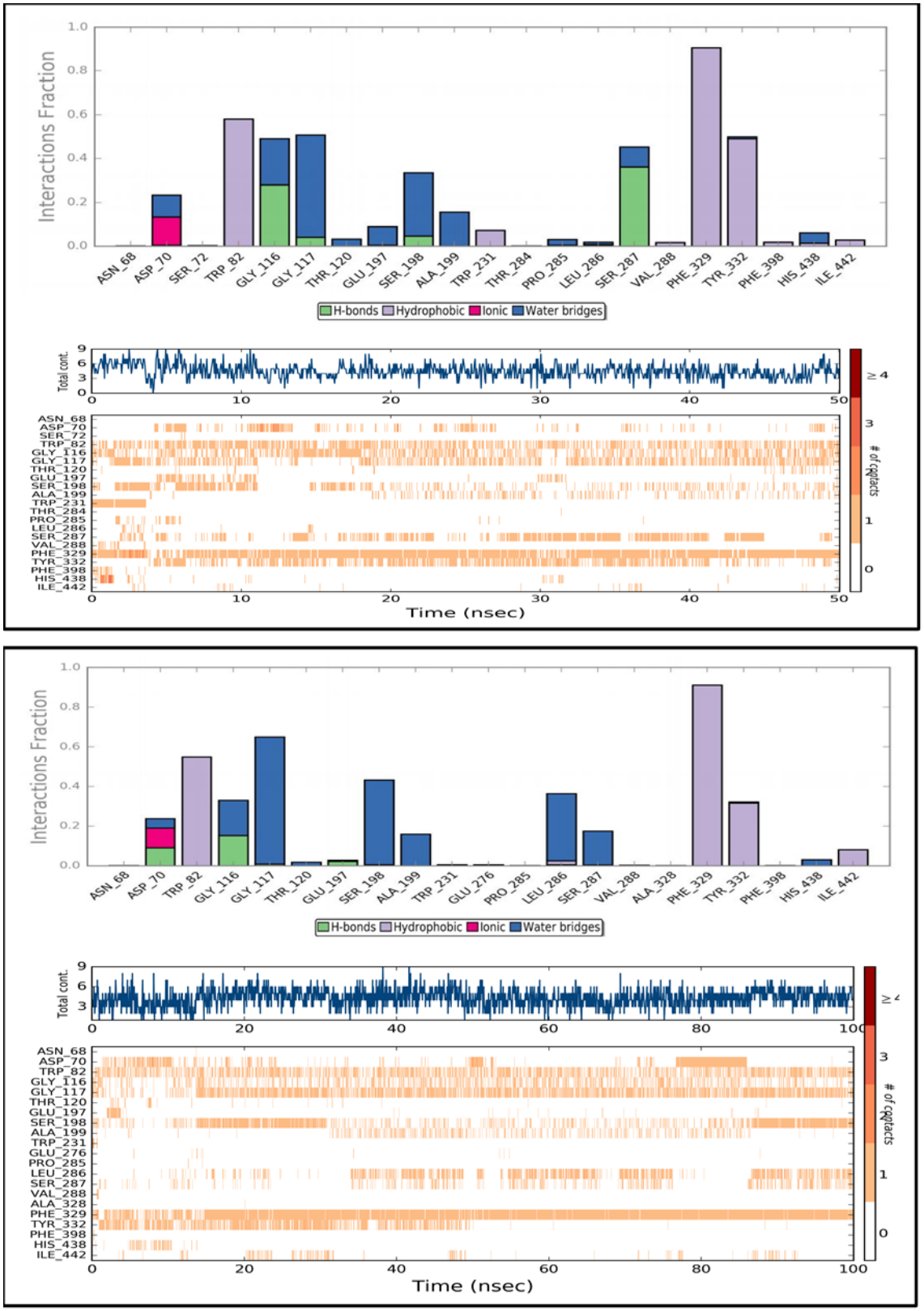

Figure 6. 40 The average interaction fractions of contact residues diagram and timeline representation of the interactions and contacts throughout the MD simulations of rivastigmine at the binding pocket of BuChE

(top: 50-ns, bottom: 100-ns)

Our goal was to analyze the structural stability of the protein-ligand complexes and determine the primary and long-standing interactions between protein and ligands. Therefore, the structural and dynamic properties of the binding pocket need to be elucidated. Throughout the MD simulations, particularly for Cα atoms of protein structures, we have performed root mean square deviations (RMSD) calculations. We have also measured the RMSD of the ligand molecules via considering 2 distinct fitting modes: (fit on protein/LigFitProt) and (fit on ligand/LigFitLig).

Using RMSD and RMSF plots, the residual deviations, and fluctuations in the complexes have been established. RMSD is managed to measure the average change in atoms' displacement for a particular frame or the ligand concerning a reference for a particular trajectory frame. To check the equilibrium of MD trajectories, RSMD is an essential parameter. It is calculated for all frames in the trajectory. RMSD plots of selected five hits are provided in (Table 6.8) and (Figures 6.41, 6.42, 6.43, and 6.44).

RMSD-time graphs show that all systems under analysis have smaller structural changes (<2.5 Å) based on the initial protein-ligand complexes, and after 50-ns and 100-ns, all complex systems show structurally stability. Figure 6.41 and 6.42 showed that donepezil had the largest increment in RMSD through 50-ns simulations and ocaperidone through 100-ns based on the graphs with AChE. While Figures 6.43 and 6.44 showed nelfinavir and risperidone with BuChE had the largest increment in RMSD Through 50 and 100-ns simulations based on the graphs and table results.

Table 6. 8 RMSD scores for the 50 and 100 ns simulations and the averages of the studied ligands

Molecules Names	AChE			BuChE		
	Cα RMSD (Å)	**LFP[a] RMSD (Å)**	**LiFL[b] RMSD (Å)**	**Cα RMSD (Å)**	**LFP[a] RMSD (Å)**	**LiFL[b] RMSD (Å)**
Donepezil50	1.950	1.328	0.582	1.369	2.973	2.074
Donepezil100	1.689	1.213	0.675	1.517	3.753	2.285
Average	**1.820**	**1.270**	**0.630**	**1.443**	**3.363**	**2.180**
Ocaperidone50	1.391	3.192	2.192	1.417	3.705	1.642
Ocaperidone100	1.850	3.201	1.662	1.451	3.714	1.593
Average	**1.620**	**3.200**	**1.927**	**1.434**	**3.710**	**1.638**
Cafedrine50	1.646	2.915	1.235	1.453	1.066	0.657
Cafedrine100	1.688	1.795	1.379	1.368	4.212	1.587
Average	**1.670**	**2.355**	**1.307**	**1.410**	**2.639**	**1.122**
Isosulpride50	1.641	4.471	1.728	1.397	2.208	1.681
Isosulpride100	1.793	3.708	1.788	1.570	2.048	1.311
Average	**1.717**	**4.089**	**1.758**	**1.483**	**2.128**	**1.496**
Risperidone50	1.660	2.072	1.107	1.463	2.827	1.215
Risperidone100	1.426	1.653	0.984	1.691	3.378	2.107
Average	**1.543**	**1.863**	**1.045**	**1.577**	**3.102**	**1.661**
Nelfinavir5-	1.653	5.683	2.211	1.464	3.442	1.832
Nelfinavir100	1.558	7.729	2.233	1.618	2.085	0.976
Average	**1.605**	**6.706**	**2.222**	**1.541**	**2.763**	**1.404**
Neostigmine50	1.400	2.416	1.171	1.471	5.187	1.062
Neostigmine100	1.476	2.388	1.093	1.388	6.168	0.833
Average	**1.438**	**2.402**	**1.132**	**1.430**	**5.677**	**0.947**
Rivastigmine50	1.642	2.523	0.660	1.304	4.142	1.640
Rivastigmine100	1.779	4.254	0.766	1.439	3.641	1.711
Average	**1.710**	**3.388**	**0.713**	**1.371**	**3.891**	**1.675**

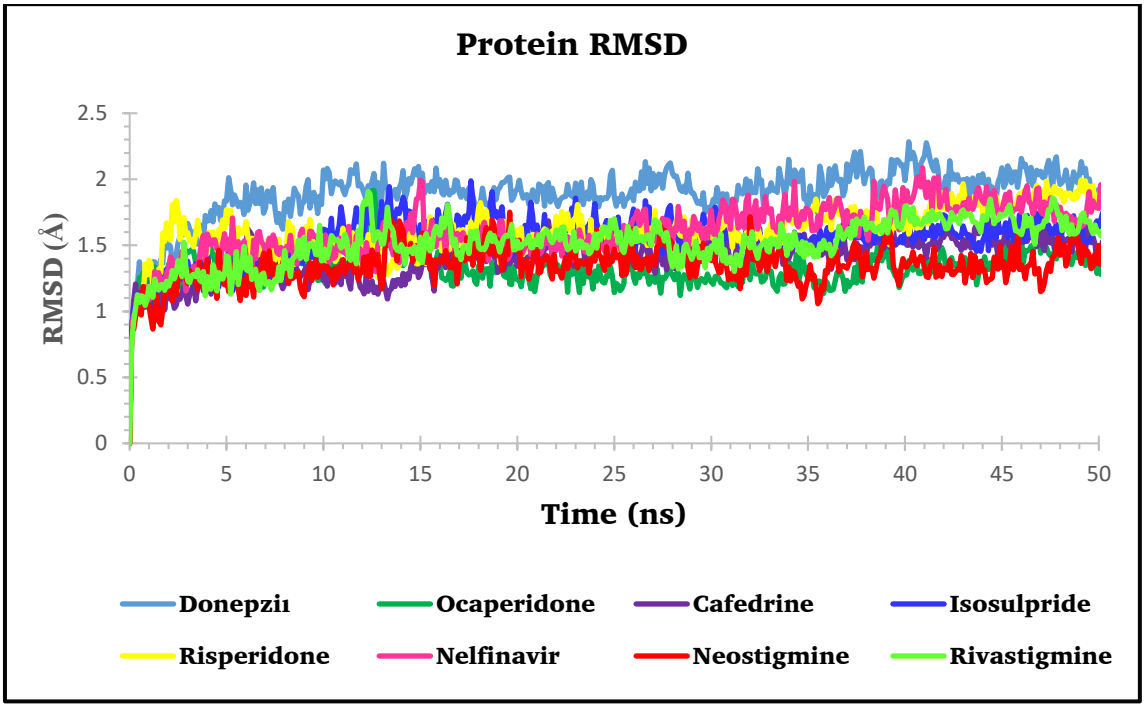

Figure 6. 41 The protein RMSD graph of the Cα atoms of the AChE throughout 50 ns MD simulations

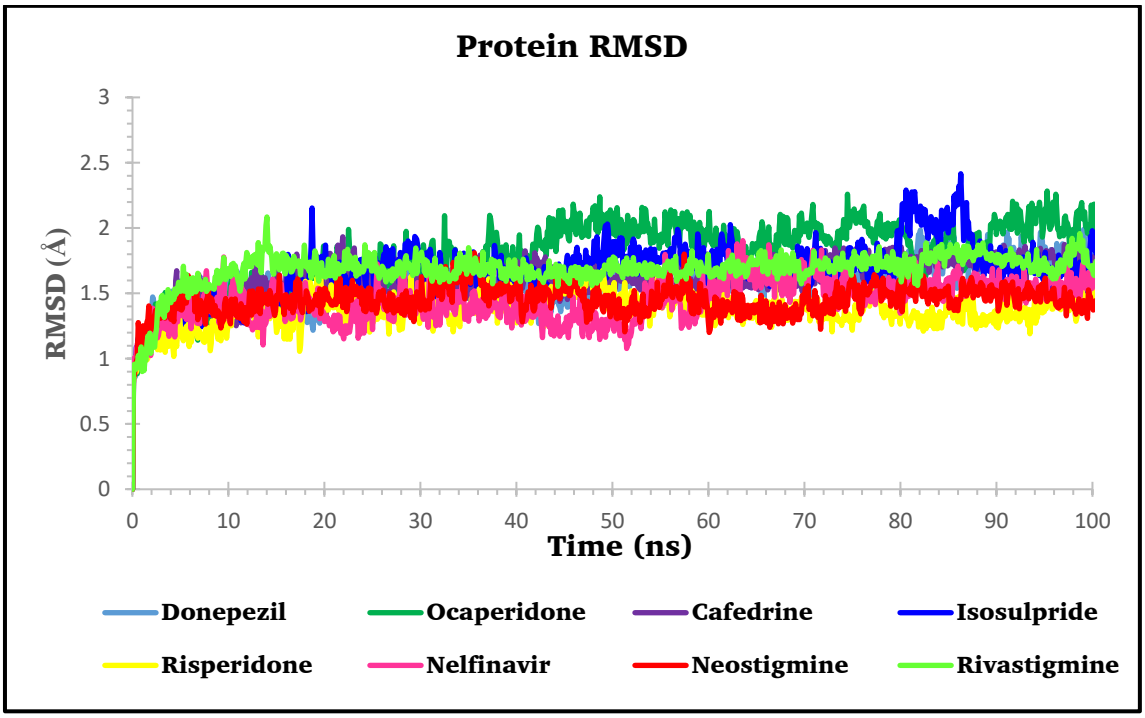

Figure 6. 42 The protein RMSD graph of the Cα atoms of the AChE throughout 100 ns MD simulations

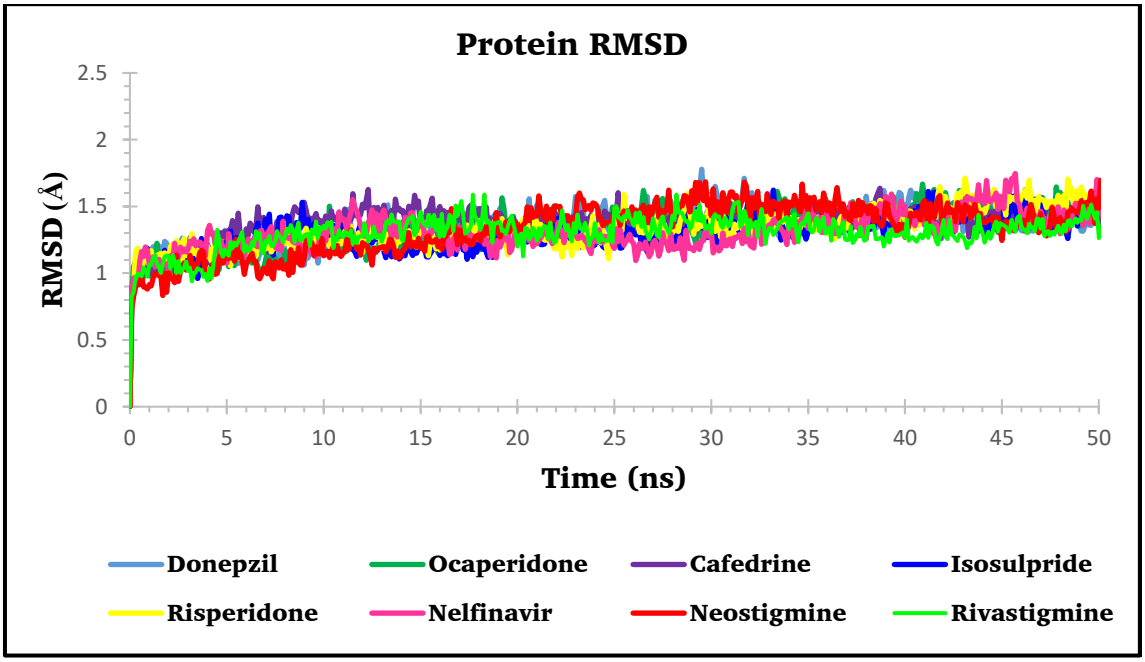

Figure 6. 43 The protein RMSD graph of the Cα atoms of the BuChE throughout 50 ns MD simulations

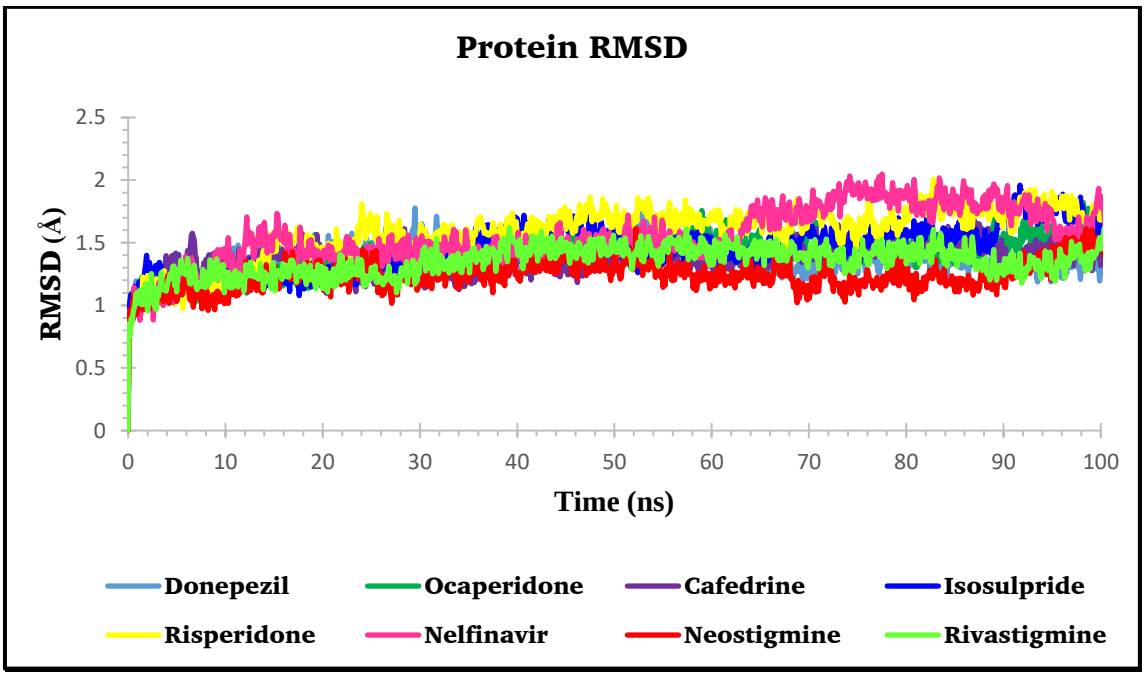

Figure 6. 44 The protein RMSD graph of the Cα atoms of the BuChE throughout 100 ns MD simulations

With LigFitProt RMSDs estimates, ligands' translational movements were plotted at the binding pocket of both enzymes, (Figures 6.45, 6.46, 6.47 and 6.48). LigFitProt RMSD plots reflect a ligand’s RMSD when the protein-ligand complex is first aligned as a reference point on the protein backbone, and the RMSDs of the ligand’s non-hydrogen atoms is determined. Table 6.8 shows the average RMSD values. The findings revealed that the analyzed compounds presented elevated disruptions in their binding site of the target enzymes through the MD simulations. It can be seen that nelfinavir, isosulpride, and rivastigmine deviate from the initial RMSD values through 50 and 100 ns MD simulations with AChE showed an average LigFitProt RMSD of 6.706, 4.089 and 3.388 Å, respectively. At the same time, reference molecules neostigmine, rivastigmine and studied ocaperidone drugs divert from the initial RMSD values with BuChE within 50 and 100 ns MD simulations. Their average values were 5.677, 3.891 and 3.710 Å, respectively. However, other molecules are more structurally stable with the protein. Thus, these four molecules diffuse from the binding pocket, but other molecules stay at the binding pocket through the MD simulations.

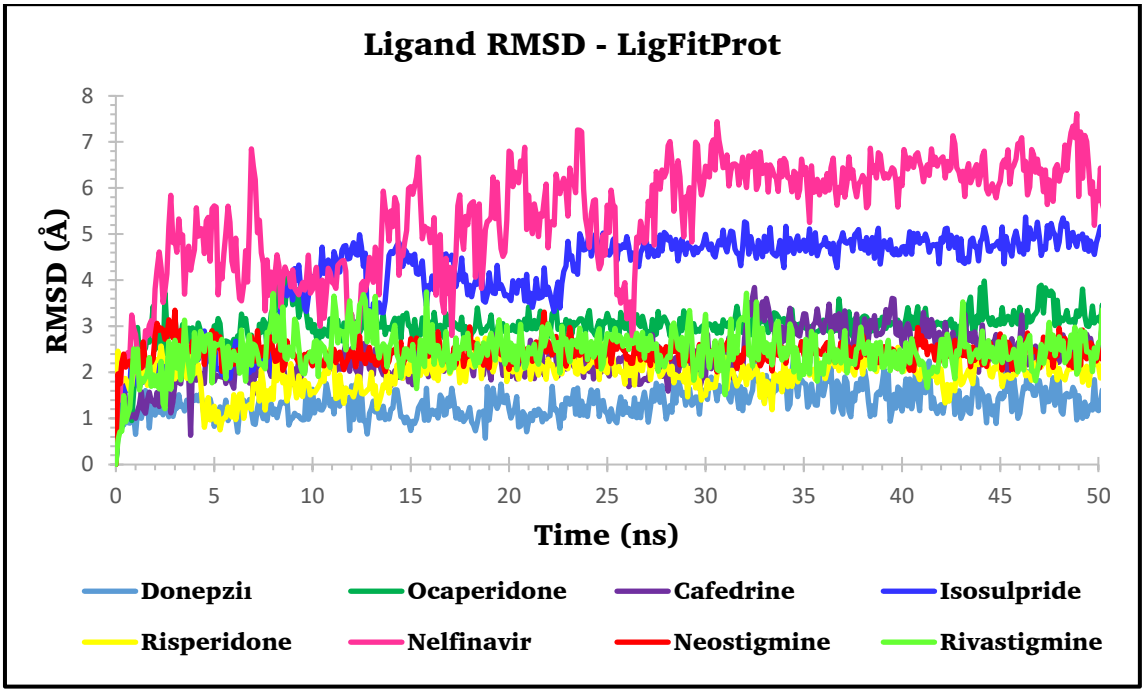

Figure 6. 45 The LigFitProt RMSD graph for the 5 hits and reference compounds with AChE (50 ns)

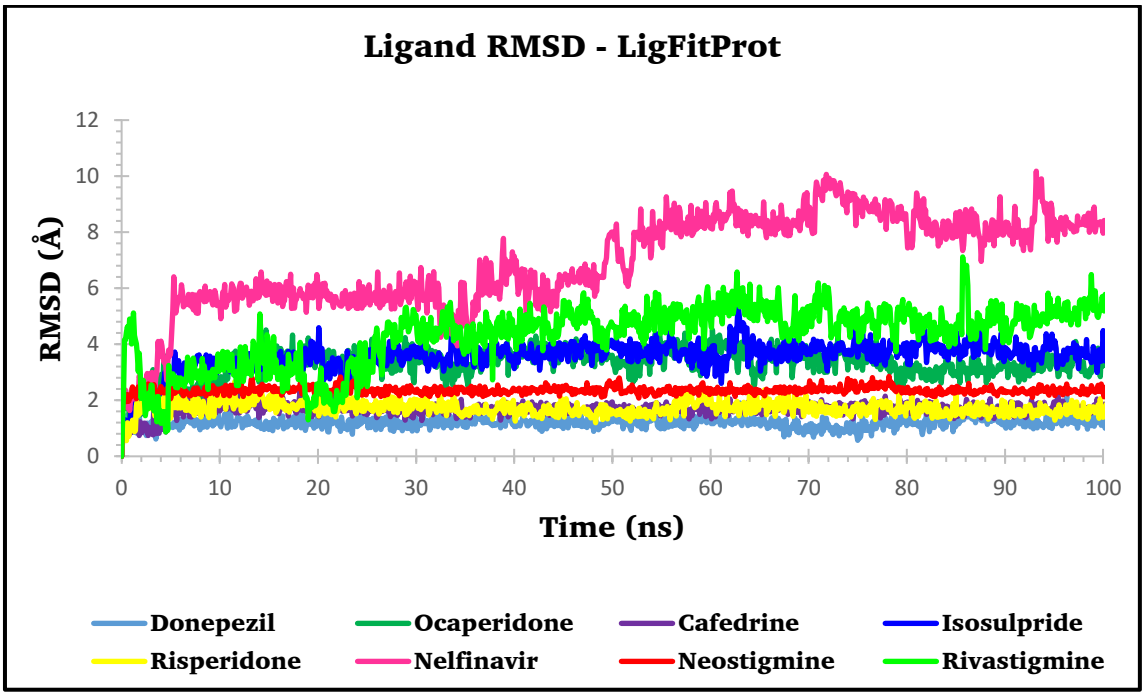

Figure 6. 46 The LigFitProt RMSD graph for the 5 hits and reference compounds with AChE (100 ns)

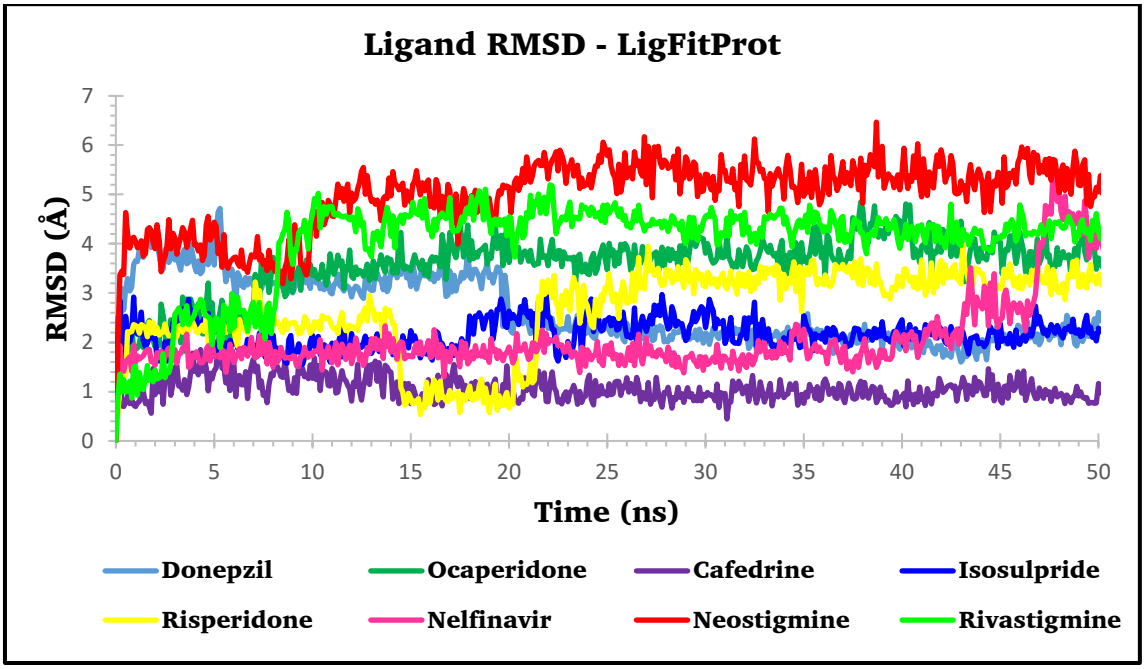

Figure 6. 47 The LigFitProt RMSD graph for the 5 hits and reference compounds with BuChE (50 ns)

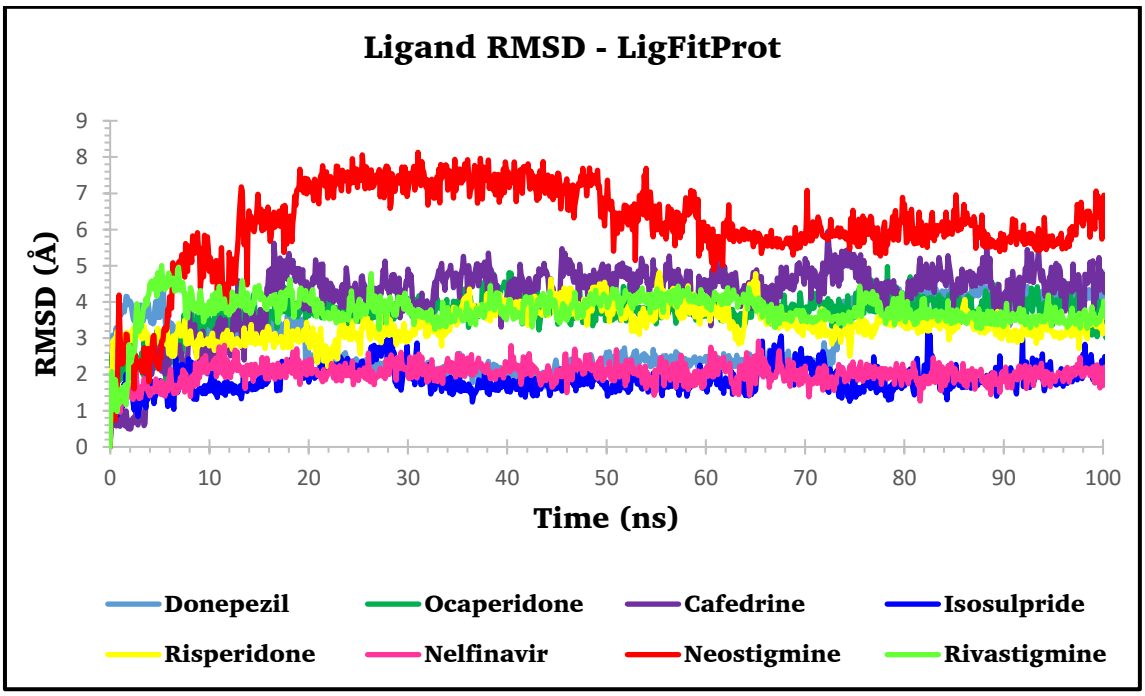

Figure 6. 48 The LigFitProt RMSD graph for the 5 hits and reference compounds with BuChE (100 ns)

Rotational motion of the ligands in the binding pocket of AChE and BuChE was also studied by using LigFitLig RMSD in (Figures 6.49, 6.50, 6.51, and 6.52). In LigFitLig RMSD plots, deviations of coordinates of non-hydrogen atoms of the ligand, based on initial conformations, are plotted. The average LigFitLig of the molecules analyzed was less than 3.0 Å, reflecting that the molecules tested do not significantly modify their rotational motion. Table 6.8 also displays the average values of LigFitLig RMSDs for the examined molecules. Nelfinavir, ocaperidone, and isosulpride show rotational motion however, other molecules are stable in the binding pocket of AChE through 50-ns and 100-ns MD simulations. At the binding pocket of AChE, all references compounds displayed very rigid behavior. Their total values were less than 1.5 Å. Nelfinavir showed the high average rotational motion of 2.211 and 2.233 Å, respectively. While with BuChE, throughout MD simulations, donepezil showed a high rotational motion of 2.074 and 2.285 Å, respectively.

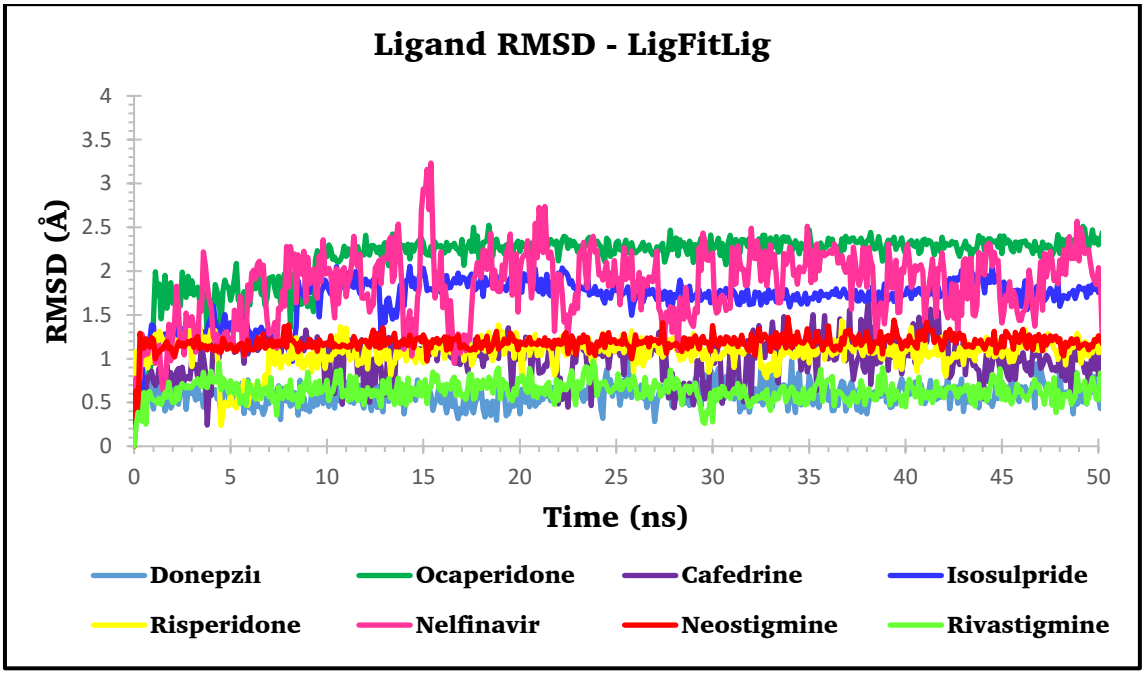

Figure 6. 49 The LigFitLig RMSD graph for the 5 hits and reference compounds with AChE (50 ns)

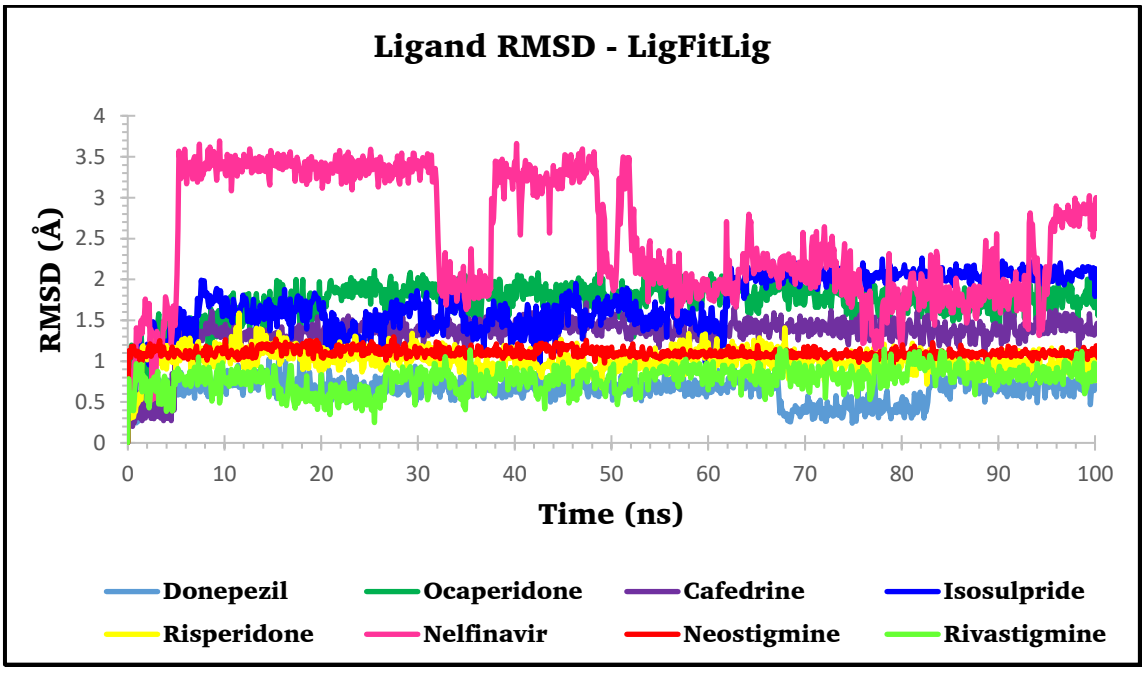

Figure 6. 50 The LigFitLig RMSD graph for the 5 hits and reference compounds with AChE (100 ns)

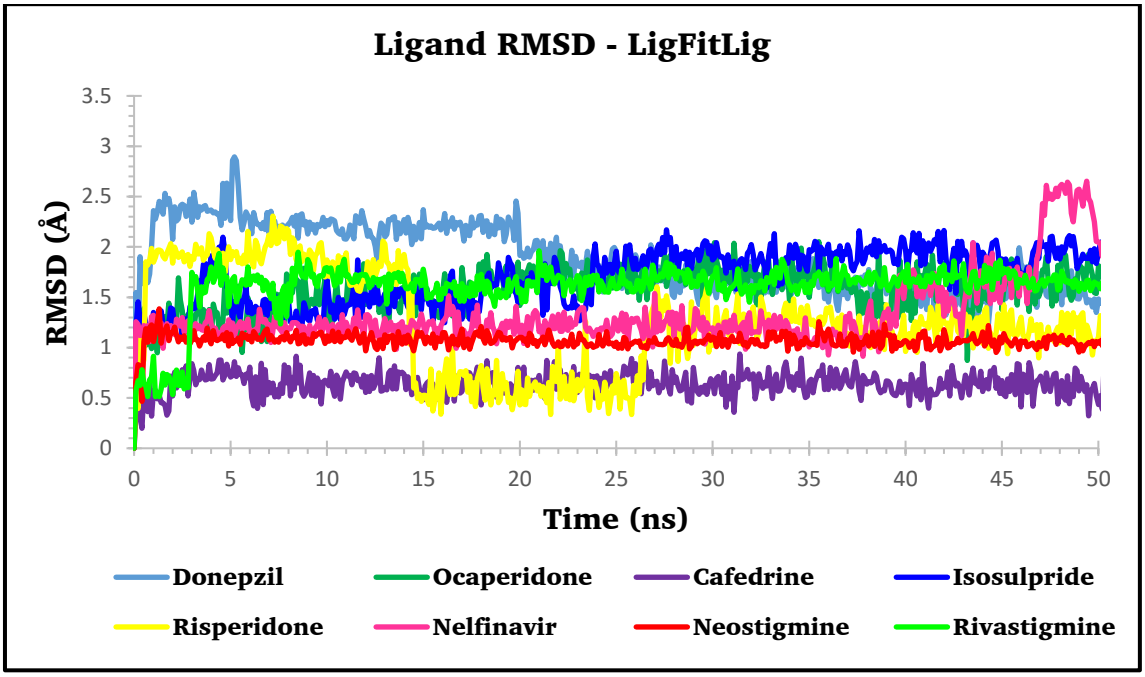

Figure 6. 51 The LigFitLig RMSD graph for the 5 hits and reference compounds with BuChE (50 ns)

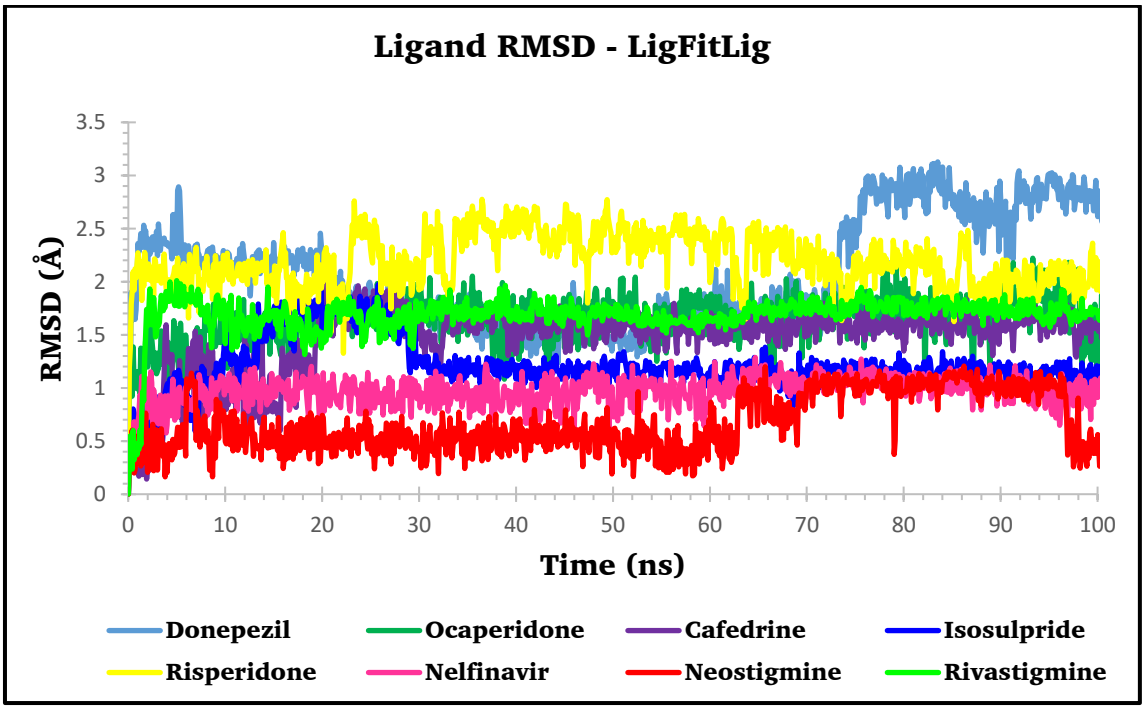

Figure 6. 52 The LigFitLig RMSD graph for the 5 hits and reference compounds with BuChE (100 ns)

Root mean square fluctuation (RMSF) values were also calculated to analyze the effect of the hits found on the target protein's backbone atoms' mobility, Figures (6.53, 6.54, 6.55, and 6.56). Generally, fluctuations are expected at the tail regions (N- and C- terminal). Furthermore, the α-helices and β-sheets are expected to remain relatively rigid through the simulation since they are secondary structural components. On the other hand, loops are expected to have more flexibility when compared. The RMSF of each amino acid residue's backbone atoms were created in complex analysis to identify the target structure's fluctuation regions. In RMSF figures through MD simulations, high RMSF values mean highly mobile areas, and low RMSF values reflect the studied system's low flexibility. All complexes' residues showed fluctuation between 1 to 4 Å except risperidone and rivastigmine, which show a fluctuation range of 5 to 7 Å with AChE in 50 and 100-ns simulations. For BuChE, risperidone and the reference drug neostigmine showed a high fluctuation range of 6 Å. Overall all complexes were stable and in an acceptable range.

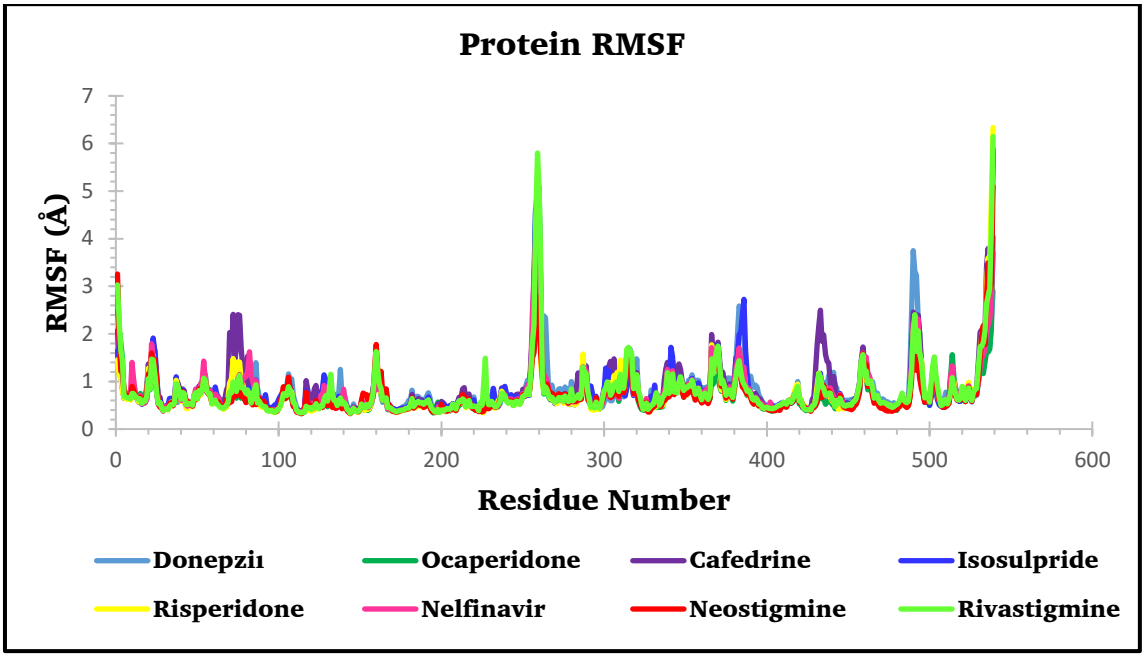

Figure 6. 53 The RMSF graphs for the 5 hits and reference compounds with AChE (50-ns)

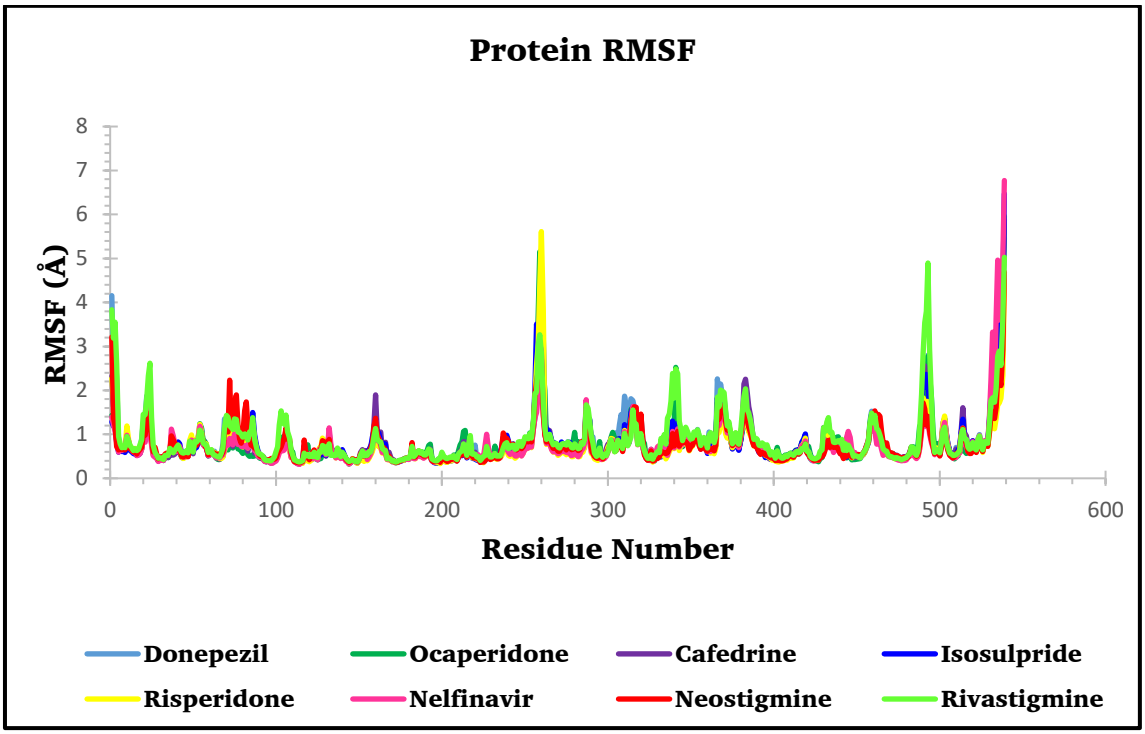

Figure 6. 54 The RMSF graphs for the 5 hits and reference compounds with AChE (100-ns)

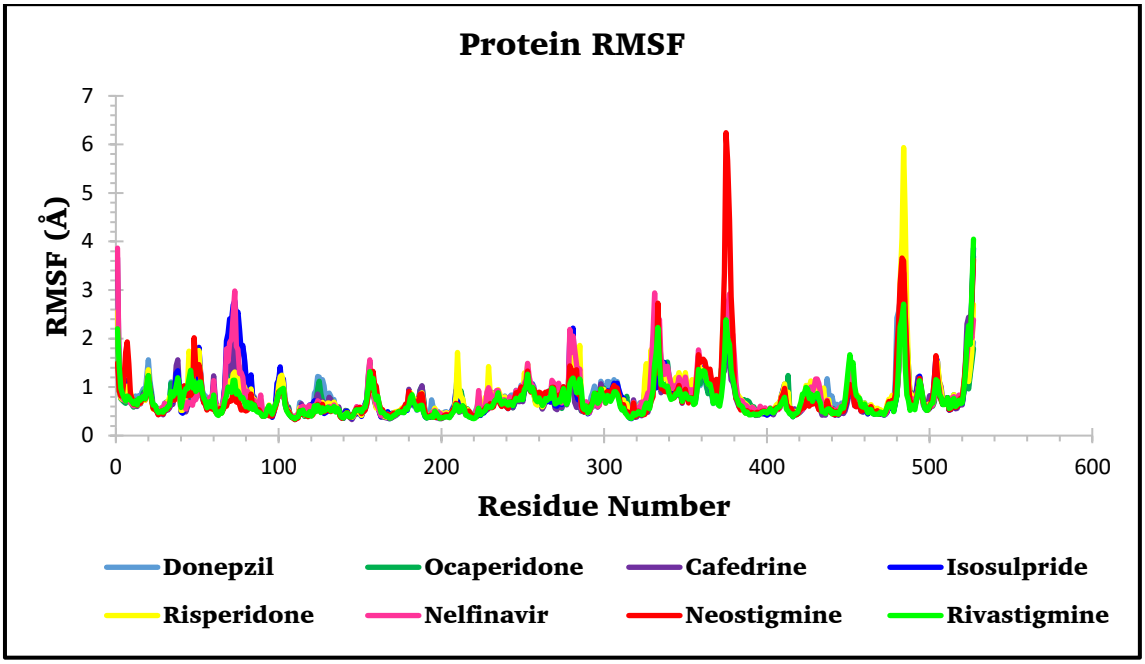

Figure 6. 55 The RMSF graphs for the 5 hits and reference compounds with BuChE (50-ns)

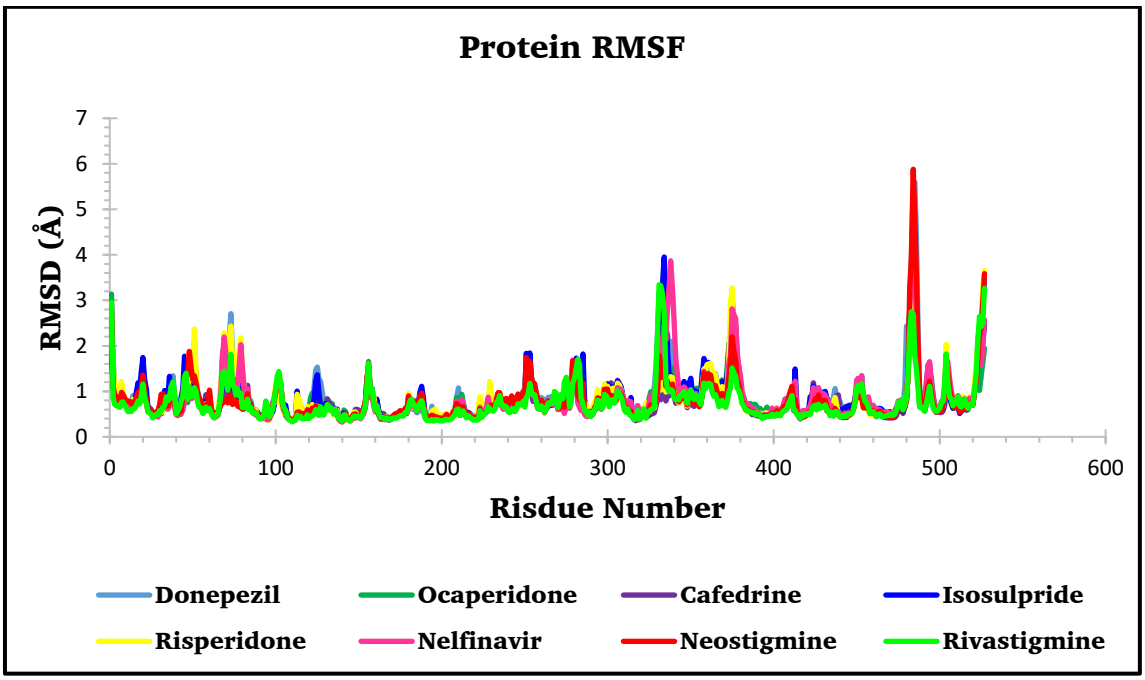

Figure 6. 56 The RMSF graphs for the 5 hits and reference compounds with BuChE (100-ns)

We have plotted the 3D of the Protein - Inhibitor complexes, 2D interaction maps, and surface filling model of the protein in Figures 6.57, 6.61, 6.65, 6.69, 6.73, 6.77, 6.81, and 6.85 for AChE and in figures 6.59, 6.63, 6.67, 6.71, 6.75, 6.97, 6.83, and 6.87 for BuChE (donepezil, ocaperidone, cafedrine, isosulpride, risperidone, nelfinavir, neostigmine, rivastigmine, respectively for AChE and then BuChE). Upper panel shows the details of 50-ns MD simulations, and the lower panel shows the details of 100-ns MD simulations.

Figures 6.58, 6.62, 6.66, 6.70, 6.74, 6.78, 6.82, and 6.86 show the conformational changes throughout the MD simulations of AChE both for the protein and the ligand. Starting conformations depicted in red color, and the final conformations depicted in blue, trajectory colored in red-white-blue scale. Upper panels show the 50-ns MD simulations and the lower panels show 100-ns MD simulations. Protein structures depicted in cartoon and ligands depicted in stick representation. Figures 6.60, 6.64, 6.68, 6.72, 6.76, 6.80, 6.84, and 6.88 show the conformational changes for the BuChE systems.

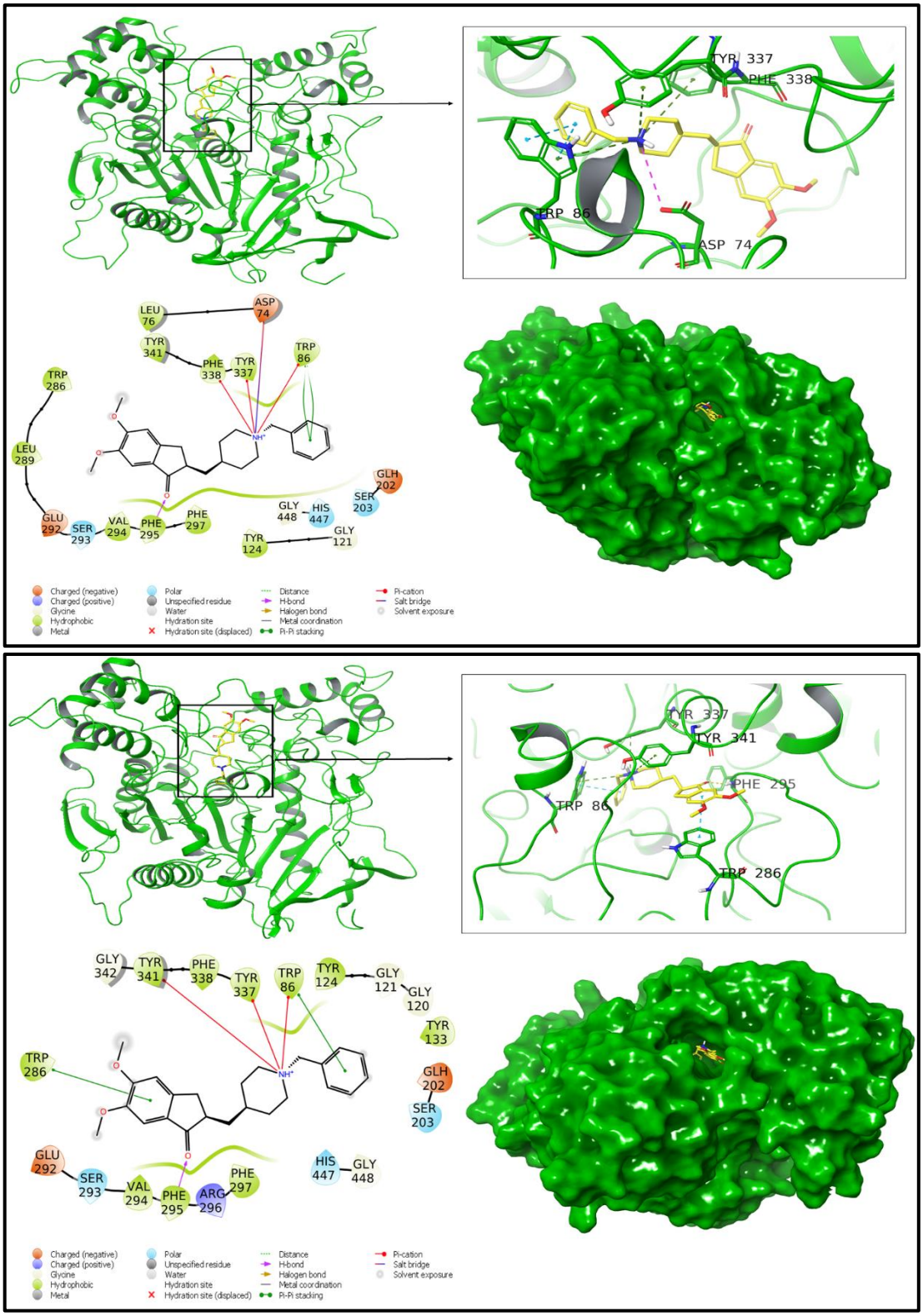

Figure 6. 57 2D and 3D ligand interaction diagrams during MD simulation of top docking pose of donepezil with AChE

(up:50-ns; dowm:100-ns)

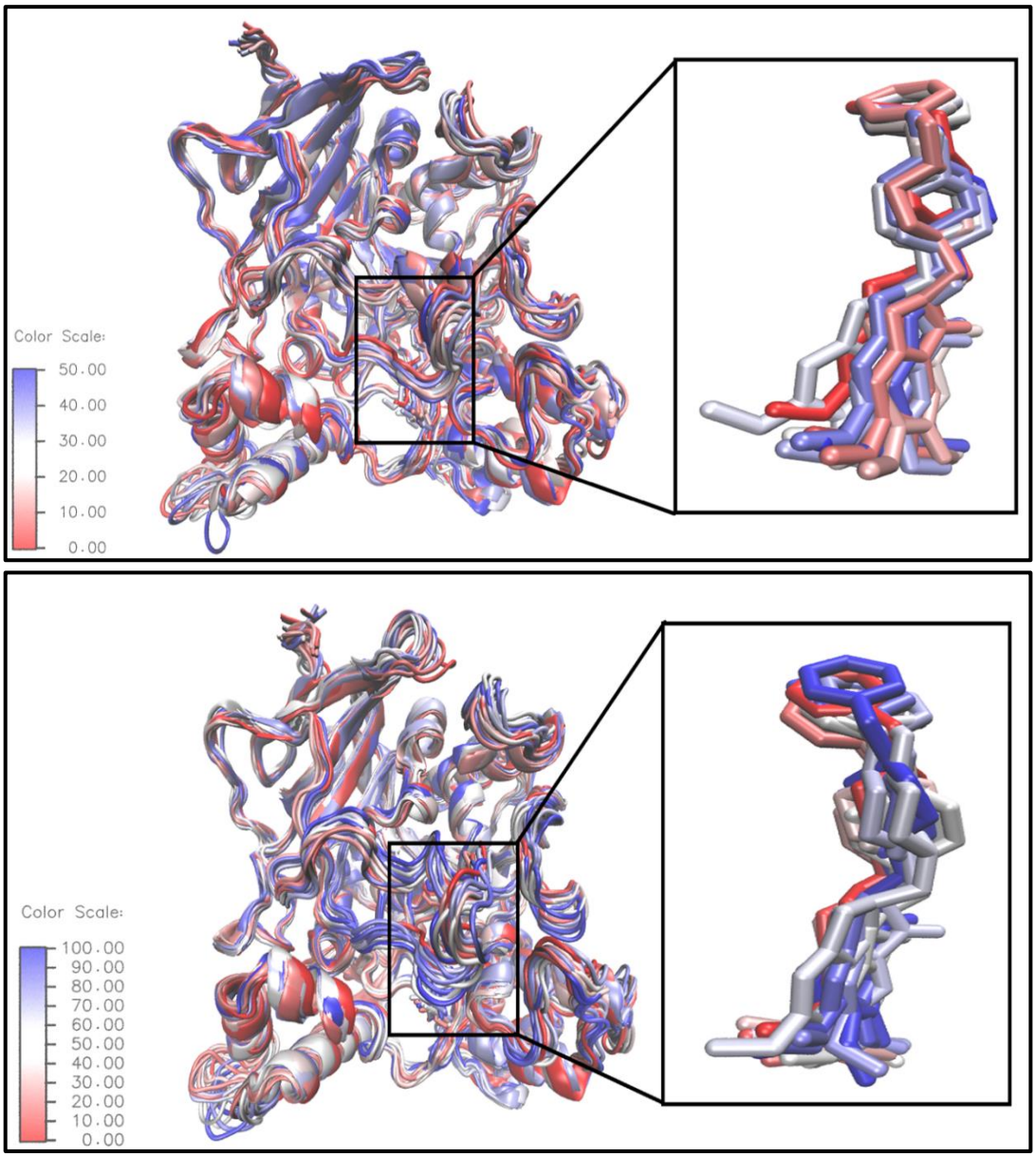

Figure 6. 58 Alignment of donepezil conformations throughout the MD simulations with AChE in a time-scale coloring (initial, red; end, blue)

(up:50-ns; dowm:100-ns)

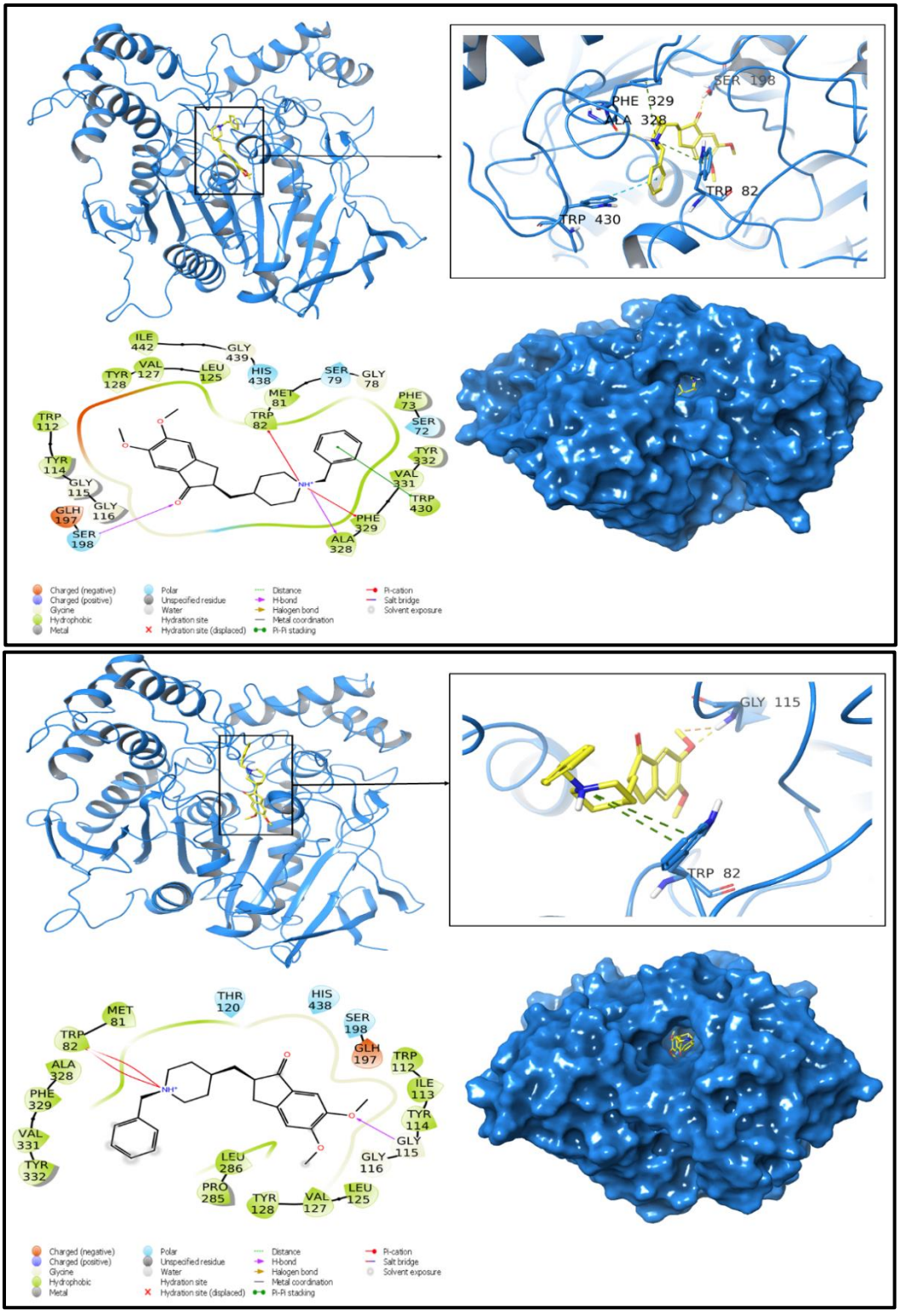

Figure 6. 59 2D and 3D ligand interaction diagrams during MD simulation of top docking pose of donepezil with BuChE

(up:50-ns; dowm:100-ns)

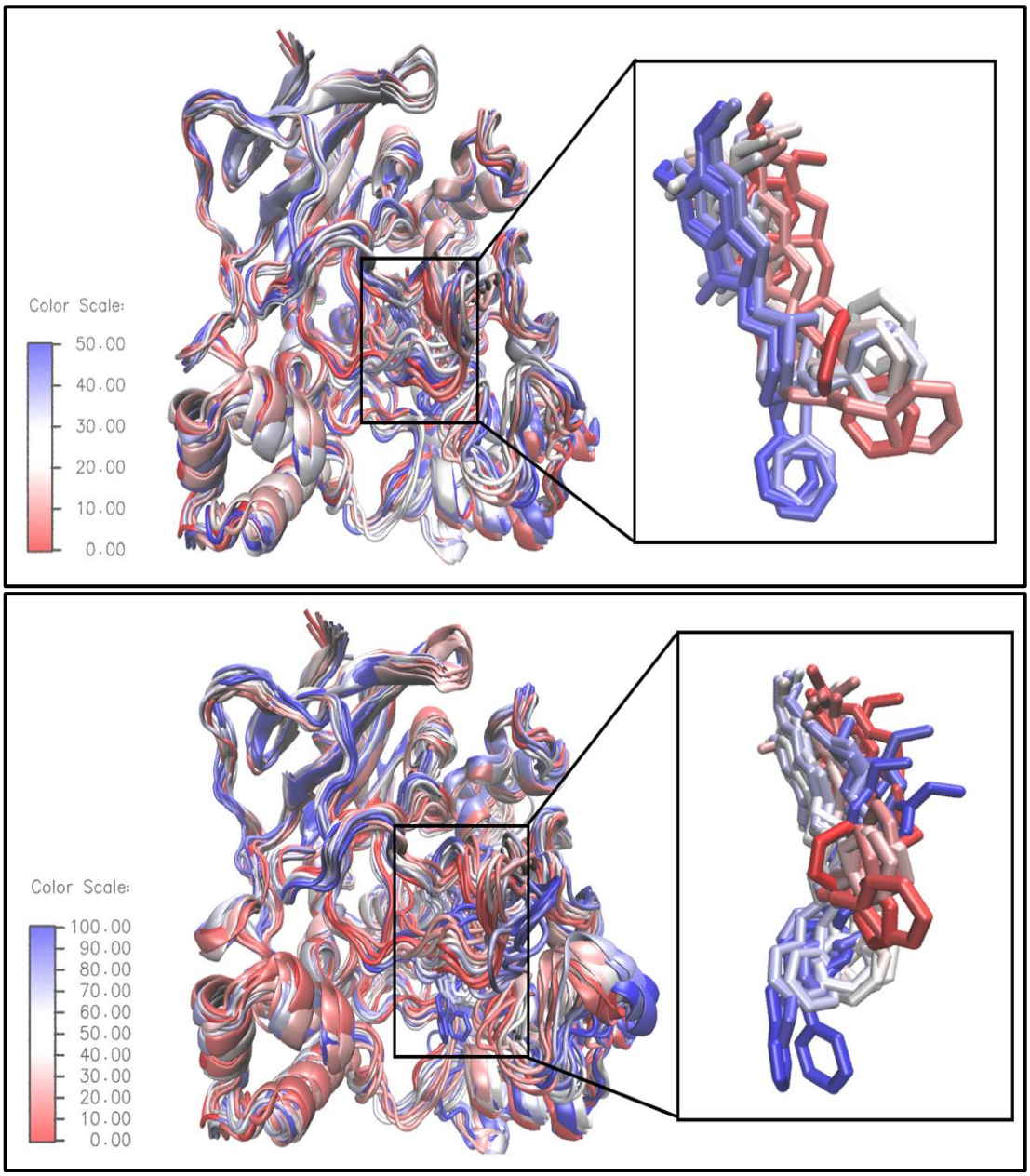

Figure 6. 60 Alignment of dnepezil conformations throughout the MD simulations with BuChE in a time-scale coloring (initial, red; end, blue)

(up:50-ns; dowm:100-ns)

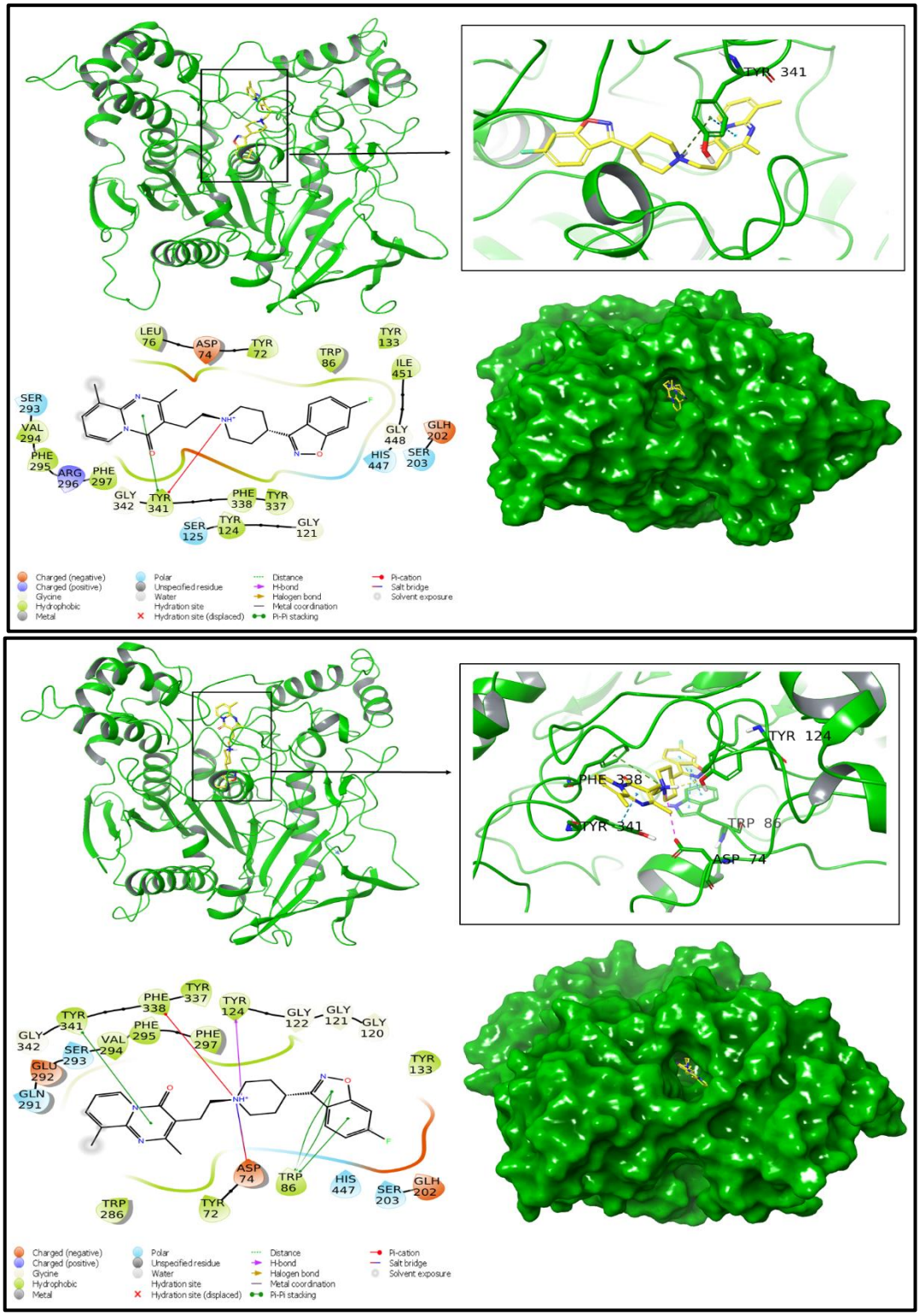

Figure 6. 61 2D and 3D ligand interaction diagrams during MD simulation of top docking pose of ocaperidone with AChE

(up:50-ns; dowm:100-ns)

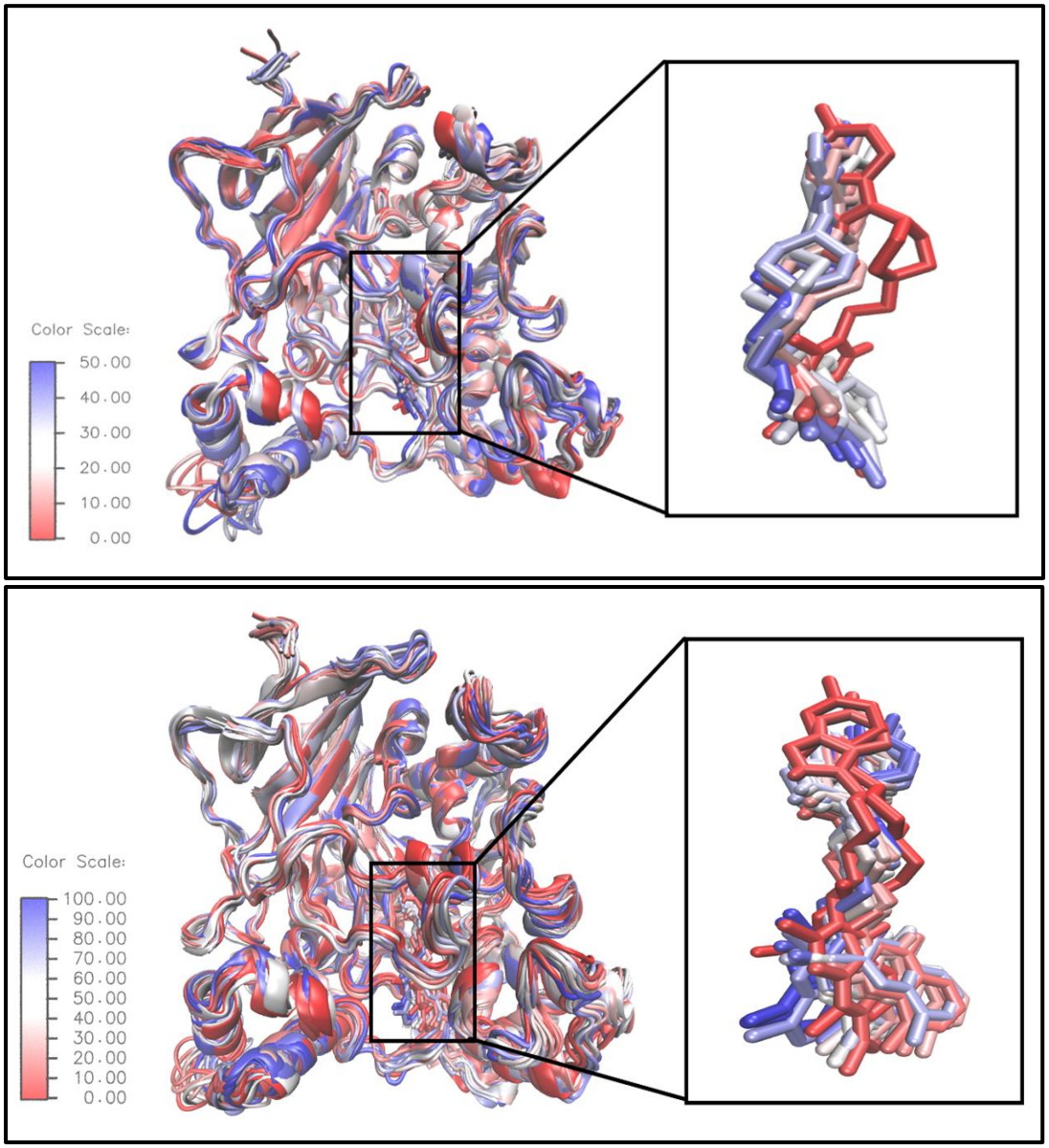

Figure 6. 62 Alignment of ocaperidone conformations throughout the MD simulations with AChE in a time-scale coloring (initial, red; end, blue)

(up:50-ns; dowm:100-ns)

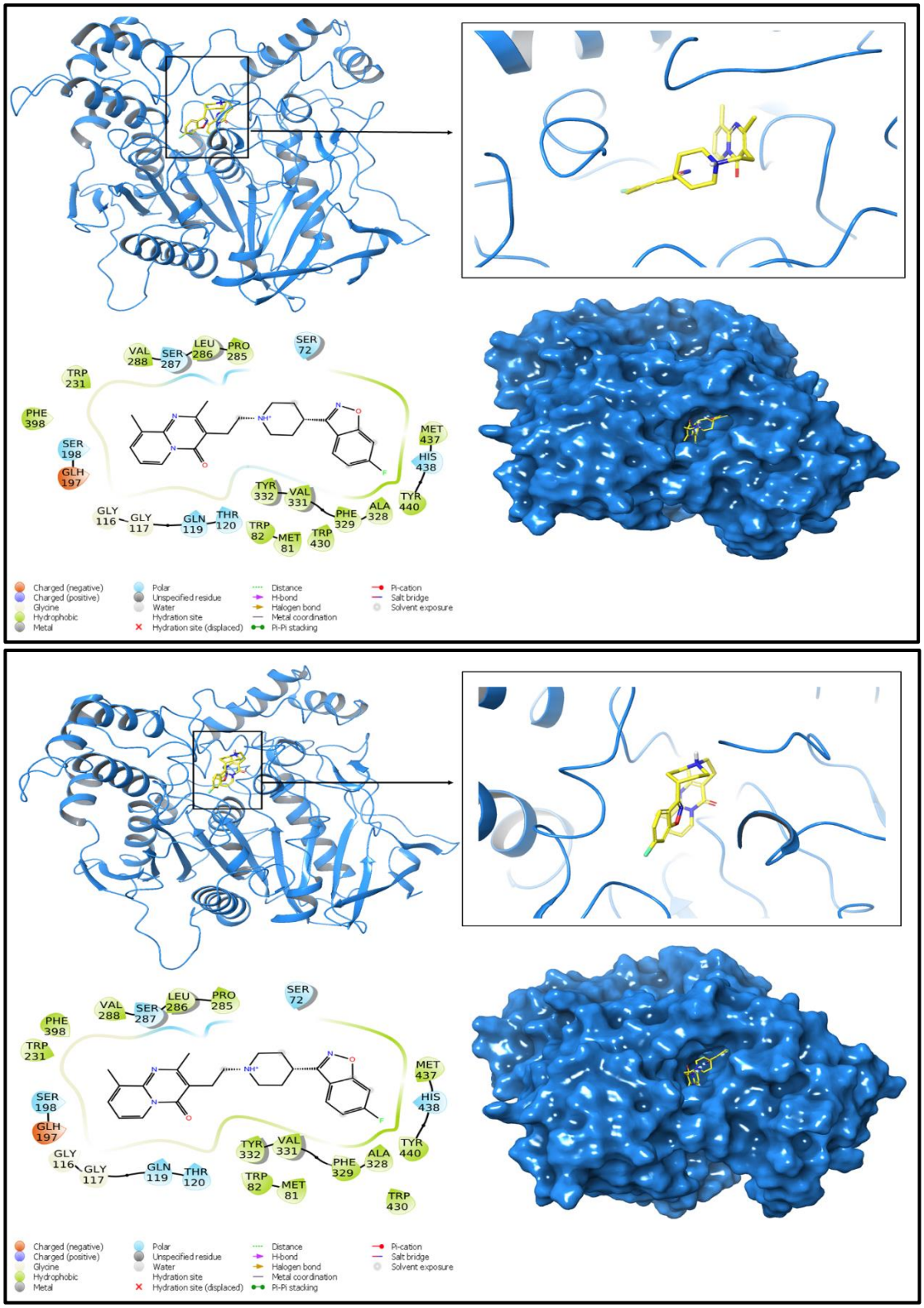

Figure 6. 63 2D and 3D ligand interaction diagrams during MD simulation of top docking pose of ocaperidone with BuChE

(up:50-ns; dowm:100-ns)

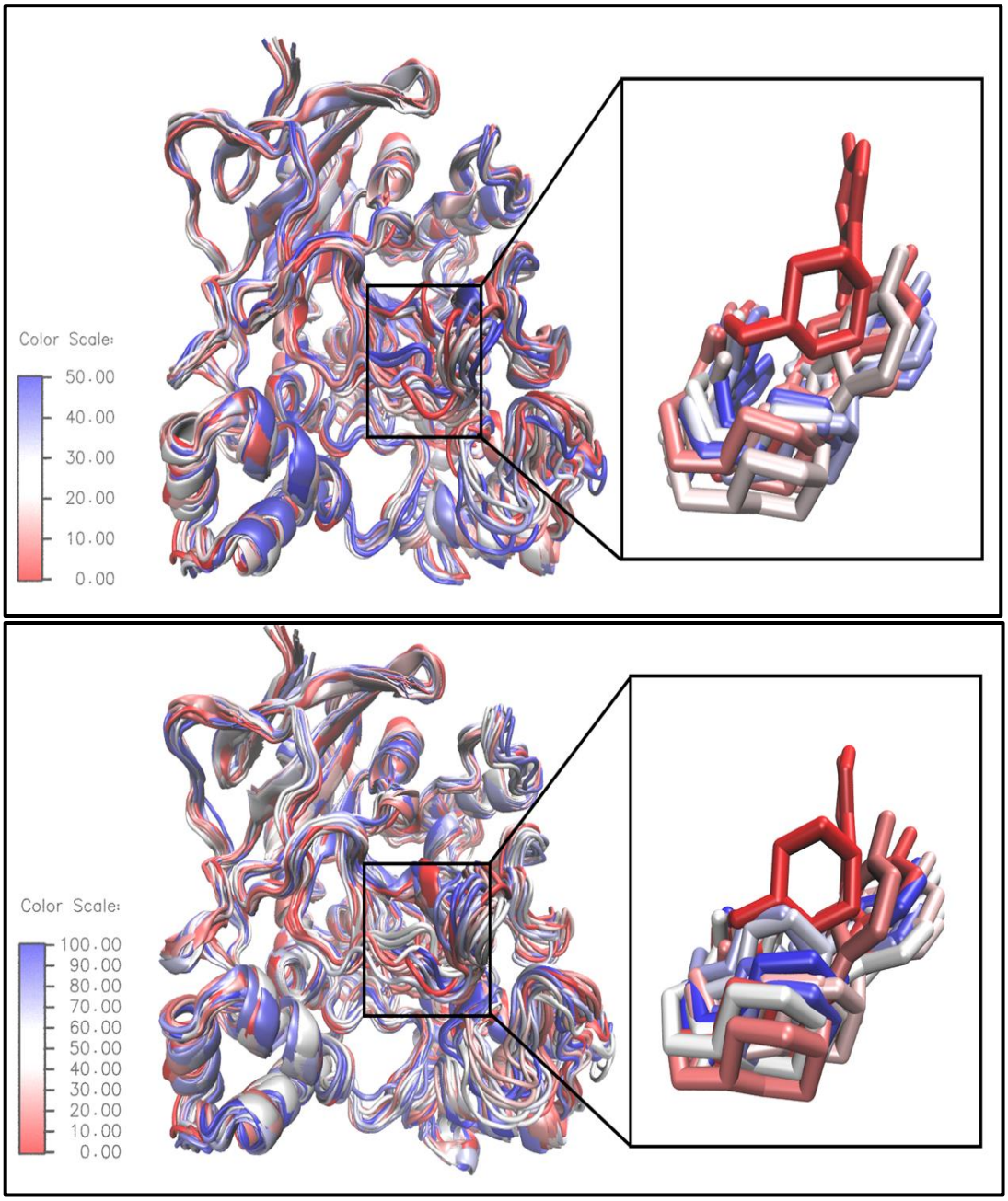

Figure 6. 64 Alignment of ocaperidone conformations throughout the MD simulations with BuChE in a time-scale coloring (initial, red; end, blue)

(up:50-ns; dowm:100-ns)

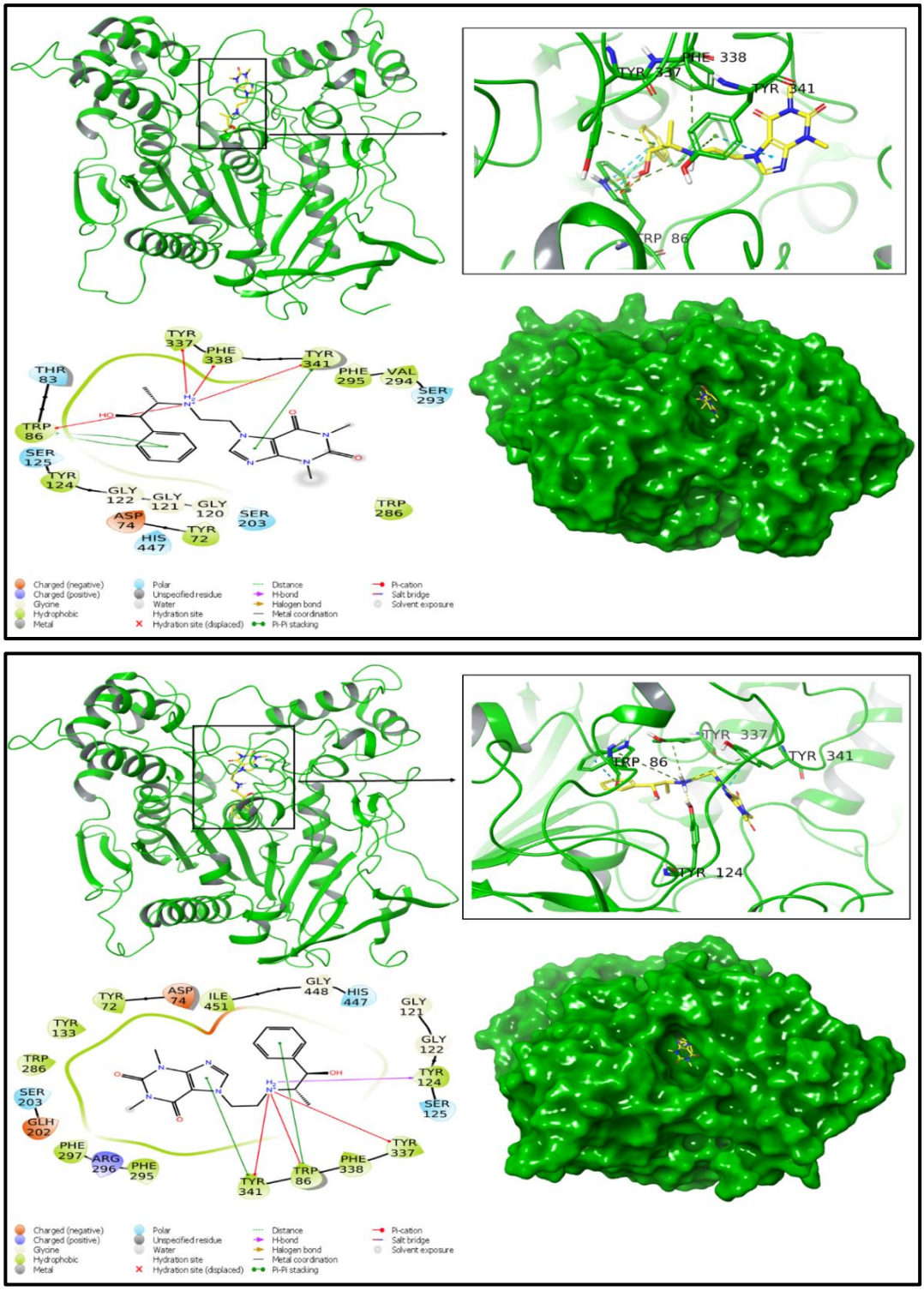

Figure 6. 65 2D and 3D ligand interaction diagrams during MD simulation of top docking pose of cafedrine with AChE

(up:50-ns; dowm:100-ns)

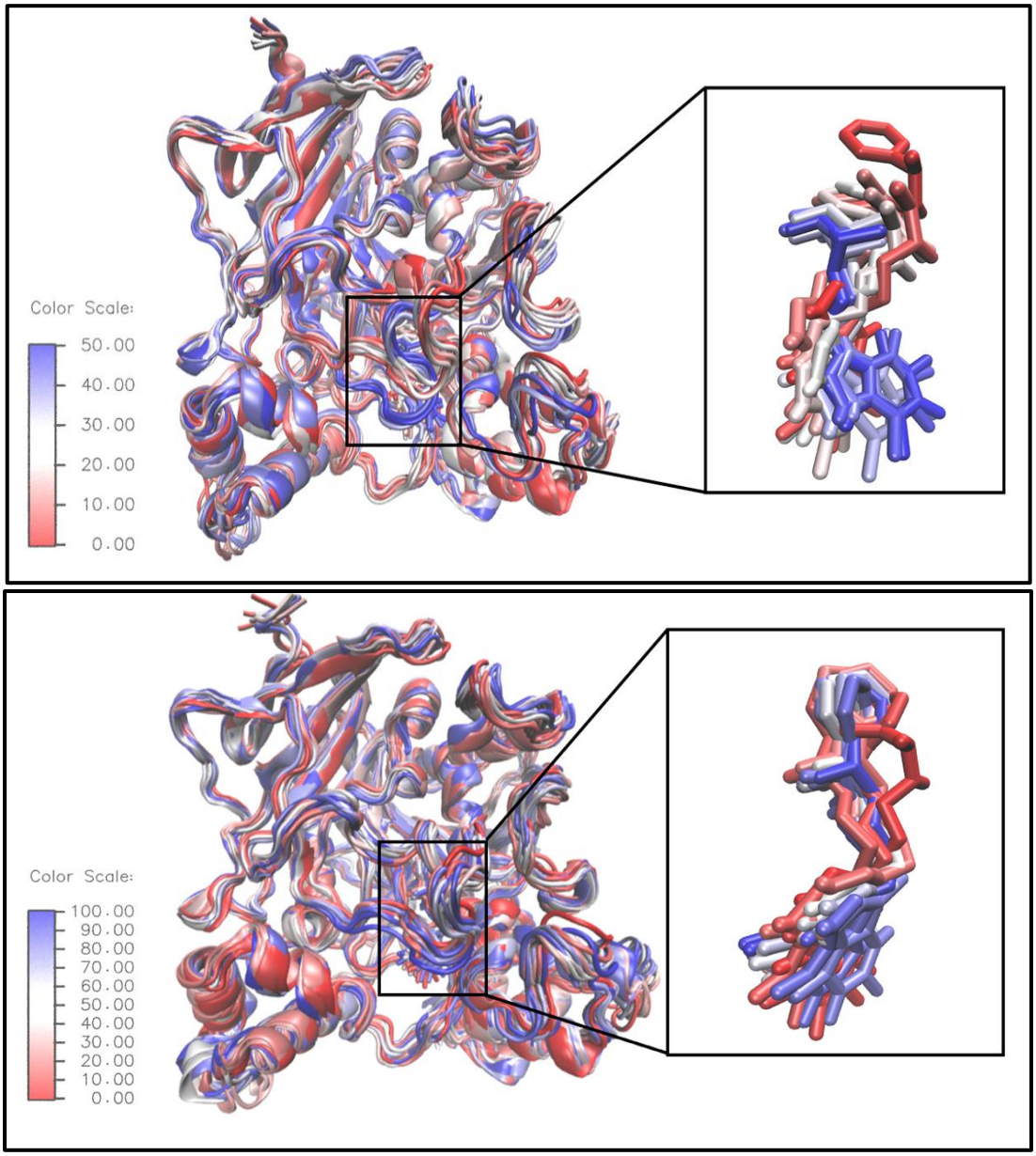

Figure 6. 66 Alignment of cafedrine conformations throughout the MD simulations with AChE in a time-scale coloring (initial, red; end, blue)

(up:50-ns; dowm:100-ns)

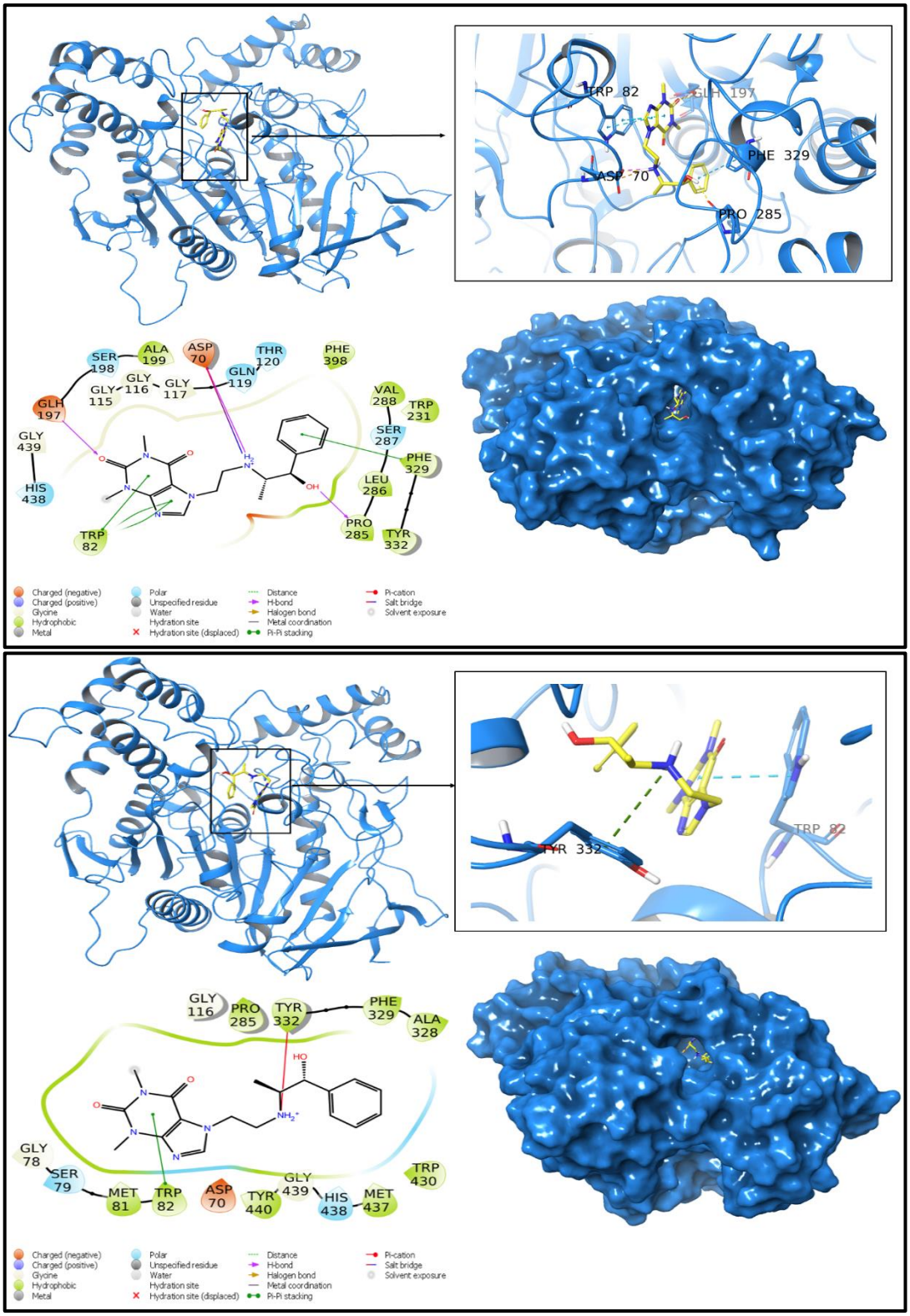

Figure 6. 67 2D and 3D ligand interaction diagrams during MD simulation of top docking pose of cafedrine with BuChE

(up:50-ns; dowm:100-ns)

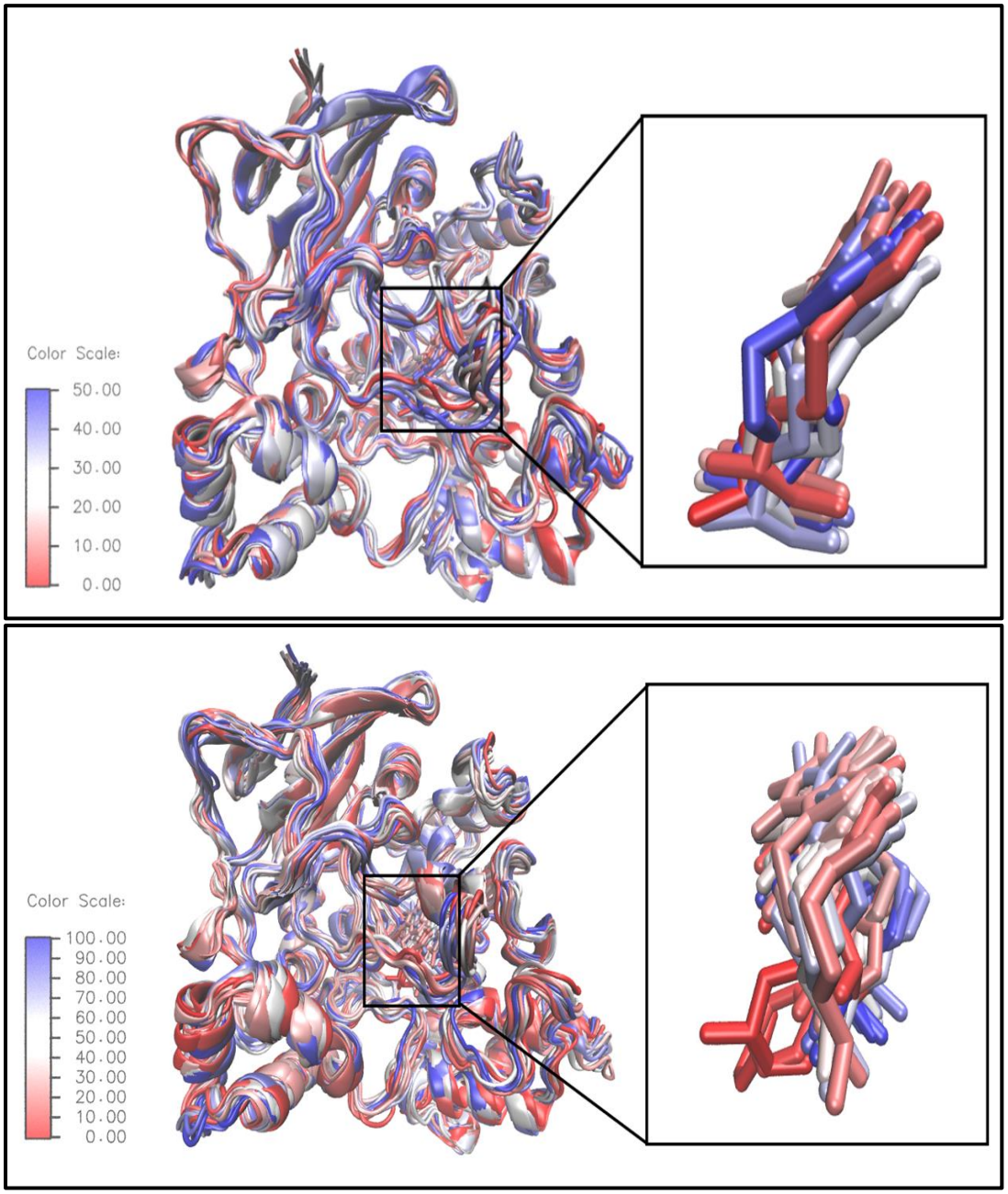

Figure 6. 68 Alignment of cafedrine conformations throughout the MD simulations with BuChE in a time-scale coloring (initial, red; end, blue)

(up:50-ns; dowm:100-ns)

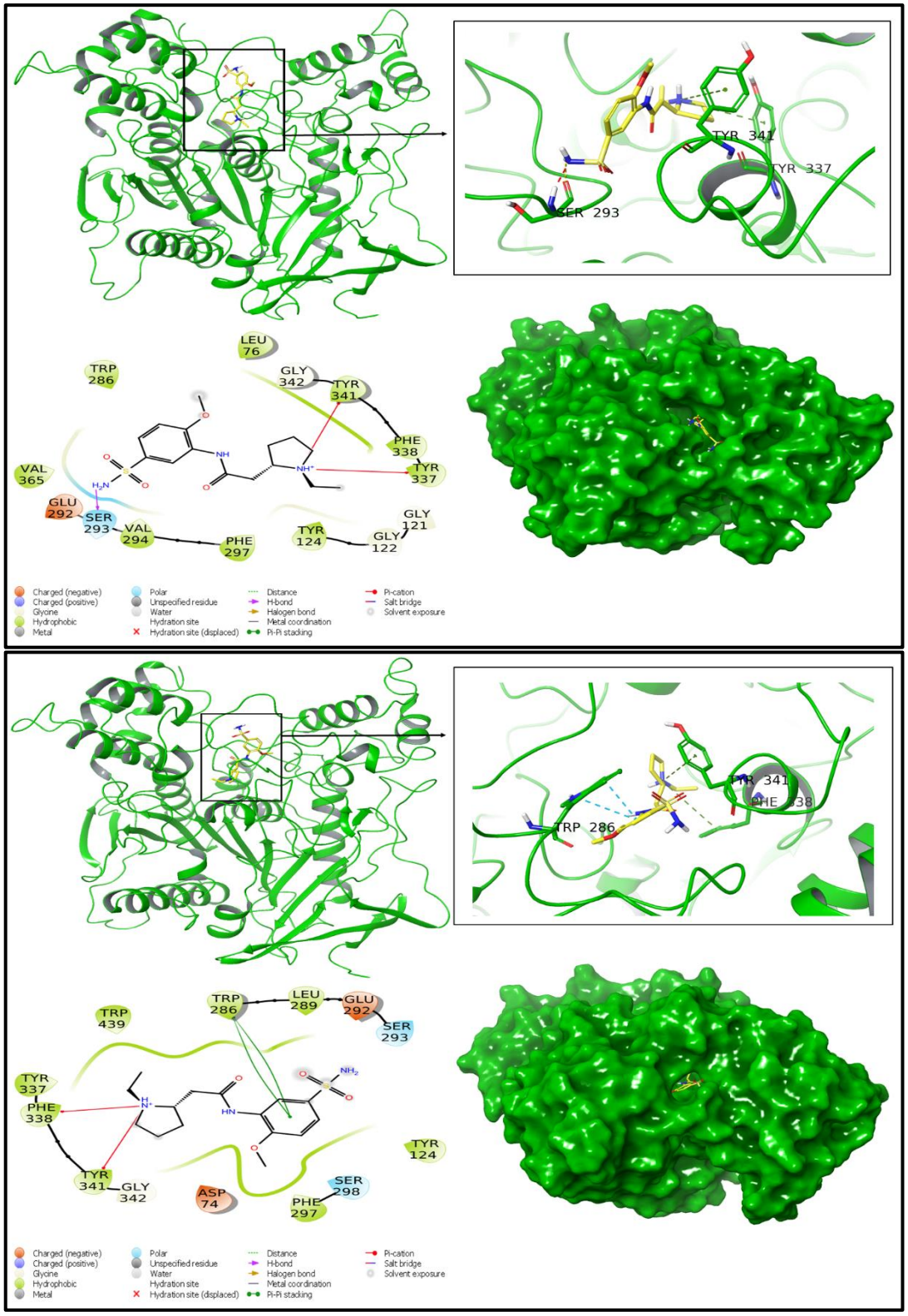

Figure 6. 69 2D and 3D ligand interaction diagrams during MD simulation of top docking pose of isosulpride with AChE

(up:50-ns; dowm:100-ns)

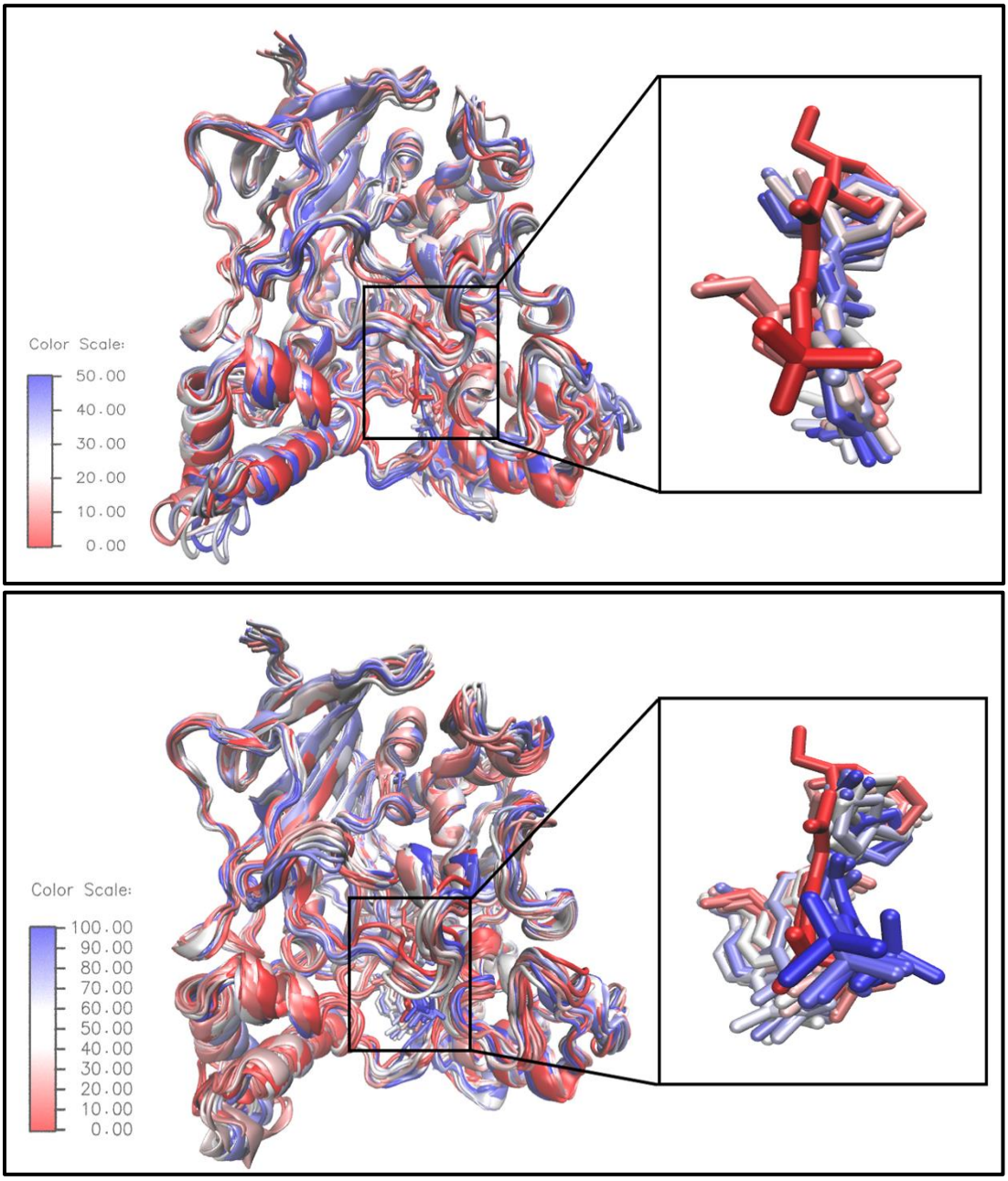

Figure 6. 70 Alignment of isosulpride conformations throughout the MD simulations with AChE in a time-scale coloring (initial, red; end, blue)

(up:50-ns; dowm:100-ns)

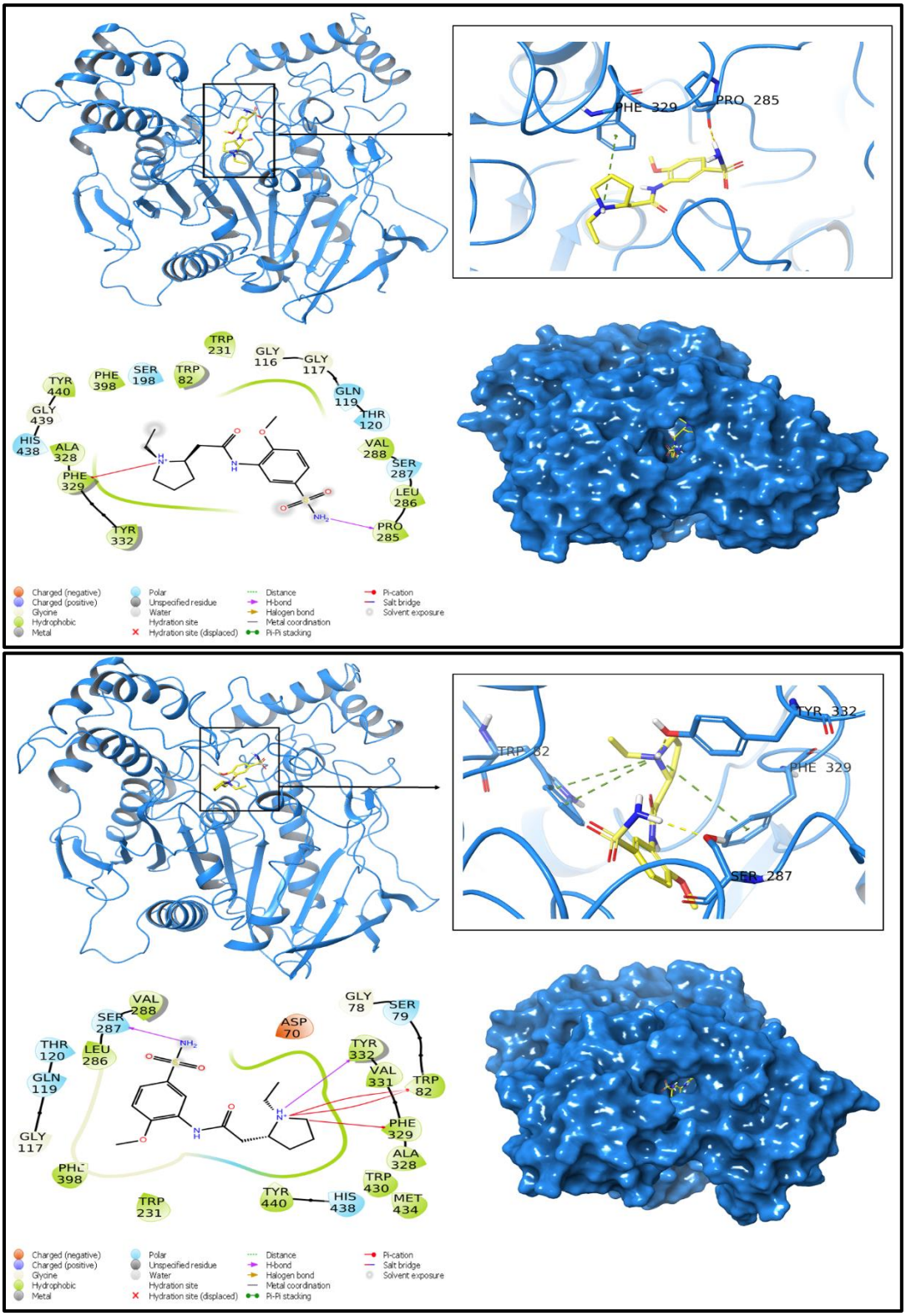

Figure 6. 71 2D and 3D ligand interaction diagrams during MD simulation of top docking pose of isosulpride with BuChE

(up:50-ns; dowm:100-ns)

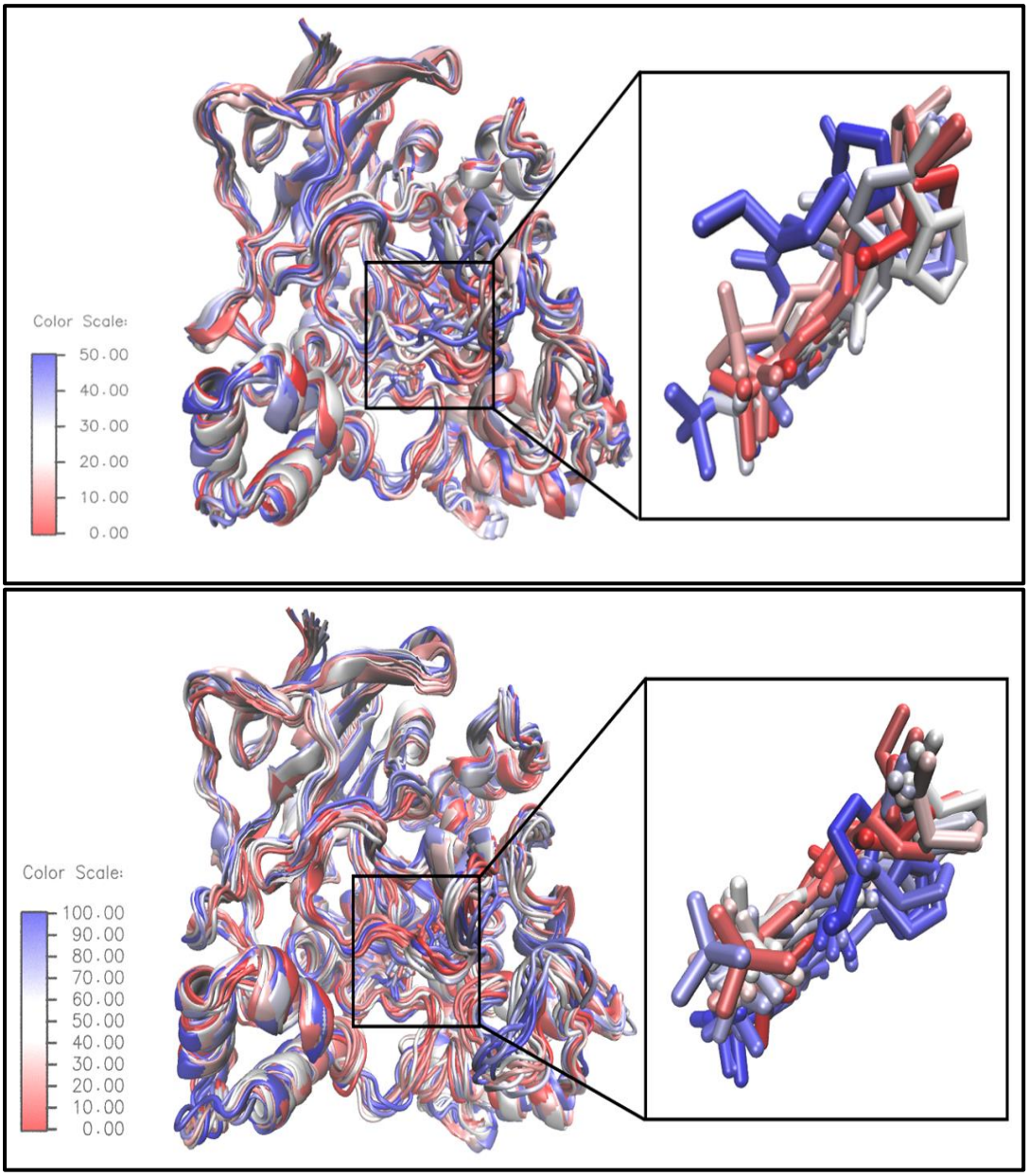

Figure 6. 72 Alignment of isosulpride conformations throughout the MD simulations with BuChE in a time-scale coloring (initial, red; end, blue)

(up:50-ns; dowm:100-ns)

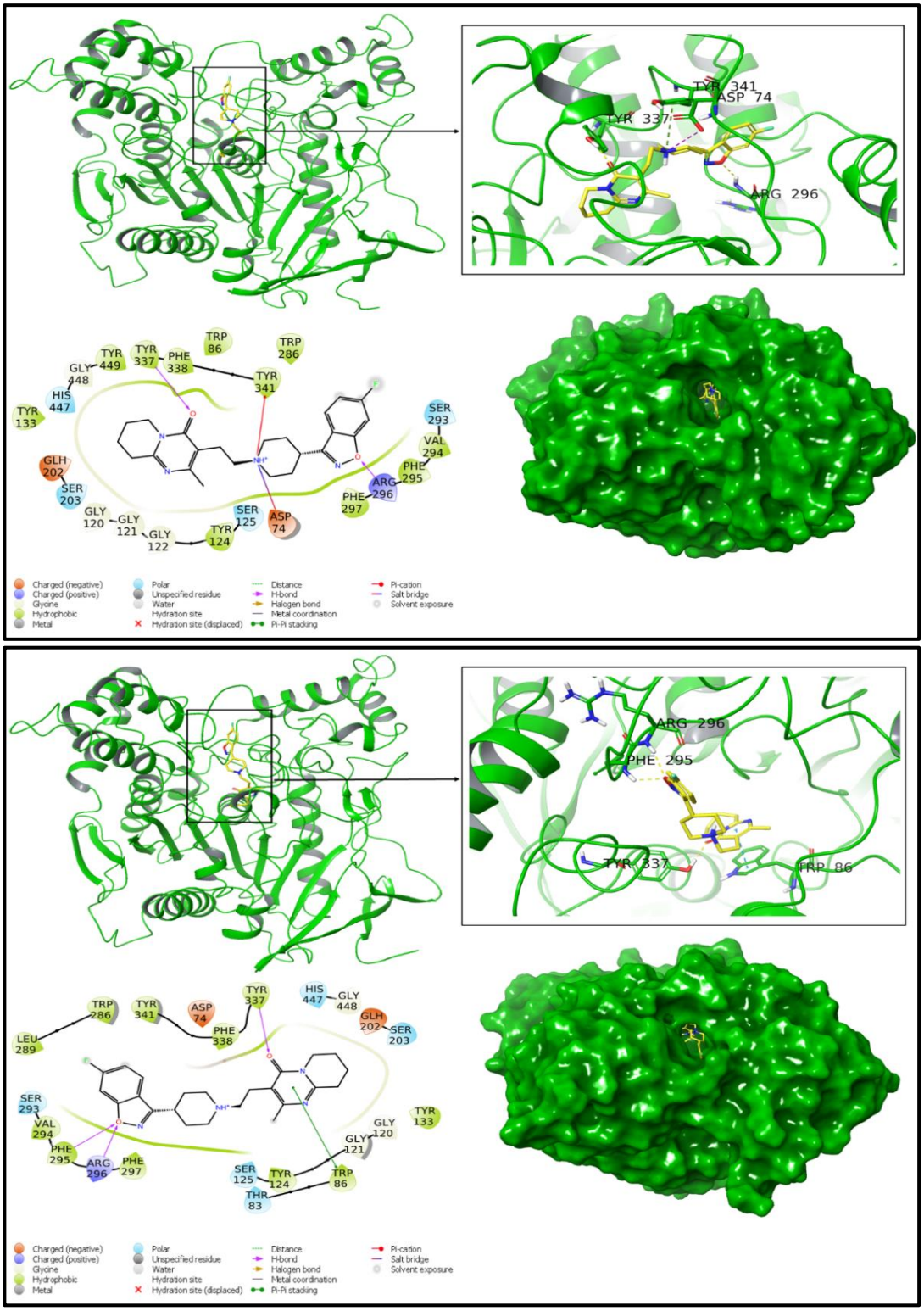

Figure 6. 73 2D and 3D ligand interaction diagrams during MD simulation of top docking pose of risperidone with AChE

(up:50-ns; dowm:100-ns)

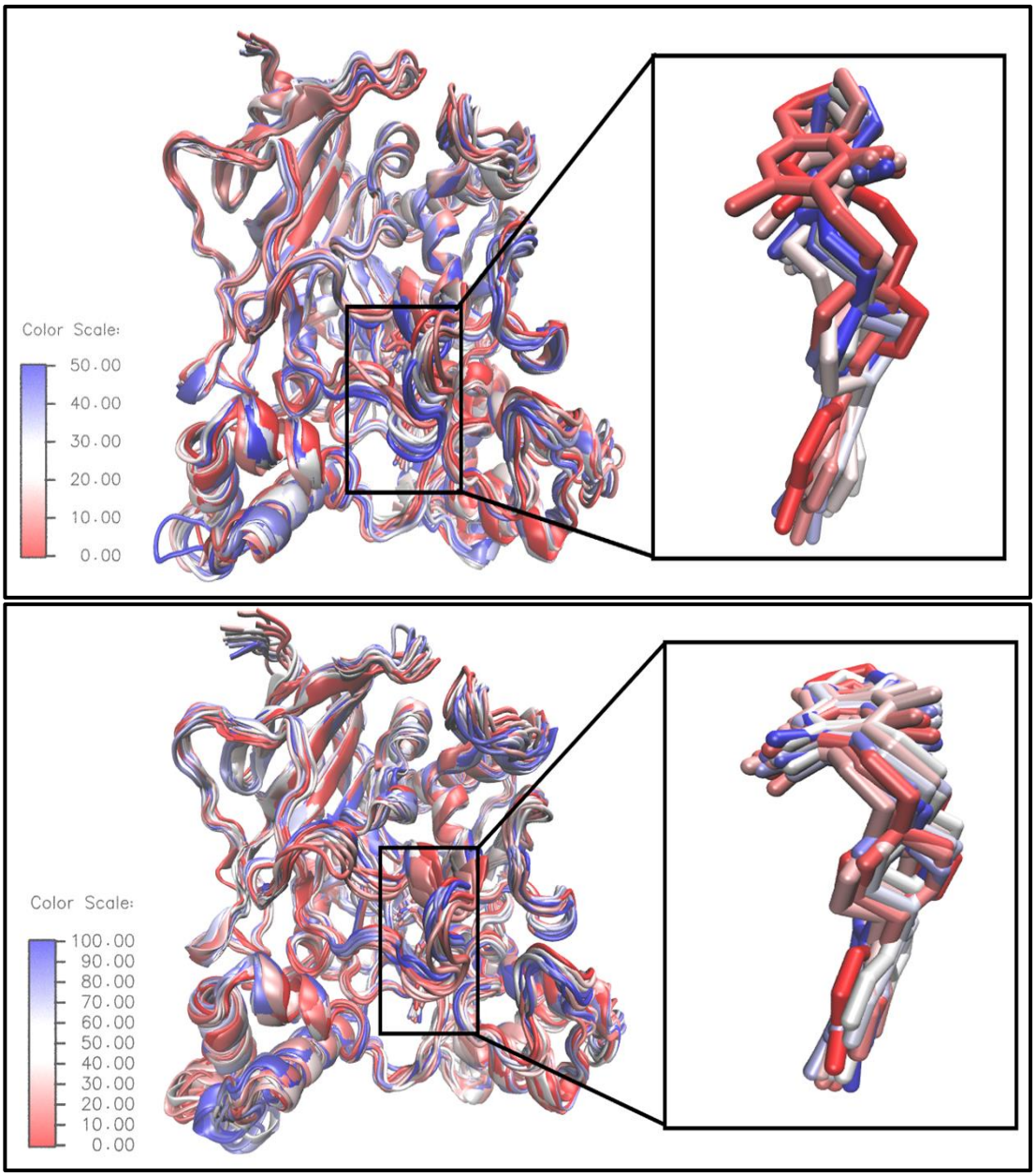

Figure 6. 74 Alignment of risperidone conformations throughout the MD simulations with AChE in a time-scale coloring (initial, red; end, blue)

(up:50-ns; dowm:100-ns)

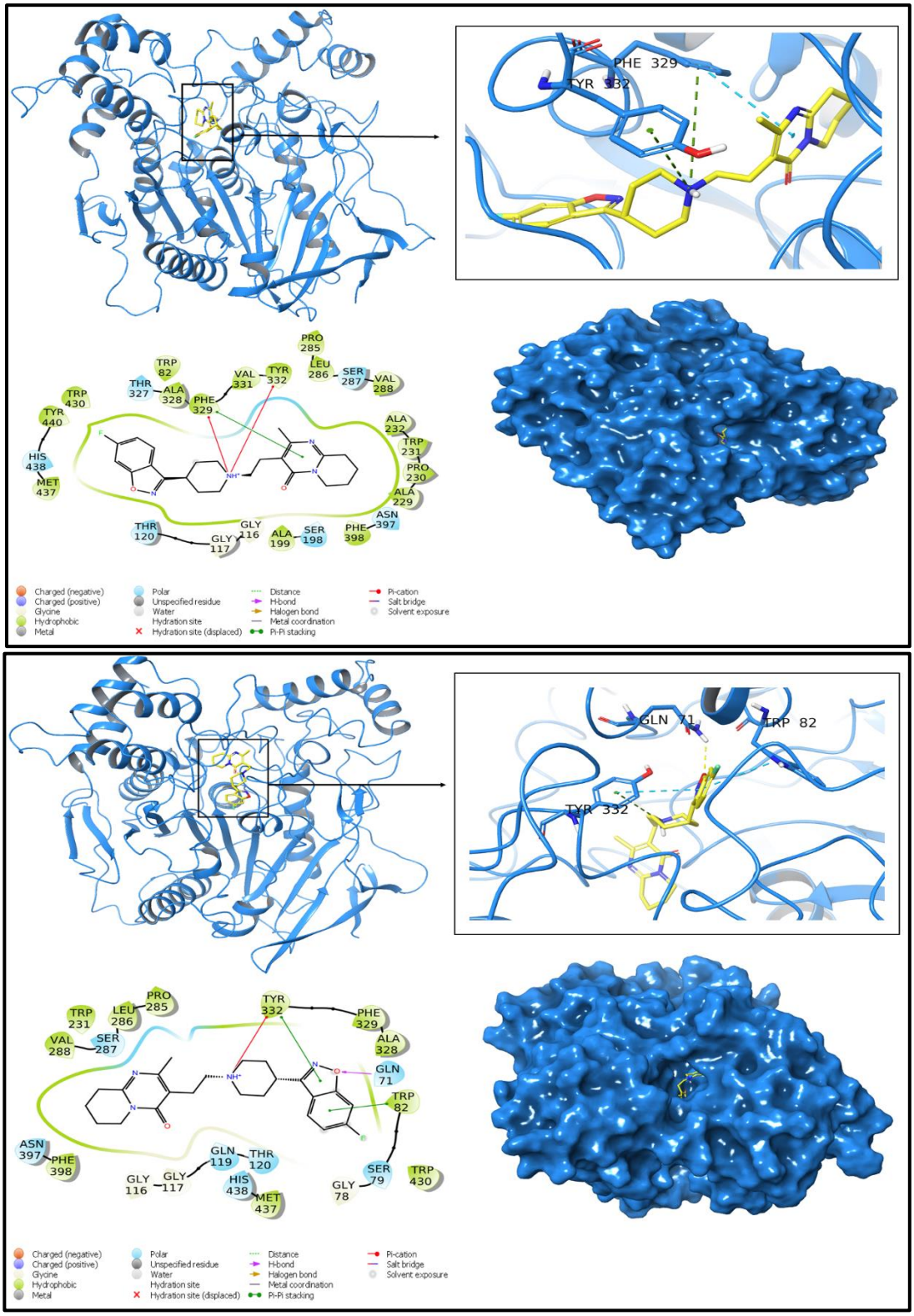

Figure 6. 75 2D and 3D ligand interaction diagrams during MD simulation of top docking pose of risperidone with BuChE during MD simulation

(up:50-ns; dowm:100-ns)

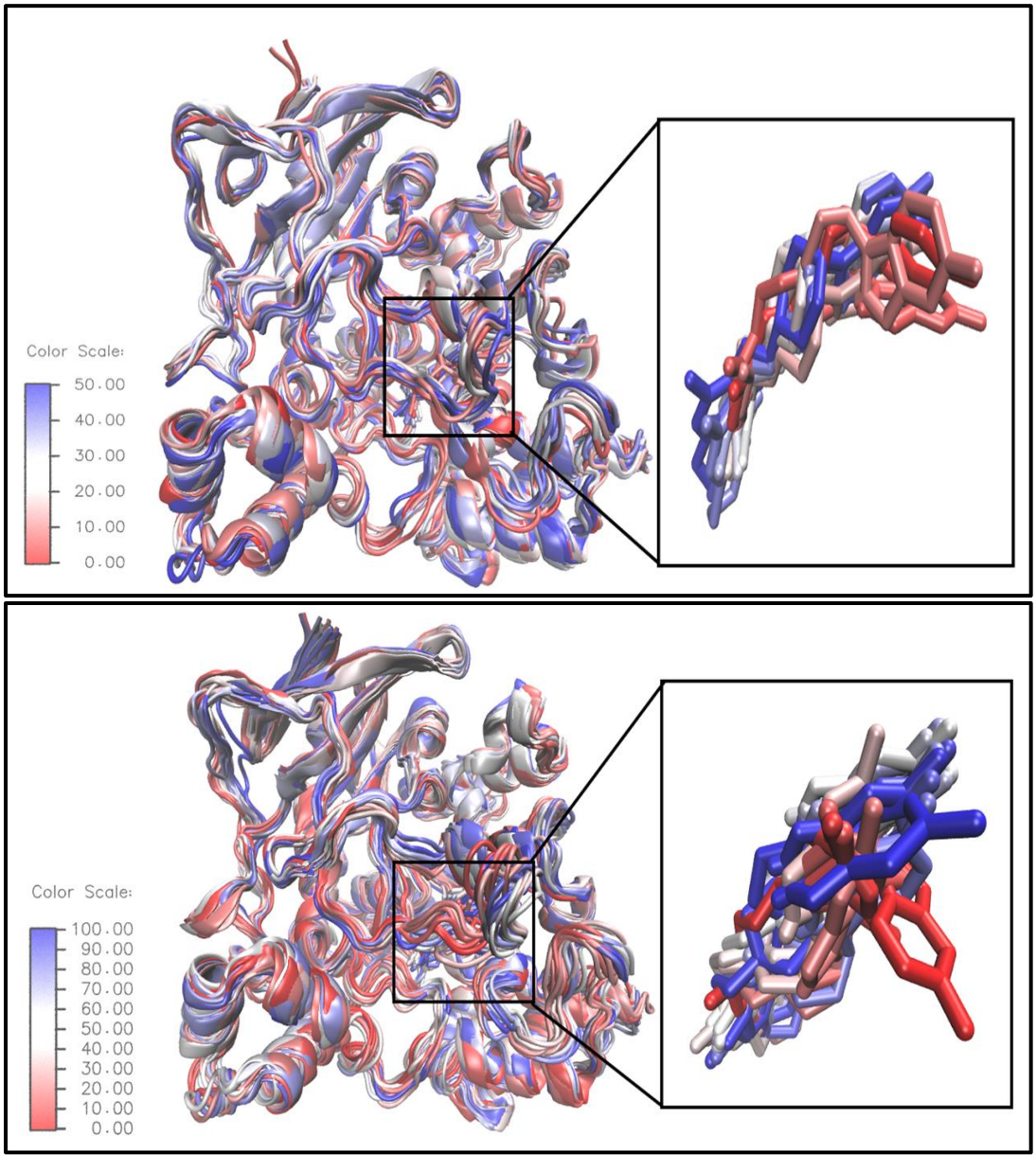

Figure 6. 76 Alignment of risperidone conformations throughout the MD simulations with BuChE in a time-scale coloring (initial, red; end, blue)

(up:50-ns; dowm:100-ns)

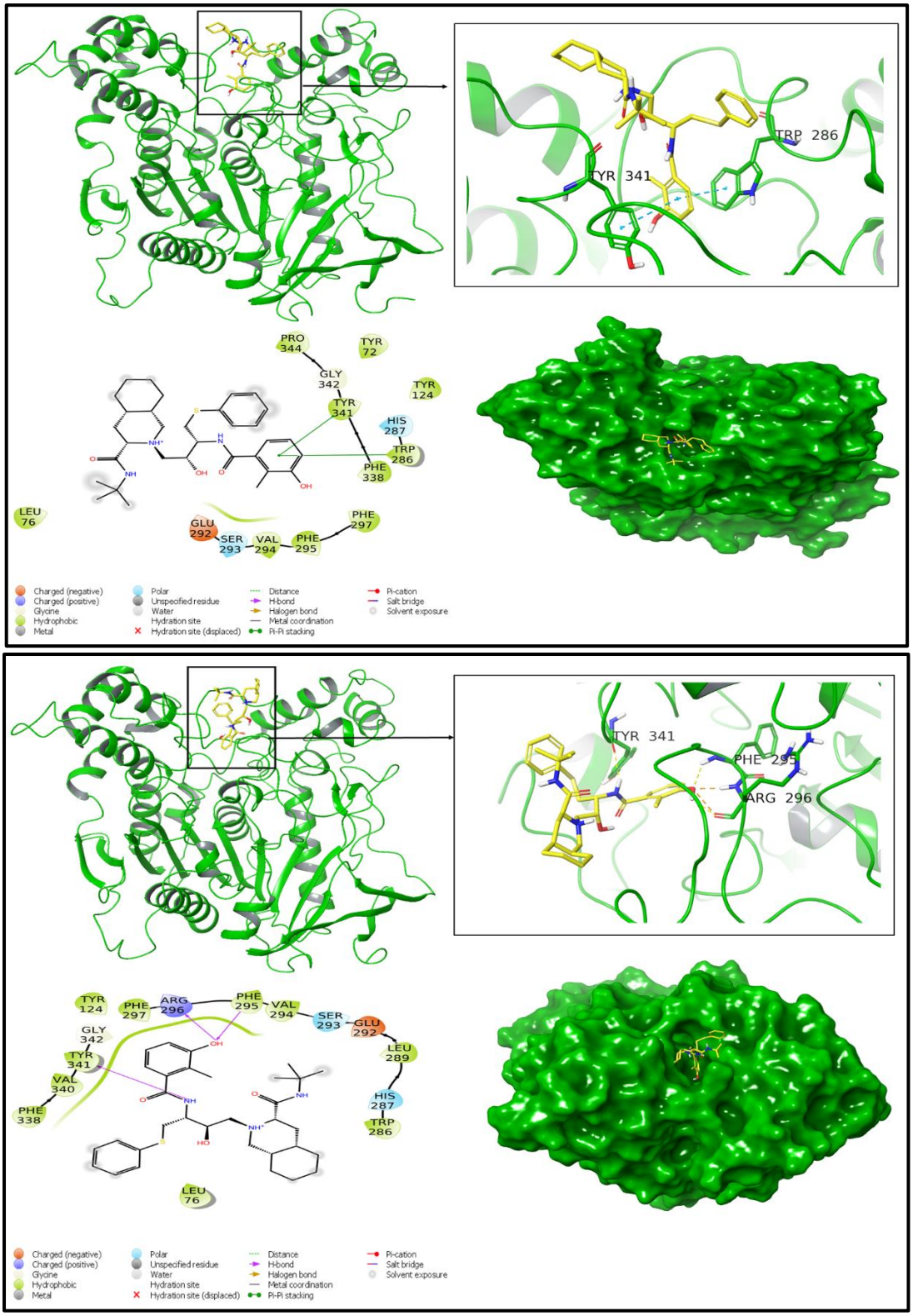

Figure 6. 77 2D and 3D ligand interaction diagrams during MD simulation of top docking pose of nelfinavir with AChE

(up:50-ns; dowm:100-ns)

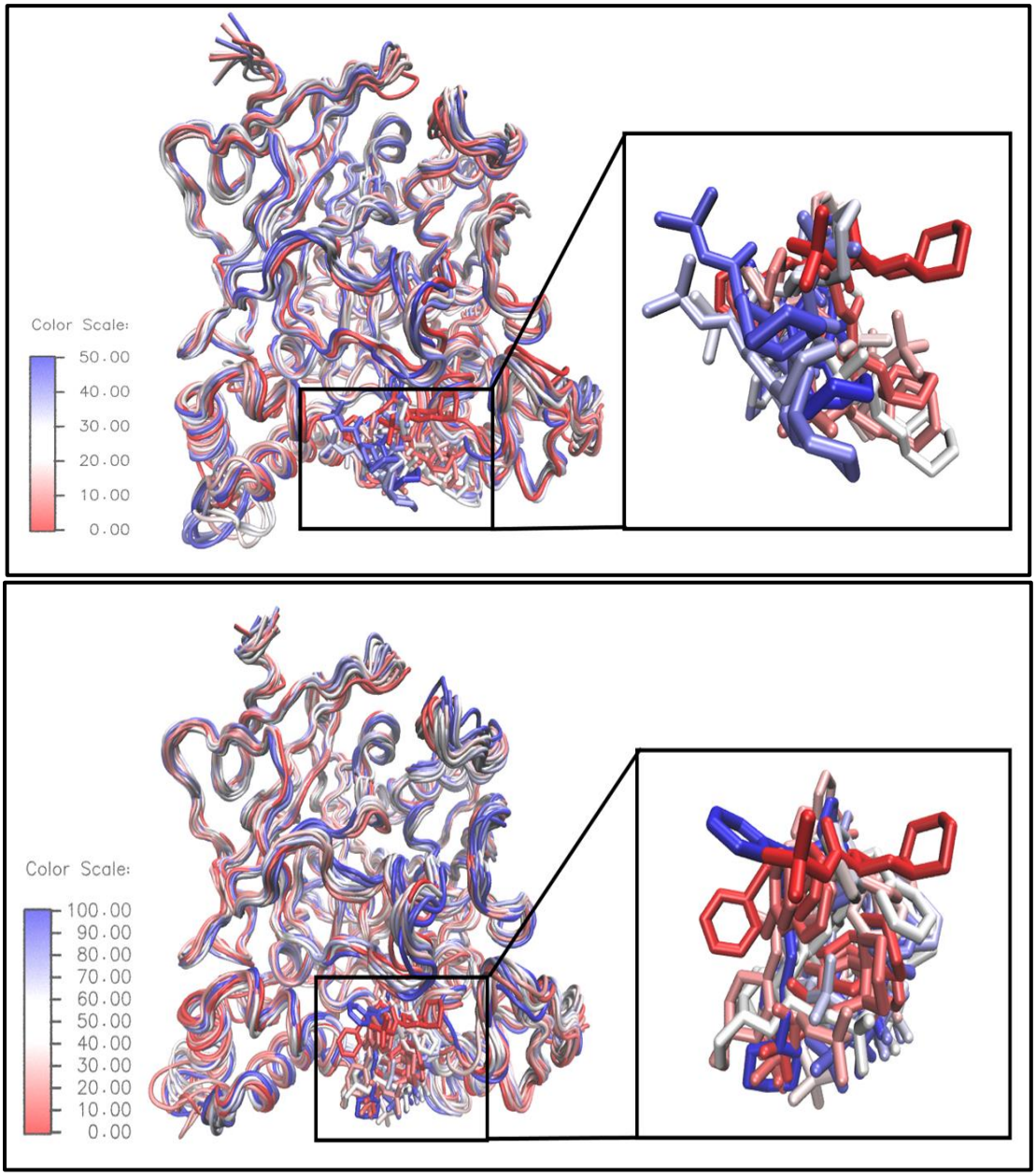

Figure 6. 78 Alignment of nelfinavir conformations throughout the MD simulations with AChE in a time-scale coloring (initial, red; end, blue)

(up:50-ns; dowm:100-ns)

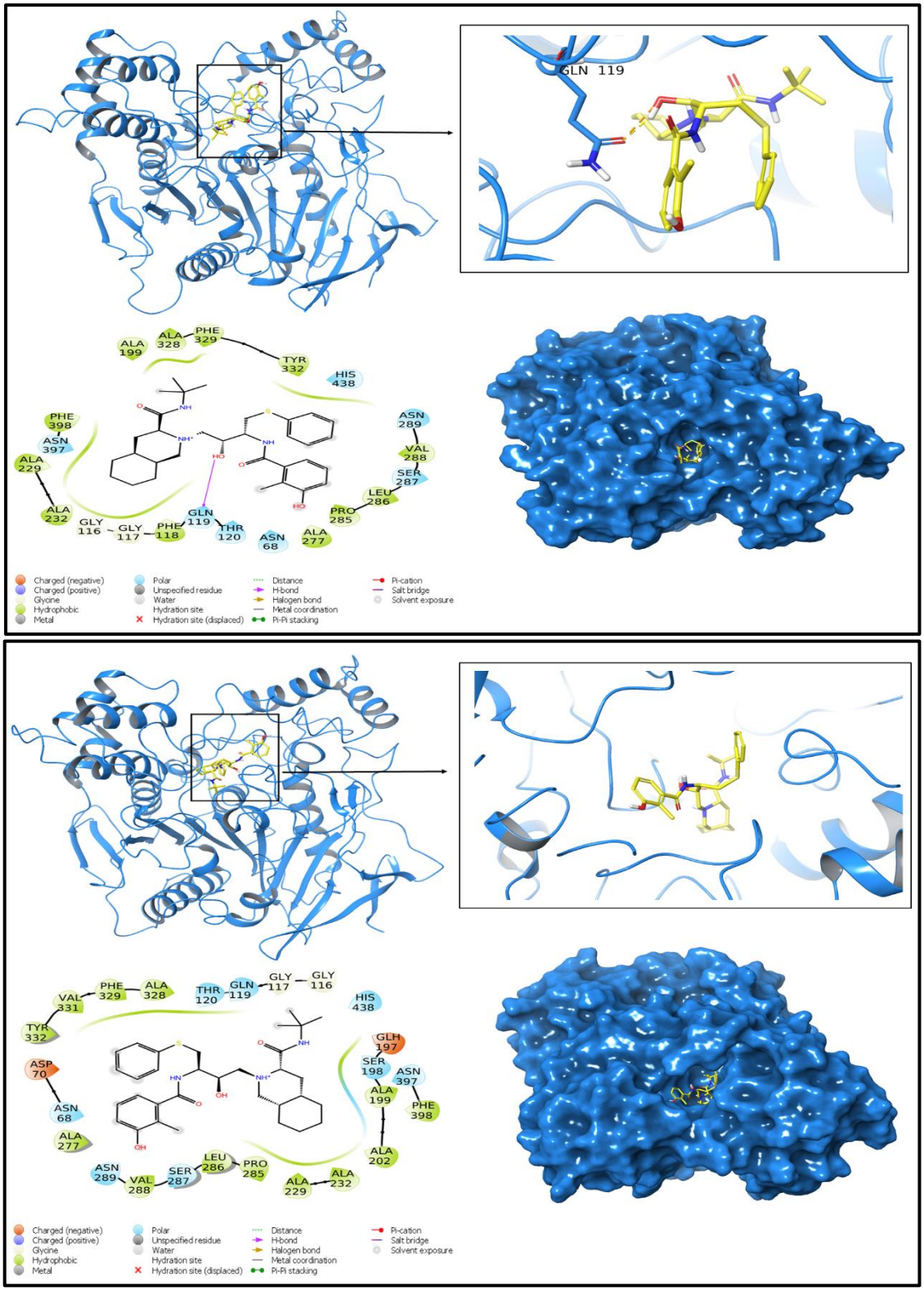

Figure 6. 79 2D and 3D ligand interaction diagrams during MD simulation of top docking pose of nelfinavir with BuChE

(up:50-ns; dowm:100-ns)

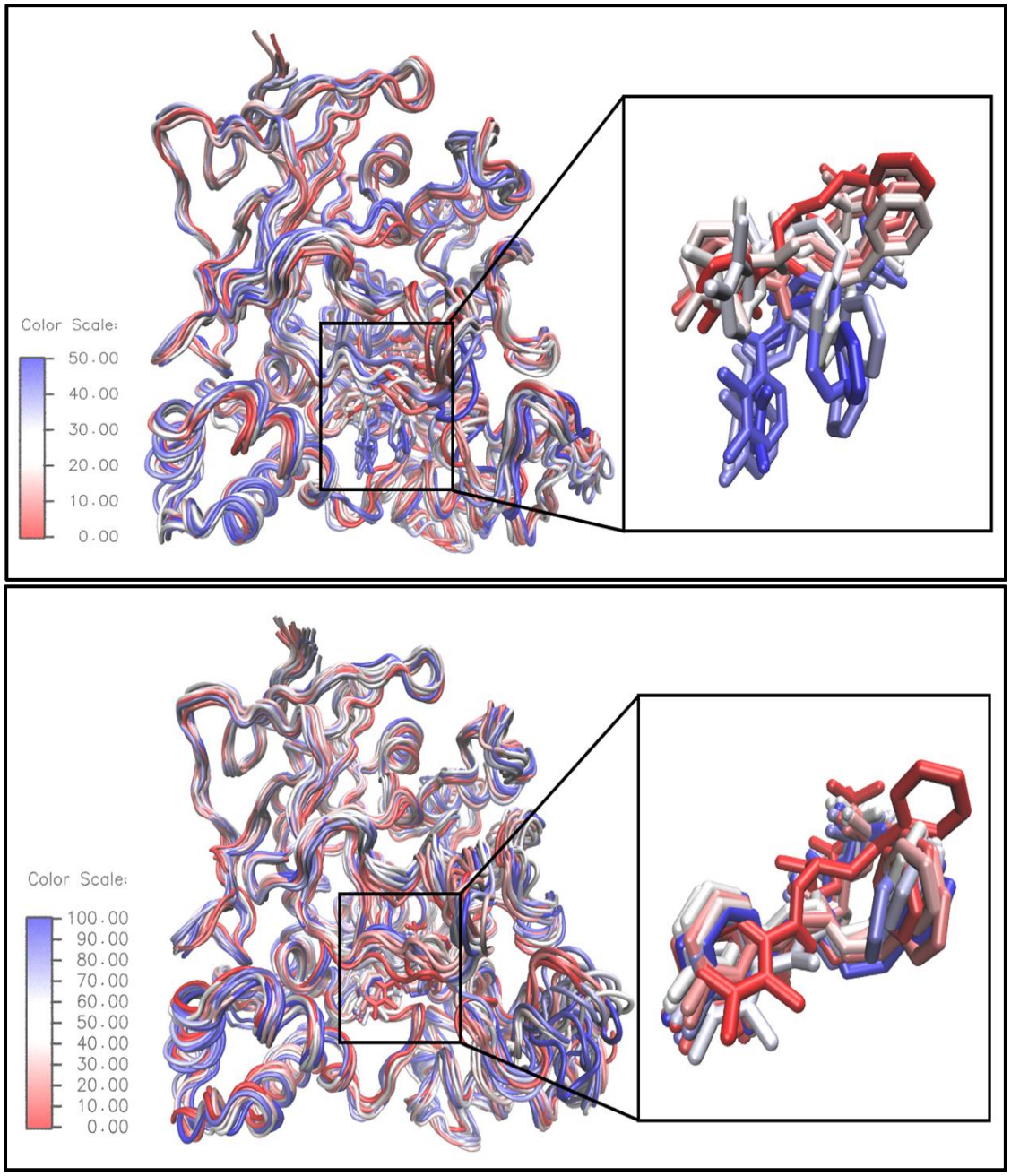

Figure 6. 80 Alignment of nelfinavir conformations throughout the MD simulations with BuChE in a time-scale coloring (initial, red; end, blue)

(up:50-ns; dowm:100-ns)

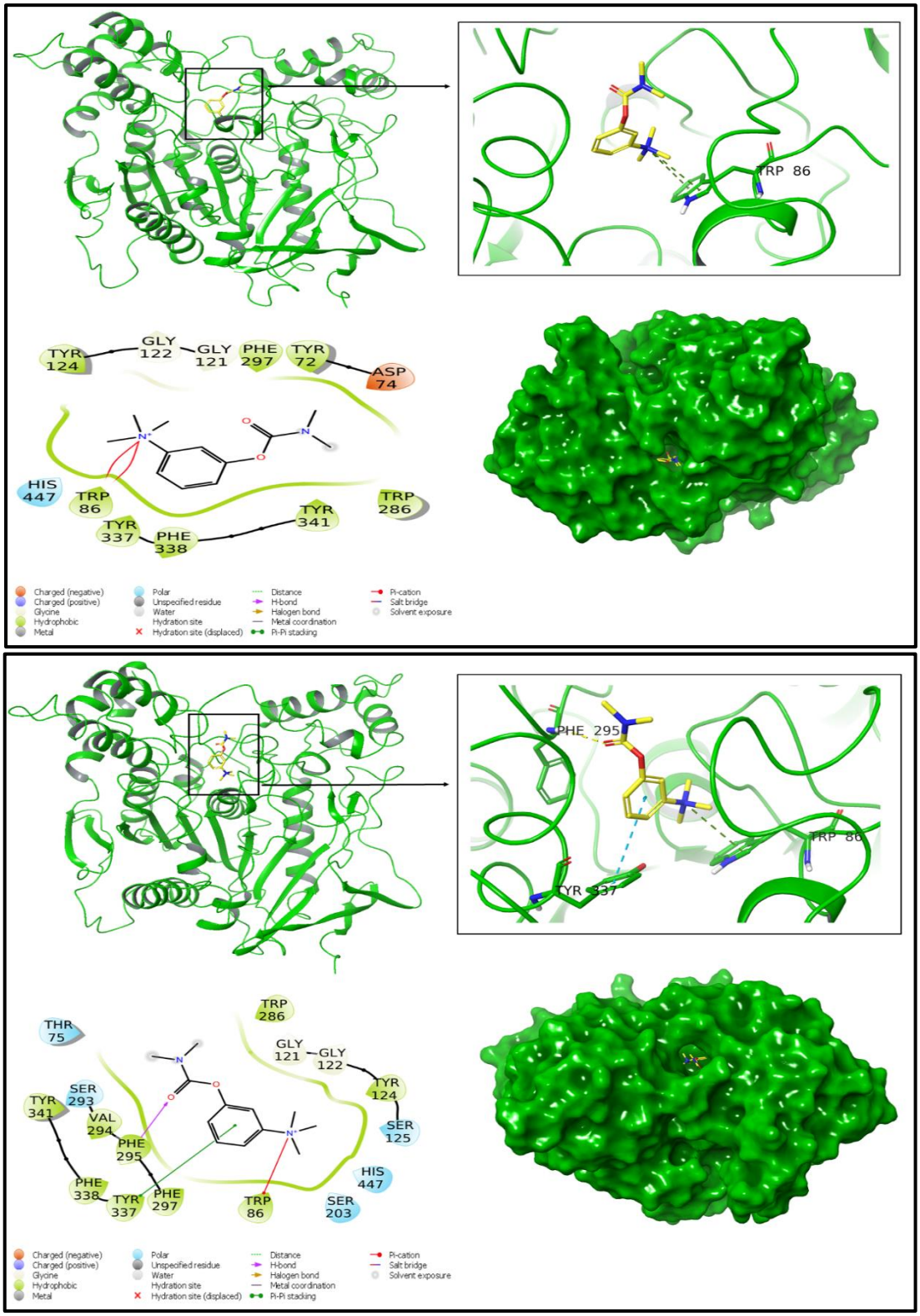

Figure 6. 81 2D and 3D ligand interaction diagrams during MD simulation of top docking pose of neostigmine with AChE

(up:50-ns; dowm:100-ns)

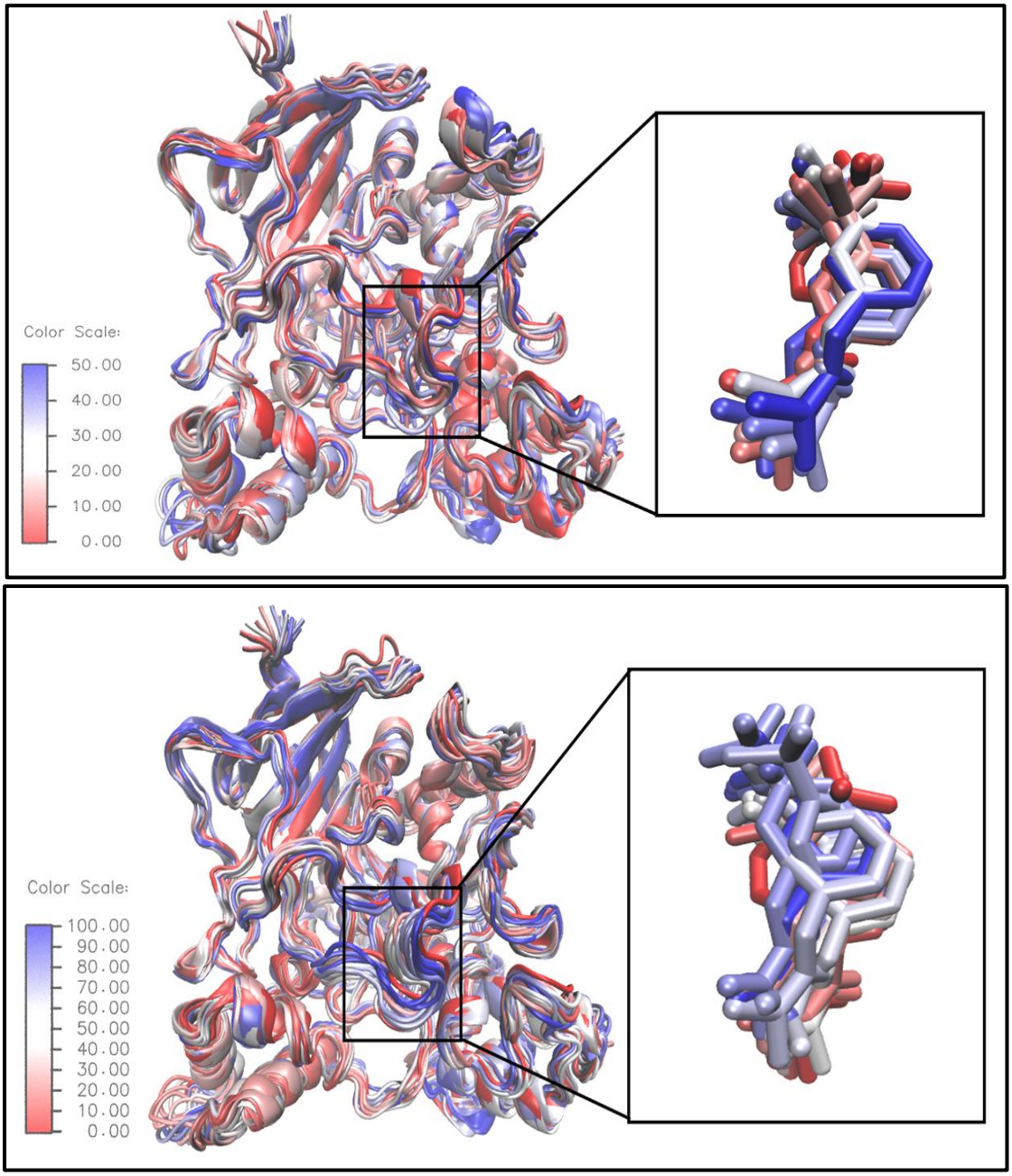

Figure 6. 82 Alignment of neostigmine conformations throughout the MD simulations with AChE in a time-scale coloring (initial, red; end, blue)

(up:50-ns; dowm:100-ns)

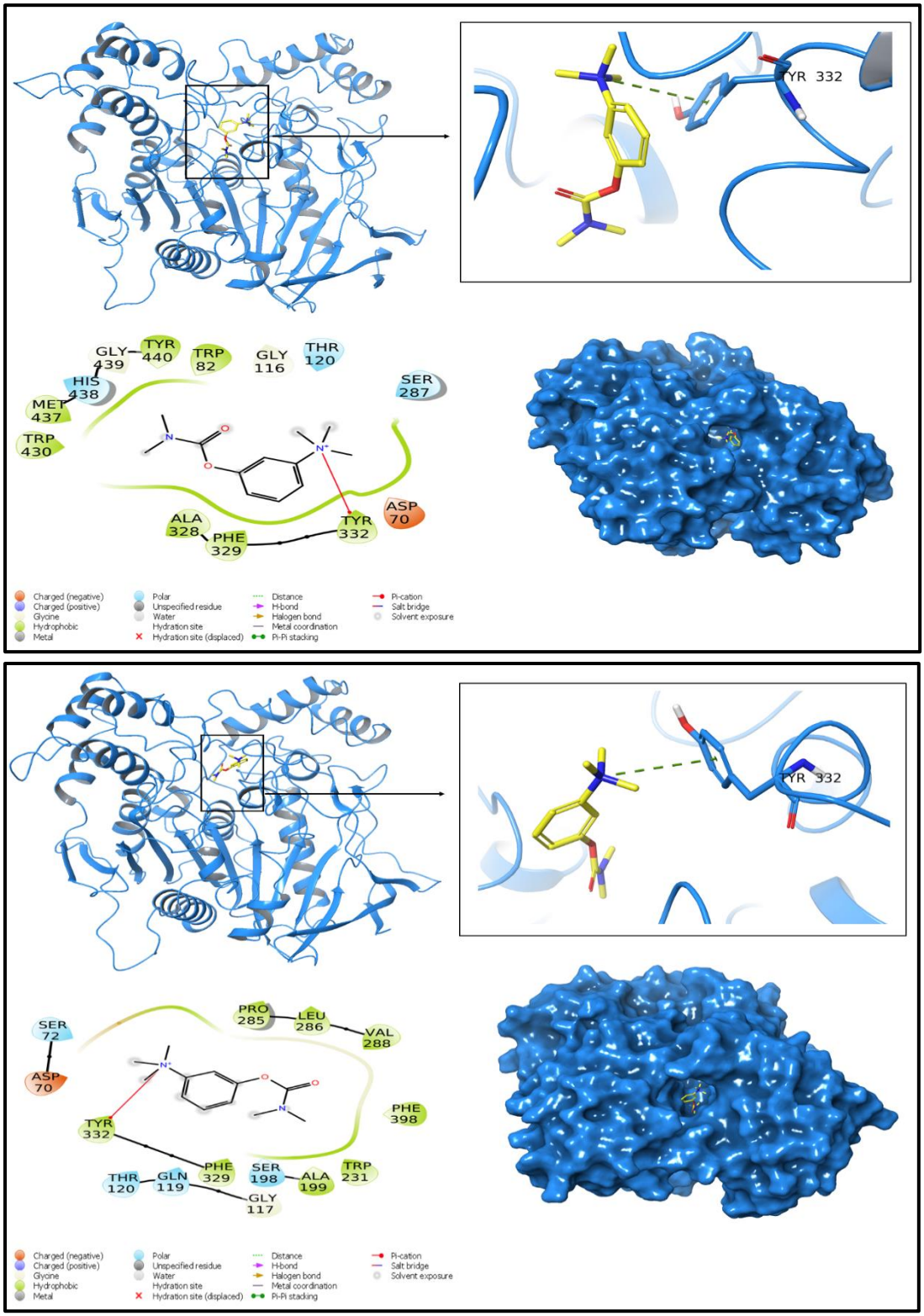

Figure 6. 83 2D and 3D ligand interaction diagrams during MD simulation of top docking pose of neostigmine with BuChE

(up:50-ns; dowm:100-ns)

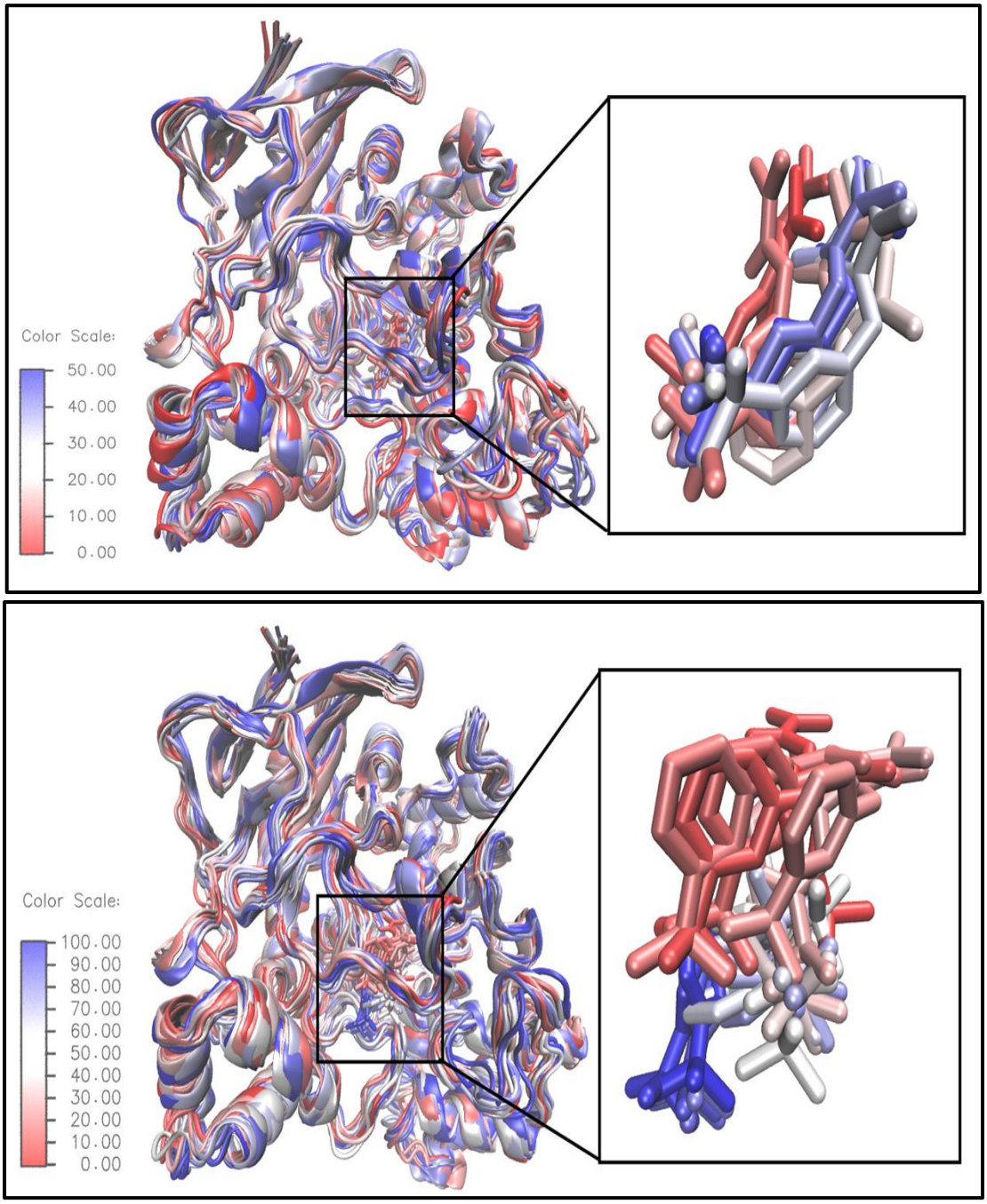

Figure 6. 84 Alignment of neostigmine conformations throughout the MD simulations with BuChE in a time-scale coloring (initial, red; end, blue)

(up:50-ns; dowm:100-ns)

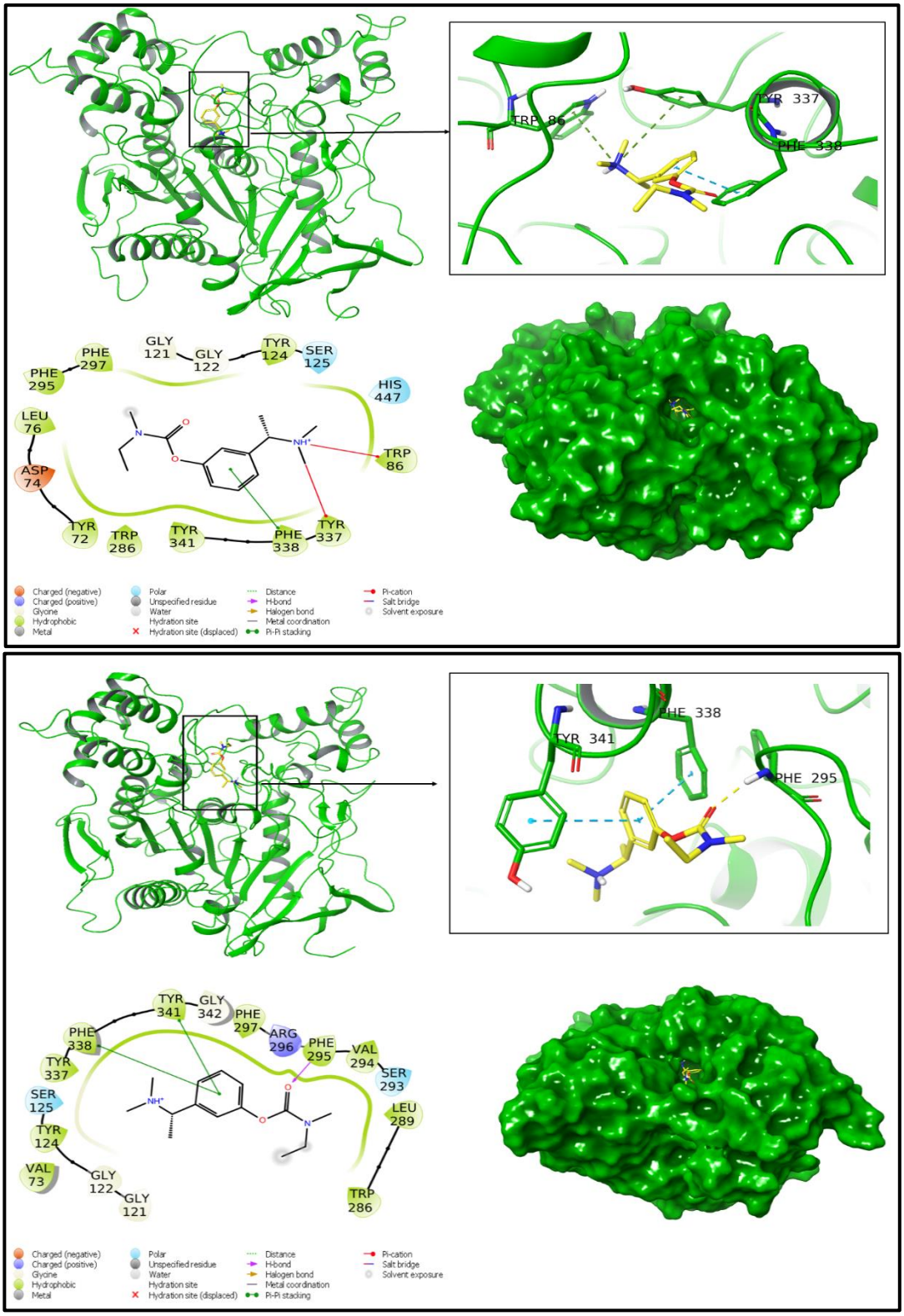

Figure 6. 85 2D and 3D ligand interaction diagrams during MD simulation of top docking pose of rivastigmine with AChE

(up:50-ns; dowm:100-ns)

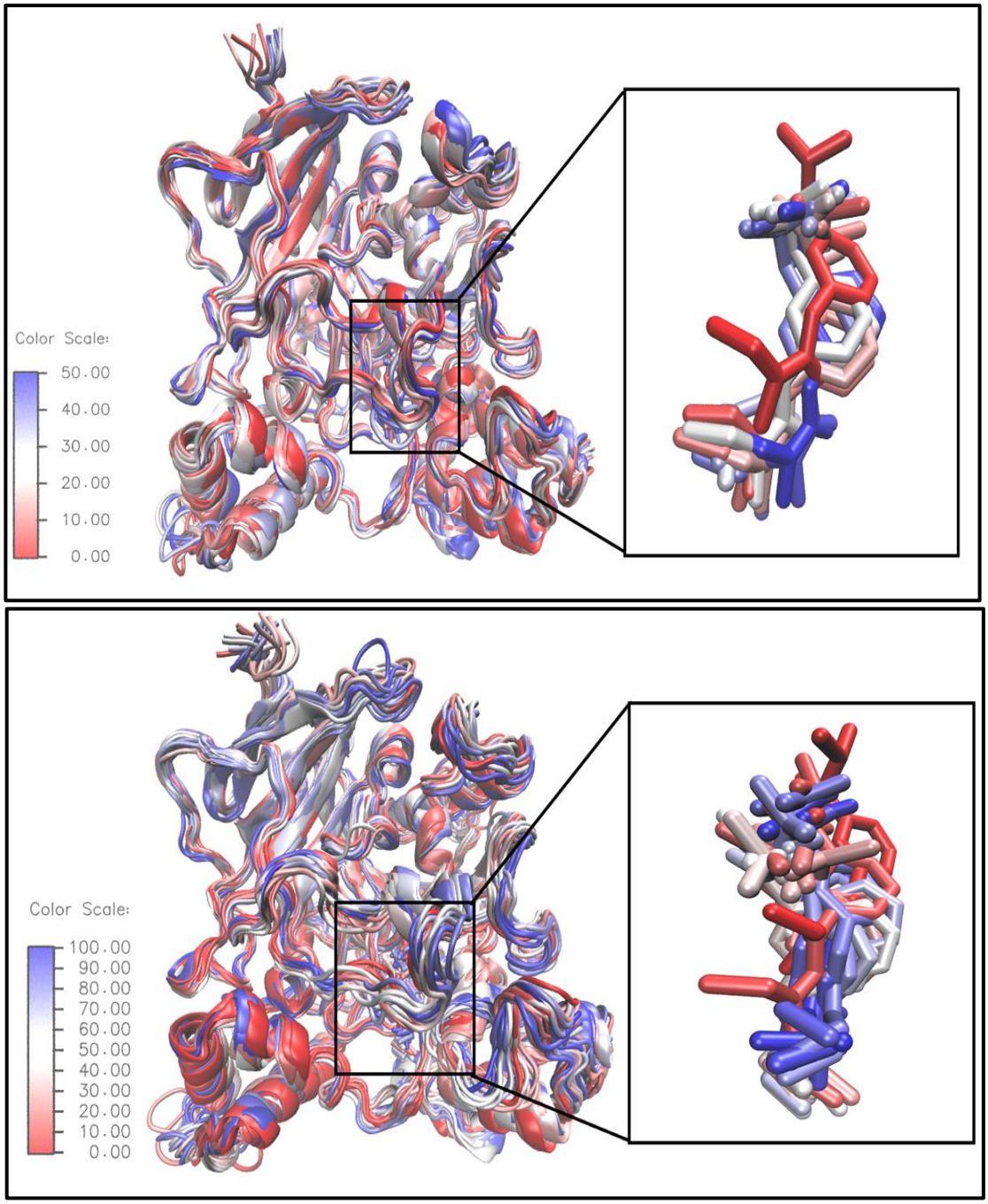

Figure 6. 86 Alignment of rivastigmine conformations throughout the MD simulations with AChE in a time-scale coloring (initial, red; end, blue)

(up:50-ns; dowm:100-ns)

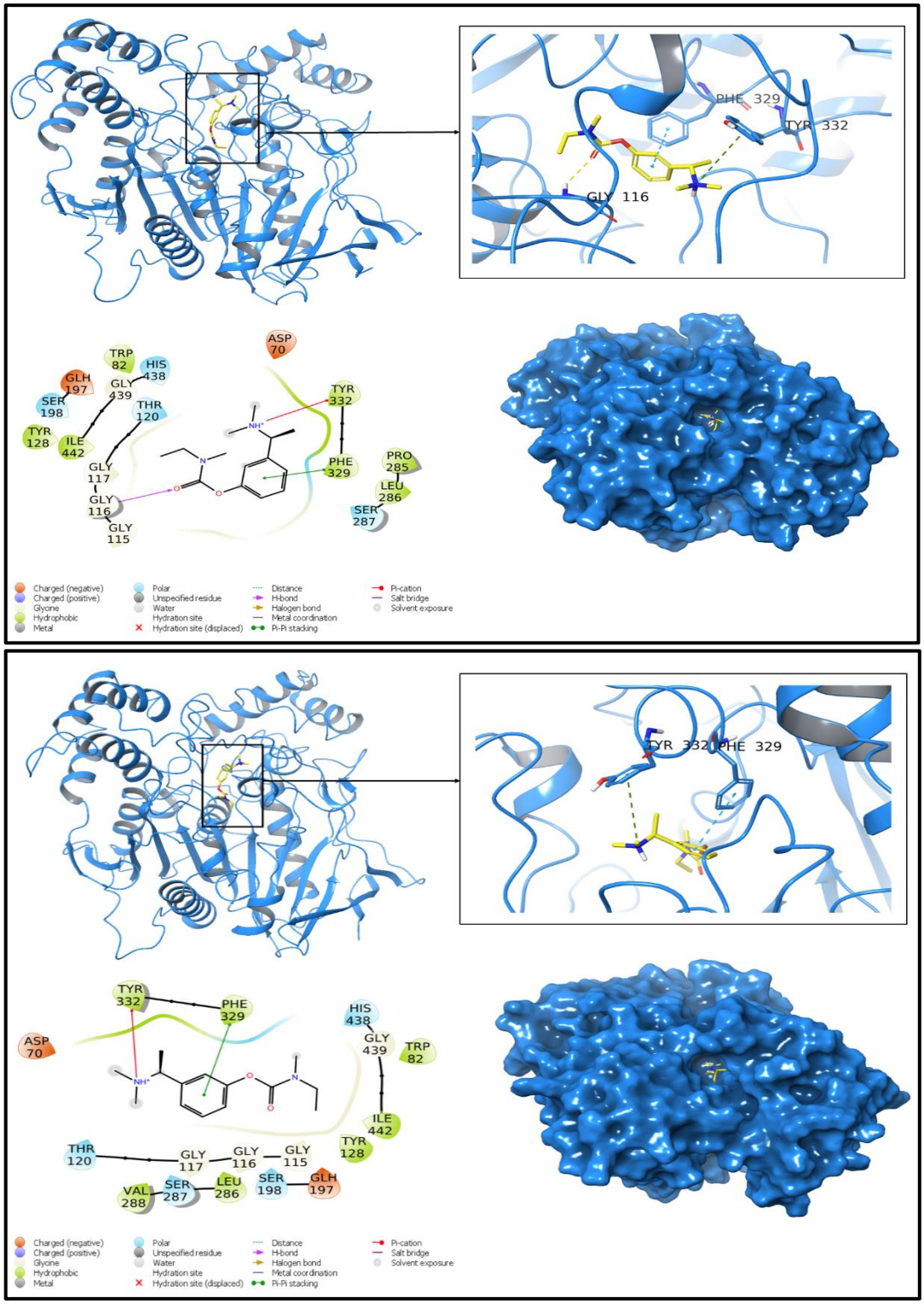

Figure 6. 87 2D and 3D ligand interaction diagrams during MD simulation of top docking pose of rivastigmine with BuChE

(up:50-ns; dowm:100-ns)

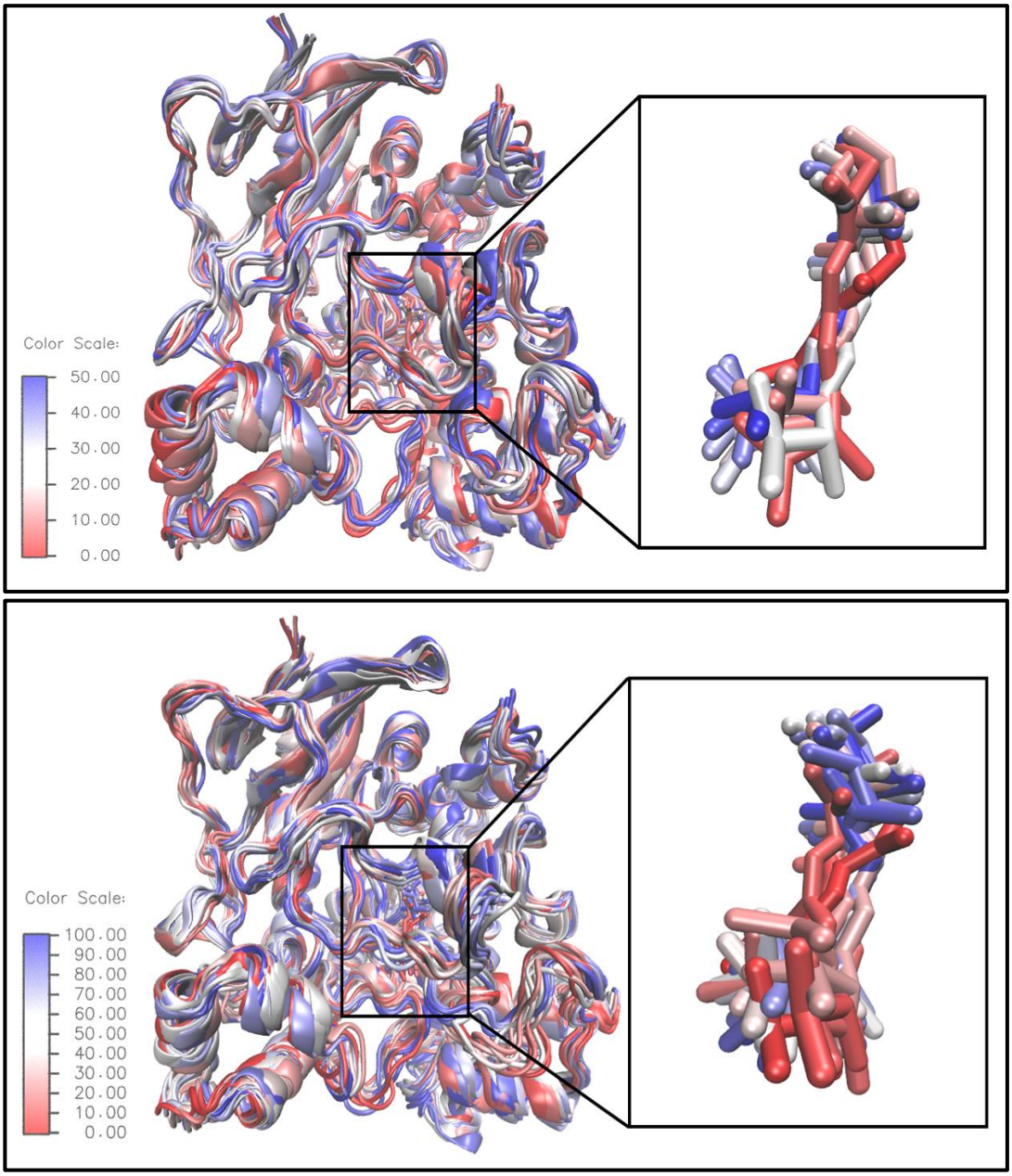

Figure 6. 88 Alignment of rivastigmine conformations throughout the MD simulations with BuChE in a time-scale coloring (initial, red; end, blue)

(up:50-ns; dowm:100-ns)

6.2 *In Vitro* Cholinesterase Activity Results and Discussion

Since enzyme inhibitors demonstrate a wide variety of behaviors, newly synthesized compounds have recently been focused on in several studies. Three hit compounds were ordered to test and confirm molecular modeling predictions and *in silico* investigations based on combined ligand-dependent and target-driven methods. described in the simulations *in silico*, and *in vitro* binding assays were performed. The concentrations of three molecules (ocaperidone, risperidone, and nelfinavir) expected to inhibit 50% of the activation of AChE and BuChE were determined from different inhibitor concentrations, and the index of selectivity (SI) reported in Table 6.9 and Figures from (6.89 to 6.94). Both AChE and BuChE inhibitions are indicated via comparing the IC_{50} values of the three chosen molecules. Select compounds can synergistically impact both enzymes, which are known to be important in AD. The IC_{50} inhibitor values were in the range of 70.23 to 89.22 nM for AChE and 36.06 to 49.37 nM for BuChE. Selected molecules showed inhibitor action in both enzymes, and their binding affinities are considered more reliable than the recognized drug neostigmine but less than rivastigmine. The best inhibition against AChE and BuChE was found with nelfinavir (IC_{50} = 70.23 nM and 36.06 nM), respectively, relative to neostigmine. Those compounds can thus be utilized as lead compounds, and with molecular tailoring experiments, their binding affinities can be strengthened. To obtain an indication of new compounds' selective cytotoxicity at an early stage in the screening procedure, we used the selectivity index (SI). A compound's SI is a widely accepted parameter used to express a molecule *in vitro* efficacy in inhibiting specific diseases. The higher the SI ratio, the theoretically more effective and safer a drug would be through *in vivo* treatment for a given AD. The *in vitro* selectivity index (defined as the ratio of the minimum inhibitory concentration of BuChE to that of the greatest inhibitory concentration of AChE) of currently used molecules were in the range of 0.24 to 0.65. Risperidone molecule was dual inhibitors of both AChE and BuChE, with high selectivity index toward both enzymes' inhibition (IS = 0.65).

Table 6. 9 AChE and BuChE inhibition results (IC_{50} nM) of selected hit molecules and references drugs (*Selectivity Index: IC_{50} of BuChE/IC_{50} of AChE)

Molecules Names	AChE (IC_{50} nM)	BuChE (IC_{50} nM)	Selectivity index*
Ocaperidone	89.22 ± 2.67	49.73 ± 1.49	0.55
Risperidone	72.30 ± 2.17	46.70 ± 1.39	0.65
Nelfinavir	70.23 ± 2.10	36.06 ± 1.08	0.51
Donepezil	37.00 ± 2.00	2,311 ± 120	62.4
Neostigmine	135.91± 1.12	84.00 ± 0.81	0.62
Rivastigmine	60.00 ± 3.11	14.10 ± 0.56	0.24

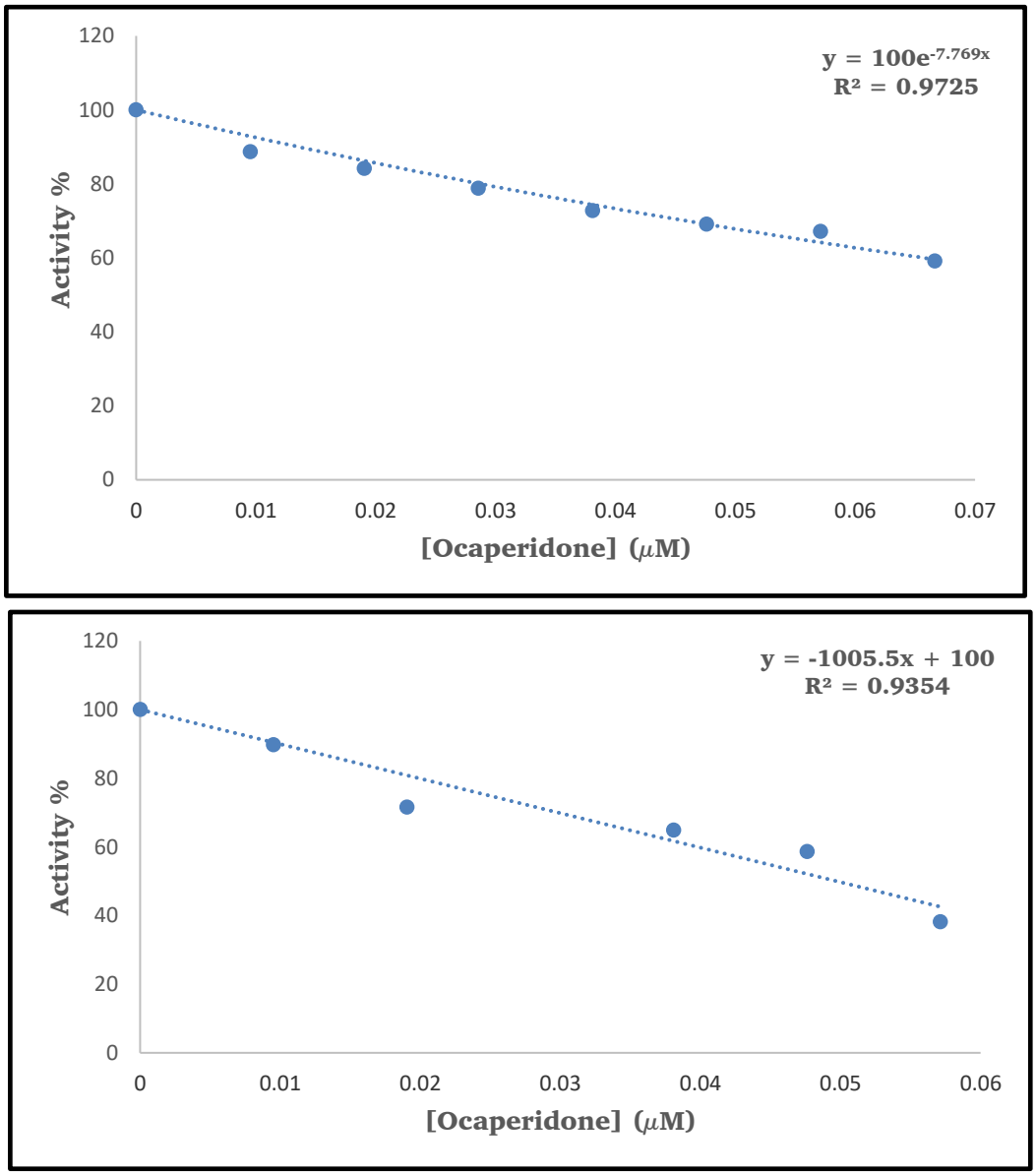

Figure 6. 89 Activity % versus ocaperidone concentration analysis graphs for AChE (up) and BuChE (down)

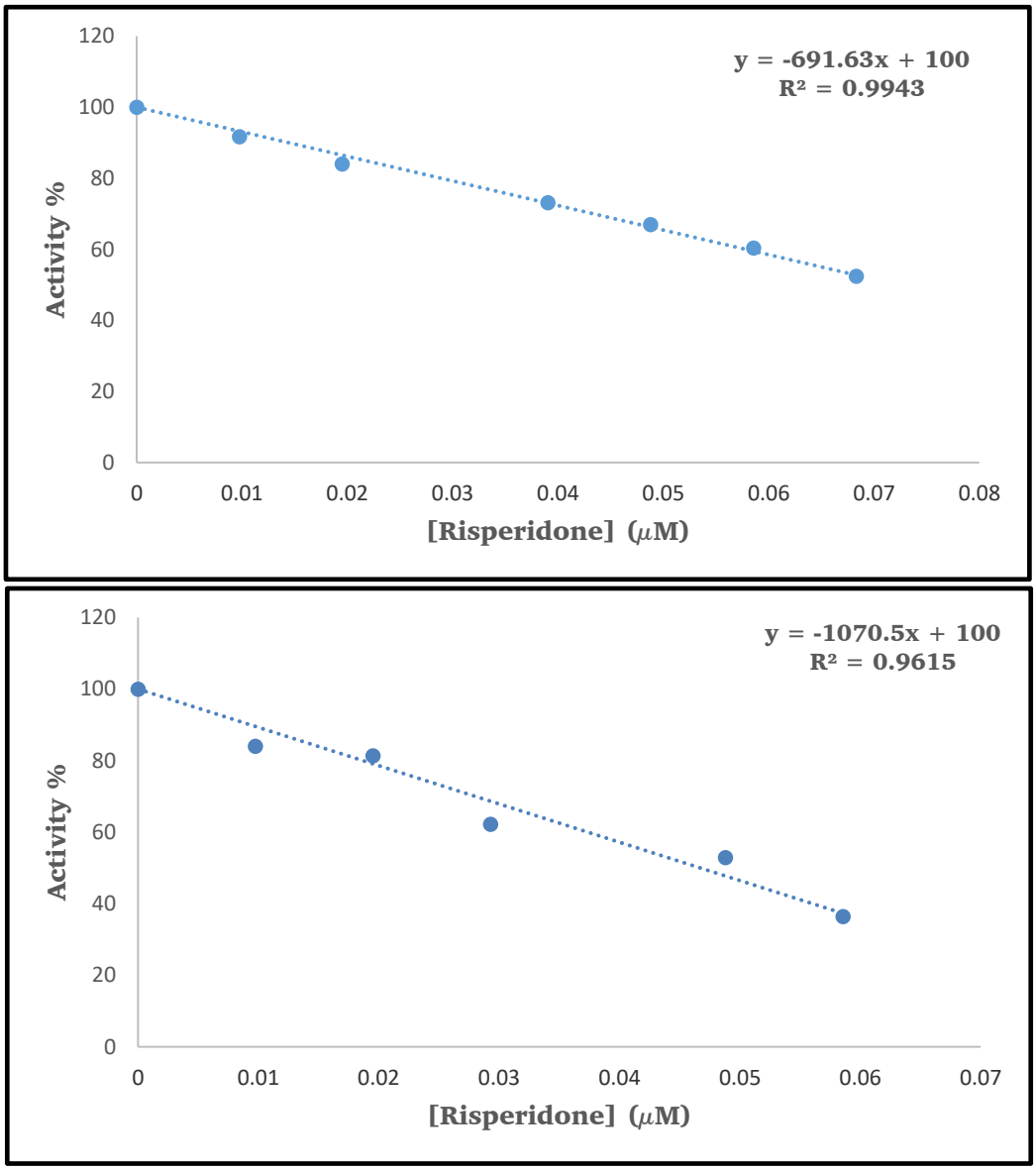

Figure 6. 90 Activity % versus risperidone concentration analysis graphs for AChE (up) and BuChE (down)

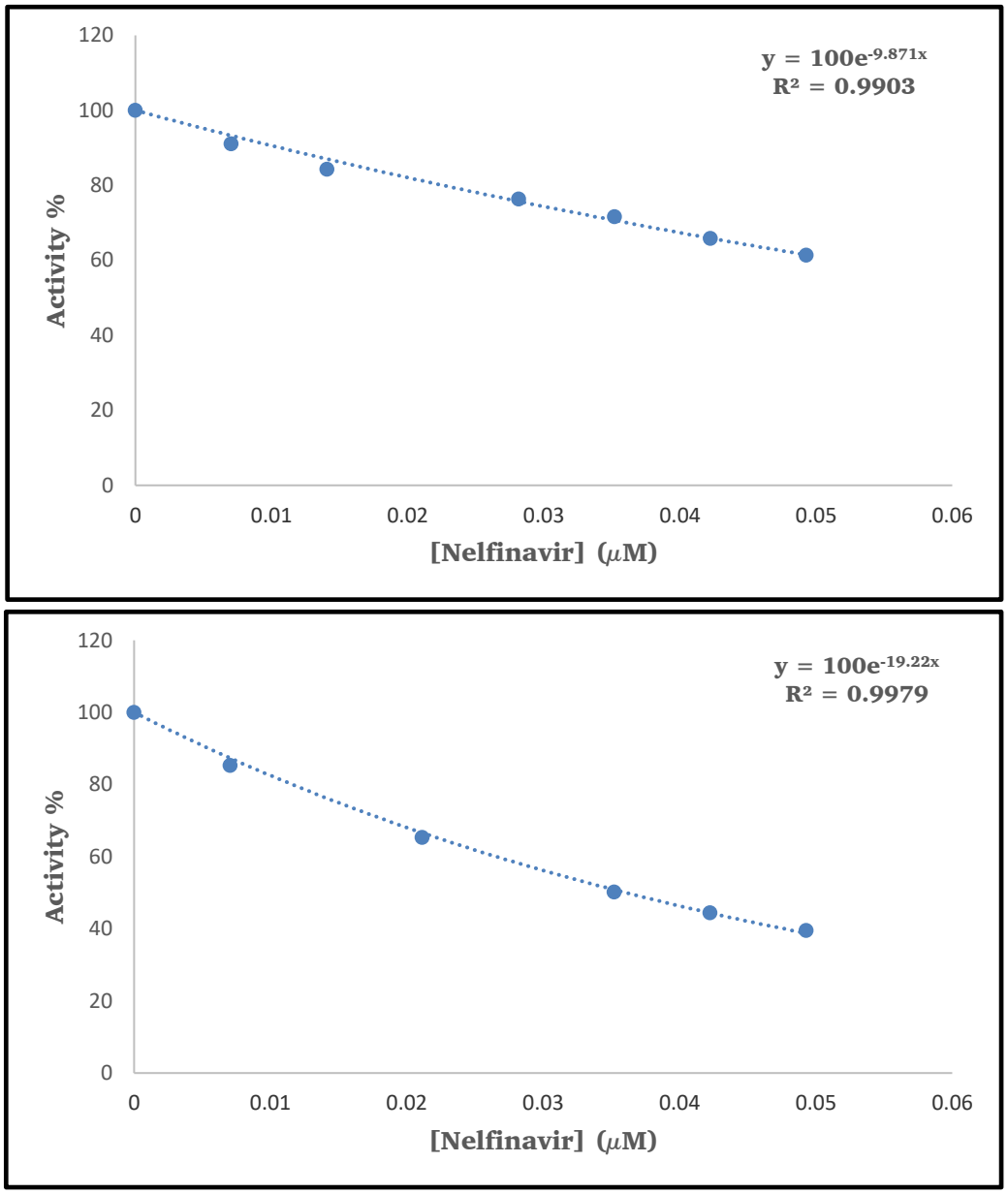

Figure 6. 91 Activity % versus nelfinavir concentration analysis graphs for AChE (up) and BuChE (down)

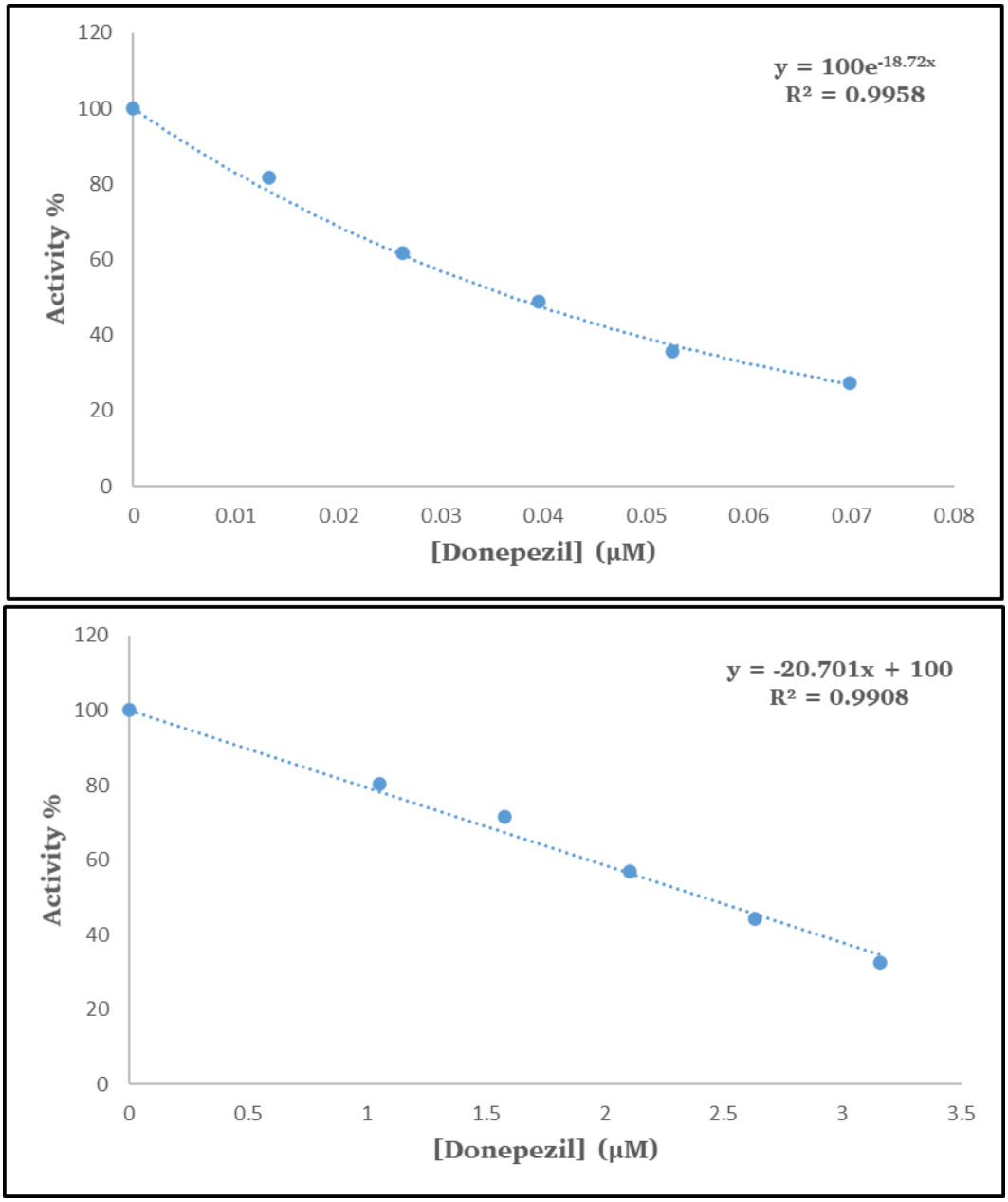

Figure 6. 92 Activity % versus donepezil concentration analysis graphs for AChE (up) & BuChE (down)

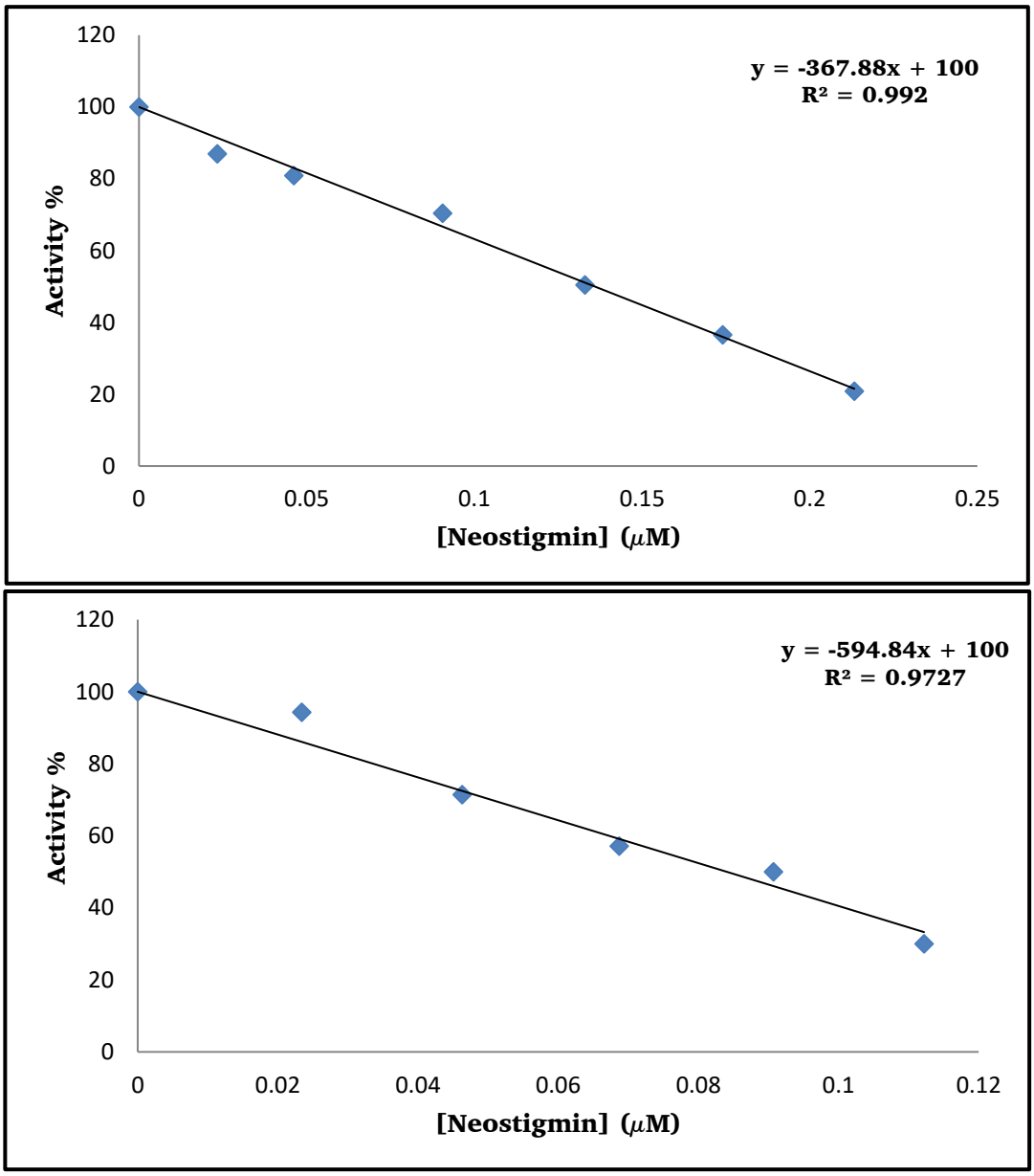

Figure 6. 93 Activity % versus neostigmine concentration analysis graphs for AChE (up) and BuChE (down)

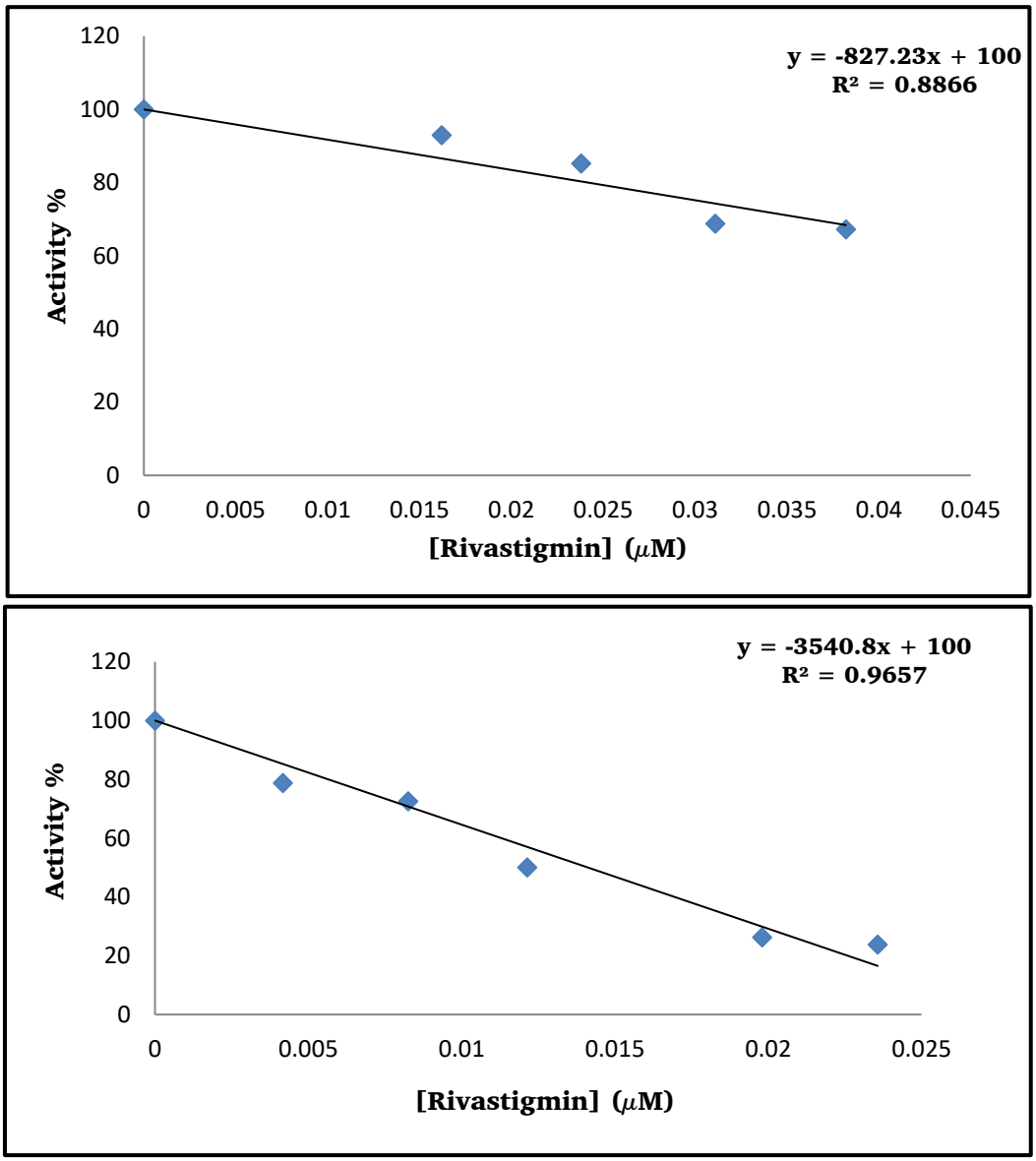

Figure 6. 94 Activity % versus rivastigmine concentration analysis graphs for AChE (up) and BuChE (down)

6.3 Conclusion

In this study, we used NPC approved and investigational drug library to repurpose existing drugs with less toxicity than the already used drugs in Alzheimer disease treatment. 7922 compounds first filtered using MetaCore™/MetaDrug™ server according to Alzheimer QSAR model. Then, 1340 compounds were obtained as possible ligands. These molecules were subjected to toxicity QSAR models in order to remove the most hazardous ones, and a final list of 10 compounds was produced. It was discovered that the studied compounds had less anticipated side effects than known inhibitors using the MetaCore™/MetaDrug™ system, which consists of 26 different toxicity QSAR models. Further evidence came from molecular modeling techniques such as docking, 50-ns, and 100-ns MD simulations, which suggested that the compounds cafedrine, risperidone, ocaperidone, and nelfinavir were conformationally stable within the binding cavity, owing to the formation of solid polar and non-polar interactions between the ligands and the active site amino acids. Both docking and MD simulations were carried out for known AChE and BuChE inhibitors, and the results showed that the studied compounds and the known inhibitors had essential amino acid profiles that were similar to one another. Among them, nelfinavir demonstrated strong inhibition of AChE and BuChE, with IC_{50} values of 70.23 and 36.06 nM, respectively, against both enzymes. All in all, these compounds have the potential to serve as novel chemotypes for the development of new ChEs inhibitors for the treatment of Alzheimer's disease. This is accomplished via properly altering the substitution pattern in the context of multifunctional anti-medicines of Alzheimer's.

REFERANCES

[1] Epperly T, Dunay MA, Boice JL. Alzheimer Disease: Pharmacologic and Nonpharmacologic Therapies for Cognitive and Functional Symptoms. American family physician. 2017;95(12):771-8.

[2] Wu J, Tian Y, Wang S, Pistolozzi M, Jin Y, Zhou T, et al. Design, synthesis and biological evaluation of bambuterol analogues as novel inhibitors of butyrylcholinesterase. European Journal of Medicinal Chemistry. 2017;126:61-71.

[3] Kurt BZ, Gazioglu I, Dag A, Salmas RE, Kayık G, Durdagi S, et al. Synthesis, anticholinesterase activity and molecular modeling study of novel carbamate-substituted thymol/carvacrol derivatives. Bioorganic and Medicinal Chemistry. 2017;25(4):1352-63.

[4] 2019 Alzheimer's disease facts and figures. Alzheimer's and Dementia. 2019;15(3):321-87.

[5] Matthews KA, Xu W, Gaglioti AH, Holt JB, Croft JB, Mack D, et al. Racial and ethnic estimates of Alzheimer's disease and related dementias in the United States (2015–2060) in adults aged ≥65 years. Alzheimer's and Dementia. 2019;15(1):17-24.

[6] Lane R, Potkin S, Enz A. Targeting Acetylcholinesterase and butyrylcholinesterase in dementia. The international journal of neuropsychopharmacology / official scientific journal of the Collegium Internationale Neuropsychopharmacologicum (CINP). 2006;9:101-24.

[7] Thompson P, Wright D, Counsell C, Zajicek J. Statistical analysis, trial design and duration in Alzheimer's disease clinical trials: A review. International psychogeriatrics / IPA. 2011;24:689-97.

[8] Chen Z, Digiacomo M, Tu Y, Gu Q, Wang S, Yang X, et al. Discovery of novel rivastigmine-hydroxycinnamic acid hybrids as multi-targeted agents for Alzheimer's disease. Eur J Med Chem. 2017;125:784-92.

[9] Orhan IE, Jedrejek D, Senol FS, Salmas RE, Durdagi S, Kowalska I, et al. Molecular modeling and in vitro approaches towards cholinesterase inhibitory effect of some natural xanthohumol, naringenin, and acyl phloroglucinol derivatives. Phytomedicine : international journal of phytotherapy and phytopharmacology. 2018;42:25-33.

[10] Auld DS, Kornecook TJ, Bastianetto S, Quirion R. Alzheimer's disease and the basal forebrain cholinergic system: relations to beta-amyloid peptides, cognition, and treatment strategies. Progress in neurobiology. 2002;68(3):209-45.

[11] Colović MB, Krstić DZ, Lazarević-Pašti TD, Bondžić AM, Vasić VM. Acetylcholinesterase inhibitors: pharmacology and toxicology. Curr Neuropharmacol. 2013;11(3):315-35.

[12] Deardorff WJ, Feen E, Grossberg GT. The Use of Cholinesterase Inhibitors Across All Stages of Alzheimer's Disease. Drugs and Aging. 2015;32(7):537-47.

[13] Pascoini AL, Federico LB, Arêas ALF, Verde BA, Freitas PG, Camps I. In silico development of new acetylcholinesterase inhibitors. Journal of biomolecular structure and dynamics. 2019;37(4):1007-21.

[14] Sahin K, Zengin Kurt B, Sonmez F, Durdagi S. Novel AChE and BuChE inhibitors using combined virtual screening, text mining and in vitro binding assays. Journal of Biomolecular Structure and Dynamics. 2020;38(11):3342-58.

[15] Sussman JL, Silman I. Computational studies on cholinesterases: Strengthening our understanding of the integration of structure, dynamics and function. Neuropharmacology. 2020;179:108265.

[16] Marucci G, Buccioni M, Ben DD, Lambertucci C, Volpini R, Amenta F. Efficacy of acetylcholinesterase inhibitors in Alzheimer's disease. Neuropharmacology. 2020:108352.

[17] Akhoon BA, Choudhary S, Tiwari H, Kumar A, Barik MR, Rathor L, et al. Discovery of a New Donepezil-like Acetylcholinesterase Inhibitor for Targeting Alzheimer's Disease: Computational Studies with Biological Validation. Journal of Chemical Information and Modeling. 2020;60(10):4717-29.

[18] Li Q, Yang H, Chen Y, Sun H. Recent progress in the identification of selective butyrylcholinesterase inhibitors for Alzheimer's disease. European Journal of Medicinal Chemistry. 2017;132:294-309.

[19] Lu T, Liu Y, Liu Y, Chen H, Han C, Feng X, et al. Discovery, biological evaluation and molecular dynamic simulations of butyrylcholinesterase inhibitors through structure-based pharmacophore virtual screening. Future Medicinal Chemistry. 2021;13(9):769-84.

[20] Macklin LJ, Schwans JP. Synthesis, biochemical evaluation, and molecular modeling of organophosphate-coumarin hybrids as potent and selective butyrylcholinesterase inhibitors. Bioorganic and medicinal chemistry letters. 2020;30(13):127213.

[21] Smith AR, Mill J, Lunnon K. The molecular etiology of Alzheimer's disease. Brain pathology (Zurich, Switzerland). 2020;30(5):964-5.

[22] Mishra N, Mandal P, Das S. ALZHEIMER'S DISEASE: FACTS AND FINDINGS. International Journal of Advanced Research. 2017;5:2386-441.

[23] Yang HD, Kim DH, Lee SB, Young LD. History of Alzheimer's Disease. Dement Neurocogn Disord. 2016;15(4):115-21.

[24] WHO. [Available from: https://www.who.int/news/item/09-12-2020-who-reveals-leading-causes-of-death-and-disability-worldwide-2000-2019#:~:text=Alzheimer's%20disease%20and%20other%20forms,Americas%20and%20Europe%20in%202019.

[25] Viña J, Lloret A. Why women have more Alzheimer's disease than men: gender and mitochondrial toxicity of amyloid-beta peptide. Journal of Alzheimer's disease : JAD. 2010;20 Suppl 2:S527-33.

[26] Alzheimer's disease facts and figures. Alzheimer's and Dementia. 2018;14(3):367-429.

[27] Schneider JA, Arvanitakis Z, Bang W, Bennett DA. Mixed brain pathologies account for most dementia cases in community-dwelling older persons. Neurology. 2007;69(24):2197-204.

[28] Viswanathan A, Rocca WA, Tzourio C. Vascular risk factors and dementia. How to move forward? 2009;72(4):368-74.

[29] Schneider JA, Arvanitakis Z, Leurgans SE, Bennett DA. The neuropathology of probable Alzheimer disease and mild cognitive impairment. Annals of Neurology. 2009;66(2):200-8.

[30] Arnaiz E, Almkvist O. Neuropsychological features of mild cognitive impairment and preclinical Alzheimer's disease. Acta neurologica Scandinavica Supplementum. 2003;179:34-41.

[31] Alzheimer's disease facts and figures. Alzheimer's and Dementia. 2020;16(3):391-460.

[32] Ullman MT. Contributions of memory circuits to language: the declarative/procedural model. Cognition. 2004;92(1):231-70.

[33] Tulving E. Precis of Elements of episodic memory. Behavioral and Brain Sciences. 2010;7(2):223-38.

[34] Saumier D, Chertkow H. Semantic memory. Current Neurology and Neuroscience Reports. 2002;2(6):516-22.

[35] Atri A. The Alzheimer's Disease Clinical Spectrum: Diagnosis and Management. The Medical clinics of North America. 2019;103(2):263-93.

[36] Long JM, Holtzman DM. Alzheimer Disease: An Update on Pathobiology and Treatment Strategies. Cell. 2019;179(2):312-39.

[37] Francis PT, Palmer AM, Snape M, Wilcock GK. The cholinergic hypothesis of Alzheimer's disease: a review of progress. Journal of neurology, neurosurgery, and psychiatry. 1999;66(2):137-47.

[38] Martorana A, Esposito Z, Koch G. Beyond the cholinergic hypothesis: do current drugs work in Alzheimer's disease? CNS neuroscience and therapeutics. 2010;16(4):235-45.

[39] Hardy J, Allsop D. Amyloid deposition as the central event in the aetiology of Alzheimer's disease. Trends in pharmacological sciences. 1991;12(10):383-8.

[40] Lott IT, Head E. Alzheimer disease and Down syndrome: factors in pathogenesis. Neurobiology of aging. 2005;26(3):383-9.

[41] Nistor M, Don M, Parekh M, Sarsoza F, Goodus M, Lopez GE, et al. Alpha- and beta-secretase activity as a function of age and beta-amyloid in Down syndrome and normal brain. Neurobiology of aging. 2007;28(10):1493-506.

[42] Zeng H, Wu X. Alzheimer's disease drug development based on Computer-Aided Drug Design. European Journal of Medicinal Chemistry. 2016;121:851-63.

[43] Mudher A, Lovestone S. Alzheimer's disease-do tauists and baptists finally shake hands? Trends in neurosciences. 2002;25(1):22-6.

[44] Goedert M, Spillantini MG, Crowther RA. Tau proteins and neurofibrillary degeneration. Brain pathology (Zurich, Switzerland). 1991;1(4):279-86.

[45] Sinyor B, Mineo J, Ochner C. Alzheimer's Disease, Inflammation, and the Role of Antioxidants. J Alzheimers Dis Rep. 2020;4(1):175-83.

[46] Deane R, Zlokovic BV. Role of the blood-brain barrier in the pathogenesis of Alzheimer's disease. Current Alzheimer research. 2007;4(2):191-7.

[47] Markesbery WR. Oxidative Stress Hypothesis in Alzheimer's Disease. Free Radical Biology and Medicine. 1997;23(1):134-47.

[48] Cataldo JK, Prochaska JJ, Glantz SA. Cigarette smoking is a risk factor for Alzheimer's Disease: an analysis controlling for tobacco industry affiliation. Journal of Alzheimer's disease : JAD. 2010;19(2):465-80.

[49] Eikelenboom P, Exel Ev, Hoozemans J, Veerhuis R, Rozemuller A, Gool WAv. Neuroinflammation@ An Early Event in Both the History and Pathogenesis of Alzheime' s Disease. Neurodegenerative Diseases. 2010;7:38 - 41.

[50] Caldwell CC, Yao J, Brinton RD. Targeting the prodromal stage of Alzheimer's disease: bioenergetic and mitochondrial opportunities. Neurotherapeutics : the journal of the American Society for Experimental NeuroTherapeutics. 2015;12(1):66-80.

[51] Du X, Wang X, Geng M. Alzheimer's disease hypothesis and related therapies. Translational Neurodegeneration. 2018;7:2.

[52] Moulton PV, Yang W. Air pollution, oxidative stress, and Alzheimer's disease. Journal of environmental and public health. 2012;2012:472751.

[53] Paul KC, Haan M, Mayeda ER, Ritz BR. Ambient Air Pollution, Noise, and Late-Life Cognitive Decline and Dementia Risk. Annual review of public health. 2019;40:203-20.

[54] Makhlouf S, Messelmani M, Zaouali J, Mrissa R. Cognitive impairment in celiac disease and non-celiac gluten sensitivity: review of literature on the main cognitive impairments, the imaging and the effect of gluten free diet. Acta neurologica Belgica. 2018;118(1):21-7.

[55] Zis P, Hadjivassiliou M. Treatment of Neurological Manifestations of Gluten Sensitivity and Coeliac Disease. Current Treatment Options in Neurology. 2019;21:1-10.

[56] Tomiyama T, Nagata T, Shimada H, Teraoka R, Fukushima A, Kanemitsu H, et al. A new amyloid variant favoring oligomerization in Alzheimer'" type dementia. Annals of Neurology. 2008;63.

[57] Tomiyama T. [Involvement of beta-amyloid in the etiology of Alzheimer's disease]. Brain and nerve = Shinkei kenkyu no shinpo. 2010;62(7):691-9.

[58] Tomiyama T, Shimada H. APP Osaka Mutation in Familial Alzheimer's Disease-Its Discovery, Phenotypes, and Mechanism of Recessive Inheritance. International journal of molecular sciences. 2020;21(4).

[59] Mendez MF. The accurate diagnosis of early-onset dementia. International journal of psychiatry in medicine. 2006;36(4):401-12.

[60] Klafki HW, Staufenbiel M, Kornhuber J, Wiltfang J. Therapeutic approaches to Alzheimer's disease. Brain : a journal of neurology. 2006;129(Pt 11):2840-55.

[61] McKhann G, Drachman D, Folstein M, Katzman R, Price D, Stadlan EM. Clinical diagnosis of Alzheimer's disease: report of the NINCDS-ADRDA Work Group under the auspices of Department of Health and Human Services Task Force on Alzheimer's Disease. Neurology. 1984;34(7):939-44.

[62] Dubois B, Feldman HH, Jacova C, Dekosky ST, Barberger-Gateau P, Cummings J, et al. Research criteria for the diagnosis of Alzheimer's disease: revising the NINCDS-ADRDA criteria. The Lancet Neurology. 2007;6(8):734-46.

[63] Burns A, Iliffe S. Alzheimer's disease. BMJ (Clinical research ed). 2009;338:b158.

[64] Bird TD. Alzheimer Disease Overview: University of Washington, Seattle, Seattle (WA); 1993 1993.

[65] Ricci G. Social Aspects of Dementia Prevention from a Worldwide to National Perspective: A Review on the International Situation and the Example of Italy. Behav Neurol. 2019;2019:8720904-.

[66] Silva MVF, Loures CMG, Alves LCV, de Souza LC, Borges KBG, Carvalho MDG. Alzheimer's disease: risk factors and potentially protective measures. Journal of biomedical science. 2019;26(1):33.

[67] Reitz C, Rogaeva E, Beecham GW. Late-onset vs nonmendelian early-onset Alzheimer disease. Neurology Genetics. 2020;6(5):e512.

[68] Swerdlow RH. Pathogenesis of Alzheimer's disease. Clin Interv Aging. 2007;2(3):347-59.

[69] Colom-Cadena M, Spires-Jones T, Zetterberg H, Blennow K, Caggiano A, DeKosky ST, et al. The clinical promise of biomarkers of synapse damage or

loss in Alzheimer’s disease. Alzheimer's Research and Therapy. 2020;12(1):21.

[70] DeTure MA, Dickson DW. The neuropathological diagnosis of Alzheimer’s disease. Molecular Neurodegeneration. 2019;14(1):32.

[71] Mishra S, Palanivelu K. The effect of curcumin (turmeric) on Alzheimer's disease: An overview. Annals of Indian Academy of Neurology. 2008;11(1):13-9.

[72] Tiwari S, Atluri V, Kaushik A, Yndart A, Nair M. Alzheimer's disease: pathogenesis, diagnostics, and therapeutics. International journal of nanomedicine. 2019;14:5541-54.

[73] Jonsson T, Atwal JK, Steinberg S, Snaedal J, Jonsson PV, Bjornsson S, et al. A mutation in APP protects against Alzheimer's disease and age-related cognitive decline. Nature. 2012;488(7409):96-9.

[74] Bergmans BA, De Strooper B. gamma-secretases: from cell biology to therapeutic strategies. The Lancet Neurology. 2010;9(2):215-26.

[75] Imahori K. The biochemical study on the etiology of Alzheimer's disease. Proc Jpn Acad Ser B Phys Biol Sci. 2010;86(1):54-61.

[76] Sanabria-Castro A, Alvarado-Echeverría I, Monge-Bonilla C. Molecular Pathogenesis of Alzheimer's Disease: An Update. Ann Neurosci. 2017;24(1):46-54.

[77] Eftekharzadeh B, Daigle JG, Kapinos LE, Coyne A, Schiantarelli J, Carlomagno Y, et al. Tau Protein Disrupts Nucleocytoplasmic Transport in Alzheimer's Disease. Neuron. 2018;99(5):925-40.e7.

[78] Tu S, Okamoto S-i, Lipton SA, Xu H. Oligomeric Aβ-induced synaptic dysfunction in Alzheimer’s disease. Molecular Neurodegeneration. 2014;9(1):48.

[79] McCormick JW, Ammerman L, Chen G, Vogel PD, Wise JG. Transport of Alzheimer's associated amyloid-β catalyzed by P-glycoprotein. PLoS One. 2021;16(4):e0250371-e.

[80] Vidal C, Zhang L. An Analysis of the Neurological and Molecular Alterations Underlying the Pathogenesis of Alzheimer's Disease. Cells. 2021;10(3):546.

[81] Rivas Nieto JC. Frontotemporal dementia: clinical, neuropsychological, and neuroimaging description. Colomb Med (Cali). 2014;45(3):122-6.

[82] Ramkumar A, Jong BY, Ori-McKenney KM. ReMAPping the microtubule landscape: How phosphorylation dictates the activities of microtubule-associated proteins. Developmental Dynamics. 2018;247(1):138-55.

[83] Ksiezak-Reding H, Pyo HK, Feinstein B, Pasinetti GM. Akt/PKB kinase phosphorylates separately Thr212 and Ser214 of tau protein in vitro. Biochimica et biophysica acta. 2003;1639(3):159-68.

[84] Sengupta A, Kabat J, Novak M, Wu Q, Grundke-Iqbal I, Iqbal K. Phosphorylation of Tau at Both Thr 231 and Ser 262 Is Required for Maximal Inhibition of Its Binding to Microtubules. Archives of biochemistry and biophysics. 1998;357(2):299-309.

[85] Cowan CM, Mudher A. Are tau aggregates toxic or protective in tauopathies? Front Neurol. 2013;4:114.

[86] Ferrari A, Hoerndli F, Baechi T, Nitsch RM, Götz J. and#x3b2;-Amyloid Induces Paired Helical Filament-like Tau Filaments in Tissue Culture *. Journal of Biological Chemistry. 2003;278(41):40162-8.

[87] d'Errico P, Meyer-Luehmann M. Mechanisms of Pathogenic Tau and Aβ Protein Spreading in Alzheimer's Disease. Frontiers in aging neuroscience. 2020;12:265.

[88] Engmann O, Giese KP. Crosstalk between Cdk5 and GSK3beta: Implications for Alzheimer's Disease. Front Mol Neurosci. 2009;2:2-.

[89] Mota IFL, de Lima LS, Santana BdM, Gobbo GdAM, Bicca JVML, Azevedo JRM, et al. Alzheimer’s Disease: Innovative Therapeutic Approaches Based on Peptides and Nanoparticles. The Neuroscientist. 2021:10738584211016409.

[90] Tönnies E, Trushina E. Oxidative Stress, Synaptic Dysfunction, and Alzheimer's Disease. Journal of Alzheimer's disease : JAD. 2017;57(4):1105-21.

[91] Larosa V, Remacle C. Insights into the respiratory chain and oxidative stress. Bioscience Reports. 2018;38(5).

[92] Guo C, Sun L, Chen X, Zhang D. Oxidative stress, mitochondrial damage and neurodegenerative diseases. Neural regeneration research. 2013;8(21):2003-14.

[93] Devine MJ, Kittler JT. Mitochondria at the neuronal presynapse in health and disease. Nature reviews Neuroscience. 2018;19(2):63-80.

[94] Anandatheerthavarada HK, Biswas G, Robin MA, Avadhani NG. Mitochondrial targeting and a novel transmembrane arrest of Alzheimer's amyloid precursor protein impairs mitochondrial function in neuronal cells. The Journal of cell biology. 2003;161(1):41-54.

[95] Murphy MP. How mitochondria produce reactive oxygen species. The Biochemical journal. 2009;417(1):1-13.

[96] Moreira PI, Carvalho C, Zhu X, Smith MA, Perry G. Mitochondrial dysfunction is a trigger of Alzheimer's disease pathophysiology. Biochimica et Biophysica Acta (BBA) - Molecular Basis of Disease. 2010;1802(1):2-10.

[97] Ansari MA, Abdul HM, Joshi G, Opii WO, Butterfield DA. Protective effect of quercetin in primary neurons against Abeta(1-42): relevance to Alzheimer's disease. The Journal of nutritional biochemistry. 2009;20(4):269-75.

[98] Mark RJ, Lovell MA, Markesbery WR, Uchida K, Mattson MP. A role for 4-hydroxynonenal, an aldehydic product of lipid peroxidation, in disruption of ion homeostasis and neuronal death induced by amyloid beta-peptide. Journal of neurochemistry. 1997;68(1):255-64.

[99] Sultana R, Perluigi M, Butterfield DA. Oxidatively modified proteins in Alzheimer's disease (AD), mild cognitive impairment and animal models of

AD: role of Abeta in pathogenesis. Acta neuropathologica. 2009;118(1):131-50.

[100] Maes O, Chertkow H, Wang E, Schipper H. Stress Gene Deregulation in Alzheimer Peripheral Blood Mononuclear Cells. 2011. p. 251-63.

[101] Ejaz HW, Wang W, Lang M. Copper Toxicity Links to Pathogenesis of Alzheimer's Disease and Therapeutics Approaches. International journal of molecular sciences. 2020;21(20).

[102] Compagnoni G, Di Fonzo A, Corti S, Comi G, Bresolin N, Masliah E. The Role of Mitochondria in Neurodegenerative Diseases: the Lesson from Alzheimer's Disease and Parkinson's Disease. Molecular Neurobiology. 2020;57.

[103] Vidal C, Zhang L. An Analysis of the Neurological and Molecular Alterations Underlying the Pathogenesis of Alzheimer's Disease. Cells. 2021;10(3).

[104] Chen Z, Zhong C. Decoding Alzheimer's disease from perturbed cerebral glucose metabolism: Implications for diagnostic and therapeutic strategies. Progress in neurobiology. 2013;108:21-43.

[105] Sokoloff L. Energetics of functional activation in neural tissues. Neurochemical research. 1999;24(2):321-9.

[106] Duelli R, Kuschinsky W. Brain glucose transporters: relationship to local energy demand. News in physiological sciences : an international journal of physiology produced jointly by the International Union of Physiological Sciences and the American Physiological Society. 2001;16:71-6.

[107] Lee T, Lee H. Shared Blood Transcriptomic Signatures between Alzheimer's Disease and Diabetes Mellitus. Biomedicines. 2021;9(1).

[108] Mosconi L, Pupi A, De Leon MJ. Brain glucose hypometabolism and oxidative stress in preclinical Alzheimer's disease. Annals of the New York Academy of Sciences. 2008;1147:180-95.

[109] Gibas K. The starving brain: Overfed meets undernourished in the pathology of mild cognitive impairment (MCI) and Alzheimer's disease (AD). Neurochemistry International. 2017;110.

[110] Greenough MA, Camakaris J, Bush AI. Metal dyshomeostasis and oxidative stress in Alzheimer's disease. Neurochemistry International. 2013;62(5):540-55.

[111] Rogers JT, Venkataramani V, Washburn C, Liu Y, Tummala V, Jiang H, et al. A role for amyloid precursor protein translation to restore iron homeostasis and ameliorate lead (Pb) neurotoxicity. Journal of neurochemistry. 2016;138(3):479-94.

[112] Huang X, Atwood CS, Hartshorn MA, Multhaup G, Goldstein LE, Scarpa RC, et al. The A beta peptide of Alzheimer's disease directly produces hydrogen peroxide through metal ion reduction. Biochemistry. 1999;38(24):7609-16.

[113] Hooda J, Shah A, Zhang L. Heme, an Essential Nutrient from Dietary Proteins, Critically Impacts Diverse Physiological and Pathological Processes. Nutrients. 2014;6(3).

[114] Faux NG, Rembach A, Wiley J, Ellis KA, Ames D, Fowler CJ, et al. An anemia of Alzheimer's disease. Molecular psychiatry. 2014;19(11):1227-34.

[115] Hong CH, Falvey C, Harris TB, Simonsick EM, Satterfield S, Ferrucci L, et al. Anemia and risk of dementia in older adults: findings from the Health ABC study. Neurology. 2013;81(6):528-33.

[116] Tiwari S, Atluri V, Kaushik A, Yndart A, Nair M. Alzheimer's disease: pathogenesis, diagnostics, and therapeutics. International journal of nanomedicine. 2019;14:5541-54.

[117] Scarpini E, Scheltens P, Feldman H. Treatment of Alzheimer's disease: current status and new perspectives. The Lancet Neurology. 2003;2(9):539-47.

[118] Olazarán J, Reisberg B, Clare L, Cruz I, Peña-Casanova J, Del Ser T, et al. Nonpharmacological therapies in Alzheimer's disease: a systematic review of efficacy. Dementia and geriatric cognitive disorders. 2010;30(2):161-78.

[119] Ballard C, Khan Z, Clack H, Corbett A. Nonpharmacological treatment of Alzheimer disease. Canadian journal of psychiatry Revue canadienne de psychiatrie. 2011;56(10):589-95.

[120] Hansen RA, Gartlehner G, Kaufer DJ, Lohr KN, Carey T. Drug Class Reviews. Drug Class Review: Alzheimer's Drugs: Final Report. Portland (OR): Oregon Health and Science University.

Copyright © 2006, Oregon Health and Science University, Portland, Oregon.; 2006.

[121] Thakur A, Kamboj P, Goswami K, Ahuja K. Pathophysiology and management of alzheimer's disease: An overview. J Anal Pharm Res. 2018;7(1).

[122] Graham WV, Bonito-Oliva A, Sakmar TP. Update on Alzheimer's Disease Therapy and Prevention Strategies. Annual review of medicine. 2017;68:413-30.

[123] Ito K, Tatebe T, Suzuki K, Hirayama T, Hayakawa M, Kubo H, et al. Memantine reduces the production of amyloid-β peptides through modulation of amyloid precursor protein trafficking. European journal of pharmacology. 2017;798:16-25.

[124] Goodman Gilman A, Hardman J, Limbird L, Molinoff P, Ruddon R. _ GOODMAN. Gilman's The Pharmacological Basis of Therapeutics.9.

[125] Nordberg A, Ballard C, Bullock R, Darreh-Shori T, Somogyi M. A review of butyrylcholinesterase as a therapeutic target in the treatment of Alzheimer's disease. The primary care companion for CNS disorders. 2013;15(2).

[126] Xu Z, Yao S, Wei Y, Zhou J, Zhang L, Wang C, et al. Monitoring Enzyme Reaction and Screening of Inhibitors of Acetylcholinesterase by Quantitative Matrix-Assisted Laser Desorption/Ionization Fourier Transform Mass

Spectrometry. Journal of the American Society for Mass Spectrometry. 2008;19(12):1849-55.

[127] Ren J, Qin C, Hu F, Tan J, Qiu L, Zhao S, et al. Habenula "cholinergic" neurons co-release glutamate and acetylcholine and activate postsynaptic neurons via distinct transmission modes. Neuron. 2011;69(3):445-52.

[128] Tiwari P, Dwivedi S, Singh MP, Mishra R, Chandy A. Basic and modern concepts on cholinergic receptor: A review. Asian Pac J Trop Dis. 2013;3(5):413-20.

[129] Kapalka GM. Chapter 4 - Substances Involved in Neurotransmission. In: Kapalka GM, editor. Nutritional and Herbal Therapies for Children and Adolescents. San Diego: Academic Press; 2010. p. 71-99.

[130] Purves D AG, Fitzpatrick D, et al., editors. Neuroscience. 2nd edition. Sunderland (MA): Sinauer Associates; 2001. Acetylcholine. Available from: https://www.ncbi.nlm.nih.gov/books/NBK11143/.

[131] Smythies J. Philosophy, perception, and neuroscience. Perception. 2009;38(5):638-51.

[132] Smythies J, de Lantremange M. The Nature and Function of Digital Information Compression Mechanisms in the Brain and in Digital Television Technology. Frontiers in systems neuroscience. 2016;10:40.

[133] Downes GB, Granato M. Acetylcholinesterase function is dispensable for sensory neurite growth but is critical for neuromuscular synapse stability. Developmental Biology. 2004;270(1):232-45.

[134] Zeynep Özdemir and Mehmet Abdullah Alagöz (November 16th 2018). Anticholinesterases STiMG, Isam Jaber Al-Zwaini and Ali AL-Mayahi, IntechOpen, DOI: 10.5772/intechopen.81994. Available from: https://www.intechopen.com/books/selected-topics-in-myasthenia-gravis/anticholinesterases.

[135] Bajda M, Wieckowska A, Hebda M, Szałaj N, Sotriffer C, Malawska B. Structure-Based Search for New Inhibitors of Cholinesterases. International journal of molecular sciences. 2013;14:5608-32.

[136] Nicolet M, Garcia L, Dreyfus PA, Verdiere-Sahuque M, Pincon-Raymond M, Rieger F. Hydrophilic and hydrophobic attachment of both globular and asymmetric acetylcholinesterase to frog muscle basal lamina sheaths. Neurochemistry International. 1987;11(2):189-98.

[137] Colović MB, Krstić DZ, Lazarević-Pašti TD, Bondžić AM, Vasić VM. Acetylcholinesterase inhibitors: pharmacology and toxicology. Curr Neuropharmacol. 2013;11(3):315-35.

[138] Assis CRD, Linhares AG, Cabrera MP, Oliveira VM, Silva KCC, Marcuschi M, et al. Erythrocyte acetylcholinesterase as biomarker of pesticide exposure: new and forgotten insights. Environmental Science and Pollution Research. 2018;25(19):18364-76.

[139] Sharma K. Cholinesterase inhibitors as Alzheimer's therapeutics (Review). Mol Med Rep. 2019;20(2):1479-87.

[140] Mehta M, Adem A, Sabbagh M. New Acetylcholinesterase Inhibitors for Alzheimer's Disease. International Journal of Alzheimerand#x2019;s Disease. 2012;2012:728983.

[141] Bacalhau P, San Juan A, Marques C, Peixoto D, Goth A, Guarda C, et al. New Cholinesterase Inhibitors for Alzheimer’s Disease: Structure Activity Studies (SARs) and Molecular Docking of Isoquinolone and Azepanone Derivatives. Bioorganic Chemistry. 2016;67.

[142] Rosenberry TL, Brazzolotto X, Macdonald IR, Wandhammer M, Trovaslet-Leroy M, Darvesh S, et al. Comparison of the Binding of Reversible Inhibitors to Human Butyrylcholinesterase and Acetylcholinesterase: A Crystallographic, Kinetic and Calorimetric Study. Molecules. 2017;22(12).

[143] Marucci G, Buccioni M, Ben DD, Lambertucci C, Volpini R, Amenta F. Efficacy of acetylcholinesterase inhibitors in Alzheimer's disease. Neuropharmacology. 2021;190:108352.

[144] Thompson PA, Wright DE, Counsell CE, Zajicek J. Statistical analysis, trial design and duration in Alzheimer's disease clinical trials: a review. International psychogeriatrics. 2012;24(5):689-97.

[145] Bajgar J. Organophosphates/nerve agent poisoning: mechanism of action, diagnosis, prophylaxis, and treatment. Advances in clinical chemistry. 2004;38:151-216.

[146] Organization WH. Organophosphorus insecticides: a general introduction: World Health Organization; 1986.

[147] Moss DE. Improving Anti-Neurodegenerative Benefits of Acetylcholinesterase Inhibitors in Alzheimer's Disease: Are Irreversible Inhibitors the Future? International journal of molecular sciences. 2020;21(10).

[148] Bai D. Development of huperzine A and B for treatment of Alzheimer's disease. Pure and Applied Chemistry. 2007;79(4):469-79.

[149] Mehta M, Adem A, Sabbagh M. New acetylcholinesterase inhibitors for Alzheimer's disease. Int J Alzheimers Dis. 2012;2012:728-983.

[150] Lockridge O, Duysen E, Masson P. Butyrylcholinesterase: Overview, Structure, and Function. 2011. p. 25-41.

[151] Mesulam MM, Guillozet A, Shaw P, Levey A, Duysen EG, Lockridge O. Acetylcholinesterase knockouts establish central cholinergic pathways and can use butyrylcholinesterase to hydrolyze acetylcholine. Neuroscience. 2002;110(4):627-39.

[152] Chen VP, Gao Y, Geng L, Stout MB, Jensen MD, Brimijoin S. Butyrylcholinesterase Deficiency Promotes Adipose Tissue Growth and Hepatic Lipid Accumulation in Male Mice on High-Fat Diet. Endocrinology. 2016;157(8):3086-95.

[153] Ha ZY, Mathew S, Yeong KY. Butyrylcholinesterase: A Multifaceted Pharmacological Target and Tool. Current protein and peptide science. 2020;21(1):99-109.

[154] Darvesh S, Hopkins D, Geula C. The biology of butyrylcholinesterase. Nature reviews Neuroscience. 2003;4:131-8.

[155] Silver A. The biology of cholinesterases. Amsterdam; New York: North-Holland Pub. Co. ; American Elsevier Pub. Co.; 1974.

[156] Gatley SJ. Activities of the enantiomers of cocaine and some related compounds as substrates and inhibitors of plasma butyrylcholinesterase. Biochemical Pharmacology. 1991;41(8):1249-54.

[157] Masson P, Froment MT, Fortier PL, Visicchio JE, Bartels CF, Lockridge O. Butyrylcholinesterase-catalysed hydrolysis of aspirin, a negatively charged ester, and aspirin-related neutral esters. Biochimica et biophysica acta. 1998;1387(1-2):41-52.

[158] Macdonald IR, Maxwell SP, Reid GA, Cash MK, DeBay DR, Darvesh S. Quantification of Butyrylcholinesterase Activity as a Sensitive and Specific Biomarker of Alzheimer's Disease. Journal of Alzheimer's Disease. 2017;58:491-505.

[159] DeBay DR, Reid GA, Pottie IR, Martin E, Bowen CV, Darvesh S. Targeting butyrylcholinesterase for preclinical single photon emission computed tomography (SPECT) imaging of Alzheimer's disease. Alzheimer's and Dementia: Translational Research and Clinical Interventions. 2017;3(2):166-76.

[160] Reid A, Darvesh S. Butyrylcholinesterase-Knockout Reduces Brain Deposition of Fibrillar β-Amyloid in an Alzheimer Mouse Model. Neuroscience. 2015;186.

[161] Maurice T, Strehaiano M, Siméon N, Bertrand C, Chatonnet A. Learning performances and vulnerability to amyloid toxicity in the

butyrylcholinesterase knockout mouse. Behavioural Brain Research. 2016;296:351-60.

[162] Diamant S, Podoly E, Friedler A, Ligumsky H, Livnah O, Soreq H. Butyrylcholinesterase attenuates amyloid fibril formation in vitro. Proc Natl Acad Sci U S A. 2006;103(23):8628-33.

[163] Panegyres P, Mamotte C, Vasikaran S, Wilton S, Fabian V, Kakulas B. Butyrycholinesterase K variant and Alzheimer's disease. Journal of neurology. 1999;246:369-70.

[164] Ilyushin DG, Haertley OM, Bobik TV, Shamborant OG, Surina EA, Knorre VD, et al. Recombinant human butyrylcholinesterase as a new-age bioscavenger drug: development of the expression system. Acta Naturae. 2013;5(1):73-84.

[165] Darvesh S, Hopkins DA, Geula C. Neurobiology of butyrylcholinesterase. Nature Reviews Neuroscience. 2003;4(2):131-8.

[166] Radić Z, Pickering NA, Vellom DC, Camp S, Taylor P. Three distinct domains in the cholinesterase molecule confer selectivity for acetyl- and butyrylcholinesterase inhibitors. Biochemistry. 1993;32(45):12074-84.

[167] Harel M, Quinn D, Nair H, Silman I, Sussman J. The X-ray structure of a transition state analog complex reveals the molecular origins of the catalytic power and substrate specificity of acetylcholinesterase. Journal of the American Chemical Society. 1996;118:2340-6.

[168] Greig NH, Lahiri DK, Sambamurti K. Butyrylcholinesterase: An Important New Target in Alzheimer's Disease Therapy. International psychogeriatrics. 2005;14(S1):77-91.

[169] Masson P, Adkins S, Gouet P, Lockridge O. Recombinant human butyrylcholinesterase G390V, the fluoride-2 variant, expressed in Chinese hamster ovary cells, is a low affinity variant. Journal of Biological Chemistry. 1993;268(19):14329-41.

[170] Masson P, Froment M-T, Gillon E, Nachon F, Lockridge O, Schopfer LM. Kinetic analysis of effector modulation of butyrylcholinesterase-catalysed hydrolysis of acetanilides and homologous esters. The FEBS Journal. 2008;275(10):2617-31.

[171] Main AR. Mode of action of anticholinesterases. Pharmacology and Therapeutics. 1979;6(3):579-628.

[172] Kamal MA, Qu X, Yu QS, Tweedie D, Holloway HW, Li Y, et al. Tetrahydrofurobenzofuran cymserine, a potent butyrylcholinesterase inhibitor and experimental Alzheimer drug candidate, enzyme kinetic analysis. Journal of neural transmission (Vienna, Austria : 1996). 2008;115(6):889-98.

[173] Taylor P, Wong L, Radić Z, Tsigelny I, Bruggemann R, Hosea NA, et al. Analysis of cholinesterase inactivation and reactivation by systematic structural modification and enantiomeric selectivity. Chem Biol Interact. 1999;119-120:3-15.

[174] Bartling A, Worek F, Szinicz L, Thiermann H. Enzyme-kinetic investigation of different sarin analogues reacting with human acetylcholinesterase and butyrylcholinesterase. Toxicology. 2007;233(1-3):166-72.

[175] Jabir NR, Khan FR, Tabrez S. Cholinesterase targeting by polyphenols: A therapeutic approach for the treatment of Alzheimer's disease. CNS neuroscience andamp; therapeutics. 2018;24(9):753-62.

[176] Surabhi S, Singh BK. COMPUTER AIDED DRUG DESIGN: AN OVERVIEW. Journal of Drug Delivery and Therapeutics. 2018;8:504-9.

[177] Cui W, Aouidate A, Wang S, Yu Q, Li Y, Yuan S. Discovering Anti-Cancer Drugs via Computational Methods. Frontiers in Pharmacology. 2020;11(733).

[178] Mavromoustakos T. Methodologies and applied strategies in the rational drug design. Current medicinal chemistry. 2011;18(17):2516.

[179] Xiang M, Cao Y, Fan W, Chen L, Mo Y. Computer-aided drug design: lead discovery and optimization. Combinatorial chemistry and high throughput screening. 2012;15(4):328-37.

[180] Baig MH, Ahmad K, Rabbani G, Danishuddin M, Choi I. Computer Aided Drug Design and its Application to the Development of Potential Drugs for Neurodegenerative Disorders. Curr Neuropharmacol. 2018;16(6):740-8.

[181] Baig MH, Ahmad K, Rabbani G, Danishuddin, Choi I. Computer Aided Drug Design and its Application to the Development of Potential Drugs for Neurodegenerative Disorders. Curr Neuropharmacol. 2017;15.

[182] Salman MM, Al-Obaidi Z, Kitchen P, Loreto A, Bill RM, Wade-Martins R. Advances in Applying Computer-Aided Drug Design for Neurodegenerative Diseases. International journal of molecular sciences. 2021;22(9).

[183] Baig MH, Ahmad K, Rabbani G, Danishuddin M, Choi I. Computer Aided Drug Design and its Application to the Development of Potential Drugs for Neurodegenerative Disorders. Curr Neuropharmacol. 2018;16(6):740-8.

[184] Zeng H, Wu X. Alzheimer's disease drug development based on Computer-Aided Drug Design. Eur J Med Chem. 2016;121:851-63.

[185] Llorach-Pares L, Nonell-Canals A, Sanchez-Martinez M, Avila C. Computer-Aided Drug Design Applied to Marine Drug Discovery: Meridianins as Alzheimer’s Disease Therapeutic Agents. Marine Drugs. 2017;15(12).

[186] Lemos A, Melo R, Moreira IS, Cordeiro MNDS. Computer-Aided Drug Design Approaches to Study Key Therapeutic Targets in Alzheimer’s Disease. In: Roy K, editor. Computational Modeling of Drugs Against Alzheimer’s Disease. New York, NY: Springer New York; 2018. p. 61-106.

[187] Kříž K, Řezáč J. Benchmarking of Semiempirical Quantum-Mechanical Methods on Systems Relevant to Computer-Aided Drug Design. Journal of Chemical Information and Modeling. 2020;60(3):1453-60.

[188] Leach AR. Molecular modelling : principles and applications. Harlow, England; New York: Prentice Hall; 2001.

[189] Imam SS, Gilani SJ, editors. Computer Aided Drug Design: A Novel Loom To Drug Discovery2017.

[190] Ferreira LG, Dos Santos RN, Oliva G, Andricopulo AD. Molecular docking and structure-based drug design strategies. Molecules. 2015;20(7):13384-421.

[191] Dos Santos RN, Ferreira LG, Andricopulo AD. Practices in Molecular Docking and Structure-Based Virtual Screening. Methods in molecular biology (Clifton, NJ). 2018;1762:31-50.

[192] Alejandra Hernández-Santoyo AYT-B, Victor, Altuzar HV-CaCM-BMtP-PaP-LD, Protein Engineering - Technology and Application, Tomohisa Ogawa, IntechOpen, DOI: 10.5772/56376. Available from: https://www.intechopen.com/books/protein-engineering-technology-and-application/protein-protein-and-protein-ligand-docking.

[193] Kitchen DB, Decornez H, Furr JR, Bajorath J. Docking and scoring in virtual screening for drug discovery: methods and applications. Nature Reviews Drug Discovery. 2004;3(11):935-49.

[194] Cramer D, and Howitt, D. L. (2004). The SAGE Dictionary of Statistics: A Practical Resource for Students in Social Sciences. London: SAGE Publications Ltd., https://doi.org/10.4135/9780857020123.

[195] Friesner RA, Banks JL, Murphy RB, Halgren TA, Klicic JJ, Mainz DT, et al. Glide: A New Approach for Rapid, Accurate Docking and Scoring. 1. Method and Assessment of Docking Accuracy. Journal of Medicinal Chemistry. 2004;47(7):1739-49.

[196] Ewing TJ, Makino S, Skillman AG, Kuntz ID. DOCK 4.0: search strategies for automated molecular docking of flexible molecule databases. J Comput Aided Mol Des. 2001;15(5):411-28.

[197] Jones G, Willett P, Glen RC, Leach AR, Taylor R. Development and validation of a genetic algorithm for flexible docking. J Mol Biol. 1997;267(3):727-48.

[198] Rarey M, Kramer B, Lengauer T, Klebe G. A fast flexible docking method using an incremental construction algorithm. J Mol Biol. 1996;261(3):470-89.

[199] Okumura H, Higashi M, Yoshida Y, Sato H, Akiyama R. Theoretical approaches for dynamical ordering of biomolecular systems. Biochim Biophys Acta Gen Subj. 2018;1862(2):212-28.

[200] Shukla R, Tripathi T. Molecular Dynamics Simulation of Protein and Protein–Ligand Complexes. In: Singh DB, editor. Computer-Aided Drug Design. Singapore: Springer Singapore; 2020. p. 133-61.

[201] Braun E, Gilmer J, Mayes HB, Mobley DL, Monroe JI, Prasad S, et al. Best Practices for Foundations in Molecular Simulations [Article v1.0]. Living journal of computational molecular science. 2019;1(1).

[202] Lippert RA, Predescu C, Ierardi DJ, Mackenzie KM, Eastwood MP, Dror RO, et al. Accurate and efficient integration for molecular dynamics simulations at constant temperature and pressure. The Journal of chemical physics. 2013;139(16):164106.

[203] Kuzmanic A, Zagrovic B. Determination of ensemble-average pairwise root mean-square deviation from experimental B-factors. Biophys J. 2010;98(5):861-71.

[204] Genheden S, Ryde U. The MM/PBSA and MM/GBSA methods to estimate ligand-binding affinities. Expert opinion on drug discovery. 2015;10(5):449-61.

[205] Wang E, Sun H, Wang J, Wang Z, Liu H, Zhang JZH, et al. End-Point Binding Free Energy Calculation with MM/PBSA and MM/GBSA: Strategies and Applications in Drug Design. Chemical reviews. 2019;119(16):9478-508.

[206] Zhang J, Zhang H, Wu T, Wang Q, van der Spoel D. Comparison of Implicit and Explicit Solvent Models for the Calculation of Solvation Free Energy in Organic Solvents. Journal of Chemical Theory and Computation. 2017;13(3):1034-43.

[207] Wilson G, Lill M. Integrating structure-based and ligand-based approaches for computational drug design. Future medicinal chemistry. 2011;3:735-50.

[208] Macalino SJ, Gosu V, Hong S, Choi S. Role of computer-aided drug design in modern drug discovery. Archives of pharmacal research. 2015;38(9):1686-701.

[209] Hoque I, Chatterjee A, Bhattacharya S, Biswas R. An Approach of Computer-Aided Drug Design (CADD) Tools for In Silico Pharmaceutical Drug Design and Development. International Journal of Advanced Research in Biological Sciences. 2017;4:60-71.

[210] Yang S-Y. Pharmacophore modeling and applications in drug discovery: challenges and recent advances. Drug Discovery Today. 2010;15(11):444-50.

[211] Dixon SL, Smondyrev AM, Knoll EH, Rao SN, Shaw DE, Friesner RA. PHASE: a new engine for pharmacophore perception, 3D QSAR model development, and 3D database screening: 1. Methodology and preliminary results. J Comput Aided Mol Des. 2006;20(10-11):647-71.

[212] Hansch C, Fujita T. p-σ-π Analysis. A Method for the Correlation of Biological Activity and Chemical Structure. Journal of the American Chemical Society. 1964;86(8):1616-26.

[213] Cherkasov A, Muratov EN, Fourches D, Varnek A, Baskin II, Cronin M, et al. QSAR modeling: where have you been? Where are you going to? Journal of medicinal chemistry. 2014;57(12):4977-5010.

[214] Neves BJ, Braga RC, Melo-Filho CC, Moreira-Filho JT, Muratov EN, Andrade CH. QSAR-Based Virtual Screening: Advances and Applications in Drug Discovery. Frontiers in Pharmacology. 2018;9(1275).

[215] Gupta PP, Bastikar VA, Bastikar A, Chhajed SS, Pathade PA. Computational Screening Techniques for Lead Design and Development. In: Singh DB, editor. Computer-Aided Drug Design. Singapore: Springer Singapore; 2020. p. 187-222.

[216] Ekins S, Andreyev S, Ryabov A, Kirillov E, Rakhmatulin EA, Sorokina S, et al. A combined approach to drug metabolism and toxicity assessment. Drug metabolism and disposition: the biological fate of chemicals. 2006;34(3):495-503.

[217] Myshkin E, Brennan R, Khasanova T, Sitnik T, Serebriyskaya T, Litvinova E, et al. Prediction of Organ Toxicity Endpoints by QSAR Modeling Based on Precise Chemical-Histopathology Annotations. Chemical Biology and Drug Design. 2012;80(3):406-16.

[218] Pathak RK, Baunthiyal M, Shukla R, Pandey D, Taj G, Kumar A. In Silico Identification of Mimicking Molecules as Defense Inducers Triggering Jasmonic Acid Mediated Immunity against Alternaria Blight Disease in Brassica Species. Frontiers in Plant Science. 2017;8(609).

[219] Pathak RK, Gupta A, Shukla R, Baunthiyal M. Identification of new drug-like compounds from millets as Xanthine oxidoreductase inhibitors for treatment of Hyperuricemia: A molecular docking and simulation study. Computational biology and chemistry. 2018;76:32-41.

[220] G M, B M, Ss V, A N, T H. Computational Drug Design and Molecular Dynamic Studies-A Review. International Journal of Biomedical Data Mining. 2017;06.

[221] Zhang S. Computer-aided drug discovery and development. Methods in molecular biology (Clifton, NJ). 2011;716:23-38.

[222] Kapetanovic IM. Computer-aided drug discovery and development (CADDD): in silico-chemico-biological approach. Chem Biol Interact. 2008;171(2):165-76.

[223] Shekhar C. In silico pharmacology: computer-aided methods could transform drug development. Chemistry and biology. 2008;15(5):413-4.

[224] Huang R, Southall N, Wang Y, Yasgar A, Shinn P, Jadhav A, et al. The NCGC pharmaceutical collection: a comprehensive resource of clinically approved

drugs enabling repurposing and chemical genomics. Science translational medicine. 2011;3(80):80ps16.

[225] Matthews BW. Comparison of the predicted and observed secondary structure of T4 phage lysozyme. Biochimica et Biophysica Acta (BBA) - Protein Structure. 1975;405(2):442-51.

[226] Banks JL, Beard HS, Cao Y, Cho AE, Damm W, Farid R, et al. Integrated Modeling Program, Applied Chemical Theory (IMPACT). Journal of computational chemistry. 2005;26(16):1752-80.

[227] Shelley J, Cholleti A, Frye L, Greenwood J, Timlin M, Uchimaya M. Epik: A software program for pKa prediction and protonation state generation for drug-like molecules. Journal of computer-aided molecular design. 2008;21:681-91.

[228] Cheung J, Rudolph MJ, Burshteyn F, Cassidy MS, Gary EN, Love J, et al. Structures of Human Acetylcholinesterase in Complex with Pharmacologically Important Ligands. Journal of Medicinal Chemistry. 2012;55(22):10282-6.

[229] Košak U, Brus B, Knez D, Šink R, Žakelj S, Trontelj J, et al. Development of an in-vivo active reversible butyrylcholinesterase inhibitor. Scientific reports. 2016;6:39495.

[230] Sastry GM, Adzhigirey M, Day T, Annabhimoju R, Sherman W. Protein and ligand preparation: parameters, protocols, and influence on virtual screening enrichments. J Comput Aided Mol Des. 2013;27(3):221-34.

[231] Cavdar H, Senturk M, Guney M, Durdagi S, Kayik G, Supuran CT, et al. Inhibition of acetylcholinesterase and butyrylcholinesterase with uracil derivatives: kinetic and computational studies. J Enzyme Inhib Med Chem. 2019;34(1):429-37.

[232] Li H, Robertson AD, Jensen JH. Very fast empirical prediction and rationalization of protein pKa values. Proteins: Structure, Function, and Bioinformatics. 2005;61(4):704-21.

[233] Shelley JC, Cholleti A, Frye LL, Greenwood JR, Timlin MR, Uchimaya M. Epik: a software program for pK(a) prediction and protonation state generation for drug-like molecules. J Comput Aided Mol Des. 2007;21(12):681-91.

[234] Halgren TA, Murphy RB, Friesner RA, Beard HS, Frye LL, Pollard WT, et al. Glide: a new approach for rapid, accurate docking and scoring. 2. Enrichment factors in database screening. J Med Chem. 2004;47(7):1750-9.

[235] Durdagi S, Aksoydan B, Erol I, Kantarcioglu I, Ergun Y, Bulut G, et al. Integration of multi-scale molecular modeling approaches with experiments for the in silico guided design and discovery of novel hERG-Neutral antihypertensive oxazalone and imidazolone derivatives and analysis of their potential restrictive effects on cell proliferation. European Journal of Medicinal Chemistry. 2018;145:273-90.

[236] Chhabra S, Sharma P, Ghoshal N. A computational docking study for prediction of binding mode of diospyrin and derivatives: Inhibitors of human and leishmanial DNA topoisomerase-I. Bioorganic and medicinal chemistry letters. 2007;17(16):4604-12.

[237] Gschwend DA, Good AC, Kuntz ID. Molecular docking towards drug discovery. Journal of Molecular Recognition. 1996;9(2):175-86.

[238] Sherman W, Day T, Jacobson MP, Friesner RA, Farid R. Novel Procedure for Modeling Ligand/Receptor Induced Fit Effects. Journal of Medicinal Chemistry. 2006;49(2):534-53.

[239] Ekhteiari Salmas R, Unlu A, Bektaş M, Yurtsever M, Mestanoglu M, Durdagi S. Virtual screening of small molecules databases for discovery of novel PARP-1 inhibitors: combination of in silico and in vitro studies. Journal of biomolecular structure and dynamics. 2017;35(9):1899-915.

[240] Cho AE, Guallar V, Berne BJ, Friesner R. Importance of accurate charges in molecular docking: quantum mechanical/molecular mechanical (QM/MM) approach. Journal of computational chemistry. 2005;26(9):915-31.

[241] Ivanova L, Tammiku-Taul J, García-Sosa AT, Sidorova Y, Saarma M, Karelson M. Molecular Dynamics Simulations of the Interactions between Glial Cell Line-Derived Neurotrophic Factor Family Receptor GFRα1 and Small-Molecule Ligands. ACS Omega. 2018;3(9):11407-14.

[242] Hoover WG. Canonical dynamics: Equilibrium phase-space distributions. Physical Review A. 1985;31(3):1695-7.

[243] Nosé S. A unified formulation of the constant temperature molecular dynamics methods. Journal of Chemical Physics. 1984;81:511-9.

[244] Martyna G, Tobias D, Klein M. Constant pressure molecular dynamics algorithms. Journal of Chemical Physics. 1994;101:4177-89.

[245] Abel R, Wang L, Harder ED, Berne BJ, Friesner RA. Advancing Drug Discovery through Enhanced Free Energy Calculations. Accounts of Chemical Research. 2017;50(7):1625-32.

[246] Hou T, Wang J, Li Y, Wang W. Assessing the Performance of the MM/PBSA and MM/GBSA Methods. 1. The Accuracy of Binding Free Energy Calculations Based on Molecular Dynamics Simulations. Journal of Chemical Information and Modeling. 2011;51(1):69-82.

[247] Hou T, Wang J, Li Y, Wang W. Assessing the performance of the molecular mechanics/Poisson Boltzmann surface area and molecular mechanics/generalized Born surface area methods. II. The accuracy of ranking poses generated from docking. Journal of computational chemistry. 2011;32(5):866-77.

[248] D L Beveridge a, DiCapua FM. Free Energy Via Molecular Simulation: Applications to Chemical and Biomolecular Systems. Annual Review of Biophysics and Biophysical Chemistry. 1989;18(1):431-92.

[249] Kollman PA, Massova I, Reyes C, Kuhn B, Huo S, Chong L, et al. Calculating Structures and Free Energies of Complex Molecules: Combining Molecular Mechanics and Continuum Models. Accounts of Chemical Research. 2000;33(12):889-97.

[250] Ellman GL, Courtney KD, Andres V, Featherstone RM. A new and rapid colorimetric determination of acetylcholinesterase activity. Biochemical Pharmacology. 1961;7(2):88-95.

[251] Durdagi S, Senturk M, Supuran C, Cavdar H, Ekinci D, Kayık G. Kinetic and In Silico Studies of Some Uracil Derivatives on Acetylcholinesterase and Butyrylcholinesterase Enzymes. J Enzyme Inhib Med Chem. 2018.

[252] Zilbeyaz K, Stellenboom N, Guney M, Oztekin A, Senturk M. Effects of aryl methanesulfonate derivatives on acetylcholinesterase and butyrylcholinesterase. Journal of Biochemical and Molecular Toxicology. 2018;32(11):e22210.

[253] Doytchinova I, Atanasova M, Valkova I, Stavrakov G, Philipova I, Zhivkova Z, et al. Novel hits for acetylcholinesterase inhibition derived by docking-based screening on ZINC database. J Enzyme Inhib Med Chem. 2018;33(1):768-76.

[254] Radić Z, Quinn DM, Vellom DC, Camp S, Taylor P. Allosteric control of acetylcholinesterase catalysis by fasciculin. The Journal of biological chemistry. 1995;270(35):20391-9.

[255] Ranjan A, Chauhan A, Jindal T. In-silico and in-vitro evaluation of human acetylcholinesterase inhibition by organophosphates. Environmental toxicology and pharmacology. 2018;57:131-40.

[256] Damuka N, Kammari K, Potshangbam AM, Rathore RS, Kondapi AK, Vindal V. Discovery of dual cation-π inhibitors of acetylcholinesterase: design, synthesis and biological evaluation. Pharmacological reports : PR. 2020;72(3):705-18.

[257] Son M, Park C, Rampogu S, Zeb A, Lee KW. Discovery of Novel Acetylcholinesterase Inhibitors as Potential Candidates for the Treatment of Alzheimer's Disease. International journal of molecular sciences. 2019;20(4).

[258] Gnatt A, Loewenstein Y, Yaron A, Schwarz M, Soreq H. Site-Directed Mutagenesis of Active Site Residues Reveals Plasticity of Human Butyrylcholinesterase in Substrate and Inhibitor Interactions. Journal of Neurochemistry. 1994;62(2):749-55.

[259] Biberoglu K, Tacal O, Akbulut H. The role of Phe329 in binding of cationic triarylmethane dyes to human butyrylcholinesterase. Archives of biochemistry and biophysics. 2011;511(1-2):64-8.

[260] Gnatt A, Loewenstein Y, Yaron A, Schwarz M, Soreq H. Site-directed mutagenesis of active site residues reveals plasticity of human butyrylcholinesterase in substrate and inhibitor interactions. Journal of neurochemistry. 1994;62(2):749-55.

[261] Ghafary S, Ghobadian R, Mahdavi M, Nadri H, Moradi A, Akbarzadeh T, et al. Design, synthesis, and evaluation of novel cinnamic acid-tryptamine hybrid for inhibition of acetylcholinesterase and butyrylcholinesterase. DARU Journal of Pharmaceutical Sciences. 2020;28(2):463-77.

[262] Masson P, Legrand P, Bartels CF, Froment MT, Schopfer LM, Lockridge O. Role of aspartate 70 and tryptophan 82 in binding of succinyldithiocholine to human butyrylcholinesterase. Biochemistry. 1997;36(8):2266-77.

[263] Zafar S, Choudhary MI, Dalvandi K, Mahmood U, Ul-Haq Z. Molecular docking simulation studies on potent butyrylcholinesterase inhibitors obtained from microbial transformation of dihydrotestosterone. Chem Cent J. 2013;7(1):164-.

[264] Asghar A, Yousuf M, Fareed G, Nazir R, Hassan A, Maalik A, et al. Synthesis, acetylcholinesterase (AChE) and butyrylcholinesterase (BuChE) activities, and molecular docking studies of a novel compound based on combination of flurbiprofen and isoniazide. RSC Advances. 2020;10:19346-52.

PUBLICATIONS FROM THE THESİS

Papers

Hind ALJANABI, Murat ŞENTÜRK and Barbaros NALBANTOĞLU (2021). "Drug Repurposing Effort for the Novel Acetylcholinesterase and Butyrylcholinesterase Targets: A Combined in silico and in vitro Study," Tob Regul Sci.™, vol. 7(6-1): 7050-7064; November (2021).

https://tobreg.org/index.php/journal/article/view/673.

Conference poster presentations

Hind ALJANABI, Barbaros NALBANTOĞLU, Serdar DURDAĞI, 2019. *In silico* and *in vitro* drug re-purposing study for the treatment of Alzheimer's disease. 7th International Bau Drug Design Congress. Istanbul/Turkey.